

Copyright
by
Sharmistha Roy
2002

The Dissertation Committee for Sharmistha Roy
Certifies that this is the approved version of the following dissertation:

Absorption of Chlorine and Mercury in Sulfite Solutions

Committee:

Gary T. Rochelle, Supervisor

David T. Allen

John G. Ekerdt

R. Bruce Eldridge

Lynn E. Katz

Absorption of Chlorine and Mercury in Sulfite Solutions

by
Sharmistha Roy, B.S.

Dissertation

Presented to the Faculty of the Graduate School of
The University of Texas at Austin
in Partial Fulfillment
of the Requirements
for the Degree of
Doctor of Philosophy

The University of Texas at Austin
August 2002

Acknowledgements

I wish to thank Professor Gary Rochelle for his guidance and support. His expertise, enthusiasm, creativity, and insight were all essential for the completion of this work. I am grateful for all the tools he has provided me for the scientific work I will accomplish in the future. I would also like to thank the other faculty members on my committee for their interest and support. Their feedback greatly enhanced this dissertation.

I want to express my appreciation for the Texas Utilities Environmental Research Steering Committee for providing financial support for me and this work. I am also grateful to the EPA for providing the funds to purchase the chlorine analyzer used in this work.

I have been fortunate to share my time with a great set of individuals in our research group: Paul Chisholm, Joe Devinentis, Lia Brodnax, Sanjay Bishnoi, Mike Dutchuk, Nicole Pauly, Norman Yeh, Amy Nowlin, Eric Chen, Susan Chi, Hongyi Dang, Stefano Freguia, Dyron Hamlin, George Goff, and Tim Cullinane. I've enjoyed working with them and am grateful for all the support they provided. They made working here enjoyable and even entertaining at times. Along with group members, I would also like to thank all of the friends and colleagues who have made the last few years such a memorable experience.

Finally, I would like to thank my family for their continuous love and support. Without them, I would not have made it to where I am now.

Absorption of Chlorine and Mercury in Sulfite Solutions

Publication No. _____

Sharmistha Roy, Ph.D.

The University of Texas at Austin, 2002

Supervisor: Gary T. Rochelle

The rate of chlorine absorption into aqueous sulfite/bisulfite, S(IV), was measured using a stirred cell reactor and a wetted wall column. Simultaneous absorption of Hg and Cl₂ in S(IV) solutions was also measured in the wetted wall column. The solution contained 0 to 10 mM S(IV) with pH ranging from 4.5 to 6. Experiments were performed at ambient temperature and pressure using 5 to 300 ppm Cl₂ and 46 ppb Hg. Absorption was modeled using the theory of mass transfer with chemical reaction. The rate constants for the Cl₂/S(IV) and Hg/Cl₂ reactions were determined to be 1.1×10^9 and 6.1×10^9 L/mol-s, respectively.

At the gas/liquid interface, chlorine reacts with S(IV) to form chloride and sulfate, and Hg is oxidized by Cl₂ to a more soluble form of Hg. The enhancement of the chlorine hydrolysis rate by the succinate buffer was quantified. Oxidants, such as HgCl₂ and NaOCl, enhanced Hg absorption. The addition of chloride had no effect on the Hg/Cl₂/S(IV) reaction rates. However, chloride did suppress chlorine hydrolysis and significantly enhanced Hg absorption with Cl₂, when no S(IV) was present. Possible reaction pathways are discussed.

These results are relevant in the simultaneous removal of Cl₂, SO₂, and Hg from flue gas. A model was developed to predict the expected Hg removal in a limestone slurry scrubber. Mercury removal decreases with increasing SO₂/S(IV). However, with low S(IV), the Cl₂ exiting the scrubber is greater. Thus, the process feasibility depends on the amount Hg and Cl₂ which can be tolerated.

Table of Contents

List of Tables	xi
List of Figures	xiii
Nomenclature	xv
Chapter 1: Introduction.....	1
1.1 Mercury pollution	1
1.1.1 Emissions	1
1.1.2 Regulations	2
1.2 Limestone slurry scrubbing.....	3
1.2.1 Proposed process for mercury removal in limestone slurry scrubbers	4
1.2.1.1 Feasibility of proposed process.....	6
1.3 Research objective and scope of work.....	7
Chapter 2: Literature Review.....	9
2.1 Characteristics of mercury	9
2.1.1 Health hazards.....	9
2.1.2 Transport cycle.....	10
2.1.3 Concentration and speciation of mercury in flue gas.....	11
2.2 Mercury control technologies	12
2.2.1 Coal cleaning	13
2.2.2 Sorbents.....	13
2.2.2.1 Carbon filter beds.....	13
2.2.2.2 Activated carbon injection	14
2.2.2.3 Calcium-based sorbents	15
2.2.2.4 Iodine-based sorbents.....	15
2.2.3 Wet scrubbing	16
2.2.3.1 Catalytic oxidation of Hg.....	16
2.2.3.2 Reagent addition to oxidize Hg.....	16
2.3 Aqueous phase reactions of mercury	17
2.3.1 Mercury absorption in chlorine oxidants	17
2.3.2 Absorption of mercury in other aqueous oxidants	20
2.3.3 Reduction of Hg(II) by S(IV)	21
2.4 Gas phase reactions of mercury	21
2.4.1 Reaction of mercury and chlorine.....	21
2.4.2 Reactions with species present in combustion flue gas	22
2.5 Aqueous phase reactions of chlorine species.....	22

2.5.1	Chlorine absorption in aqueous solutions	22
2.5.2	Reactions among aqueous chlorine oxidants	24
2.5.3	Reactions of S(IV) with chlorine oxidants.....	25
2.6	Summary	27
Chapter 3:	Mass Transfer with Chemical Reaction	28
3.1	Chlorine absorption model.....	28
3.2	Mercury absorption model.....	32
Chapter 4:	Experimental Apparatus and Methods.....	33
4.1	Description of stirred cell reactor apparatus	33
4.2	Gas source and flow path for stirred cell reactor	35
4.3	Methods for chlorine analysis.....	36
4.3.1	Electrochemical chlorine analyzer	36
4.3.2	IMS chlorine analyzer.....	36
4.3.3	Absolute chlorine analysis through wet chemical methods.....	37
4.3.3.1	Basis and rationale	37
4.3.3.2	Initial analytical methods.....	38
4.3.3.3	Final wet chemical methods to determine Cl ₂ concentration.....	38
4.4	Chlorine analyzer calibration procedure.....	39
4.4.1	Calibration of electrochemical analyzer	40
4.4.2	Calibration of the IMS analyzer.....	42
4.5	Stirred cell reactor solution and analysis	43
4.6	Iodometric titration for S(IV).....	45
4.7	Wetted wall column design.....	46
4.7.1	Basis and rationale	46
4.7.2	Description of wetted wall column.....	47
4.8	Wetted wall column solution flow path and analysis	49
4.9	Gas flow path for chlorine absorption in wetted wall column.....	51
4.10	Gas source and flow path for mercury absorption	51
4.11	Mercury sample conditioning system	53
4.11.1	Initial testing	53
4.11.2	Final configuration.....	55
4.12	Cold vapor atomic absorption (CVAA) mercury analyzer	55
4.12.1	Mercury analyzer calibration	56
4.13	Typical experimental procedure	58
Chapter 5:	Characterizing Wetted Wall Column.....	59
5.1	Gas film mass transfer coefficient	59
5.1.1	Experimental method.....	59
5.1.2	Theory	60
5.1.3	Results and discussion	62
5.2	Liquid film mass transfer coefficient.....	65

5.2.1	Experimental method	66
5.2.2	Theory	66
5.2.3	Results and discussion	68
5.3	Gas/liquid contact area.....	70
5.3.1	Basis and rationale	70
5.3.2	Experimental method	70
5.3.3	Theory	71
5.3.4	Results and discussion	72
Chapter 6:	Chlorine Absorption in Stirred Cell Reactor	76
6.1	Approximate reaction rate for chlorine with S(IV) at pH 4.5	76
6.1.1	Experimental method	76
6.1.2	Tabulated results	77
6.1.3	Discussion	80
6.2	Chlorine absorption as a function of agitation.....	88
6.2.1	Experimental method	88
6.2.2	Tabulated results	89
6.2.3	Discussion	91
6.3	Effect of succinate buffer on chlorine absorption at pH 4.5	92
6.3.1	Experimental method	93
6.3.2	Tabulated results	93
6.3.3	Discussion	94
6.4	S(IV) oxidation at pH 4.5 by chlorine and oxygen.....	96
6.4.1	Experimental method	96
6.4.2	Tabulated results	96
6.4.3	Discussion	97
6.5	Absorption at pH 4.5 using electrochemical chlorine analyzer	100
6.5.1	Experimental method	101
6.5.2	Tabulated results	101
6.5.3	Discussion	102
6.5.3.1	Effect of chloride	104
6.6	Absorption at pH 6 to 8.5 using electrochemical analyzer	105
6.6.1	Experimental method	105
6.6.2	Tabulated results	106
6.6.3	Discussion	106
6.7	Summary	106
Chapter 7:	Chlorine Absorption in Wetted Wall Column	108
7.1	Chlorine absorption in wetted wall column at pH 4.7	108
7.1.1	Experimental method	108
7.1.2	Tabulated results	109
7.1.3	Discussion	110

7.1.3.1 Regressed rate constant.....	111
7.1.3.2 Section profiles	113
7.1.3.3 Model sensitivity.....	118
7.2 Chlorine absorption in wetted wall column at pH 5.7	123
7.2.1 Experimental method.....	123
7.2.2 Tabulated results	124
7.2.3 Discussion.....	124
7.2.3.1 Regressed $k_{2,\text{buf}}$ at pH 5.7	125
7.2.3.2 Regressed $k_{2,\text{S(IV)}}$ at pH 5.7.....	127
7.2.3.3 Effect of 0.1 M NaCl	130
7.3 Comparison of S(IV) reaction rates with $\text{Cl}_2/\text{HOCl}/\text{OCl}^-$	130
7.4 Summary	130
Chapter 8: Simultaneous Absorption of Mercury and Chlorine.....	132
8.1 Absorption of mercury and chlorine into S(IV) at pH 4.7	132
8.1.1 Experimental method.....	132
8.1.2 Tabulated results	133
8.1.3 Discussion.....	134
8.1.3.1 Regressing $k_{2,\text{Hg}}$ at pH 4.7.....	134
8.1.3.2 Section profiles	138
8.2 Absorption of mercury and chlorine into S(IV) at pH 5.7	145
8.2.1 Experimental method.....	145
8.2.2 Tabulated results	145
8.2.3 Discussion.....	146
8.2.3.1 Regressed $k_{2,\text{Hg}}$ at pH 5.7	147
8.2.3.2 Model sensitivity.....	148
8.3 Effect of mercuric chloride at pH 5.7	152
8.3.1 Experimental method.....	152
8.3.2 Tabulated results	153
8.3.3 Discussion.....	153
8.4 Effect of sodium hypochlorite and chloride.....	157
8.4.1 Theory	157
8.4.2 Experimental method.....	159
8.4.3 Tabulated results	160
8.4.4 Discussion.....	161
8.4.4.1 Overview of data.....	161
8.4.4.2 Analysis of results obtained by previous researchers	163
8.4.4.3 Analysis of this work in the context of previous work	165
8.4.4.4 Parallel reactions.....	166
8.5 Implications on mercury removal in a typical limestone slurry scrubber.....	171
8.5.1 Other factors affecting Hg removal in a limestone slurry scrubber.....	175

8.6 Summary	176
Chapter 9: Conclusions and Recommendations	179
9.1 Conclusions.....	179
9.1.1 Chlorine absorption in succinate buffer/S(IV).....	179
9.1.2 Simultaneous absorption of mercury and chlorine	180
9.1.3 Predicting Hg removal in a limestone slurry scrubber.....	181
9.2 Recommendations.....	181
9.2.1 Understanding Hg/Cl ₂ reaction pathway	181
9.2.2 Experimental conditions to simulate limestone slurry scrubber	182
9.2.3 Improved Hg analytical capabilities	182
Appendix A: Gas film mass transfer coefficient for stirred cell.....	184
Appendix B: Liquid film mass transfer coefficient for stirred cell.....	187
Appendix C: Chloride analysis through ion chromatography	196
Appendix D: S(IV) analysis through iodometric titration	197
Appendix E: Calculation of D _{Cl₂-N₂} using Chapman-Enskog theory	199
Appendix F: Liquid film mass transfer coefficient for wetted wall.....	200
Appendix G: NaOCl Analysis through Iodometric Titration	205
Bibliography	206
Vita.....	219

List of Tables

Table 1.1. Mercury emissions from combustion sources	2
Table 4.1 Analyzing Hg in the presence of chlorine	54
Table 5.1 Data used to obtain gas film mass transfer coefficient	62
Table 5.2 Liquid film mass transfer coefficients	69
Table 5.3 Data used to calculate area.....	73
Table 6.1. Chlorine and oxygen absorption with variable S(IV) at pH 4.5 in 50 mM succinate buffer with 1.15 L/min gas and at n_g/n_L of 700 to 730 rpm	77
Table 6.2. Chlorine absorption in S(IV) at pH 4.5 in 50 mM succinate buffer with 1.15 L/min gas and at n_g/n_L of 700 to 730 rpm	79
Table 6.3. Chlorine absorption in S(IV) at pH 4.5 in 5 mM succinate buffer with 1.18 L/min gas and at n_g/n_L of 745 rpm	80
Table 6.4. Chlorine (21.2 ppm inlet) absorption in S(IV) solutions with 5 mM buffer at various agitation rates	89
Table 6.5. Chlorine absorption with varying buffer concentration in pH 4.5 with 1.15 L/min gas at n_g/n_L of 700 rpm.....	94
Table 6.6. S(IV) depletion resulting from oxygen absorption at pH 4.5 in 50 mM succinate buffer with 1.15 L/min gas and at n_g/n_L of 700 to 730 rpm	96
Table 6.7. Chlorine absorption in S(IV) at pH 4.5, measured with electrochemical analyzer, in 50 mM succinate buffer with 1.2 L/min gas	102
Table 6.8. Chlorine absorption at pH 6 to 8.5 with 1.2 L/min gas, measured using electrochemical sensor analyzer	106
Table 7.1. Chlorine absorption in S(IV) at pH 4.5 – 4.7 with 5 mM succinate buffer in wetted wall column	109
Table 7.2. Chlorine section profile at 23.5 ppm and 0.01 mM S(IV)	114
Table 7.3. Chlorine section profile at 23.5 ppm and 0.06 mM S(IV)	115
Table 7.4. Chlorine profile at 23.5 ppm and 1 mM S(IV)	117
Table 7.5. Parameters used for base case model sensitivity analyses at pH 4.7	118
Table 7.6. Chlorine absorption in buffered S(IV) at pH 5.65 – 5.75	124
Table 7.7. Parameters used in model for pH 5.7 chlorine absorption.....	125
Table 7.8 Comparison of K_a values at 9.5°C and 25°C	126
Table 7.9 Correlation for $k_{2,buf}$ as a function K_a at ambient temperature.....	127
Table 7.10. Reaction rates of S(IV) with chlorine species at 25°C	130
Table 8.1. Mercury and chlorine absorption in buffered S(IV) at pH 4.7	133
Table 8.2. Parameters used to regress Hg/Cl_2 reaction rate at pH 4.7	135

Table 8.3. Mercury section profile at 7.6 ppm Cl ₂ and 0.01 mM S(IV)	138
Table 8.4. Mercury section profile at 7.6 ppm Cl ₂ and 9 mM S(IV)	139
Table 8.5. Mercury section profile at 22.4 ppm Cl ₂ and 0.01 mM S(IV)	141
Table 8.6. Mercury section profile at 22.4 ppm Cl ₂ and 9 mM S(IV)	142
Table 8.7 Mercury and chlorine absorption in buffered S(IV) at pH 5.65 to 5.75 ...	145
Table 8.8 Parameters used to model Hg and Cl ₂ absorption at pH 5.7	146
Table 8.8 Absorption of Hg and Cl ₂ in buffered HgCl ₂ at pH 5.64 to 5.66.....	153
Table 8.9 Predicted and observed Hg absorption in HgCl ₂ with Cl ₂ present	156
Table 8.10 Predicted and observed Hg flux in HgCl ₂ without Cl ₂	157
Table 8.11 Absorption of Hg and Cl ₂ in NaOCl/0.1 M NaCl at pH 5.76	160
Table 8.12 Absorption of Hg and Cl ₂ in S(IV)/0.1 M NaCl at pH 5.76	161
Table 8.13 Mercury absorption in NaOCl/NaCl at pH 5 to 11, Hg _{in} = 98 ppb (Zhao, 1997)	169
Table 8.14 Mercury flux predictions in 0.1 M NaCl at pH 5.76.....	169
Table 8.15. Parameters used to predict mercury removal in a scrubber at 25°C ...	172
Table 8.16. Predicted Hg penetration in a scrubber with Cl ₂ injection at inlet.....	174
Table 8.17. Predicted Hg penetration in a scrubber with Cl ₂ injection near top.....	175
Table A-1. Gas film mass transfer coefficient (k _g) for stirred cell reactor, obtained using IMS analyzer	184
Table A-2. Gas film mass transfer coefficient (k _g) for stirred cell reactor, obtained using electrochemical analyzer	184
Table A-3. Parameters for gas film mass transfer correlations.....	186
Table B-1. Data used to determine k_{L,Cl_2}^0 correlations for stirred cell reactor	187
Table B-2. Liquid film mass transfer coefficient for stirred cell reactor	194
Table F-1. Data used to determine k_{L,Cl_2}^0 at 2.26 mL/s	200
Table F-2. Data used to determine k_{L,Cl_2}^0 at 2.96 mL/s	202

List of Figures

Figure 1.1. Chlorine injection for Hg removal in limestone slurry scrubbing.....	5
Figure 1.2. Mass transfer boundary layer	6
Figure 4.1. Stirred cell reactor apparatus	34
Figure 4.2. Typical calibration of electrochemical sensor analyzer	41
Figure 4.3. Electrochemical analyzer calibration with bad cell.....	42
Figure 4.4 Typical IMS analyzer calibration	43
Figure 4.5 Wetted wall column.....	48
Figure 4.6 Flow diagram for chlorine absorption in wetted wall column	50
Figure 4.7 Gas flow path for mercury/chlorine absorption.....	52
Figure 4.8 Typical CVAA calibration	57
Figure 5.1. Correlations for gas film mass transfer coefficient in wetted wall.....	64
Figure 5.2 Obtaining area of wetted wall column.....	75
Figure 6.1. Chlorine absorption in buffered S(IV) in stirred cell reactor, $k_{2,S(IV)} = 2 \times 10^9$ L/mol-s.....	82
Figure 6.2. Chlorine penetration in buffered S(IV) in stirred cell, $k_{2,S(IV)} = \text{b}$	85
Figure 6.3. Chlorine penetration in buffered S(IV) in stirred cell reactor, $k_{2,S(IV)} = 2.5 \times 10^8$ L/mol-s.....	86
Figure 6.4. Chlorine penetration in buffered S(IV) in stirred cell reactor, $k_{2,S(IV)} = 2 \times 10^9$ L/mol-s.....	87
Figure 6.5. Data limited by k_g of stirred cell reactor	92
Figure 6.6. Obtaining kinetics for Cl_2 absorption in succinate buffer at pH 4.5	95
Figure 6.7. S(IV) oxidation by 275 ppm chlorine and 14.5% oxygen.....	98
Figure 6.8. S(IV) oxidation by 21 ppm chlorine and 20.5% oxygen.....	99
Figure 6.9. Electrochemical analyzer data overlaid onto IMS data.....	103
Figure 6.10. Chlorine absorption in 0 – 2 mM S(IV) in 50 mM buffer using electrochemical analyzer.....	104
Figure 6.11. Effect of chloride on Cl_2 absorption in S(IV), obtained from data using electrochemical analyzer.....	105
Figure 7.1. Comparison of predicted fluxes in wetted wall column to that in stirred cell at pH 4.7 using $k_{2,S(IV)} = 2 \times 10^9$ L/mol-s	111
Figure 7.2. Chlorine penetration in buffered S(IV), $k_{2,S(IV)} = 1.0 \times 10^9$ L/mol-s, in wetted wall column at pH 4.7	112
Figure 7.3. Chlorine penetration in buffered S(IV) in stirred cell reactor, $k_{2,S(IV)} = 1.0 \times 10^9$ L/mol-s.....	113

Figure 7.4 Effect of varying k_g on predicted chlorine penetration	119
Figure 7.5 Effect of varying $k_{L,S(IV)}^o$ on predicted chlorine penetration	120
Figure 7.6. Effect of varying area on chlorine penetration	121
Figure 7.7 Effect of varying $k_{2,S(IV)}$ on chlorine penetration.....	122
Figure 7.8. Chlorine absorption in buffered S(IV) at pH 5.7, $k_{2,S(IV)} = 1.4 \times 10^9$ L/mol-s	128
Figure 7.9 Chlorine penetration in buffered S(IV) at pH 5.7, $k_{2,S(IV)} = 1.4 \times 10^9$ L/mol-s	129
Figure 8.1. Predicted Hg penetration at various Cl_2 and S(IV) at pH 4.7 to 4.8.....	136
Figure 8.2 Mercury penetration in S(IV) at pH 4.7, $k_{2,Hg} = 6.2 \times 10^9$ L/mol-s	137
Figure 8.3. Concentration profile at 22.4 ppm Cl_2 and 0.01 mM S(IV)	144
Figure 8.4. Concentration profile at 22.4 ppm Cl_2 and 9 mM S(IV)	144
Figure 8.5. Mercury penetration in S(IV) at pH 5.7, $k_{2,Hg} = 6.0 \times 10^9$ L/mol-s.....	148
Figure 8.6. Effect of varying $k_{g,Hg}$ on predicted Hg penetration.....	149
Figure 8.7. Effect of varying $k_{2,Hg}$ on predicted Hg penetration	150
Figure 8.8. Effect of varying $k_{2,S(IV)}$ on predicted Hg penetration.....	151
Figure 8.9. Hg penetration in buffered $HgCl_2$ at pH 5.65	155
Figure 8.10. Mercury penetration in buffered NaOCl/0.1 M NaCl at pH 5.76	162
Figure 8.11. Using parallel reaction model to correlate data with NaOCl/NaCl.....	170
Figure A-1. Data and correlations for gas film mass transfer coefficient.....	186
Figure B-1. Extracting k_{L,Cl_2}^o at 729 rpm	189
Figure B-2. Extracting k_{L,Cl_2}^o at 305 rpm	190
Figure B-3. Extracting k_{L,Cl_2}^o at 504 rpm	190
Figure B-4. Extracting k_{L,Cl_2}^o at 734 rpm	191
Figure B-5. Extracting k_{L,Cl_2}^o at 699 rpm	191
Figure B-6. Extracting k_{L,Cl_2}^o at 228 rpm	192
Figure B-7. Extracting k_{L,Cl_2}^o at 600 rpm	192
Figure B-8. Extracting k_{L,Cl_2}^o at 306 rpm	193
Figure B-9. Extracting k_{L,Cl_2}^o at 514 rpm	193
Figure B-10. Extracting k_{L,Cl_2}^o at 718 rpm	194
Figure B-11. Data and correlations for physical liquid film mass transfer coefficient for stirred cell reactor.....	195
Figure F-1. Extracting k_{L,Cl_2}^o at 2.26 mL/s for wetted wall column	203
Figure F-2. Extracting k_{L,Cl_2}^o at 2.96 mL/s for wetted wall column	204

Nomenclature

a	activity ($\text{kmol/m}^3 = \text{mol/L}$)
A	gas/liquid contact area (m^2)
A^-	generic anion
C_{Cl_2}	concentration of chlorine in liquid ($\text{mol/L} = \text{M} = \text{kmol/m}^3$)
$[\text{Cl}^-]$	concentration of chloride in liquid (M)
d	inner diameter of wetted wall column (m)
D_{Cl_2}	diffusion coefficient for chlorine in water (m^2/s)
D_{Hg}	diffusion coefficient for mercury in water (m^2/s)
$D_{\text{S(IV)}}$	diffusion coefficient for S(IV) in water (m^2/s)
E	enhancement factor (dimensionless)
FC	mass flow controller
G	gas flow rate to reactor (m^3/s or L/min)
h	height of wetted wall column (m)
HA	generic acid
H_{Cl_2}	Henry's law constant for chlorine ($\text{atm}\cdot\text{m}^3/\text{kmol}$)
H_{Hg}	Henry's law constant for mercury ($\text{atm}\cdot\text{m}^3/\text{kmol}$)
I	ionic strength
IMS	ion mobility spectrometry
K	equilibrium constant
k_g	individual gas film mass transfer coefficient ($\text{kmol/s}\cdot\text{atm}\cdot\text{m}^2$)
$k_{\text{L,Cl}_2}^0$	individual physical liquid film mass transfer coefficient for chlorine (m/s)
K_{OG}	overall gas phase mass transfer coefficient ($\text{kmol/s}\cdot\text{atm}\cdot\text{m}^2$)
$k_{1,\text{H}_2\text{O}}$	first order rate constant for chlorine hydrolysis reaction (s^{-1})
$k_{2,\text{buf}}$	second order rate constant for chlorine/succinate buffer reaction ($\text{m}^3/\text{kmol}\cdot\text{s}$)
$k_{2,\text{Hg}}$	second order rate constant for mercury/chlorine reaction ($\text{m}^3/\text{kmol}\cdot\text{s}$)
$k_{2,\text{Hg(II)}}$	second order rate constant for mercury/Hg(II) reaction ($\text{m}^3/\text{kmol}\cdot\text{s}$)
$k_{2,\text{S(IV)}}$	second order rate constant for chlorine/S(IV) reaction ($\text{m}^3/\text{kmol}\cdot\text{s}$)
$k_{2,\text{OH}}$	second order rate constant for chlorine/hydroxide reaction ($\text{m}^3/\text{kmol}\cdot\text{s}$)
M_A	molecular weight of species A
N_{Cl_2}	flux of chlorine ($\text{kmol/m}^2\cdot\text{s}$)
N_g	number of gas phase mass transfer units, defined as $k_g A/G$ (dimensionless)
n_g	gas phase agitation rate (rpm)
n_L	liquid phase agitation rate (rpm)
P	total pressure (atm)

P_{Cl_2}	partial pressure of chlorine (atm)
$P_{Cl_2,b}^*$	partial pressure of chlorine in equilibrium with chlorine in bulk liquid (atm)
pK_a	negative logarithm of acid dissociation constant
Q_L	liquid flow rate (m^3/s)
R	gas constant ($8.205 \times 10^{-5} m^3 \cdot atm/mol \cdot ^\circ C$)
Re	Reynolds number ($dv\rho/\mu$)
Sc	Schmidt number ($\mu\rho/D$)
Sh	Sherwood number ($k_g d/D$)
t	time (s)
T	temperature ($^\circ C$ or K)
u_{surf}	velocity of surface fluid in wetted wall column (m/s)
V	reactor volume (m^3)
W	wetted perimeter of wetted wall column
y_{Hg}	mole fraction of mercury in the gas phase (dimensionless)

Subscripts

b	in bulk
CO_2	for carbon dioxide
Cl_2	for chlorine
i	at gas/liquid interface
Hg	for Hg
in	inlet
$init$	initial
L	liquid
o	outlet
$S(IV)$	for S(IV)
T	total

Greek

δ	film thickness (m)
ε/k	energy parameter for Lennard Jones equation (K)
γ	activity coefficient
η	parameter used to determine liquid film mass transfer coefficient
μ	viscosity (kg/m-s)
Θ	parameter used to determine liquid film mass transfer coefficient
ρ	density (kg/m^3)
σ_{AB}	Lennard-Jones collision diameter (m)

τ	surface exposure time in wetted wall column (s)
Ω_D	collision integral in Lennard-Jones potential

Chapter 1: Introduction

1.1 MERCURY POLLUTION

Mercury (Hg) pollution is an important problem because of its behavior in the environment (bioaccumulation) and the potential for deleterious health effects. By the end of 2004, the Environmental Protection Agency (EPA) will issue the final regulations on controlling mercury emissions from coal burning power plants (EPA, 2000). Plants will have until 2007 to implement these rules. Even though mercury control technologies do exist, many are not effective for the removal of the low concentration of mercury compounds that are present in the flue gas of power plants. Therefore, more research is needed to develop a cost-effective Hg control technology which power plants will be willing to implement. Furthermore, a better understanding of the mass transfer and chemical kinetics of these processes is still needed.

1.1.1 Emissions

Roughly 50 to 75% of the mercury input to the atmosphere results from human activities. The best point estimate of annual anthropogenic U.S. emissions of mercury was 158 tons in 1994-95. About 87% of these anthropogenic emissions are from combustion sources such as coal-fired power plants, municipal waste combustors, medical waste incinerators, and hazardous waste combustors (Keating et al., 1997; Sznoppek and Goonan, 2000). The EPA has regulated all of these sources, except for the power plants, since the mid-late 1990's. Table 1.1 shows a breakdown of the mercury emissions from the major combustion sources (Keating et al., 1997). Also, recent data from 1999 suggest that coal-fired utility boilers emit between 42 to

45 tons of mercury per year in the U.S., which agrees with the data in Table 1.1 (Milobowski et al., 2001; Chu et al., 2001). Estimates from the 1999 data suggest that coal-fired power plants emit 18 tons of oxidized mercury and 26 tons of elemental mercury per year (Chu et al., 2001).

Table 1.1. Mercury emissions from combustion sources

Source	% of Total Emissions (1994-1995 data)
Coal-fired utility boilers	33
Municipal waste combustors	19
Commercial/industrial boilers	18
Medical waste incinerators	10
Hazardous waste combustors	4.4
Residential boilers	2.3
Total from combustion	87

Combustion of coal and of municipal solid waste releases mercury (Hg) and mercuric chloride (HgCl_2) vapors in the flue gas. The total composition of Hg is typically 0.01 to 0.1 ppm in incinerator gas and 0.001 to 0.01 ppm in coal-fired flue gas. Even though the concentrations seem low, the threshold limit value (TLV) for Hg is only $0.1 \mu\text{g}/\text{m}^3$ (0.01 ppb), and the 8 hr TWA is only $0.05 \mu\text{g}/\text{m}^3$. The concentration of mercury in ambient air is typically 2 to 5 ng/m^3 (0.25 to 0.6 ppt), except near emission sources, where it can be considerably higher (Hall, 1992; Schroeder et al., 1991; Seigneur et al., 1994). The long-range transport of mercury makes mercury control a global issue.

1.1.2 Regulations

Coal-fired power plants are the biggest source of anthropogenic mercury emissions in the U.S., yet they are currently not regulated. On December 14, 2000,

EPA announced that mercury emissions from coal-fired power plants would be regulated under Title III of the Clean Air Act Amendments of 1990 (EPA, 2000; Richardson et al., 2001). Regulations should be proposed by 2003. EPA plans to issue the final rules by December 15, 2004 (EPA, 2000), and is expected to require compliance by December 2007 (Richardson et al., 2001). Therefore, mercury removal research is of current interest. A variety of control strategies are currently under development.

1.2 LIMESTONE SLURRY SCRUBBING

The flue gas from coal-fired power plants contains sulfur dioxide (SO_2) and hydrogen chloride (HCl) at much higher concentrations than the mercury compounds (Niksa and Helble, 2001). Limestone slurry scrubbing is often used to remove SO_2 and HCl from these flue gases. Wet flue gas desulfurization (FGD) systems are currently installed for SO_2 removal on about 25% of the coal-fired utility generating capacity in the U.S. (Milobowski et al., 2001). Limestone slurry scrubbing processes comprise 70% of the market for flue gas desulfurization, and 80% of installed FGD systems worldwide are wet scrubbers (Oskarsson et al., 1997). Furthermore, Phase II of the Acid Rain SO_2 Reduction Program, which began in 2000, further restricts total SO_2 emissions and affects both large and small power plants (EPA, 2001). Scrubbers may need to be installed to meet these required emissions reductions. Therefore, FGD scrubbing will most likely continue to be an important part of maintaining environmental quality.

FGD is a mature technology that has low capital costs, high SO_2 removal efficiency, and is easy to retrofit. For coal-fired utility boilers already equipped with these scrubbing systems, the incremental cost of any elemental mercury removal achieved is minimal (Milobowski et al., 2001). Therefore, it would be economically beneficial if a reagent could be added to the existing scrubber to remove the mercury.

In order for the proposed process to be feasible, the new reagent should not negatively impact operation and SO₂ removal performance.

Limestone slurry scrubbing is typically accomplished in countercurrent spray contactors (Brogren and Karlsson, 1997). Figure 1.1 shows a diagram of a limestone slurry scrubber. The flue gas containing sulfur dioxide enters the bottom of the spray tower. The scrubber typically operates at 55°C. The gas counter-currently contacts limestone slurry, which is sprayed into the absorber through a series of spray headers. The SO₂ is absorbed into the spray, while the cleaned gas exits the top of the absorber. Fresh limestone slurry is fed to the hold tank and circulated to the top of the scrubber. The fresh slurry is typically at pH 5 to 6 with 0.1 to 10 mM sulfite, S(IV). After the spray contacts the gas, the absorbed SO₂ causes the pH to decrease to 3 to 5 and the S(IV) to increase to 2 to 10 mM. In the hold tank, the S(IV) is oxidized by air to sulfate, S(VI).

1.2.1 Proposed process for mercury removal in limestone slurry scrubbers

Since mercuric chloride is very soluble in water, it is readily absorbed by aqueous solutions in conventional scrubbers (Noble et al., 1993). However, elemental mercury is not very soluble in water and is not readily absorbed in simple aqueous solutions (Zhao and Rochelle, 1998). However, it should be possible to remove Hg by conventional aqueous scrubbing technologies with the addition of reagents to produce chlorine, which will oxidize the Hg to a more soluble form through reaction in the mass transfer boundary layer. Some researchers, such as Zhao (1997) and Livengood and Mendelsohn (1997), have had success in removing Hg via reactions with chlorine oxidants. Mercury reacts with chlorine to form mercuric chloride, HgCl₂, which is very soluble (Indu et al., 1997) and can thus be easily removed through aqueous scrubbing. Even though previous researchers have seen that mercury reacts with chlorine, they have not quantified the reaction kinetics.

Therefore, further research is warranted. Figure 1.1 depicts the proposed process in a limestone slurry scrubber.

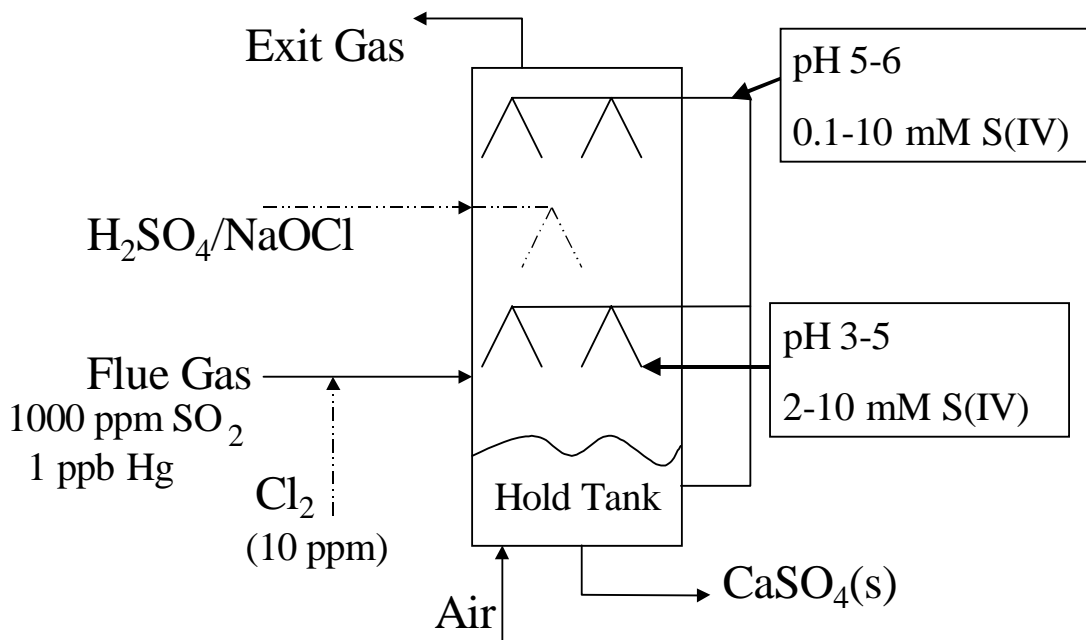


Figure 1.1. Chlorine injection for Hg removal in limestone slurry scrubbing

In the proposed technology, either hypochlorite solution will be sprayed into the scrubber to generate chlorine in-situ or chlorine gas (< 10 ppm) will be directly injected into the gaseous feed as shown in Figure 1.1. The chlorine cannot be introduced with the bulk solution. If an oxidant were put in the bulk solution, it would be completely depleted by reaction with dissolved S(IV). Hypochlorite will release Cl₂ upon acidification by absorption of SO₂ and HCl or by addition of sulfuric acid. The Cl₂ should react with elemental Hg in the solution at the gas/liquid interface and should greatly enhance the rate of absorption of Hg. The mercury will be oxidized and absorbed into the scrubber solution. The chlorine will also react at the gas/liquid interface with any elemental Hg formed by sulfite reduction of HgCl₂ in the bulk solution.

Figure 1.2 shows a diagram of the simplified concentration profiles in the mass transfer boundary layer of this process in a limestone slurry scrubber. Mercury, chlorine, and sulfur dioxide will be simultaneously absorbed from the gas phase. Near the gas/liquid interface, Cl_2 will react with the absorbed SO_2 , S(IV) , to produce chloride and sulfate, S(VI) . There should also be a small amount of chlorine left at the interface to oxidize the Hg to HgCl_2 .

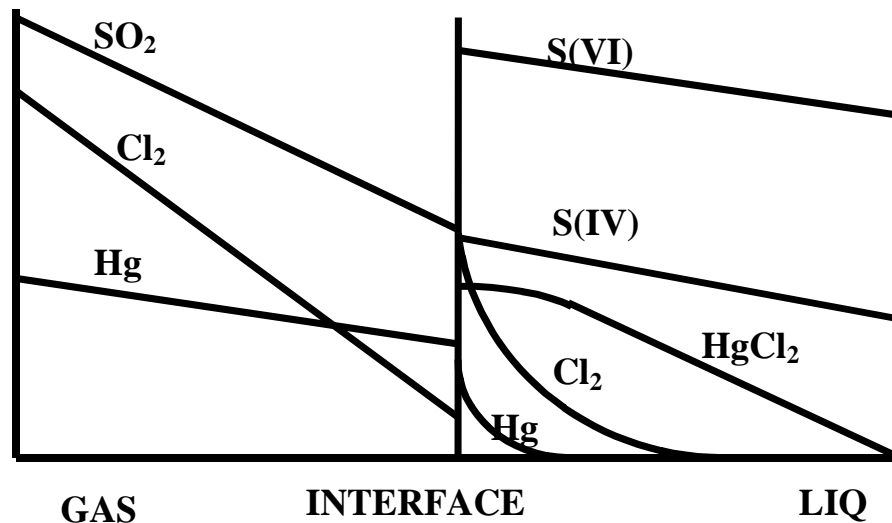


Figure 1.2. Mass transfer boundary layer

1.2.1.1 Feasibility of proposed process

The success of this approach requires that the mercury react with the chlorine before it gets reduced by the dissolved SO_2 present as S(IV) . S(IV) represents sulfur in the +4 oxidation state (sulfite and bisulfite). Therefore, the kinetics of the reactions between mercury, chlorine, and S(IV) need to be quantified in order to determine if the proposed process is feasible in controlling Hg emissions. Also, all of the chlorine must be absorbed before the gas exits the scrubber. Therefore, the optimal situation would be to have the S(IV) react quickly with Cl_2 , but not so rapidly that there is no Cl_2 left at the interface to react with the Hg . If the chlorine at the interface is depleted

completely by the S(IV)/SO₂, then staged injections of chlorine into the scrubber may be a better option. Another option is adding another oxidant, such as hydrogen peroxide (H₂O₂), with the chlorine. The H₂O₂ will oxidize the S(IV) so that the S(IV) will not deplete the chlorine at the interface.

In order for the process to be practical, the chlorine cannot impact the gas or solution chemistry. This can be accomplished as long as only a small amount of chlorine (under 20 ppm) is needed to remove the Hg. The formation of chlorinated hydrocarbons will not be a problem since these reactions do not occur until much higher temperatures (Chen and Rochelle, 2000).

Another practical consideration is that the process cannot generate much additional waste. This should not be a problem because currently the slurry already has some HgCl₂ in it. This process would just add some more to the slurry. Since the mercury amounts are so small, the waste slurry will probably just be handled in the same manner in which it is currently handled.

1.3 RESEARCH OBJECTIVE AND SCOPE OF WORK

The primary objective of this work is to understand the kinetics of systems containing mercury, chlorine, and S(IV). Mercury and chlorine absorption was measured in a gas/liquid contactor with known mass transfer properties. The absorption was modeled in order to extract kinetics. An understanding of these kinetics is needed in order to develop a technology that will remove both Hg and HgCl₂ through aqueous scrubbing with chlorine. The gaseous chlorine oxidant should react with elemental Hg in the solution at the gas/liquid interface and greatly enhance the rate of absorption of Hg. This work provides kinetics data which may be important in other processes (than scrubbers in power plants) that contain mercury, chlorine, and/or S(IV).

The kinetics of these systems have not been studied before, but previous researchers have studied similar systems. Zhao (1997) demonstrated that mercury could be absorbed into sodium hypochlorite/chloride solutions at high pH and postulated that free chlorine was the active species reacting with Hg. However, Zhao was not able to obtain reproducible data in the pH range of a limestone slurry scrubber (pH 3 to 6) since chlorine was being stripped and reacting with the Hg on the moist surfaces of the reactor. Therefore, further research is warranted. Simultaneous absorption of mercury and chlorine need to be conducted at low/intermediate pH in a gas/liquid contactor that minimizes surface and bulk gas reactions.

The chapters in this dissertation present the applicable theory, experimental methods and procedures, results and conclusions for the absorption of Hg and Cl₂ in aqueous S(IV) solutions. This work begins by discussing previous literature. Chapter 2 presents background information on characteristics of Hg, transport cycle, health risks, and existing control technologies for mercury removal. Mercury and chlorine absorption reactions are also detailed. Chapter 3 uses mass transfer with chemical reaction theory to formulate the models used in the data analysis. Chapter 4 provides the details for the experimental equipment, analytical methods, and procedures. Chapter 5 contains the experimental results of the characterization of the mass transfer properties of the newly constructed wetted wall column. Chapter 6 presents the experimental results and discussion of the chlorine absorption experiments conducted in the stirred cell reactor. Chapter 7 contains the experimental results of the chlorine absorption experiments in the wetted wall column, which resulted in the extraction of rate constants. Chapter 8 discusses the results from the simultaneous absorption of mercury and chlorine experiments in the wetted wall. Chapter 9 summarizes the conclusions and gives recommendations for further study.

Chapter 2: Literature Review

This chapter presents a comprehensive literature review. The first section provides general background information on mercury, explaining why mercury pollution is so hazardous and a global problem. The second section describes the current mercury control technologies and problems and explains why further research is still needed. The rest of the chapter details the reactions between mercury and chlorine compounds. These reactions will be important in understanding the chemical systems in this work.

2.1 CHARACTERISTICS OF MERCURY

2.1.1 *Health hazards*

Concentrations of mercury in air and water are usually low and of little direct concern, although accidental exposures to elemental mercury can pose a threat (Keating et al., 1997). Inhalation of any form of mercury can cause severe respiratory tract damage. Mercury is a cumulative toxicant that attacks the central nervous system and kidneys. Organic forms of mercury, such as dimethyl or methyl mercury, are the most hazardous.

The absorption of elemental mercury occurs rapidly through the lungs. It can easily cross both placental and blood-brain barriers. Inorganic mercury is readily absorbed through the skin, but has a limited capacity for penetrating the blood-brain or placental barriers (Keating et al., 1997).

Methyl mercury is almost completely absorbed into the blood. It is rapidly and extensively absorbed through the gastrointestinal tract and distributed to all tissues. Methyl mercury bioaccumulates in tissue and can easily pass the blood-brain

and placental barriers to cause permanent brain damage. Fish consumption dominates the pathway for human and wildlife exposure to methyl mercury. Epidemics of mercury poisoning following high dose exposures to methyl mercury demonstrated that neurotoxicity is the health effect of greatest concern when methyl mercury exposure occurs to the developing fetus (Keating et al., 1997).

2.1.2 Transport cycle

The form of mercury in ambient air is predominantly gaseous elemental mercury. Elemental mercury has a high volatility and long life span. It has a residence time of one to two years in the atmosphere. Thus, elemental mercury vapor and small particulates of divalent inorganic mercury compounds can be widely dispersed and travel thousands of miles from emission sources. The long-range transport of mercury makes mercury control a world-wide issue (Keating et al., 1997).

Measured data and modeling indicate that the amount of mercury mobilized and released into the atmosphere has increased since the beginning of the ice age. Releases from human activities today are adding to the mercury reservoirs that already exist in land, water, and air. Anthropogenic emissions of mercury to the air rival or exceed natural inputs. Natural inputs include mercury from volcanic eruptions and mercury that is re-emitted from soil, forests, oceans, etc. This mercury may be emitted resulting from natural biological and geological processes drawing from a reservoir of mercury which resulted from an anthropogenic source. Mercury cycles in the environment because of natural and anthropogenic activities (Keating et al., 1997).

Mercury is deposited in water and soil. Most of the mercury in water, soil, sediments, plants, and animals is in the form of inorganic mercury salts and organic forms of mercury (e.g., methyl mercury). All forms of mercury can be converted to methyl mercury (the most lethal form of mercury) by bacteria. The methyl mercury

accumulates most efficiently in the aquatic food web (Keating et al., 1997). In lakes, methyl mercury is concentrated up the food chain so that the predator fish have methyl mercury concentrations 7 million times higher than the surrounding water. Nearly all of the mercury that accumulates in fish tissue is methyl mercury. Inorganic mercury, which is less efficiently absorbed and more readily eliminated from the body than methyl mercury, does not tend to bioaccumulate.

The inorganic forms of mercury (either bound to airborne particles or in a gaseous form) are readily removed from the atmosphere by precipitation and are also dry deposited. Wet deposition is the primary mechanism for transporting mercury from the atmosphere to surface waters and land. Contaminated sediments at the bottom of surface waters can serve as an important mercury reservoir. Mercury has a long retention time in soils. Even after mercury deposits, it can be emitted back to the atmosphere. Mercury undergoes a series of complex chemical and physical transformations as it cycles between the atmosphere, land, and water (Keating et al., 1997).

Computer simulations suggest that about a third of U.S. anthropogenic emissions are deposited within the continental United States. Models suggest that the rest is transported outside the U.S. and diffuses into the global reservoir. The simulations show that about three times as much mercury is being added to the global reservoir from U.S. sources as is being deposited from it. The highest deposition rates are predicted to occur in the southern Great Lakes and Ohio River valley, the Northeast and scattered areas in the South. Humid locations have higher deposition rates than arid locations (Keating et al., 1997).

2.1.3 Concentration and speciation of mercury in flue gas

Combustion of coal releases mercury (Hg) and mercuric chloride (HgCl_2) vapors in the flue gas. The total composition of Hg is less than 0.01 ppm in coal-fired

flue gas (Niksa and Helble, 2001). The amount and speciation of mercury emitted from a coal-fired power plant depends on the coal type, boiler operation parameters, and environmental controls installed (Chu et al., 2001; Richardson et al., 2001; Weilert and Randall, 2001).

The speciation of mercury can impact its removal in the system (Afonso, 2001; Richardson et al., 2001). Oxidized mercury, such as HgCl_2 , can be easily removed through existing aqueous scrubbers. Elemental mercury is not removed by aqueous scrubbing since it is relatively insoluble in water (Niksa and Helble, 2001).

The form of mercury depends on the type of coal burned, fuel constituents, and operating conditions and varies from one plant to another (Keating et al., 1997). The chlorine content in coal is an important parameter in determining the percentage mercury removal and speciation since greater chlorine content in the coal resulted in greater quantities of oxidized mercury (Afonso, 2001; Chu et al., 2001). Elemental Hg can be a big fraction of the total mercury, especially if the plant is burning coal that is high in mercury and low in chlorine content, such as Texas lignite and Powder River Basin coal.

2.2 MERCURY CONTROL TECHNOLOGIES

Elemental mercury is the most volatile among trace metal compounds and can pass through conventional air pollution control devices (Rodriguez et al., 2001). Furthermore, since the speciation of mercury varies from plant to plant, there is no single control technology that removes all forms of mercury from all sources. Most of the control technologies that have been developed are for higher concentration Hg sources and are not as effective in the low Hg concentration ranges, which are relevant to power plants (Keating et al., 1997). Various control technologies are detailed in this section.

2.2.1 Coal cleaning

Effectiveness of mercury reduction by conventional coal cleaning ranges from 0 to 64%, with an overall average reduction of 21% (Keating et al., 1997). This variation in mercury removal results from different cleaning techniques, different Hg analytical techniques, and different mercury concentrations in the raw coal.

Conventional cleaning methods include mechanical devices using pulsating water or air currents to physically stratify and remove impurities. Another method is dense media washing which uses heavy liquid solutions, usually consisting of magnetite, to separate coal from its impurities (Keating et al., 1997).

Advanced coal cleaning methods such as selective agglomeration and column froth flotation can increase the amount of mercury removed by conventional cleaning methods alone. However, the potential impact on post-combustion form and control of the remaining Hg has not been thoroughly researched. The chemical cleaning techniques may result in a different form of mercury under combustion and post-combustion conditions. Also, cleaned coal can cause mercury mass transfer limitations in emissions control systems (Keating et al., 1997).

2.2.2 Sorbents

Using sorbents is one of the most promising technologies for mercury removal from power plants which do not require wet scrubbers for SO₂ control (Sjostrom et al., 2001). Sorbents that have been researched for reducing mercury emissions include those that are carbon, calcium, or iodine-based. The large quantity of sorbent needed and the high costs associated with it are the major drawbacks to using sorbents (Rostam-Abadi et al., 2001).

2.2.2.1 Carbon filter beds

In addition to mercury, carbon filter beds can remove organic pollutants, such as dioxins and furans, and acid gases such as SO₂ and HCl. The flue gas flows

horizontally through the filter bed, while the adsorbent migrates through the filter. The size of a carbon filter bed depends on the flue gas flow rate. Carbon filter beds have been used on power plants in Germany since the late 1980s. Although mercury control was not the primary purpose of installing the beds, reduction of mercury is observed. Potential negative impacts associated with carbon filter beds include disposing of the spent carbon, formation of “hot spots” in the bed that can result in bed fires, and the potential emissions during the coal-charring segment of the carbon activation processes (Keating et al., 1997).

2.2.2.2 Activated carbon injection

This control technology involves the injection of powdered activated carbon into flue gas upstream of an air pollution control device, such as electrostatic precipitators and fabric filters. This process has primarily been developed to remove mercury from municipal waste combustors and municipal waste incinerators. Gas phase oxidized mercury is readily captured by activated carbon, while elemental mercury has a much lower affinity for carbon. Activated carbon contains multiple internal pores with a very high specific surface area. The activated carbon can adsorb a broad range of trace contaminants in addition to mercury. Efficient distribution of the carbon in the flue gas is very important for this process (Keating et al., 1997).

The application of activated carbon to utility flue gas cannot be directly scaled from the application at municipal waste combustors due to the composition differences. At power plants, small concentrations of mercury are contained in a large volume of gas, and large amounts of activated carbon are needed to provide adequate contact between the carbon particles and mercury. The level of mercury control in utility flue gas depends on properties such as gas volume, temperature, and concentration; these properties are distinctly different from those in municipal waste combustors (Keating et al., 1997).

Research is currently being conducted to study the feasibility of activated carbon injection for removal of mercury in the flue gas of coal-fired power plants (Rostam-Abadi et al., 2001; Sjoström et al., 2001). Activated carbon sorbents were prepared from a variety of precursor materials and evaluated in laboratory tests to determine their ability to remove mercury and mercuric chloride. Tests showed that biomass-based carbons performed better than other carbons in capturing elemental Hg, while tire and lignite-based carbons had larger adsorption capacities for mercuric chloride (Rostam-Abadi et al., 2001).

Sorbents are affected by flue gas composition, mercury speciation, sorbent characteristics (such as size), and process conditions (such as temperature). Results have shown that although general trends between different sorbents exist, sorbent performance is usually site specific depending on the exact nature of the flue gas (Sjoström et al., 2001).

2.2.2.3 Calcium-based sorbents

Adding certain oxidants to calcium-based sorbents results in significant improvement in the removal of Hg, SO₂, and NO_x from simulated flue gases. Calcium-based sorbents are typically based on lime or silicate. These sorbents readily adsorb mercuric chloride, but do not readily adsorb elemental Hg unless modifications are made to the sorbent production process. Bench-scale tests showed that adding oxidants to lime-based sorbents during their production process can significantly increase the elemental mercury uptake capabilities of these sorbents (Singer et al., 2001).

2.2.2.4 Iodine-based sorbents

Recent bench-scale experiments showed that high capture efficiencies (> 98%) of elemental mercury were achieved using potassium iodide sorbent particles.

The iodide oxidized the elemental Hg and captured the oxidized forms (Rodriguez et al., 2001).

2.2.3 Wet scrubbing

As previously mentioned, wet scrubbing can remove oxidized forms of mercury, such as mercuric chloride. Therefore, if the elemental mercury is oxidized either in the scrubber or upstream of the scrubber, mercury removal can occur.

2.2.3.1 Catalytic oxidation of Hg

Many power plants use selective catalytic reduction (SCR) to reduce NO_x emissions. The effectiveness of a SCR catalyst to oxidizing the elemental Hg in flue gas has been investigated. Bench-scale tests have shown that flue gas treated by the SCR catalyst has a greater percentage of oxidized mercury (90 to 95%) than untreated gas (50 to 80%) (Milobowski et al., 2001).

Pilot-scale and full-scale tests also indicate that some commercial SCR catalysts are capable of oxidizing Hg (Richardson et al., 2001). Catalysts tested included titanium-vanadium based, palladium-based, and iron-based. The Ti/V-based catalysts were generally capable of oxidizing elemental Hg in flue gas at temperatures expected in SCR processes. Other metal-based catalysts were capable of oxidizing Hg at lower temperatures (< 200°C), but not at SCR conditions (Richardson et al., 2001). Drawbacks of catalytic oxidation include catalyst deactivation over time. A lot of catalyst is needed to oxidize the mercury. The catalyst deactivation rate depends on the site conditions (Blythe et al., 2001).

2.2.3.2 Reagent addition to oxidize Hg

As mentioned before, it would be economically beneficial if a reagent could be added to an existing scrubber to remove mercury. Babcock and Wilcox and McDermott Technology are developing a proprietary reagent and testing it in one of their pilot plant facilities (Milobowski et al., 2001). The initial formulation of the

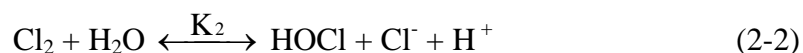
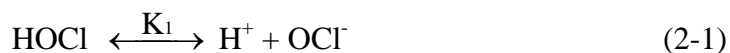
reagent did not improve mercury removal because of the reagent's inability to suppress the emission of elemental mercury from the wet scrubber. Therefore, an alternate reagent was tested which resulted in increased mercury removal (Milobowski et al., 2001).

2.3 AQUEOUS PHASE REACTIONS OF MERCURY

2.3.1 *Mercury absorption in chlorine oxidants*

Previous researchers have performed screening experiments on mercury removal through reaction with chlorine oxidants. Zhao and Rochelle (1999) investigated Hg absorption in sodium hypochlorite (NaOCl)/chloride (NaCl) solutions in the same stirred cell reactor which was used initially in this work. Zhao showed that low pH, high temperature, and high Cl^- concentration favored Hg absorption.

In aqueous hypochlorite solution, the distribution of hypochlorite (OCl^-), hypochlorous acid (HOCl), and chloride (Cl^-) depends on solution pH and chloride concentration, $[\text{Cl}^-]$. Since lower pH results in higher Hg removal, Zhao postulated that free Cl_2 is the active species that reacts with Hg. Thus, she developed a correlation which she postulated would predict Hg absorption at any pH, $[\text{Cl}^-]$, $[\text{NaOCl}]_T$. The activity of free Cl_2 can be obtained from the following two equilibria:



The values for K_1 and K_2 at 25°C are $3.00 \times 10^{-8} \text{ M}$ (Atkins, 1990; Morris, 1966) and $3.94 \times 10^{-4} \text{ M}^2$ (Connick and Chia, 1959), respectively. Thus, at low pH (high H^+) and high Cl^- , the formation of Cl_2 is favored. The chlorine reacts with the Hg to form HgCl_2 in an apparent overall second order reaction and greatly enhances the rate of Hg absorption. The overall reaction is:



The rate constant was obtained from modeling the Hg absorption using surface renewal theory for mass transfer with fast chemical reaction in the boundary layer. The rate constant measured by Zhao in hypochlorite solutions at pH 9 to 11 was 1.7×10^{15} L/mol-s at 25°C and 1.4×10^{17} L/mol-s at 55°C. These rate constants predict that substantial enhancement of mercury absorption occurs with only 0.1 ppb of chlorine. However, since these rate constants are much greater than the diffusion-limited rate (Connors, 1990), the kinetics observed by Zhao do not represent the elementary reaction mechanism.

Zhao also investigated Hg absorption in hypochlorite/chloride solutions at lower pH, but the data were not reproducible. When the pH was less than 9 and the chloride concentration was high, the observed Hg absorption would decrease with time. Zhao postulated that this decrease resulted from chlorine being stripped from the solution. Therefore, at low to intermediate pH ranges, kinetic information could not be obtained. Thus, Zhao was not able to get good data in the pH range of a limestone slurry scrubber.

Zhao also conducted preliminary experiments with simultaneous absorption of chlorine and Hg in the stirred cell reactor. Results demonstrated that 1 to 10 ppm of chlorine can be effective in removing 0.1 ppm Hg (Zhao and Rochelle, 1999). However, Zhao could not obtain any kinetic data because the chlorine reacted with mercury on the surfaces of the reactor, in addition to reaction in the gas/liquid interface. Furthermore, Zhao did not have a sample conditioning system before the mercury analyzer. Therefore, the Hg removal observed may have been due to factors other than reaction in the mass transfer boundary layer.

Nene and Rane (1981) also measured the absorption of elemental Hg in sodium hypochlorite/chloride solutions at pH 2 to 11 and modeled the Hg absorption using the theory of mass transfer with chemical reaction. Nene and Rane correlated different rate constants for each set of experimental conditions (pH, $[\text{Cl}^-]$, $[\text{NaOCl}]_T$);

they did not develop a global model, utilizing a single rate constant, which would predict Hg absorption at any pH, $[\text{Cl}^-]$, $[\text{NaOCl}]_{\text{T}}$. The authors stated that mercury could be effectively removed from gases by scrubbing with hypochlorite solutions. These solutions are active over a wide pH range and even at low concentrations of available chlorine. The authors stated that the reaction was first order in both mercury and hypochlorite, and the reaction rate depended on the pH and the chloride concentration. They observed that the rate of reaction with HOCl (low pH) was 100 times higher than the rate with OCl^- (high pH). They postulated that this was due to the higher oxidation potential in acidic solutions. The presence of sodium chloride also greatly enhanced the mercury absorption rate at both low and high pH.

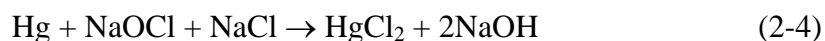
Nene and Rane (1981) also absorbed mercury into potassium hypochlorite/chloride solutions and observed that the reaction rate was faster with potassium than with sodium. Once again, the addition of chloride (as KCl) enhanced the reaction rate.

Livengood and Mendelsohn (1997) performed screening experiments on Hg removal in a gas bubbler. They found that hypochlorite solutions provided about 40 to 50% Hg removal with nitric oxide (NO) and SO_2 present. They postulated that NO enhanced mercury removal because NO reacted with chlorine to yield nitrosyl chloride (Stoddart, 1944), which then reacted with Hg. Their conclusion for the reaction of Hg in the presence of NO was that nitrosyl chloride probably reacts faster with Hg than chlorine does. They also found that 3.6% chloric acid (HClO_3) provided 70% Hg removal with NO and 50% removal with NO and SO_2 . Addition of SO_2 did lower mercury absorption, but did not completely stop it. Livengood and Mendelsohn also performed experiments with bromine and iodine, but they concluded that these were not as effective as chlorine compounds in removing Hg.

Skipnik et al. (1979) said that Hg removal with an acidic chlorine-containing solution can be represented by two mechanisms: (1) chlorine from the solution is

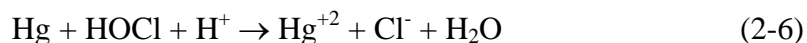
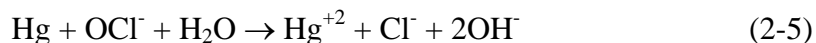
swept into the gas phase where it oxidizes the Hg and (2) Hg diffuses from the gas into the solution and reacts with the chlorine. Their experiments showed that when the chlorine/mercury ratio is less than 20:1, mercurous chloride is the primary product formed. At ratios greater than 20:1, the oxidation of Hg with chlorine yields mercuric chloride. This reaction takes place rapidly (in 1-2 seconds). Other researchers have also shown that mercurous ion is readily oxidized to mercuric in the presence of excess oxidant (Davies et al., 1973). Furthermore, Lindqvist (1991) showed that mercuric ion is unstable at pH greater than 3. Schroeder et al. (1991) stated that in dilute solutions of mercury, the mercurous ion (Hg_2^{+2}) is usually not stable and disproportionates.

Skripnik et al. (1979) also showed that oxidation of Hg can occur in alkaline medium in the presence of hypochlorite/chloride. The overall reaction was:

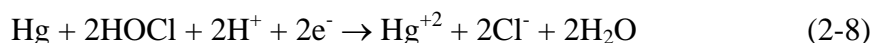
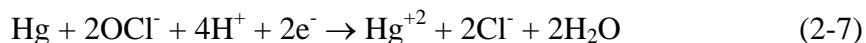


They found that the oxidation of Hg is still fast under these conditions, but the reaction is twice as fast in acid because of higher oxidizing potentials in acid.

Lin and Pehkonen (1999) propose the following overall reactions:



Another proposed reaction scheme for mercury oxidation by hypochlorite species is (Schroeder et al., 1991):



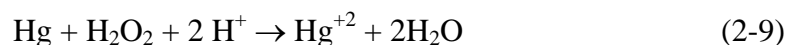
2.3.2 Absorption of mercury in other aqueous oxidants

Researchers have also investigated other Hg reactions, as listed by Lin and Pehkonen (1998), Lindqvist (1991), Schroeder et al. (1991), and Seigneur et al.

(1994). Elemental Hg is readily oxidized to mercuric ion by the addition of an oxidizing agent. Kaczur (1996) details the use of chloric acid to oxidize and remove Hg. Chloric acid is a strong oxidizer which is capable of simultaneous removal of SO₂, NO_x, and elemental Hg (Kaczur, 1996).

Iverfeldt and Lindqvist (1986) and Munthe (1992) discuss mercury absorption in ozone solutions. The absorption of elemental Hg by water was increased by three orders of magnitude by ozone (Iverfeldt and Lindqvist, 1986). Ozone also oxidizes Hg in the gas phase. The second order reaction rate for the aqueous reaction of mercury with ozone was determined to be $(4.7 \pm 2.2) \times 10^7$ L/mol-s at room temperature (Munthe, 1992).

Elemental Hg can also be oxidized by hydrogen peroxide (H₂O₂) at pH less than 5.5 (Schroeder et al., 1991). The overall reaction is:



This reaction can be catalyzed by the presence of Fe⁺³. At pH higher than 5.5, the hydrogen peroxide will reduce the oxidized Hg to elemental Hg (Schroeder et al., 1991).

2.3.3 Reduction of Hg(II) by S(IV)

Divalent mercury (mercuric ion, Hg⁺²) can be reduced to elemental Hg by aqueous sulfite solutions (Munthe et al., 1991). The proposed mechanism involves the formation of an unstable intermediate, HgSO₃, which decomposes to produce Hg⁺, which is then rapidly reduced to elemental mercury, Hg⁰.

2.4 GAS PHASE REACTIONS OF MERCURY

2.4.1 Reaction of mercury and chlorine

Mercury is known to react with Cl₂ in the gas phase to form mercuric chloride (Hall et al., 1991, Edwards et al., 2001, Niksa and Helble, 2001; Skare and Johansson, 1992; Yarwood and Niki, 1990). Niksa and Helble (2001) present a detailed 8-step

mechanism for this reaction. Mercury reacts with Cl_2 in the gas phase with a reaction rate constant of $2 \times 10^5 \text{ L/mol-s}$ at 20°C (Hall, 1992). The reaction was surface-catalyzed; it was observed to be heterogeneous since reaction occurred on the surfaces (both moist and dry surfaces) as well as in the bulk gas (Hall, 1992; Medhekar et al., 1979; Menke and Wallis, 1980; Schroeder et al., 1991). Hall's lab-scale experiments showed that the reaction rate was relatively independent of temperature from 20°C to 700°C . Thus, the apparent activation energy is probably not greater than 10 kJ/mol . Mercury removal via gas phase reaction with chlorine can be quantified using this rate constant and a typical commercial gas phase residence time of 2 seconds. If the gas inlet were 1 ppb Hg and 10 ppm chlorine, 0.84 ppb Hg would exit the scrubber. Therefore, gas phase reaction with chlorine is not enough to remove Hg.

2.4.2 Reactions with species present in combustion flue gas

Hall (1992) investigated reactions of mercury with several gases, including oxygen, hydrogen chloride (HCl), nitrogen dioxide (NO_2), ammonia (NH_3), sulfur dioxide (SO_2), and hydrogen sulfide (H_2S). Elemental Hg is readily oxidized by HCl at room temperature and at elevated temperatures (up to 900°C). The reaction rate between Hg and NO_2 is slower. The oxidation of Hg by oxygen to mercuric oxide (HgO) is enhanced by the presence of a catalyst, such as activated carbon. Elemental Hg does not react with NH_3 , N_2O , SO_2 , or H_2S . This was expected since these gases are either reducing or inert (Hall et al., 1991).

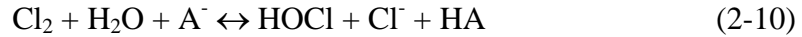
2.5 AQUEOUS PHASE REACTIONS OF CHLORINE SPECIES

2.5.1 Chlorine absorption in aqueous solutions

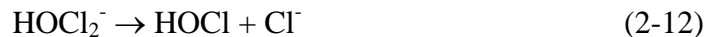
There are several reactions that contribute to chlorine absorption in aqueous solutions. At a pH of 3 to 10.5 (with no S(IV) present), chlorine hydrolysis to form hypochlorous acid and hydrochloric acid is the dominant reaction controlling chlorine

absorption (Spalding, 1962; Lifshitz and Perlmutter-Hayman, 1960). This reaction is relatively slow, $k_{1,H_2O} = 15.4 \text{ s}^{-1}$ at 25°C (Brian et al., 1966). Under typical limestone slurry scrubber conditions, if 10 ppm Cl_2 were injected into the gaseous feed, 8.5 ppm Cl_2 would exit if chlorine absorption in water were the only reaction enhancing chlorine absorption. Therefore, the chlorine hydrolysis reaction alone will not cause the chlorine at the gas-liquid interface to be depleted.

Chlorine hydrolysis can be enhanced by the presence of buffer anions (Wang and Maregerum, 1994; Lifshitz and Perlmutter-Hayman, 1962). The following overall reaction occurs:



The kinetics of this reaction have been studied for the following anions (A^-): acetate, chloroacetate, and formate (Lifshitz and Perlmutter-Hayman, 1962; Lifshitz and Perlmutter-Hayman, 1961). Lifshitz and Perlmutter-Hayman only studied rates with anions of weak monoprotic acids at 9.5°C . They correlated the reaction rates with the acid dissociation constant (K_a) and showed that at lower pK_a values (stronger acids), the hydrolysis rate enhancement was slower. They also proposed the following mechanism:

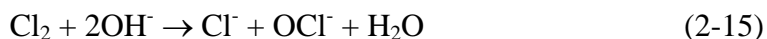


The rate-determining step is the first reaction, the proton transfer step.

At a pH greater than 10.5, the reaction of chlorine and hydroxide is the dominant reaction (Hikita et al., 1973; Spalding, 1962).



Equation 2-13 is the rate-determining step. At high pH, the overall reaction can be written as Equation 2-15.



This reaction is relatively fast, $k_{2,\text{OH}} = 1.57 \times 10^9 \text{ L/mol-s}$ (Ashour et al., 1996); thus, at high pH, there will be very little chlorine at the gas/liquid interface.

Chlorine can also react with sulfite to form chloride and sulfate (Askew and Morisani, 1989; Gordon et al., 1990).



This reaction has not been studied much; thus, the kinetics have not been quantified.

2.5.2 Reactions among aqueous chlorine oxidants

The only chlorine species discussed in the previous sections have been chlorine, chloride, hypochlorous acid, and hypochlorite. In a more complex system, there may be other chlorine species present, including chlorite (ClO_2^-), chlorous acid (HClO_2), chlorate (ClO_3^-), chloric acid (HClO_3), and chlorine dioxide (ClO_2). Much research has been done on the reactions among these chlorine oxidants in solution. These reactions will be important if other chlorine species are present.

Adam et al. (1992) have studied the decomposition of HOCl to chlorate at pH 5 to 8 through the formation of the $\text{Cl}_2\text{O} \cdot \text{H}_2\text{O}$ intermediate. They observed the maximum decomposition rate to occur at pH 6.89 (Adam et al., 1992). Kieffer and Gordon (1968) have studied the disproportionation of chlorous acid. Burke et al. (1993) have studied chlorine dioxide formation by reduction of sodium chlorate with hydrogen peroxide in aqueous sulfuric acid.

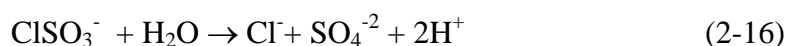
Various researchers have studied the reaction between chlorite and hypochlorous acid to produce chlorine dioxide through the formation of the Cl_2O_2 intermediate (Fabian and Gordon, 1992; Gordon and Tachiyashiki, 1991; Peintler et al., 1990; Tang and Gordon, 1984). The complex formation reactions of the chlorite

ion have also been studied (Fabian and Gordon, 1991; Gordon and Emmenegger, 1966). Aieta and Roberts (1986b) studied the absorption of chlorine into chlorite solutions to produce chlorine dioxide and chlorate. The reaction rate constant at 293 K and zero ionic strength was 1.62×10^4 L/mol-s (Aieta and Roberts, 1986b). In acidic solutions, chlorate reacts with chloride to produce chlorine dioxide and chlorine (Hong et al., 1967).

Other chlorine species that can exist include Cl_2^- (Robertson and Williams, 1964; Castner and Kanzig, 1957), Cl_3^+ (Gutmann, 1972; West and Rollefson, 1936; Ropp et al., 1957), Cl_3^- (Zimmerman and Strong, 1957; Sherril and Izard, 1931; Halford, 1940; Gutmann, 1972; Huheey, 1983), and Cl_5^- (Gutmann, 1972).

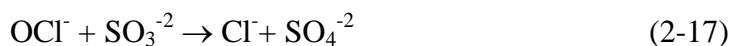
2.5.3 Reactions of S(IV) with chlorine oxidants

Even though the $\text{Cl}_2/\text{S(IV)}$ reaction kinetics have not been studied, researchers have investigated S(IV) reactions with various chlorine oxidants. Hypochlorous acid (HOCl) and hypochlorite (OCl^-) can react with sulfite (SO_3^{-2}) (Fogelman et al., 1989). Hypochlorous acid reacts as follows:



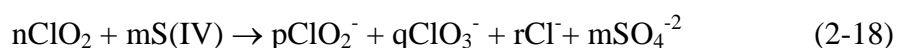
The first reaction has a rate constant of 7.6×10^8 L/mol-s at 25°C and ionic strength of 0.5. The second reaction, which is the rate of hydrolysis of the chlorosulfate intermediate, has a rate constant of 270 s^{-1} (Yiin and Margerum, 1988).

Hypochlorite reacts with sulfite as shown below (Lister and Rosenblum, 1963):



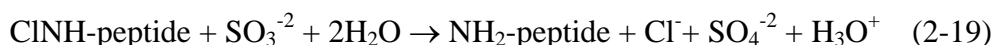
The rate of oxidation of sulfite with HOCl is more than four orders of magnitude faster than the rate with OCl⁻. A shift in mechanism is proposed to account for the huge increase in reactivity (Fogelman et al., 1989).

Suzuki and Gordon (1978) investigated the reaction of chlorine dioxide (ClO₂) with S(IV) in basic (pH 8 – 13) solutions, where S(IV) represents sulfur in the +4 oxidation state (primarily sulfite and bisulfite). The overall stoichiometry is:



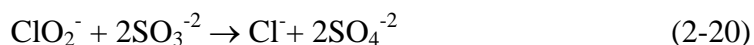
The coefficients n, m, p, q, and r depend on both the pH and the specific buffer solution used. The major reaction products are chlorite and sulfate, with only minor amounts of chlorate and chloride. The reaction was first order in total S(IV) and first order in ClO₂. The overall second order rate constants at pH 8.7, 10.0, and 11.5 were determined to be 7.5 x 10⁵, 8.6 x 10⁵, and 1.2 x 10⁶ L/mol-s, respectively. The chlorite formed can be further reduced by the S(IV), but this reaction is relatively slow under these conditions. However, the reaction between chlorite and S(IV) is rapid in acid (Halperin and Taube, 1952).

Reactions of S(IV) with chlorine oxidants are important in water and wastewater treatment. Here, sulfite is used to deplete residual chlorine (such as chloramines and chloropeptides) which remains after water disinfection using chlorine. A monochloropeptide reacts with sulfite as shown (Jensen and Helz, 1998).



Jensen and Helz (1998) say that usually bisulfite (HSO₃⁻) is a much poorer reducing agent than sulfite (SO₃²⁻). So, reaction rates of chlorine oxidants are much faster with sulfite than with bisulfite.

Sulfite is also used to remove chlorite (which can result from using chlorine dioxide as a disinfectant) from treated water. The reaction is (Gordon et al., 1990):



2.6 SUMMARY

Mercury pollution is a global problem. The mercury emissions from power plants add significantly to the total mercury in the global reservoir, and therefore, a cost-effective control technology needs to be developed and implemented. Currently, there is no recommended technology to reduce mercury emissions from power plants. Thus, more research needs to be conducted in order to understand the chemistry of these systems, which will lead to the development of a control technology. Specifically, this work will be most relevant for mercury control at coal-fired power plants that already have scrubbers. This work focuses on adding a reagent to an existing limestone slurry scrubber to reduce Hg emissions.

Even though other researchers have observed that chlorine reacts with mercury and S(IV), there is no kinetic data on these aqueous reactions. However, there are data on other reactions with mercury and chlorine oxidants. These reactions are relevant to the understanding of the Hg/Cl₂/S(IV) system. Various researchers have shown that by the addition of an oxidant elemental mercury can be easily oxidized to Hg⁺² and absorbed into aqueous solutions. Previous researchers have observed that the Hg/Cl₂ reaction is catalyzed by surfaces; therefore, in order to extract kinetics, absorption must be conducted in a gas/liquid contactor that minimizes solid surfaces. Previous researchers have also shown that S(IV) is a strong reducing agent, but Hg can still be oxidized in its presence if a strong oxidizing agent is present.

The major contribution of this work is to understand the chemistry of aqueous systems containing Hg/Cl₂/S(IV). This work provides absorption data and rate constants for the reactions among Hg, Cl₂, and S(IV) at low/intermediate pH ranges. This data can be used to predict mercury removal in limestone slurry scrubbers.

Chapter 3: Mass Transfer with Chemical Reaction

This chapter discusses the theory of mass transfer with chemical reaction in the boundary layer. The models used in analyzing the data are developed.

3.1 CHLORINE ABSORPTION MODEL

Chlorine absorption into S(IV) solutions occurs by mass transfer with simultaneous chemical reaction. Chlorine must first diffuse from the bulk gas to the gas liquid interface with the flux (N_{Cl_2}) given by:

$$N_{Cl_2} = k_g (P_{Cl_2,b} - P_{Cl_2,i}) \quad (3-1)$$

Then, chlorine absorption into the liquid occurs by mass transfer with fast chemical reaction in the boundary layer with the same flux:

$$N_{Cl_2} = \frac{Ek_{L,Cl_2}^o (P_{Cl_2,i} - P_{Cl_2,b}^*)}{H_{Cl_2}} \quad (3-2)$$

According to surface renewal theory (Danckwerts, 1970), the enhancement factor (E) can be expressed as (Critchfield, 1988; Shen, 1997; Zhao, 1997):

$$E = \sqrt{1 + \frac{D_{Cl_2}}{k_L^o} (k_{1,H_2O} + k_{2,buf} [buffer]_i + k_{2,OH} [OH^-]_i + k_{2,S(IV)} [S(IV)]_i)} \quad (3-3)$$

which incorporates the reactions which contribute to chlorine absorption. If the enhancement of chlorine absorption by the buffer and S(IV) are the two dominant reactions and if equilibrium effects are negligible, then the flux expression simplifies to Equation 3-4. The assumptions above were validated by the experiments

conducted. Equation 3-4 models mass transfer with fast, pseudo-first order irreversible reaction.

This result (Equation 3-4) is the same for both surface renewal and penetration theories. The absorption in the stirred cell reactor is modeled using surface renewal theory, while the absorption in the wetted wall column is modeled using penetration theory. For a fast reaction, both theories simplify to the same result.

$$N_{Cl_2} = Ek_{L,Cl_2}^o \frac{P_{Cl_2,i}}{H_{Cl_2}} = \frac{P_{Cl_2,i}}{H_{Cl_2}} \sqrt{D_{Cl_2} (k_{2,S(IV)} [S(IV)]_i + k_{2,buf} [buffer]_i)} \quad (3-4)$$

The enhancement factor expression is derived assuming that the chlorine/S(IV) reaction is first order in chlorine and first order in S(IV). If this model is correct, the extracted rate constant, $k_{2,S(IV)}$, can be used to extrapolate chlorine removal at low chlorine concentrations. The corresponding rate expression is:

$$\text{reaction rate} = k_{2,S(IV)} [Cl_2][S(IV)] \quad (3-5)$$

The concentrations and physical properties (diffusivity, D , and Henry's law constant, H) are known. At 25°C, the Henry's law constant for chlorine, H_{Cl_2} , was taken to be 16.7 atm·m³/kmol (Brian et al., 1966), and the diffusion coefficient for chlorine through water, D_{Cl_2} , was taken to be 1.48 x 10⁻⁹ m²/s (Spalding, 1962). The chlorine flux was determined experimentally from the gas phase material balance. The value for $k_{2,buf}$ was determined by quantifying the rate of chlorine absorption into succinate buffer. Thus, the only unknown is the rate constant for the chlorine/S(IV) reaction.

The interfacial liquid S(IV) concentration is obtained by assuming that Cl_2 reacts with S(IV) at the gas/liquid interface with a stoichiometry of one mole S(IV) per mole chlorine.

$$N_{Cl_2} = N_{S(IV)} = k_{L,S(IV)}^o ([S(IV)]_b - [S(IV)]_i) \quad (3-6)$$

$$[S(IV)]_i = [S(IV)]_b - \frac{N_{Cl_2}}{k_{L,S(IV)}^o} \quad (3-7)$$

The partial pressure of chlorine at the interface can be calculated from Equation 3-1, and the interfacial S(IV) concentration can be obtained from Equation 3-7. The interfacial buffer concentration is assumed to be the same as the concentration of buffer in the bulk. Thus, Equation 3-4 simplifies to Equation 3-8.

$$N_{Cl_2} = \frac{1}{H_{Cl_2}} \left(P_{Cl_2,b} - \frac{N_{Cl_2}}{k_g} \right) \sqrt{D_{Cl_2} \left(k_{2,S(IV)} \left([S(IV)]_b - \frac{N_{Cl_2}}{k_{L,S(IV)}^o} \right) + k_{2,buf} [buffer] \right)} \quad (3-8)$$

In the stirred cell reactor, the bulk concentrations are known since the gas and liquid phases are well mixed. The partial pressure of chlorine in the bulk is equivalent to the chlorine exiting the stirred cell reactor and can therefore be rewritten in terms of the inlet chlorine concentration through a gas phase material balance. Thus, Equation 3-9 is the resulting model used in analyzing the data from the stirred cell reactor.

$$N_{Cl_2} = \frac{1}{H_{Cl_2}} \left(P_{Cl_2,in} - \frac{N_{Cl_2} A}{G} - \frac{N_{Cl_2}}{k_g} \right) \sqrt{D_{Cl_2} \left(k_{2,S(IV)} \left([S(IV)]_b - \frac{N_{Cl_2}}{k_{L,S(IV)}^o} \right) + k_{2,buf} [buffer] \right)} \quad (3-9)$$

In order to analyze the wetted wall column data, the model must be integrated since the gas and liquid concentrations are not constant throughout the column. Therefore, Equation 3-8 must be integrated to obtain the bulk concentrations at each point in the column. In order to do this, the model divided the column into many small sections. In each section, the flux and corresponding bulk concentrations were calculated. In the first section (in the bottom of the column), the bulk chlorine and S(IV) were initialized to the chlorine entering and S(IV) exiting, respectively. The flux for the section was calculated using Equation 3-8. The new bulk concentrations

for the next section were calculated from the previous sections' values and the newly calculated flux:

$$P_{Cl_2, new} = P_{Cl_2, old} - \frac{N_{Cl_2} dA}{G} \quad (3-10)$$

$$[S(IV)]_{new} = [S(IV)]_{old} + \frac{N_{Cl_2} dA}{Q_L} \quad (3-11)$$

Then, the new flux was once again calculated using the new bulk values. This process was continued until the values for the top of the column were calculated. Given the chlorine and S(IV) concentrations at the bottom of the column, the model calculated the overall chlorine flux and penetration ($Cl_{2,out}/Cl_{2,in}$) in the wetted wall column. The model values were compared with the measured flux and penetration.

The rate constant can only be extracted if the chlorine absorption is controlled by kinetics. When the S(IV) concentration is high relative to the chlorine concentration, the chlorine flux is limited by the resistance in the gas phase, and the flux from Equation 3-1 simplifies to:

$$N_{Cl_2} = k_g P_{Cl_2, b} \quad (3-12)$$

Under these conditions, there is essentially no chlorine at the interface since all the chlorine reacts with S(IV) as soon as the chlorine reaches the interface. Thus, the chlorine absorption only depends on how fast the chlorine diffuses from the bulk gas to the gas/liquid interface, not on the kinetics.

When the chlorine concentration is high relative to the S(IV) concentration, the flux is limited by S(IV) depletion at the interface. This means that there is essentially no S(IV) at the interface since whatever S(IV) diffuses to the interface is readily depleted through reaction with chlorine. Under these conditions, the flux in Equation 3-6 simplifies to:

$$N_{Cl_2} = N_{S(IV)} = k_{L, S(IV)}^0 [S(IV)]_b \quad (3-13)$$

showing that the flux of chlorine is linear with the bulk S(IV) concentration.

3.2 MERCURY ABSORPTION MODEL

Mercury absorption also occurs by mass transfer with fast irreversible chemical reaction in the boundary layer. Thus, the mercury flux is given by:

$$N_{Hg} = \frac{P_{Hg,i}}{H_{Hg}} \sqrt{D_{Hg} k_{2,Hg} [Cl_2]_i} \quad (3-14)$$

The corresponding rate expression is:

$$\text{reaction rate} = k_{2,Hg} [Hg][Cl_2] \quad (3-15)$$

As before, the interfacial concentrations can be written in terms of the bulk, and the new Hg bulk concentration can be calculated using the new calculated flux:

$$N_{Hg} = \frac{1}{H_{Hg}} \left(P_{Hg,b} - \frac{N_{Hg}}{k_{g,Hg}} \right) \sqrt{D_{Hg} k_{2,Hg} \left[\frac{1}{H_{Cl_2}} \left(P_{Cl_2,b} - \frac{N_{Cl_2}}{k_{g,Cl_2}} \right) \right]} \quad (3-16)$$

$$P_{Hg,new} = P_{Hg,old} - \frac{N_{Hg} dA}{G} \quad (3-17)$$

At 25°C, the Henry's constant and diffusivity for mercury through water was taken from Zhao (1997) to be 8.91 atm-m³/kmol (Clever et al., 1985) and 1.19 x 10⁻⁹ m²/sec (Nene and Rene, 1981; Sitaraman, 1963).

Since the concentrations change throughout the column, the bulk concentrations in each section must be calculated. Once the model (Equation 3-8) calculates the chlorine concentration for each section, the mercury flux and concentration are also calculated (Equations 3-16 and 3-17) for each section until the top of the column is reached.

Chapter 4: Experimental Apparatus and Methods

This chapter details the apparatus and methods used to perform the mercury and chlorine absorption experiments. Detailed descriptions of the stirred cell reactor and wetted wall column are provided. The gas and liquid flow paths, typical operating procedures, and analytical procedures are also discussed.

4.1 DESCRIPTION OF STIRRED CELL REACTOR APPARATUS

Initial chlorine absorption experiments were performed at ambient temperature (22 to 25°C) and atmospheric pressure in the well-characterized stirred cell contactor with Teflon surfaces shown in Figure 4.1 (Zhao and Rochelle, 1999; Zhao, 1997). Teflon (PFA) tubing, fittings (TFE), and valves (PFA) were used for all the connections. All of the tubing and fittings were 1/4", except for those used in the main flow line after the addition of dilution air. These were 3/8" in order to accommodate the higher gas flow rates. Mass flow controllers are labeled as "FC."

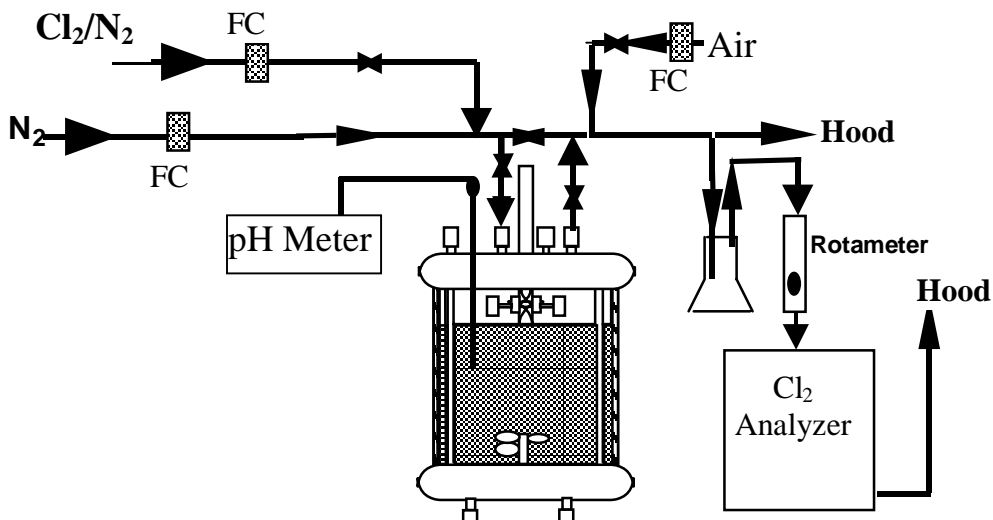


Figure 4.1. Stirred cell reactor apparatus

The stirred cell contactor allowed gas/liquid contact, for which mass transfer properties were known or measured, at a known interfacial area (A) of $8.1 \times 10^{-3} \text{ m}^2$. The stirred tank reactor simulates absorption of the gas (such as Cl_2) across the gas-liquid interface of a droplet, bubble, or packing in a commercial absorber. The cylindrical reactor had a 0.01 m inner diameter and 0.016 m height. The reactor vessel consisted of a thick glass cylinder with Teflon-coated 316 stainless steel plates sealed to the top and bottom by thick gasket clamps. Four equally-spaced, Teflon-coated, 316 stainless steel baffles were welded to the bottom plate. The length of the baffles was long enough to extend to the main body of the gas phase. The bottom plate contained ports for liquid inlet and outlet. The top plate contained ports for the gas inlet and outlet, solution injection, and pH probe. The total volume of the reactor was $1.295 \times 10^{-3} \text{ m}^3$.

The stirred cell contactor was equipped with Teflon-coated independently controlled agitators for gas and liquid phase mixing. Each agitator was driven by a Fisher StedFast Stirrer (Model SL 1200). The geometry of the agitators is given in Zhao (1997). The gas inlet was at the near center of the top plate, directly above the

gas agitator blade, to ensure that the inlet gas was properly mixed. The addition of reflective tape to the stirrer shafts allowed the agitator speed measurement using a hand-held digital tachometer. The mass transfer coefficients (k_g , k_L^o) were a function of the agitation rates. The general form of the correlation is shown in Equation 4-1. Data and correlations used to obtain the k_g and k_L^o are in Appendix A and B, respectively.

$$k_g \text{ or } k_L^o = A(n_g \text{ or } n_L)^b \quad (4-1)$$

4.2 GAS SOURCE AND FLOW PATH FOR STIRRED CELL REACTOR

Gas feed was prepared by quantitatively mixing 0.1% Cl_2 (1000 ppm in N_2) with nitrogen. The flow rates of all gas streams were controlled by Brooks mass flow controllers. The flow controllers for chlorine had to periodically be changed due to inaccurate flows possibly resulting from corroded parts. These controllers were always flushed with nitrogen after every experiment.

The synthesized gas stream, typically at a flow rate of 1.2 L/min, was continuously fed to the reactor. Valves were used to control the flow path of the gas, whether it entered the reactor or bypassed it for calibration. After exiting the reactor, the gas stream was diluted with house air and a portion of the gas was continuously analyzed for chlorine. The majority of the gas was vented to the hood. The portion that went to the analyzer first went through an empty 125-mL Erlenmeyer flask which was connected after the reactor outlet to capture any water vapor or liquid. Since this flask stayed empty throughout an experiment, no liquid exited the reactor through the gas outlet. When the chlorine concentration to the reactor was less than 30 ppm, approximately 3 L/min of dilution air was used. When the chlorine concentration was greater, 36 L/min of dilution air was used. The chlorine analyzer output was connected to a strip chart recorder. The flux of chlorine (rate of chlorine absorption)

was calculated from the gas phase material balance. An analyzer with an electrochemical sensor (NOVA Model 540P) was initially used. Later experiments were done using ion mobility spectrometry (Molecular Analytics AirSentry 10-Cl2). Both analyzers had a 4 – 20 mA output, which was converted to 1 – 5 V signal using a 250 Ω resistor. This voltage output was connected to a strip chart recorder (Soltec Model 1242).

4.3 METHODS FOR CHLORINE ANALYSIS

4.3.1 *Electrochemical chlorine analyzer*

The analyzer contains an electrochemical sensor with a platinum measuring electrode and silver reference electrode. The electrolyte used is a 3% lithium chloride solution. The electrolyte continuously weeps over the active surface of the sensor. When the chlorine contacts the electrochemical sensor, it reacts to form silver chloride (AgCl) which releases two electrons. The current produced is proportional to the chlorine concentration. This analyzer drifts during an experiment and also has a longer response time than the IMS analyzer. It can take several minutes before the analyzer signal stabilizes after the chlorine concentration is increased. Nitrogen dioxide (NO₂) and sulfur dioxide (SO₂) interfere with the electrochemical sensor analysis.

4.3.2 *IMS chlorine analyzer*

The analyzer is based on ion mobility spectrometry (IMS), similar in principle to time-of-flight mass spectrometry (Bacon et al., 1998). The sample is passed over a semi-permeable membrane through which the chlorine diffuses. Purified dry instrument air (supplied externally) sweeps the chlorine from the interior of the membrane and into an ionization region supplied with a β^- source (Ni⁶³). The ionized molecules then drift through a cell under the influence of an electric field. An electronic shutter grid allows periodic introduction of the ions into a drift tube where

they separate based on charge, mass, and shape. Smaller ions move faster than larger ions through the drift tube and arrive at the detector. The current created at the detector is amplified, measured as a function of time, and a spectrum is generated. A microprocessor evaluates the spectrum for the chlorine and determines the concentration based on peak height.

The IMS analyzer is linear throughout the entire range and can detect chlorine at very low concentrations. The IMS analyzer also has much better repeatability than the electrochemical sensor analyzer. There is essentially no drift, and the analyzer responds within seconds (much faster response time than the electrochemical sensor analyzer). The IMS cell is very sensitive to pressure, which is why the analyzer was always calibrated under the same conditions as an experiment. According to the manufacturer (Molecular Analytics), the following do not interfere with the chlorine analysis: CO₂, Hg, SO₂, NO, hydrocarbons, and chlorinated hydrocarbons. However, NO₂ and HCl do interfere with the IMS analysis due to peak overlap at high concentrations.

4.3.3 Absolute chlorine analysis through wet chemical methods

4.3.3.1 Basis and rationale

The absolute gas phase chlorine concentration was measured using a wet chemical method. During these analyses, the gas flowed from the cylinder through the same tubing it would normally flow through in an experiment. The absolute chlorine concentration was measured (instead of relying on that of the gas supplier) since the analysis would yield the actual chlorine concentration that the reactor sees by accounting for chlorine loss between the cylinder and reactor (such as adsorption in tubing). At the beginning and end of each experiment, the tubing was flushed with nitrogen. Since no chlorine was detected by the analyzer under these conditions, chlorine desorption from tubing was assumed to be negligible.

For most of the data analyses, absolute values for the chlorine concentration do not matter as much since relative chlorine concentrations are the important parameter. Usually in the data interpretation, the flux (or outlet chlorine) is normalized by the chlorine concentration, which is why only relative values are important. Also, in order to calculate the fraction gas film resistance (which is used to analyze some of the data), only relative concentrations are needed. The absolute value of the chlorine concentration does matter if only chlorine flux is looked at alone without normalizing it.

4.3.3.2 Initial analytical methods

Various ways of analyzing the chlorine absorbed were investigated. Many of these methods involved measuring the chloride formed as a result of chlorine absorption. One method used consisted of titrating the solution containing chloride with silver nitrate to produce silver chloride (Kolthoff and Stenger, 1947; Scott, 1939). Adsorption indicators can be used to determine the endpoint (Finlayson, 1992; Kolthoff and Stenger, 1947). Potentiometric (Carson, 1953; Nagy et al., 1975; Lisensky and Reynolds, 1991; Prokopov, 1970; Serjeant, 1984; Zettimeisl and Laurence, 1977) and amperometric (Coulson and Cavanagh, 1960; Lingane, 1954; Shaffer et al., 1948; Stock, 1965) methods could also be used. These methods involve measuring either the voltage or the current generated from chloride formation using a silver electrode and a reference electrode.

4.3.3.3 Final wet chemical methods to determine Cl_2 concentration

The absolute chlorine concentration was first analyzed by sparging chlorine into a potassium iodide solution buffered at pH 5. Chlorine reacts with iodide to form iodine, which is then titrated with sodium thiosulfate to give the chlorine concentration (Harris, 1987; Kolthoff and Belcher, 1957; Franson, 1995; Scott, 1939; White, 1986). Later, the absolute chlorine was analyzed by sparging chlorine into

sodium sulfite/sodium hydroxide solution at pH 12.5 and then analyzing the chloride concentration using ion chromatography. Typical solution composition was 0.04 M Na_2SO_3 /0.1 M NaOH. The gas was usually sparged into the solution for 10 to 30 minutes. For each mole of chlorine absorbed, two moles of chloride are formed. This method resulted in a chlorine concentration 1.4 times greater than what was obtained using the potassium iodide method.

The sulfite method gave more reproducible results and recovered more of the chlorine than the previously used potassium iodide method. For both of these methods, the zero was calibrated by supplying only nitrogen (without chlorine) through the tubing. Also, different chlorine concentrations were used in the experiment in order to verify the wet chemical method. Using the sulfite analysis, the cylinder chlorine concentration (after passing from the cylinder through the tubing) was 840 ppm, while Air Products stated that the cylinder concentration was 1000 ppm. Air Products also stated that the cylinder chlorine concentration may decrease over time, but they were not sure what the time span would be. A basis of 840 ppm was assumed for all of the data discussed in this work which were taken using this chlorine cylinder. The simultaneous mercury and chlorine absorption experiments were done with a different cylinder, which had a concentration of 914 ppm, compared to Air Products' value of 962 ppm.

4.4 CHLORINE ANALYZER CALIBRATION PROCEDURE

The chlorine analyzer was calibrated at the beginning and end of each experimental series to check for analyzer drift. There was essentially no drift for the IMS analyzer. During calibration, the gas flow rate was identical to that in an experiment. Other than bypassing the reactor, the gas flow path during calibration was the same as during an experimental run. To calibrate the analyzer zero, nitrogen (without chlorine) was supplied and diluted with house air. To calibrate the span, the gas flow rates were adjusted to give different chlorine concentrations spanning the

range of interest. For the later experiments (those analyzed by IMS), both dry gas and wet gas calibrations were done to ensure that moisture did not affect the analyzer reading. Wet gas calibrations were done by having the nitrogen (not the chlorine) go through the stirred cell reactor filled with aqueous solution. For chlorine concentrations less than 30 ppm, there was a slight difference in wet and dry gas calibrations, probably resulting from the increased humidity of the gas. Therefore, wet calibrations were always used whenever experiments were conducted in the stirred cell reactor in which the chlorine concentration would be less than 30 ppm.

4.4.1 Calibration of electrochemical analyzer

As previously mentioned, the electrochemical analyzer drifted during experiments. Therefore, throughout an experiment, the calibration was frequently checked. Another problem with this analyzer was that the calibration was not completely linear over the entire range; it was linear over the upper and lower ranges of the chlorine concentration. Therefore, a multi-point (7 to 9-point) calibration was usually performed. Figure 4.2 shows a typical calibration.

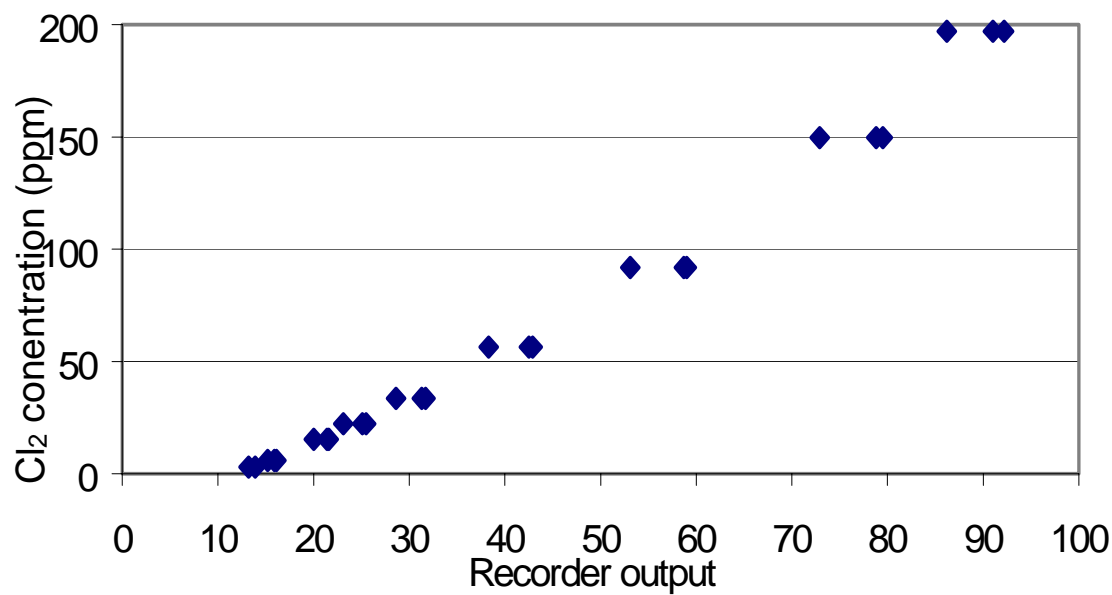


Figure 4.2. Typical calibration of electrochemical sensor analyzer

However, there were some experiments in which the calibration was worse due to a problem with the electrochemical cell not being completely full of electrolyte. Figure 4.3 shows a typical calibration under these conditions.

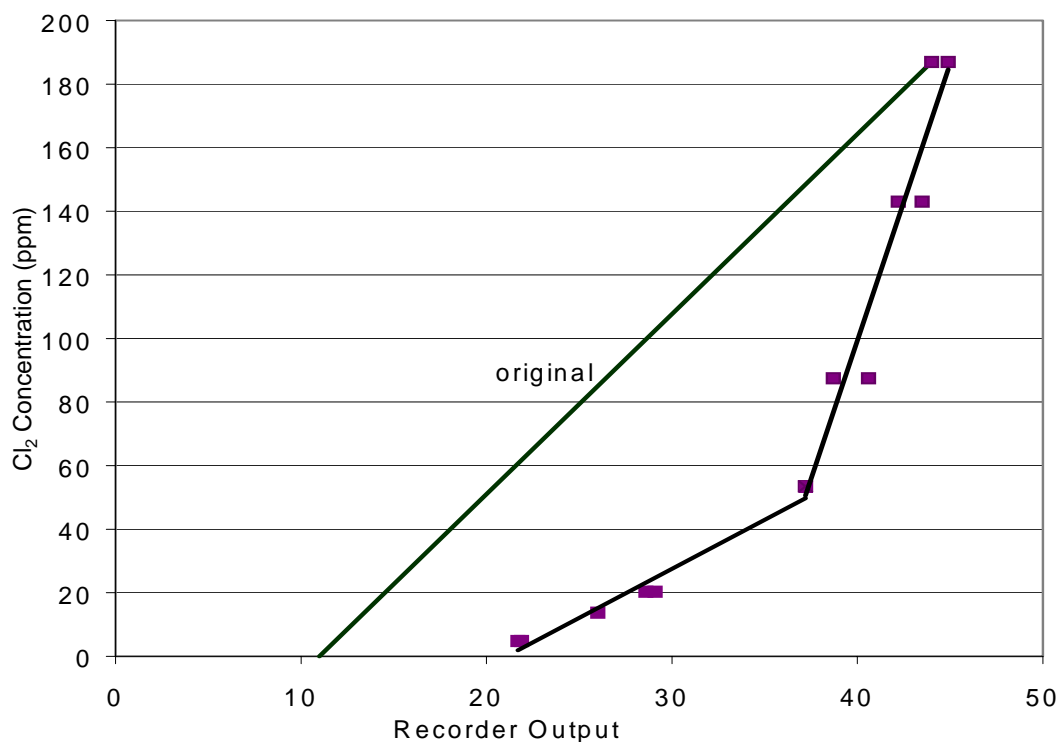


Figure 4.3. Electrochemical analyzer calibration with bad cell

The “original” line represents what the calibration would be if the analyzer was linear.

4.4.2 Calibration of the IMS analyzer

Initially, a 10-point calibration was done to test the linearity. However, the analyzer was observed to have excellent repeatability and linearity. Therefore, during experiments, only a 3-point calibration (plus zero) was conducted. Calibration was checked at the end to verify that no significant drift occurred. Figure 4.4 shows a typical calibration.

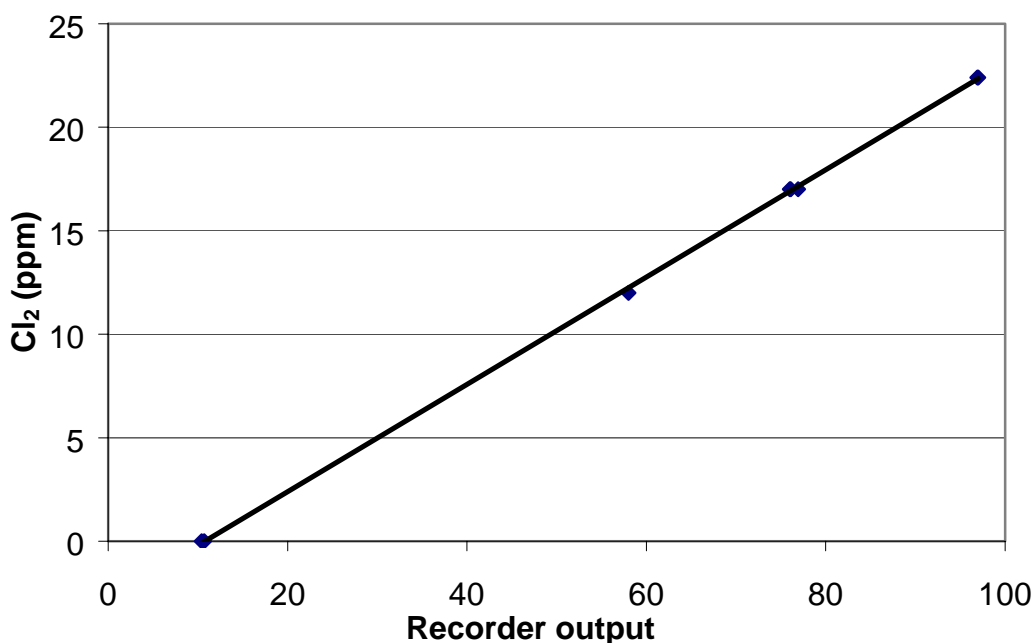


Figure 4.4 Typical IMS analyzer calibration

4.5 STIRRED CELL REACTOR SOLUTION AND ANALYSIS

The reactor contained the aqueous S(IV) solution, ranging from 0 to 10 mM, used in absorbing chlorine. The reactor fluid volume in a typical experiment was $1.06 \times 10^{-3} \text{ m}^3$; thus, the liquid level was slightly below the gas phase agitator. Distilled water was first added to the reactor. For experiments at $\text{pH} \approx 4.5$, the reactor solution was buffered by injecting a stock solution of equimolar succinic acid/sodium hydroxide. The solution needed to be buffered to ensure that the pH at the gas/liquid interface was constant. Succinate buffer was used because it is not volatile and buffers at the desired pH. Furthermore, succinic acid (or glutaric acid) is often used as an organic acid additive in limestone slurry scrubbing. The buffer concentration in the reactor ranged from 5 to 50 mM total succinate. The S(IV) solution was obtained by injecting a stock solution containing equimolar sodium bisulfite (obtained from sodium meta-bisulfite, Certified A.C.S., Fisher Scientific)

and sodium sulfite (Powder, Reagent A.C.S., Spectrum Chemical). For experiments at $\text{pH} > 7$, stock solutions of only sodium sulfite were used.

Liquid samples (2 to 25 mL, depending on S(IV) concentration) were periodically taken from the bulk of the reactor and analyzed for S(IV) concentration by iodometric titration (Ayres, 1968; Harris, 1987; Kolthoff and Belcher, 1957; Kolthoff et al., 1969). During some experiments, 3 mL samples were withdrawn and analyzed for the reaction products, chloride and sulfate, using ion chromatography. However, it was discovered that sulfate analysis could not be done in buffered solutions due to peak overlap. Also, we attempted to use the ion chromatograph (IC) to obtain an independent S(IV) measurement. This method involved binding the S(IV) with formaldehyde before injecting into the IC. This method was later discontinued since it was not as reproducible as the iodometric titration method. The ion chromatograph and iodometric titration procedures are detailed in Appendix C and D, respectively. Withdrawing samples did not affect the reaction since each withdrawal was followed by subsequent injection of fluid.

The pH of the bulk reactor solution was continuously monitored and recorded using a strip chart recorder (0 – 100 mV input). The pH probe (Accumet Pencil-Thin Epoxy Body-Gel Filled) was calibrated by placing it into a standard pH 4 and pH 7 buffer solution. After calibration, the pH probe was inserted into the reactor fluid for continuous pH monitoring of the bulk reactor fluid. The pH was measured to verify that the experiments were being conducted at the desired pH. The concentration of each S(IV) species (bisulfite and sulfite) can be calculated by knowing the pH and total S(IV) concentration. In the buffered S(IV) experiments, essentially all of the S(IV) was present as bisulfite since the pH was much lower than the pK_a of the sulfite/bisulfite reaction ($\text{pK}_a = 7$).

4.6 IODOMETRIC TITRATION FOR S(IV)

After the S(IV) sample was withdrawn from the stirred cell reactor, it was directly injected into excess iodine solution to avoid air oxidation to sulfate. The S(IV) reduced the iodine to iodide. The excess iodine was titrated with sodium thiosulfate. When the yellow color of the iodide started to fade (as the iodine was reduced to iodide by the thiosulfate), a couple drops of starch indicator were added to enhance the endpoint detection. The endpoint was reached when the blue solution turned clear.

The S(IV) concentration was determined from the difference between the amount of thiosulfate used to titrate the excess iodine and the amount needed if no S(IV) were added to the iodine. The difference indicates how much of the iodine reacted with S(IV).

The S(IV) analysis procedure was modified as experiments were done. The accuracy and precision were improved with procedural modifications such as checking blanks and verifying standard solutions daily and withdrawing larger samples from the reactor. However, at very low S(IV), the difference to determine the amount of iodine which reacted with S(IV) was very low. At times, it was close to the errors in measurements (buret readings). Thus, the expected precision at S(IV) concentrations below 0.09 mM is ± 0.04 mM. For example, when the S(IV) concentration is reported as 0.08 mM, the actual concentration could range from 0.04 to 0.12 mM. However, the S(IV) concentrations were more precise in the wetted wall column experiments, due to modifications such as withdrawing larger samples (than stirred cell) and using lower concentration standards.

4.7 WETTED WALL COLUMN DESIGN

4.7.1 *Basis and rationale*

The existing stirred cell contactor could not be used for the simultaneous absorption because the mercury will react with the chlorine on the solid surfaces (such as on the gas agitator and the top of the reactor). A new contactor was designed to minimize reactions in the bulk gas and on the solid surfaces. The contactor also needed higher mass transfer coefficients in order to precisely extract rate constants for fast reactions. Wetted wall columns designed by other researchers were investigated in order to obtain the proposed design (Aieta, 1984; Aieta and Roberts, 1986a; Astarita et al., 1983; Blauwhoff and Van Swaaij, 1985; Danckwerts, 1970; Fickert et al., 1998; Gilliland et al., 1958; Gilliland and Sherwood, 1934; Greenwelt, 1926; Kiil, 1998; Li and Lai, 1995; Pacheco, 1998; Utter et al., 1992; Vivian and Peaceman, 1956; Yih and Shen, 1988).

Short, skinny columns are typically used since the fluid and mass transfer properties are well-characterized (Astarita et al., 1983). However, this type of column would have a small gas/liquid contact area. An area similar to that of the stirred cell contactor was desired. If the area were too small, there would not be a statistically significant concentration change. Therefore, the column either needed to be wide or tall. A wide column would result in a lower gas phase mass transfer coefficient because of the additional resistance in the gas phase. In tall columns, flow is typically not well characterized due to ripples at random spots (Astarita et al., 1983; Dankwerts, 1970). Therefore, designing a tall column in which the fluid was periodically disturbed and renewed was attempted.

The final design consisted of a column divided into several short skinny sections. This allowed reproducible flow patterns, a contact area similar to the stirred cell reactor, and good mass transfer properties. The total unwetted solid surface was

minimized to reduce Hg removal by reaction with chlorine on solid surfaces. The space between sections was minimized. The total gas volume in the contactor was also minimized to enhance gas film mass transfer and to minimize any bulk gas reaction of chlorine and Hg.

4.7.2 Description of wetted wall column

Figure 4.5 depicts the constructed wetted wall column. The column consists of a glass tube divided into five 6-cm sections. The liquid solution is collected and refreshed between sections. The column has a 1-cm ID, 108 cm² area, and a total height of 31 cm. Gas flows into the bottom of the column through a 3/8" OD glass tube and counter-currently contacts the liquid. This glass tube has a smooth, sharp edge (ground outward as shown in Figure 4.5) in order to ensure no liquid enters it. All surfaces in contact with gas are either glass or teflon to avoid adsorption of Hg and Cl₂ on surfaces. All experiments were conducted at ambient temperature.

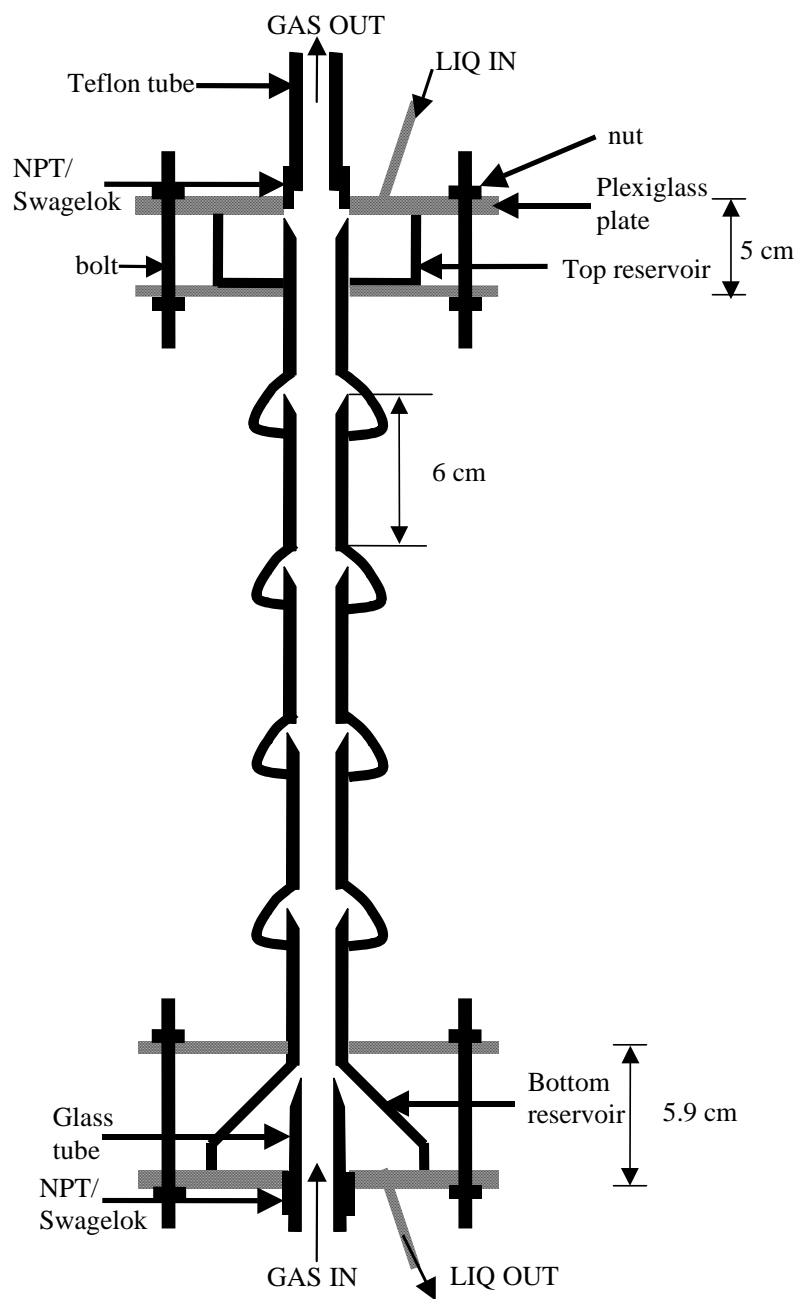


Figure 4.5 Wetted wall column

Aqueous solution enters the top glass reservoir (which is maintained full of liquid throughout an experiment), and the liquid enters the column and distributes

itself evenly. To aid in an even liquid distribution, the inside face of the tube (in each of the 5 sections) was ground downward. Liquid is collected in the bottom glass reservoir and pumped using a gear pump (Micropump variable-speed pump with suction shoe head). The top and bottom reservoirs were created by glass-blowing. The top reservoir holds approximately 25 mL of liquid, while the bottom reservoir holds about 30 – 40 mL. Both reservoirs were constructed out of thick-walled glass. The bottom reservoir was blown at a 45° angle as shown in Figure 4.5. The glass reservoirs are directly attached to the column. The top and bottom seals are provided by O-rings, which are between the glass and plexiglass. The plexiglass plates are bolted on the four corners; nuts provide the compressive force on tightening. The liquid inlet and outlet were constructed out of 1/4" OD plexiglass tubing and were attached to the plexiglass plates. The plexiglass plates were threaded so that the gas inlet and outlet fittings could be connected. The gas outlet fitting was a 3/8" NPT to 3/8" Swagelok connection. When the fitting was completely closed (touching the glass column), no liquid could enter the column. During an experiment, the fitting was adjusted to obtain smooth flow. Smooth, fully-wetted flow was observed by using a strobe light. A level was used to ensure that the column was aligned vertically. The 3/8" glass gas outlet tubing was inserted through a 3/8" NPT to 3/8" Swagelok fitting. The fitting was screwed into the bottom plexiglass plate. The glass tube was inserted through the fitting until positioned at the desired height.

4.8 WETTED WALL COLUMN SOLUTION FLOW PATH AND ANALYSIS

Figure 4.6 shows a flow diagram of the complete wetted wall apparatus with all the supporting equipment. The liquid solution was stored in a reservoir constructed out of a plexiglass tube and sealed with O-rings and plexiglass plates on the top and bottom of the reservoir. The top plate contained ports for the pH probe (same probe as in stirred cell), thermocouple probe (Omega T type, model TTSS-

14G-12), solution injection, and liquid outlet. The liquid inlet port was located on the bottom side of the reservoir. The reservoir volume was either 0.7 L or 3.1 L (could easily be interchanged). A Micropump gear pump was used to circulate the liquid through the system. The liquid flow rate was measured using a Gilmont Accucal rotameter. The range of operating liquid flow rates was very narrow (2 to 3.5 mL/s) due to the flow stability and entrainment. The typical flow rate was 2.26 mL/s. The fluid temperature was monitored in the reservoir and in the liquid outlet from the column. Both temperature probes were connected to a display meter (Omega DP462-T). A pH probe was in the reservoir to continuously measure the pH of the bulk solution. The solution inside the the plexiglass reservoir was continuously stirred using a magnetic stirrer (Corning hot plate stirrer model PC-351).

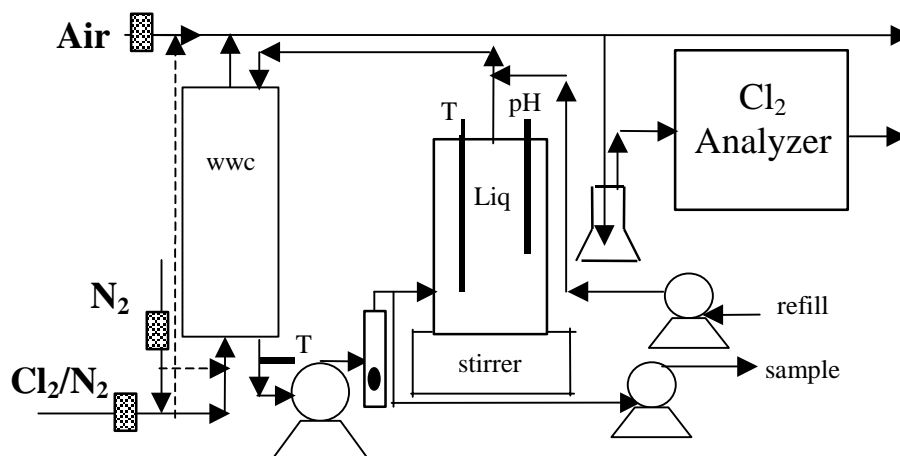


Figure 4.6 Flow diagram for chlorine absorption in wetted wall column

A two-head Masterflex peristaltic pump was used to withdraw samples of the solution exiting the column, while adding fluid to the reservoir to retain the liquid level. Liquid samples were periodically taken from the liquid outlet and analyzed using iodometric titration. The sample was pumped directly into an Erlenmeyer flask with iodine solution. Therefore, air oxidation was avoided. The sample size ranged from 20 to 50 mL, depending on the S(IV) concentration. A bigger sample size

resulted in greater precision in the measurements of S(IV) concentration. A more precise buret was also used in these experiments. The peristaltic pump was also used to adjust liquid level in the column as needed.

4.9 GAS FLOW PATH FOR CHLORINE ABSORPTION IN WETTED WALL COLUMN

As with the stirred cell experiments, gas flow rates were controlled by mass flow controllers. The synthesized gas stream, typically ranging from 5 to 10 L/min, was continuously fed to the column. The dashed lines in Figure 4.6 represent alternate flow paths. The chlorine and nitrogen can both bypass the column, or the chlorine alone can bypass the column. As with the stirred cell reactor, valves (not pictured) are used to control flow path. The hatched rectangles represent the mass flow controllers. The column could not operate at gas flow rates greater than 10 L/min because liquid would be forced out through the gas exit. After exiting the column, the gas was diluted with air. Most of the gas was vented to the hood, while a portion of it passed through a knockout flask before entering the IMS analyzer. The IMS analyzer contained an internal eductor that drew the amount of gas necessary for analysis.

4.10 GAS SOURCE AND FLOW PATH FOR MERCURY ABSORPTION

Gaseous elemental mercury was generated using a commercially available permeation tube (VICI Metronics High Emission Tube-SR, 10 cm length) which continuously emits a known amount of mercury into a known dilution flow rate. The permeation tube was inside a glass U-tube (supplied by the manufacturer) and immersed in a water bath with temperature maintained at 90°C using a Lauda Immersion Circulator. The permeation rate at 90°C was 1801 ng/min. The water bath was filled with distilled water, as suggested by the manufacturer. The bath was monitored and re-filled as water evaporated. A constant water depth ensured a constant heating area for the U-tube. By maintaining a reservoir of the liquid mercury

at a constant temperature in the water bath, the mercury vapor pressure remains constant and provides the constant driving force for diffusion through the membrane wall. Approximately 100 cc/min of nitrogen flowed through the permeation tube to ensure sufficient heat exchange. As before, all gas flows were controlled by mass flow controllers.

The liquid solution flow path for the simultaneous Hg/Cl₂ absorption experiments is identical to that shown in Figure 4.6. The gas flow path has been slightly modified and is shown in Figure 4.7. As before, valves (as shown in Figure 4.7) are used to control flow path (bypass or through column). The mercury and chlorine bypass lines were kept separate to prevent reaction. During an experimental run, the Hg/N₂ gas stream joined the Cl₂/N₂ stream before entering the wetted wall column. Typical chlorine and mercury concentrations entering the column were 25 ppm and 50 ppb, respectively. The total gas flow to the reactor was usually 5 L/min.

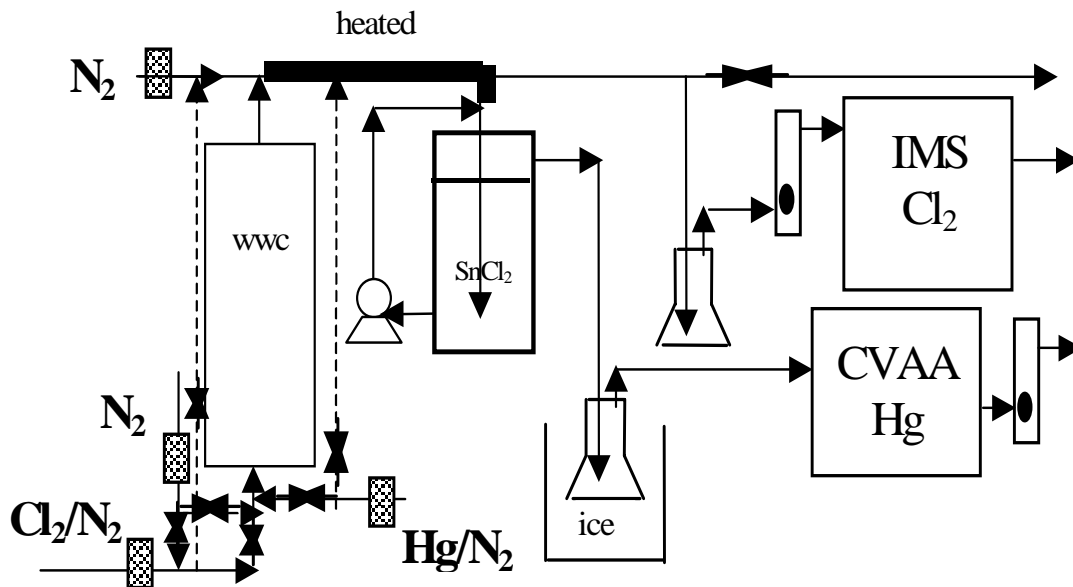


Figure 4.7 Gas flow path for mercury/chlorine absorption

After the gas exited the column, it was usually diluted with pure nitrogen. Dilution flow was typically at 8 L/min, resulting in a total gas flow of 13 L/min after

dilution. Most of the gas was sent to an acidic potassium permanganate (0.1 M KMnO_4 in 10% H_2SO_4) scrubber to remove Hg before being vented to the hood. About 1 L/min of gas was sent through the IMS analyzer to be continuously analyzed for chlorine. A rotameter with valve was used to regulate flow to the IMS analyzer. A valve in the main line was used to regulate the flow for mercury analysis. Approximately 200 to 250 cc/min gas was analyzed for mercury. The Hg analytical system is detailed in the next section. A rotameter placed after the Hg analyzer was used to monitor gas flow to the analyzer. All the gas streams went through the permanganate scrubber before being vented to the hood.

4.11 MERCURY SAMPLE CONDITIONING SYSTEM

4.11.1 Initial testing

Since Hg reacts with Cl_2 on surfaces, analyzing for Hg in the presence of Cl_2 is difficult. During the initial experiments, as soon as the Cl_2 flow was started, the Hg concentration would instantly decrease to zero. For these tests, the entering gas was always dry (did not pass through a wet column). Also, for these initial tests, the pump loop shown across the SnCl_2 impinger in Figure 4.7 was not present. Throughout these tests, the impinger design (constructed out of glass) was modified as needed. Good contact of the gas with the impinger solution, without the introduction of more surfaces, was essential. Table 4.1 summarizes the effects of the different configurations initially tested.

Table 4.1 Analyzing Hg in the presence of chlorine

Configuration	Hg _{in} (ppb)	Cl _{2in} (ppm)	Effect on Hg
Empty impinger	16.8	8.6	Decreases to 0
Acidic SnCl ₂ /soda lime	16.8	1.5	Decreases to 0
Basic SnCl ₂ /ice bath	34	1	Decreases slowly
	34	2	Decreases faster
	16.8	0.5	Decreases slowly
	16.8	8.6	Decreases to 0
Pumping SnCl ₂ through impinger	16.8	8.6	No effect—see all Hg

In the first trial, there was no solution in the impinger. Also, the knockout flask was present, but was not immersed in an ice bath. Since the gas was dry, no drying agent was needed. Even though the gas was dry, Hg was still removed by reaction with Cl₂ on the surfaces.

In the next trial, the impinger contained 10 wt % stannous chloride (SnCl₂) and 20 wt % HCl. After the impinger, the gas was dried by passing through a tube filled with soda lime. Acidic SnCl₂ solution is commonly used to reduce all oxidized forms of Hg to elemental Hg (Blythe et al., 2001; Richardson et al., 2001; Sjoström et al., 2001). The SnCl₂ should also reduce the chlorine to chloride. However, experiments showed that the analyzer still could not see any Hg in the presence of Cl₂. This was because the acidic SnCl₂ was not completely reducing all of the chlorine. Therefore, the remaining chlorine was being adsorbed on the soda lime and reacting with the Hg. Other researchers did not have this problem with the acidic SnCl₂ because their gases did not contain chlorine; typical flue gas contains SO₂, NO_x, and HCl, but no Cl₂.

For the next set of trials, the acidic SnCl_2 was replaced by a basic SnCl_2 solution. Under basic conditions, SnCl_2 still effectively reduces all oxidized forms of Hg to elemental. The solution composition used was 20 wt % sodium hydroxide and 2 wt % stannous chloride. At high pH, the chlorine should be completely absorbed. Since soda lime may absorb Hg, it was removed. The gas was now dried by passing through an Erlenmeyer flask, which was immersed in an ice bath. With this configuration, the analyzer could see the Hg in the presence of chlorine. However, as the chlorine concentration was increased, the Hg concentration would decrease.

4.11.2 Final configuration

A configuration was eventually developed to analyze for Hg in the presence of Cl_2 . After the gas exits the column, it is heated (via heating tape surrounding the teflon tube) to minimize moisture (and avoid Hg/Cl_2 reactions on the moist surfaces). The gas is sparged into the impinger containing the $\text{SnCl}_2/\text{NaOH}$ solution. The basic SnCl_2 solution reduces any oxidized Hg to elemental Hg and reacts with (and removes) the chlorine. As shown in Figure 4.7, the solution was continuously pumped through the impinger, at an approximate flow rate of 0.6 mL/s, using a peristaltic pump. Since the solution was pumped, entering at the top with the gas, the impinger tube was constantly being washed by the reducing solution. Good contact of the gas with the solution is maintained without introducing more surface for the mercury to react with chlorine. After flowing through the impinger, the gas is dried by flowing through a knockout flask immersed in an icebath before entering the mercury analyzer for continuous analysis. This method (adding the impinger solution pump) allows the analyzer to see all the Hg, even in the presence of chlorine.

4.12 COLD VAPOR ATOMIC ABSORPTION (CVAA) MERCURY ANALYZER

A cold vapor atomic absorption spectrometry (LDC Analytical, Model 3200) analyzer was used to continuously analyze for gas phase elemental mercury. This

analyzer is identical to the instrument used by Zhao (1997). The analyzer uses a photometric detector that measures the luminous intensity of monochromatic light that has passed through the sample and compares it with the luminous intensity of an equal light beam of fixed value. This analyzer is specifically designed to measure ultraviolet light at a wavelength of 253.7 nm. The mercury concentration is linear with the absorbance at this wavelength. The cell path length is 10 cm. Chlorine did not interfere with the mercury analyzer.

4.12.1 Mercury analyzer calibration

Due to the low experimental mercury concentrations, less than 5% of the full-scale range of the analyzer was used. At this low range (0 – 50 mV output), the calibration drifted often. Therefore, a three-point calibration (plus zero) was done at the beginning and end of the experiment. Also, during an experiment, the calibration was periodically checked. The calibration was always linear over the desired concentration range. The analyzer usually responded within a few seconds, but sometimes, it took several minutes for the concentration to stabilize. Figure 4.8 shows a typical calibration.

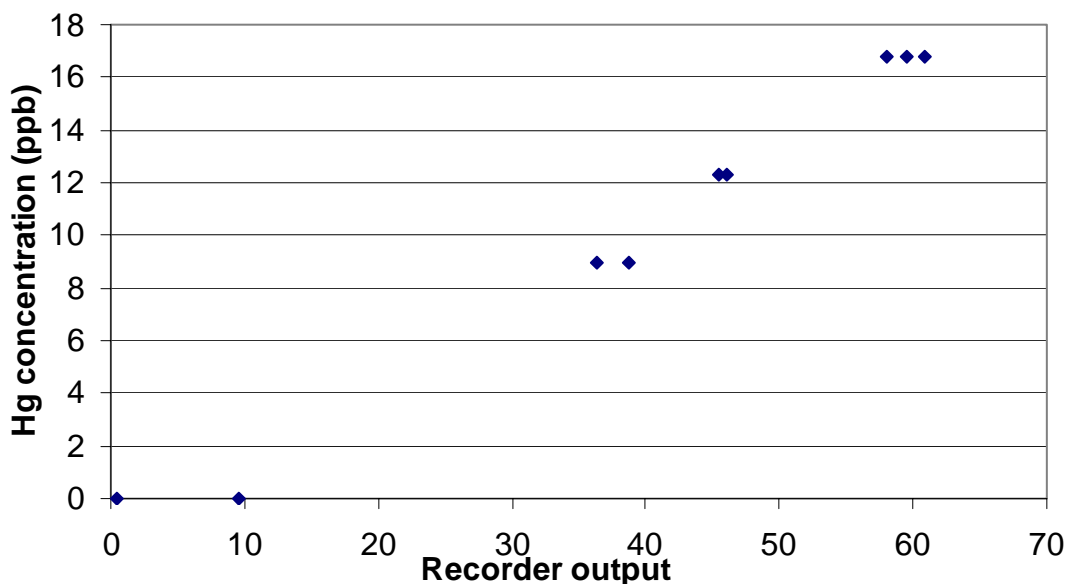


Figure 4.8 Typical CVAA calibration

The analyzer was always turned on (to avoid warm-up issues for the source lamp) with no gas flow. During calibration, the gas flow rate was identical to that in an actual experiment. The flow through the CVAA was always maintained at approximately 200 – 250 cc/min. To calibrate the analyzer zero, only nitrogen was run through the system. The time for the zero to stabilize ranged from 30 minutes to 2 hours. After the zero stabilized, the nitrogen flow through the mercury permeation tube was started. It generally took one hour for the mercury concentration to stabilize after flow was started through the permeation tube. After stabilizing, the nitrogen dilution flow was changed in order to obtain different mercury concentrations to obtain the linear calibration. The analyzer was calibrated by passing a known concentration of Hg through the dry wetted wall column. In order to verify that moisture (resulting from a wet column) did not affect the analyzer, a wet calibration was also done. The wet calibration yielded the same signal as the dry calibration. When the Hg goes through the column, with either water or buffer flowing, the

concentration is the same as going through a dry column. Therefore, neither water nor buffer absorbs any detectable Hg. The analyzer calibration was also done both with and without chlorine to ensure that the chlorine did not significantly reduce the Hg signal.

4.13 TYPICAL EXPERIMENTAL PROCEDURE

This section summarizes the typical operating procedure for the simultaneous absorption of mercury and chlorine in the wetted wall column. The plexiglass reservoir was first filled with succinate buffer (or distilled water). The impinger was filled with the $\text{SnCl}_2/\text{NaOH}$ solution. The pH probe and the analyzers were calibrated. Flow was started through the column. The gas outlet fitting was adjusted, the column level was verified, and more fluid was added as necessary to ensure smooth flow through the column with no air bubbles present in any of the tubing. The iodine and thiosulfate standards were verified, and several blanks (buffer samples with no S(IV) present) were analyzed.

The appropriate valves were opened/closed to start the flow of $\text{Hg}/\text{Cl}_2/\text{N}_2$ through the wetted wall column. The chlorine concentration was varied, S(IV) was injected, solution samples were withdrawn, and so forth.

At the end of the experiment, the calibration (of the CVAA and IMS) was checked, the liquid waste was properly disposed, and the wetted wall column and plexiglass reservoir were cleaned by flushing distilled water through the system.

Chapter 5: Characterizing Wetted Wall Column

In order to extract reaction kinetics from absorption data, knowledge of the mass transfer coefficients and the contact area is essential. The mass transfer characteristics of the wetted wall column were determined experimentally. The overall resistance to mass transfer is equal to the sum of the resistances in the gas and liquid phases:

$$\frac{1}{K_{OG}} = \frac{1}{k_g} + \frac{H}{Ek_L^o} \quad (5-1)$$

If a reaction is very fast (high E) and/or if the gas is extremely soluble in the liquid (high H), the last term vanishes, and the overall gas mass transfer coefficient is equivalent to the individual gas film mass transfer coefficient. Therefore, k_g can be easily determined by absorbing a gas into a liquid which has a rapid reaction rate. On the other hand, if the gas has a low solubility (low H) and does not react quickly in the liquid, the resistance in the liquid film dominates the overall mass transfer resistance. Thus, to determine the liquid film mass transfer coefficient, gas should be desorbed from a liquid in which the gas is not very soluble. These criteria led to the experiments which were conducted to characterize the wetted wall column. Mass transfer coefficients are independent of chlorine concentration.

5.1 GAS FILM MASS TRANSFER COEFFICIENT

5.1.1 *Experimental method*

The gas phase mass transfer coefficient was obtained by measuring chlorine absorption into 0.25 M sodium hydroxide (NaOH) in the wetted wall column. The 700 mL plexiglass reservoir was used for all experiments. Some experiments were

also done at 1.0 M NaOH to verify that the absorption was gas film controlled. The chlorine concentration was measured using the IMS analyzer. The typical chlorine inlet concentration was 22 ppm, but it was varied from 20 to 280 ppm. The gas flow rate was varied from 1 to 10 L/min, resulting in a Reynolds number (Re) range in the column of 170 to 1400. The liquid flow rate was usually at 2.26 mL/s. Since this was the first absorption experiment conducted in the wetted wall column, some procedures were modified throughout these experiments. The flow path was varied, and the liquid level in the column had to occasionally be adjusted.

5.1.2 Theory

Since the chlorine/hydroxide reaction is very fast, there is negligible resistance in the liquid phase; thus, K_{OG} is equivalent to k_g . Under complete gas film control, the chlorine at the interface is negligible relative to the bulk. Thus, the gas film mass transfer coefficient can be calculated from:

$$k_g = \frac{N_{Cl_2}}{P_{Cl_2,b}} \quad (5-2)$$

The bulk concentration was taken to be the log mean average of the inlet and outlet concentrations. This was valid since under gas film control, the overall gas phase mass transfer coefficient was constant throughout the column. If the overall mass transfer coefficient varied throughout the column (as it does in experiments that are used to extract kinetics), then an integrated method, as discussed in Chapter 3, must be employed.

Hobler (1966) develops a correlation for the gas phase mass transfer coefficient, which applies to laminar flow in a wetted wall column. Laminar flow does not become stable until a certain distance from the inlet. Therefore, the local mass transfer coefficient decreases with distance from the inlet. In practice, the local

coefficient is not of interest; the average value over the height of the column (h) is the value needed (Hobler, 1966).

Using dimensional analysis, the mass transfer coefficient (written in terms of the Sherwood number) can be expressed as a general function (Hobler, 1966):

$$Sh = KRe^A Sc^B (d/h)^C \quad (5-3)$$

An analytical approach can be used to determine the exponents (A, B, and C) and the constant (K). Hobler (1966) states the following correlations:

$$Sh = 0.5ReSc(d/h), \quad \text{if } ReSc(d/h) < 4.5 \quad (5-4)$$

$$Sh = 1.62[ReSc(d/h)]^{1/3}, \quad \text{if } ReSc(d/h) > 13 \quad (5-5)$$

Equation 5-4 is derived assuming fully developed flow (parabolic velocity distribution). This assumption may be valid for gas flow through a long tube, in which the laminar flow has had time to fully develop.

Equation 5-5 is derived assuming a constant velocity in the whole cross-section. This assumption is most valid for unstable flow, in which the column is short or the flow is very high that it does not have enough time to fully develop. The column designed in this work falls in this category if the gas flow is greater than 3 L/min (which it usually is). Below 3 L/min, the flow may be fully developed; so Equation 5-4 may be applicable. However, at these low flow rates, the values from Equation 5-4 are very similar to those from Equation 5-5 (within 15 to 20%).

Even though an analytical correlation for k_g exists, it is always important to calibrate the apparatus to see if it agrees with the model (Astarita et al., 1983). To obtain the expression that best correlates the experimental data, the general relationship (Equation 5-3) reported by Hobler (1966) was assumed. For the absorption experiments, the physical properties were never varied. Thus, the k_g is essentially only a function of the gas flow rate.

5.1.3 Results and discussion

The data used to obtain k_g are tabulated in Table 5.1.

Table 5.1 Data used to obtain gas film mass transfer coefficient

Q_L (mL/s)	G (L/min)	[OH] ⁻ (M)	Cl _{2,in} (ppm)	Cl _{2,o} (ppm)	Cl _{2,LM} (ppm)	N _{Cl2} (kmol/s)	$k_g A$ (mol/s-atm)	k_g (mol/s-atm-m ²)
2.26	1.18	0.25	21.9	1.9	8.2	1.64E-11	0.00200	0.186
2.26	2.14	0.25	23.9	5	12.1	2.81E-11	0.00232	0.215
2.26	1.16	0.25	270	22.2	99.2	2.00E-10	0.00201	0.186
2.26	2.8	0.25	144.5	31	73.7	2.21E-10	0.00299	0.277
2.26	1.18	0.25	21.9	1.75	8.0	1.65E-11	0.00207	0.192
2.26	2.14	0.25	23.7	4.86	11.9	2.80E-11	0.00235	0.218
2.26	1.18	0.25	21.6	1.79	8.0	1.62E-11	0.00204	0.189
2.26	2.14	0.25	23.7	4.42	11.5	2.87E-11	0.00250	0.231
2.26	1.16	0.25	280	23.2	103.1	2.07E-10	0.00201	0.186
2.26	1.18	0.25	21.9	1.71	7.9	1.65E-11	0.00209	0.194
2.26	1.18	0.25	21.6	1.75	7.9	1.63E-11	0.00206	0.191
4.3	1.18	0.25	21.6	1.1	6.9	1.68E-11	0.00244	0.226
2.26	2.14	0.25	23.7	4.48	11.5	2.86E-11	0.00248	0.229
2.26	2.14	0.25	23.7	4.15	11.2	2.91E-11	0.00259	0.240
4.3	2.14	0.25	23.7	3.92	11.0	2.94E-11	0.00267	0.248
4.3	1.16	0.25	280	18.5	96.2	2.11E-10	0.00219	0.203
2.26	2.14	0.25	23.7	4.3	11.4	2.88E-11	0.00254	0.235
4.3	2.14	0.25	23.6	3.7	10.7	2.96E-11	0.00275	0.255
2.26	2.14	0.25	23.8	3.91	11.0	2.96E-11	0.00268	0.249
2.26	2.14	0.25	23.75	4.36	11.4	2.88E-11	0.00252	0.233
2.26	4.78	0.25	23.5	7.28	13.8	5.38E-11	0.00389	0.360
2.26	4.78	0.25	23.5	7.06	13.7	5.46E-11	0.00399	0.370
2.26	4.78	0.25	23.5	7.09	13.7	5.45E-11	0.00398	0.368
2.26	4.78	0.25	23.5	6.89	13.5	5.51E-11	0.00407	0.377
2.26	4.78	0.25	23.7	6.5	13.3	5.71E-11	0.00429	0.398
2.26	2.14	1	23.8	4.35	11.4	2.89E-11	0.00253	0.234
2.26	2.14	1	23.8	4.5	11.6	2.87E-11	0.00248	0.229
2.26	2.14	1	23.8	4.21	11.3	2.91E-11	0.00257	0.238
2.26	2.14	1	23.8	4.07	11.2	2.93E-11	0.00262	0.243
2.26	4.78	0.25	23.5	7.1	13.7	5.44E-11	0.00397	0.368
2.26	4.78	0.25	23.5	7	13.6	5.48E-11	0.00402	0.372
2.26	4.78	0.25	23.5	6.8	13.5	5.54E-11	0.00412	0.381
2.26	4.78	0.25	76.8	20.7	42.8	1.86E-10	0.00435	0.403
2.26	4.78	0.25	76.8	20	42.2	1.89E-10	0.00447	0.414
2.26	4.78	0.25	76.4	20	42.1	1.87E-10	0.00445	0.412
2.26	4.78	0.25	76.4	19.1	41.3	1.90E-10	0.00460	0.426
2.26	4.78	0.25	76.4	20.7	42.7	1.85E-10	0.00433	0.401

2.26	9.52	0.25	45.5	14.6	27.2	2.04E-10	0.00751	0.696
2.26	9.52	0.25	45.5	14.2	26.9	2.07E-10	0.00770	0.713
2.26	4.78	0.25	76.2	20.96	42.8	1.83E-10	0.00428	0.397
2.26	4.78	0.25	76.2	20.5	42.4	1.85E-10	0.00436	0.404
2.26	4.78	0.25	76.6	20.5	42.6	1.86E-10	0.00438	0.405
4.3	4.78	0.25	76.2	15.8	38.4	2.00E-10	0.00522	0.484
2.26	9.52	0.25	45.5	14.7	27.3	2.04E-10	0.00747	0.692
2.26	9.52	0.25	45.5	14.25	26.9	2.07E-10	0.00768	0.711
2.26	9.52	0.25	45.6	14.7	27.3	2.04E-10	0.00748	0.693
2.26	9.52	0.25	45.6	14.25	27.0	2.07E-10	0.00769	0.712
2.26	9.52	0.25	23.6	7.7	14.2	1.05E-10	0.00740	0.686
2.26	9.52	0.25	23.8	7.4	14.0	1.08E-10	0.00772	0.715
2.26	9.52	0.25	23.6	7.6	14.1	1.06E-10	0.00749	0.694
2.26	9.52	0.25	24.2	8.5	15.0	1.04E-10	0.00692	0.641
2.26	9.52	0.25	24.2	8.36	14.9	1.05E-10	0.00703	0.651

The correlation developed was:

$$Sh = 0.82[ReSc(d/h)]^{0.64} \quad (5-6)$$

Figure 5.1 depicts the above correlation and the data for obtaining k_g . Only values at a liquid flow rate of 2.26 mL/s were used to correlate k_g . At the higher flow of 4.3 mL/s, gas bubbles were drawn through the liquid outlet, and the chlorine outlet concentration sometimes fluctuated. These effects resulted in greater absorption.

The experiments using 1 M NaOH yielded the same result as those in 0.25 M NaOH. Since the 1 M NaOH did not result in additional absorption, complete gas film control was confirmed. The absorption was limited by the rate of chlorine diffusion in the gas phase, not by the Cl_2/OH reaction kinetics.

The data in Table 5.1 show that the percent chlorine removal increases with decreasing gas flow rate. This result occurs because at the lower flow, the gas has more contact with the absorbing solution. At a typical gas flow of 5 to 10 L/min, the maximum chlorine removal that can occur in the wetted wall column (resulting from complete gas film control) is 70%. At a flow rate of 1.2 L/min, the maximum chlorine removal is 91%.

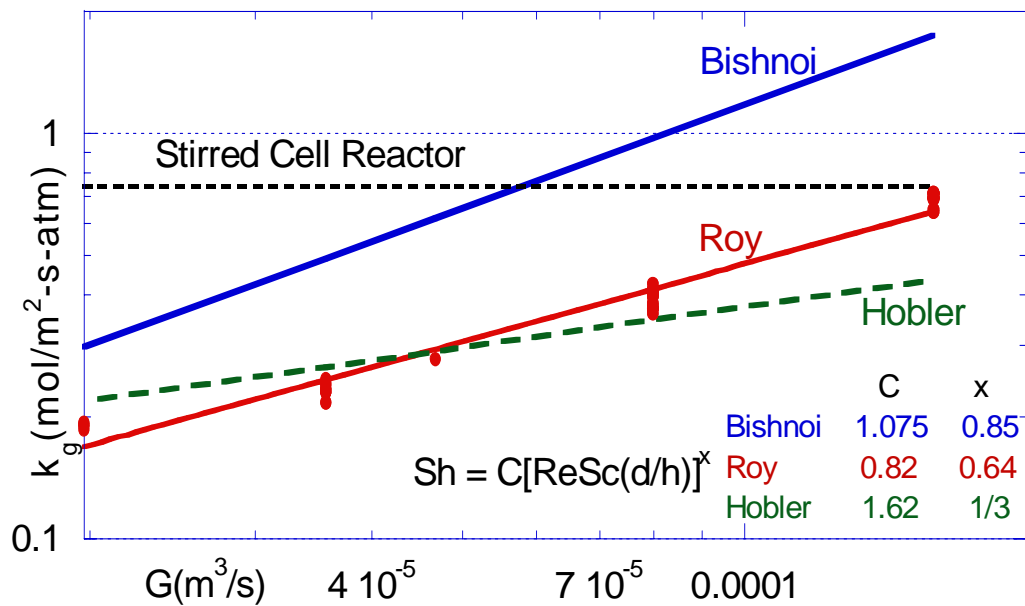


Figure 5.1. Correlations for gas film mass transfer coefficient in wetted wall

The gas film mass transfer coefficient increases with gas flow rate. At a typical gas flow from 5 to 10 L/min, the k_g ranged from 0.4 to 0.7 mol/s-atm-m². Figure 5.1 also shows correlations obtained by other researchers, as well as a typical k_g value from the stirred cell reactor. Only at high flow rates (10 L/min) does the wetted wall k_g equal the stirred cell k_g . The scatter in the data occurs because of modifications made throughout the experiments. Changes in gas flow path and liquid level probably resulted in the minor deviations.

The Hobler relationship, Equation 5-5, is closest to the correlation developed in this work. The small discrepancies probably result from the fact that the column geometry is slightly different than a simple tube.

The results obtained by Bishnoi (2000) are much higher. The column used in his work had a very different geometry and flow path. The liquid solution flowed along the outside of the tube (instead of wetting the inside). The gas entered the column through a small opening. Upon entering the column, the gas velocity

suddenly decreased (due to increase in diameter) as the gas entered the annulus. These end effects may result in a higher absorption rate, leading to higher values for k_g . Also, the column that Bishnoi used was a short (9.1 cm) column; scaling up his empirical correlation to a column, which is three times taller, may not be valid.

This section has detailed the measurement of the gas film mass transfer coefficient for Cl_2 . In order to model Hg absorption, the gas film mass transfer coefficient for Hg ($k_{g,\text{Hg}}$) must be determined. From looking at Equation 5-6, the gas film mass transfer coefficient depends on geometry, diffusivity, density, and viscosity. The addition of Hg does not affect the density or viscosity of the gas. Furthermore, the geometry does not change for the Hg absorption experiments. Therefore, the difference in k_g should only be related to the difference in diffusivities.

The diffusivity of Cl_2 through N_2 was calculated using the Chapman and Enskog equation (Hines and Maddox, 1985; Hirschfelder et al., 1954) to be $0.123 \text{ cm}^2/\text{s}$. Detailed calculations are in Appendix E. The diffusivity of Hg through N_2 was calculated to be $0.13 \text{ cm}^2/\text{s}$, and this value was verified by other sources (Zhao, 1997; Mullaly and Jacques, 1924; Spier, 1940; Nakayama, 1968). Since the diffusivities are essentially the same value (ratio of 1.057), the gas film mass transfer coefficient is assumed to be the same for Hg as that for Cl_2 .

5.2 LIQUID FILM MASS TRANSFER COEFFICIENT

The physical liquid phase mass transfer coefficient was obtained by measuring chlorine desorption from hypochlorous acid (HOCl) solution in 0.1 M HCl at ambient temperature. The chlorine formation resulted from the following reaction:



At low pH and high chloride, the formation of chlorine is favored.

5.2.1 Experimental method

In a typical experiment, sodium hypochlorite (NaOCl) was injected into the 700 mL plexiglass reservoir, which contained 0.1 M HCl. The total volume of liquid circulating through the system was approximately 750 mL. At a flow rate of either 5 or 10 L/min, nitrogen gas flowed over the solution, desorbing chlorine. Throughout an experiment, more NaOCl was injected as necessary. The chlorine was analyzed using the IMS analyzer. Due to the narrow range of liquid operating rates, the liquid flow could not be varied much. The typical flow was 2.26 mL/s.

5.2.2 Theory

The liquid film mass transfer coefficient can be determined by correlating the chlorine concentration as a function of time. Liquid phase mass balance gives:

$$V \frac{dC_{Cl_2}}{dt} = -k_{L,Cl_2}^o A (C_{Cl_2,b} - C_{Cl_2,i}) \quad (5-8)$$

With excess gas, the chlorine at the interface is negligible compared to the chlorine in the bulk liquid. Thus, the mass balance in Equation 5-8 can be simplified and rearranged to yield:

$$\frac{dC_{Cl_2}}{C_{Cl_2,b}} = -\frac{k_{L,Cl_2}^o A}{V} dt \quad (5-9)$$

Integrating the above differential equation results in:

$$C_{Cl_2,b} = C_{Cl_2,init} \exp\left(-\frac{k_{L,Cl_2}^o A}{V} t\right) \quad (5-10)$$

Since the gas phase flux equals the liquid phase flux:

$$\frac{G(P_{Cl_2,out} - P_{Cl_2,in})}{RT} = k_{L,Cl_2}^o A (C_{Cl_2,b} - C_{Cl_2,i}) \quad (5-11)$$

Since there is no chlorine in the entering gas, $P_{Cl_2,in} = 0$, and since the interfacial chlorine concentration is much less than the bulk chlorine concentration:

$$P_{Cl_2,out} = \frac{RT}{G} k_{L,Cl_2}^o A C_{Cl_2,b} \quad (5-12)$$

Combining the gas balance with the liquid balance and taking natural logarithms results in:

$$\ln P_{Cl_2,out} = \ln \left(\frac{RT C_{Cl_2,init} k_{L,Cl_2}^o A}{G} \right) - \frac{k_{L,Cl_2}^o A}{V} t \quad (5-13)$$

Therefore, from a plot of $\ln P_{Cl_2,out}$ vs time, the liquid film mass transfer coefficient can be extracted from the slope.

The measured physical liquid film mass transfer coefficient can be analyzed using a fundamental model developed by Pigford (1941). Pacheco (1998) found that this model predicted the experimental data within 15%. This method relies on solving the continuity equation for diffusion into a falling liquid film. The model assumes a parabolic velocity profile in the liquid phase and a uniform concentration of the diffusing species at the gas/liquid interface (Pacheco, 1998).

The mass transfer coefficient is given as a function of the parameter $\eta = D\tau/\delta^2$, where τ is the surface contact time calculated from the surface velocity and the height of the contactor (h/u_{surf}) and δ is the film thickness calculated by Equation 5-16. For the diffusing gas A, this model leads to the following expressions.

$$\Theta = \frac{[A]_i^L - [A]_o^{L,out}}{[A]_i^L - [A]_o^{L,in}} = 0.7857 \exp(-5.121\eta) + 0.1001 \exp(-39.21\eta) + 0.036 \exp(-105.6\eta) + 0.0181 \exp(-204.7\eta) \quad \text{for } \eta > 0.01 \quad (5-14)$$

$$\Theta = \frac{[A]_i^L - [A]_o^{L,out}}{[A]_i^L - [A]_o^{L,in}} = 1 - 3\sqrt{\frac{\eta}{\pi}} \quad \text{for } \eta < 0.01 \quad (5-15)$$

The film thickness and the velocity at the surface of the liquid are determined by solving the momentum balance for a falling film (Bird et al., 1960), where W is the wetted perimeter length.

$$\delta = \sqrt[3]{\frac{3\rho_L Q}{\mu_L g W}} \quad (5-16)$$

$$u_{\text{surf}} = \frac{\rho_L g \delta^2}{2\mu_L} \quad (5-17)$$

The mass transfer coefficient is then obtained by Equation 5-18.

$$k_{L,A}^o = \frac{Q_L}{A}(1 - \Theta) \quad (5-18)$$

For this work, η was always less than 0.01; therefore, Equation 5-15 was used. Using Equation 5-15, the model is equivalent to the expression derived using penetration theory to calculate the liquid film mass transfer coefficient in the laminar flow regime.

5.2.3 Results and discussion

The raw data are tabulated in Appendix F, along with figures showing the best-fit lines. The slopes from these lines was used to calculate the liquid film mass transfer coefficient, as shown in Equation 5-13. Table 5.2 summarizes the calculated k_{L,Cl_2}^o values.

Table 5.2 Liquid film mass transfer coefficients

Q_L (mL/s)	k_{L,Cl_2}^o (cm/s)
2.26	0.00931
2.26	0.00895
2.26	0.00986
2.26	0.00972
2.26	0.00922
2.26	0.00844
2.26	0.00868
2.96	0.0110

At a flow rate of 2.26 mL/s, the k_{L,Cl_2}^o values range from 0.0084 to 0.0099 cm/s, with an average value of 0.009 cm/s. The k_{L,Cl_2}^o value is higher than the stirred cell value of 0.0024 cm/s. The k_{L,Cl_2}^o value is similar to values typical of wetted wall columns, 0.005 to 0.02 cm/s (Astarita et al., 1983). Therefore, we were successful in constructing a column that had a k_{L,Cl_2}^o value similar to the values in short columns.

The liquid film mass transfer coefficient increases with liquid flow rate. However, the liquid flow rate could not be varied over a wide range in the wetted wall column. At lower flow rates, the column was not fully wetted. At much higher flow rates, bubbles entered the liquid lines. The average value at 2.26 mL/s and the value at 2.96 mL/s are within 15% of the model prediction. Therefore, it was concluded that the value obtained experimentally was valid. Practically, a more precise value is not needed since the absorption in S(IV) experiments are not very sensitive to the liquid film mass transfer coefficient.

In order to calculate the $S(IV)$ at the interface, the liquid film mass transfer coefficient for $S(IV)$ was needed. The value for chlorine was converted to a value for $S(IV)$ by correcting for the diffusion coefficients:

$$k_{L,S(IV)}^o = k_{L,Cl_2}^o \sqrt{\frac{D_{S(IV)}}{D_{Cl_2}}} \quad (5-19)$$

The diffusivity for $S(IV)$ through water was taken to be $1.33 \times 10^{-9} \text{ m}^2/\text{s}$ (Chang, 1979). Applying this correction resulted in a typical value of 0.0085 cm/s .

5.3 GAS/LIQUID CONTACT AREA

5.3.1 Basis and rationale

The area of the column was experimentally determined by absorbing carbon dioxide into sodium hydroxide solutions. For simple wetted wall columns, the gas/liquid contact area is given by the geometric surface area. However, in the column used in this work, the space in between sections may result in a greater area.

Also, ripples in the liquid may result in a greater gas/liquid contact area. At a typical flow of 2.26 mL/s , the Reynolds number of the film is 333. When the Reynolds number is between 25 and 1000, the flow is characterized as laminar with ripples. During an experiment, the top three sections of the column were observed to not have any ripples. However, some rippling was seen in the bottom sections. Therefore, it was decided to verify the area experimentally.

5.3.2 Experimental method

Carbon dioxide (CO_2) was absorbed into 0.1 M and 0.5 M NaOH at ambient temperature and pressure. The 700 mL plexiglass reservoir was used for these experiments, and the liquid solution flow path was identical to that discussed previously. The liquid flow was 2.26 mL/s .

Gas feed was prepared by quantitatively mixing 0.5% CO₂ (5000 ppm CO₂ in N₂) with pure N₂. The gas flow path is similar to that shown in Figure 4.6, except that the Cl₂ was replaced by CO₂. Also, the gas was not diluted after exiting the column, and there was no vent before the analyzer. Thus, all of the gas that entered the column went to the CO₂ analyzer. The gas flow rate to the column was varied from 1 to 5 L/min, and the CO₂ inlet concentration was varied from 200 to 550 ppm.

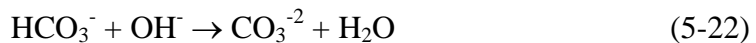
After exiting the column, the gas went through a 125-mL Erlenmeyer flask immersed in an ice bath before entering the CO₂ analyzer (Horiba PIR-2000). The analyzer used infrared spectroscopy to continuously measure the CO₂ concentration. The lowest range of the analyzer, 0 to 0.05% (500 ppm), was used, with an output of 0 to 1 V. The analyzer had excellent repeatability (no drift) and response times. Since the analyzer response was quadratic, a 6-point (plus zero) calibration was usually conducted. Dry and wet gas calibrations resulted in the same CO₂ signal.

5.3.3 Theory

Since the kinetics of the CO₂/OH reaction are well known, the area can be calculated from absorption data using the model for mass transfer with chemical reaction. The model is analogous to Equations 3-4 and 3-14.

$$N_{\text{CO}_2} = \frac{A P_{\text{CO}_2 i}}{H_{\text{CO}_2}} \sqrt{D_{\text{CO}_2} k_2 [\text{OH}^-]_i} \quad (5-20)$$

At high pH, the CO₂/OH reaction can be written as (Dankwerts, 1970):



The second reaction is instantaneous; thus, the overall reaction rate is given by the reaction rate for the first step (Dankwerts, 1970; Pinsent et al., 1956):

$$\log k_2 (\text{L/mol} \cdot \text{s}) = 13.635 - \frac{2895}{T(\text{K})} \quad (5-23)$$

The rate constant was corrected for ionic strength (I) by Astarita et al. (1983).

$$\log k_{\text{corr}} = \log k_2 + 0.08I \quad (5-24)$$

The Henry's law constant and the diffusion coefficient for CO₂/H₂O were obtained from Bishnoi (2000).

$$H_{\text{CO}_2} (\text{atm} \cdot \text{L/mol}) = 17107 \exp\left(\frac{-1886.1}{T(\text{K})}\right) \quad (5-25)$$

$$D_{\text{CO}_2} (\text{cm}^2/\text{s}) = 0.024 \exp\left(\frac{-2122}{T(\text{K})}\right) \quad (5-26)$$

These values also need to be corrected for ionic strength. The correction for the Henry's law constant is (Dankwerts, 1970; Pohorecki and Moniuk, 1987):

$$\log\left(\frac{H}{H_o}\right) = -SI \quad (5-27)$$

The parameter S consists of contributions of the ions and the gas:

$$S = h_{\text{Na}} + h_{\text{OH}} + h_{\text{CO}_2} = 0.091 + 0.066 - 0.019 = 0.138 \quad (5-28)$$

The viscosity (μ) correction was applied to the diffusivity. Viscosities for the sodium hydroxide solutions were obtained from the Lide (2000).

$$D_2 = \frac{D_1 \mu_1}{\mu_2} \quad (5-29)$$

After the physical properties and rate constant were corrected for ionic strength, they were used, along with the absorption data, to calculate the area as shown in Equation 5-20.

5.3.4 Results and discussion

Table 5.3 tabulates the data.

Table 5.3. Data used to calculate area

T (K)	D _{CO2} (m ² /s)	H _{CO2} (atm/M)	k ₂ (L/mol-s)	k _{corr} (L/mol-s)	G (L/min)	[OH] ⁻ (M)	CO _{2,in} (ppm)	CO _{2,o} (ppm)	N _{CO2} (kmol/s)	A (m ²)
294	1.715E-09	27.12	6138	6253	2.18	0.1	236.5	183.7	7.993E-11	0.0117
294	1.715E-09	27.12	6138	6253	2.18	0.1	236.5	183	8.099E-11	0.0119
294	1.715E-09	27.12	6138	6253	2.18	0.1	236	183	8.024E-11	0.0118
296.2	1.809E-09	28.44	7264	7399	1.29	0.1	399	261.6	1.231E-10	0.0113
296.2	1.809E-09	28.44	7264	7399	1.29	0.1	399	263.8	1.211E-10	0.0111
296.2	1.809E-09	28.44	7264	7399	1.29	0.1	398.2	263.8	1.204E-10	0.0110
296.2	1.809E-09	28.44	7264	7399	1.29	0.1	399	260	1.245E-10	0.0115
296.2	1.809E-09	28.44	7264	7399	1.29	0.1	311	203.5	9.63E-11	0.0114
296.2	1.809E-09	28.44	7264	7399	1.29	0.1	311	205.5	9.451E-11	0.0111
296.2	1.809E-09	28.44	7264	7399	1.29	0.1	312	203.5	9.72E-11	0.0115
296.2	1.809E-09	28.44	7264	7399	1.29	0.1	311	205.5	9.451E-11	0.0111
295.8	1.792E-09	28.20	7047	7178	4.77	0.1	547	479	2.253E-10	0.0121
295.8	1.792E-09	28.20	7047	7178	4.77	0.1	539	474	2.153E-10	0.0117
295.8	1.792E-09	28.20	7047	7178	4.77	0.1	541	474	2.219E-10	0.0121
295.8	1.792E-09	28.20	7047	7178	4.77	0.1	299	263.9	1.163E-10	0.0113
295.8	1.792E-09	28.20	7047	7178	4.77	0.1	305	264	1.358E-10	0.0133
295.8	1.792E-09	28.20	7047	7178	4.79	0.1	206.5	181.2	8.407E-11	0.0120
293.9	1.579E-09	23.83	6091	6679	1.29	0.5	399	193	1.845E-10	0.0098
293.9	1.579E-09	23.83	6091	6679	1.29	0.5	400.6	193.4	1.856E-10	0.0098
293.9	1.579E-09	23.83	6091	6679	1.29	0.5	311	149.6	1.446E-10	0.0099
293.9	1.579E-09	23.83	6091	6679	1.29	0.5	309.2	149.6	1.43E-10	0.0098
293.9	1.579E-09	23.83	6091	6679	1.29	0.5	312	149.6	1.455E-10	0.0100
295.4	1.638E-09	24.62	6835	7494	2.18	0.5	236	150	1.302E-10	0.0092
295.4	1.638E-09	24.62	6835	7494	2.18	0.5	237.5	150.4	1.319E-10	0.0093
295.4	1.638E-09	24.62	6835	7494	2.18	0.5	236	149.1	1.316E-10	0.0094
295.5	1.642E-09	24.67	6887	7552	4.77	0.5	540	423.6	3.856E-10	0.0097
295.5	1.642E-09	24.67	6887	7552	4.77	0.5	537	423.6	3.756E-10	0.0095
295.5	1.642E-09	24.67	6887	7552	4.77	0.5	300	233	2.219E-10	0.0102
295.5	1.642E-09	24.67	6887	7552	4.77	0.5	299.2	232.8	2.2E-10	0.0101
295.5	1.642E-09	24.67	6887	7552	4.77	0.5	301.4	232.8	2.272E-10	0.0105

Table 5.3 shows that the data at 0.5 M NaOH yield a lower area than the data at 0.1 M. The average area using the 0.5 M data is $98 \pm 4 \text{ cm}^2$, while the average area using the 0.1 M data is $116 \pm 6 \text{ cm}^2$. At higher ionic strength, the solution is more

viscous. The more viscous solution could result in less ripples and more stable flow, which would lower the area. However, the viscosity change is too small (1.112 cp compared to 1.027 cp at 0.1 M NaOH) to account for this big a change. The calculated film thickness is not much different either. Also, from observing the fluid flow during experiments, there did not seem to be any differences in the fluid mechanics. Therefore, it seems unlikely that the gas/liquid contact area would vary with ionic strength.

The difference in the area calculations at the two NaOH concentrations could arise from the ionic strength corrections. For the 0.1 M NaOH data, the ionic strength corrections only have minor effects. The corrections are greater for the 0.5 M NaOH data, especially the Henry's law constant correction, which results in a 15% decrease in the calculated area. The ionic strength corrections resulted from other researchers varying ionic strength over a wide range, assuming all other factors are constant, and correlating the new rate with the ionic strength. Perhaps, the correlations over-correct for the small change in concentration that occurs in these experiments.

If an average is taken of all of the data, the area is $108 \pm 10 \text{ cm}^2$. Figure 5.2 plots the data. The lines represent the flux calculated from Equation 5-15 using the average area of 108 cm^2 .

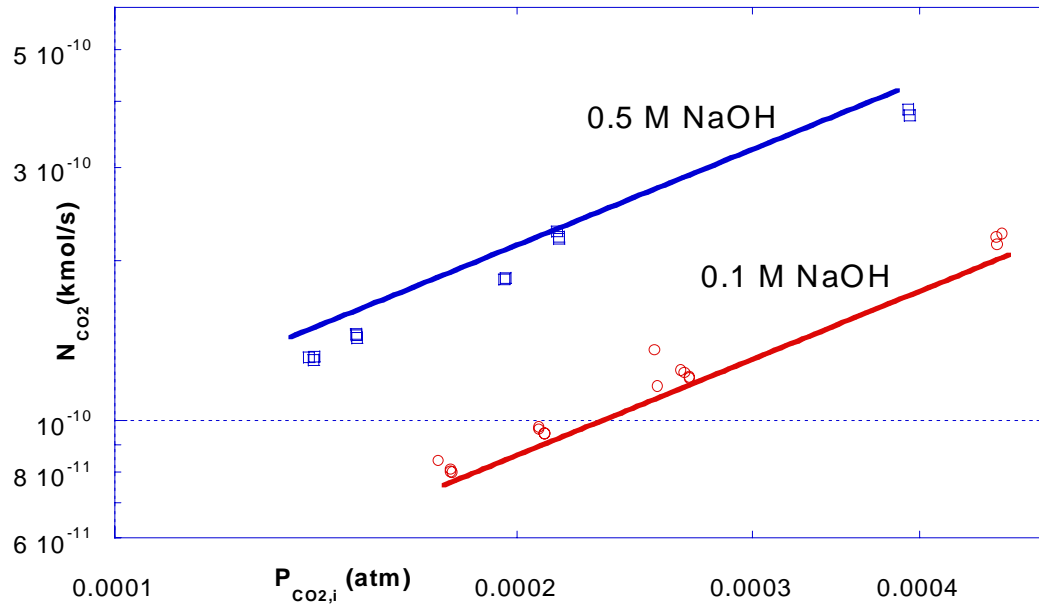


Figure 5.2 Obtaining area of wetted wall column

The area for the wetted wall column is slightly greater than the stirred cell area of 81 cm^2 . The area is also slightly greater than the geometric surface area of the column, which is approximately 102 cm^2 . The value for the area used for all calculations was 108 cm^2 .

Chapter 6: Chlorine Absorption in Stirred Cell Reactor

This chapter presents the results of the chlorine absorption experiments conducted in the stirred cell reactor at ambient temperature. All of the solutions were buffered at a pH of approximately 4.5, except for the preliminary data discussed in Section 6.6. The enhancement of the chlorine hydrolysis rate by the succinate buffer was quantified at this pH. Chlorine was absorbed into buffered S(IV) solutions to obtain kinetic data. The effects of adding oxygen to the inlet gas and adding chloride to the solution were investigated. Model predictions on mercury removal in a typical limestone slurry scrubber are also discussed in this chapter.

6.1 APPROXIMATE REACTION RATE FOR CHLORINE WITH S(IV) AT pH 4.5

The rate constant for the reaction of Cl_2 with S(IV) was too rapid to be precisely measured using the existing stirred cell reactor, due to mass transfer limitations. However, an order of magnitude estimate of the rate constant is feasible using the data discussed in this section. The data were modeled using Equation 3-9.

6.1.1 *Experimental method*

The absorption of chlorine into buffered S(IV) solutions was measured in the stirred cell reactor. The chlorine was analyzed using the IMS analyzer. The gas flow rate to the reactor was approximately 1.2 L/min. The gas and liquid agitation speeds ranged from 700 to 740 rpm. During an experiment, the absorption of chlorine into the buffer was first measured. After this measurement, the experiments consisted of 1) injecting S(IV) into the reactor, 2) withdrawing samples for analysis as the S(IV) was depleted, 3) injecting more S(IV) and analyzing samples. Throughout a single experimental series, the chlorine inlet concentration was usually kept constant.

Throughout all the experiments, the chlorine inlet ranged from 21 to 276 ppm. For the experiments containing oxygen (O₂), the chlorine was diluted with house air (instead of pure N₂), before entering the reactor.

6.1.2 Tabulated results

The data discussed in this section are tabulated in the following tables. Each series represents data obtained in a single day, collected over the course of 5 to 6 hours. The points are listed in chronological order. Table 6.1 displays the first data set, including data with oxygen. Most of the data with oxygen were at high S(IV) concentrations in order to quantify S(IV) oxidation rates and see if chlorine catalyzes S(IV) oxidation. These data are discussed in more detail in Section 6.4. Table 6.2 displays the final set of chlorine absorption data in 50 mM buffer (50 mM succinic acid-50 mM NaOH), and Table 6.3 displays chlorine absorption data in 5mM (5mM succinic acid-5mM NaOH) buffer.

Table 6.1. Chlorine and oxygen absorption with variable S(IV) at pH 4.5 in 50 mM succinate buffer with 1.15 L/min gas and at n_g/n_L of 700 to 730 rpm

Series	[S(IV)] _{bulk} (mM)	Cl _{2,in} (ppm)	Cl _{2,out} (ppm)	N _{Cl2} (kmol/m ² -s)	O ₂ (%)
A	0*	276	235	4.09E-09	0
	0*	276	242	3.37E-09	0
	0	276	150	1.26E-08	0
	1.15	276	94.6	1.82E-08	0
	0.78	129	21.6	1.10E-08	0
	0.634	21	2.5	1.93E-09	0
	4	276	33.8	2.43E-08	0
	4	129	10.8	1.21E-08	0
	4	129	13.2	1.19E-08	0
	4	21	0.33	2.14E-09	0
B	0*	276	225	5.10E-09	0
	0*	276	236	3.99E-09	0
	0	276	151	1.25E-08	0
	3.85	276	34.5	2.42E-08	0
	2.44	276	39.3	2.37E-08	0

	1.86	276	39.7	2.37E-08	0
C	0	276	149	1.27E-08	0
	5.04	276	37.5	2.39E-08	0
	3	276	38.5	2.38E-08	0
	1.74	276	43.7	2.33E-08	0
D	0*	21	15.6	5.46E-10	0
	0*	21	17	4.05E-10	0
	0	21	8.3	1.28E-09	0
	5	21.2	1.3	2.01E-09	0
E	0	264	134	1.26E-08	14.5
	4.43	264	32.7	2.24E-08	14.5
	3.83	264	28	2.29E-08	14.5
	3.22	264	31.7	2.25E-08	14.5
	2.02	264	39	2.18E-08	14.5
	1.37	264	41.9	2.15E-08	14.5
	0.664	264	116	1.44E-08	14.5
	0.35	264	159	1.02E-08	14.5
F	0	21	8.1	1.31E-09	0
G	0	21.2	8	1.33E-09	0
	0.26	21.2	3.8	1.76E-09	0
	0.176	21.2	4.7	1.66E-09	0
	1.08	21.2	2.2	1.92E-09	0
	1.05	21.2	2.04	1.93E-09	0
	1.02	21.2	2.15	1.92E-09	0
	3.74	21.2	0.9	2.05E-09	0
	3.44	21.2	1.2	2.02E-09	0
	3.43	21.2	1	2.04E-09	0
	3.59	21.2	1	2.04E-09	0
H	0	21.2	7.9	1.34E-09	20.5
	0.519	21.2	2.99	1.84E-09	20.5
	0.336	21.2	3.6	1.78E-09	20.5
	0.18	21.2	4.3	1.70E-09	20.5
	1.56	21.2	1.5	1.99E-09	20.5
	1.18	21.2	1.9	1.95E-09	20.5
	0.642	21.2	2.5	1.89E-09	20.5
	4.74	21.2	0.8	2.06E-09	20.5
	4.23	21.2	0.94	2.04E-09	20.5
	3.88	21.2	1	2.04E-09	20.5

* not buffered; absorption in pure water

Table 6.2. Chlorine absorption in S(IV) at pH 4.5 in 50 mM succinate buffer with 1.15 L/min gas and at n_g/n_L of 700 to 730 rpm

Series	[S(IV)] _{bulk} (mM)	Cl _{2,in} (ppm)	Cl _{2,out} (ppm)	N _{Cl2} (kmol/m ² -s)
A	0	263.9	134.1	1.26E-08
	0	263.9	142.3	1.18E-08
	0.38	263.9	154.0	1.06E-08
	0.169	263.9	163.5	9.73E-09
	0.59	263.9	131.2	1.29E-08
	0.334	263.9	171.7	8.93E-09
	0.208	263.9	178.2	8.30E-09
	1.56	263.9	43.3	2.14E-08
	1.22	263.9	49.8	2.07E-08
	4.95	263.9	29.9	2.27E-08
	10	263.9	23.0	2.33E-08
B	0	21.2	4.35	1.70E-09
	0	21.2	4.89	1.65E-09
	0.182	21.2	3.67	1.77E-09
	0.075	21.2	7.75	1.36E-09
	0.276	21.2	3.84	1.75E-09
	0.178	21.2	4.62	1.67E-09
	1.38	21.2	2	1.94E-09
	1.32	21.2	2	1.94E-09
	5.23	21.2	0.7	2.07E-09
	10	21.2	0.3	2.11E-09
C	0	263.9	132.5	1.27E-08
	0	263.9	142.2	1.18E-08
	0.27	263.9	153.5	1.07E-08
	0	263.9	163.5	9.73E-09
	0.61	263.9	125.0	1.35E-08
	0.437	263.9	160.0	1.01E-08
	1.25	263.9	46.5	2.11E-08
	0.74	263.9	94.7	1.64E-08
	4.7	263.9	32.0	2.25E-08
	10	263.9	24.9	2.32E-08
D	0	21.2	7.25	1.41E-09
	0.183	21.2	4.24	1.71E-09
	0.098	21.2	6.68	1.46E-09
	0.26	21.2	3.83	1.75E-09
	0.128	21.2	5.69	1.56E-09
	1.43	21.2	2.2	1.92E-09
	1.39	21.2	2.2	1.92E-09
	5.45	21.2	0.6	2.08E-09

Table 6.3. Chlorine absorption in S(IV) at pH 4.5 in 5 mM succinate buffer with 1.18 L/min gas and at n_g/n_L of 745 rpm

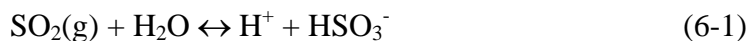
Series	[S(IV)] _{bulk} (mM)	Cl _{2,in} (ppm)	Cl _{2,out} (ppm)	N _{Cl₂} (kmol/m ² -s)
E	0	21.2	12.9	8.39E-10
	0.213	21.2	4.33	1.70E-09
	0.155	21.2	5.51	1.58E-09
	0.103	21.2	8.88	1.24E-09
	0.089	21.2	13.6	7.63E-10
	1.48	21.2	2.23	1.91E-09
F	0	21.2	13.0	8.21E-10
	0.117	21.2	7.49	1.38E-09
	0.076	21.2	11.6	9.66E-10
	0.064	21.2	13.51	7.73E-10
	0.06	21.2	15.1	6.17E-10
	0.15	21.2	6.09	1.52E-09
	0.12	21.2	9.26	1.20E-09

6.1.3 Discussion

Figure 6.1 depicts the chlorine flux as a function of the bulk S(IV) concentration. Data at two chlorine inlet concentrations of 265 ppm (actually 264 to 276 ppm as shown in Tables 6.1 and 6.2) and 21 ppm are shown. The points at 0.01 mM S(IV) are actually in succinate buffer with no S(IV). The inverted triangles in Figure 6.1 represent points in which oxygen was added to the inlet gas. All the data are in 50 mM succinate buffer except for the points represented by the squares with diagonal lines which are in 5 mM buffer.

At low pH and high S(IV), SO₂(g) production occurs. Therefore, data in experiments with greater than 5 mM S(IV) for the 265 ppm inlet and greater than 1 mM S(IV) for the 21 ppm inlet were discarded because SO₂ was stripped from the reactor and reacted with Cl₂ on the damp surfaces of downstream equipment. The

additional chlorine removal is due to the increased levels of gaseous SO₂, which forms at high S(IV) concentrations, in the reactor:



At pH 4.5, 5 mM S(IV) results in generation of about 70 ppm SO₂. Therefore, the existing stirred cell contactor cannot be used for experiments at high S(IV)/low pH since SO₂ would form inside the reactor.

The curves are calculated using Equation 3-9. The gas flow rate (1.18 L/min) and mass transfer coefficients used in the model were representative of the experimental data. The gas and liquid phase mass transfer coefficients (k_g and $k_{L,S(IV)}^o$) in the model were 0.75 mol/s-atm-m² and 2.45 x 10⁻⁵ m/s, respectively. The rate constant of the chlorine/S(IV) reaction ($k_{2,S(IV)}$) was chosen to best fit the data. The buffer rate constant was obtained by measuring chlorine absorption as a function of buffer concentration; these results will be detailed in Section 6.3.

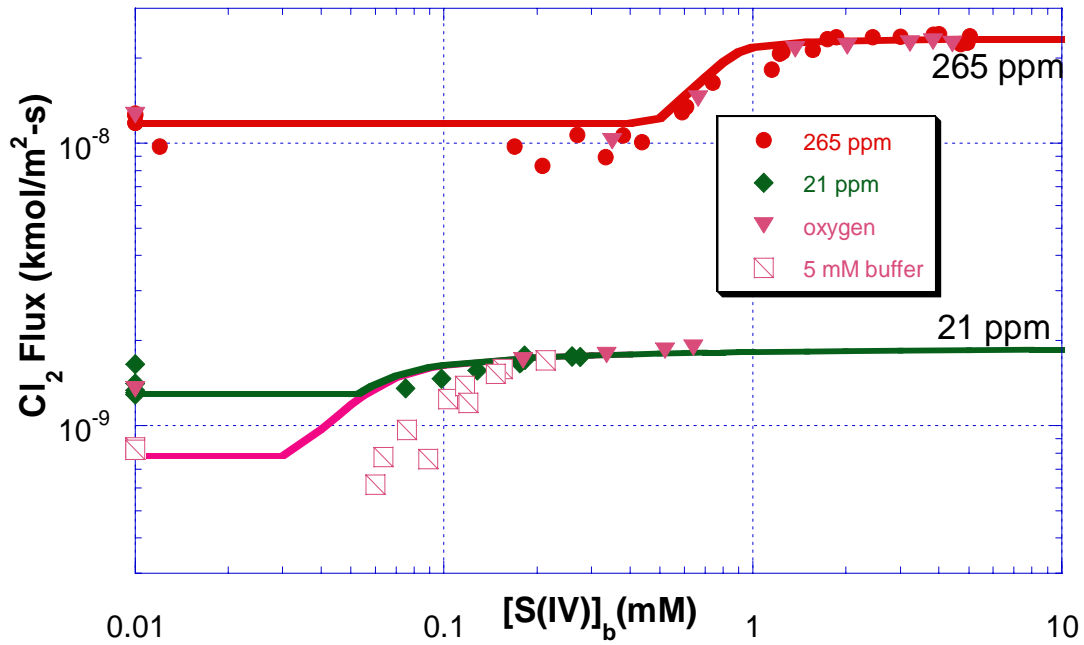


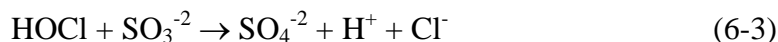
Figure 6.1. Chlorine absorption in buffered S(IV) in stirred cell reactor, $k_{2,S(IV)} = 2 \times 10^9 \text{ L/mol-s}$

Figure 6.1 shows that at high S(IV), the chlorine flux does not depend on the S(IV) concentration since the limit of gas film resistance is approached. At lower chlorine concentrations, gas film control is achieved at lower S(IV) since it takes less S(IV) to react with the chlorine.

Figure 6.1 also shows that at low S(IV), the flux is limited (in some cases inhibited) by the buffer-enhanced chlorine hydrolysis reaction. In this region, the flux depends mainly on the buffer reaction rate. However, the data show that when very little S(IV) was injected, the chlorine flux was less than what it was initially in buffer alone. Thus, S(IV) inhibited chlorine absorption at very low S(IV) concentrations. At a chlorine concentration of 265 ppm and S(IV) concentration of 0.5 mM, the flux was equivalent to the flux in buffer alone. When the S(IV) concentration was lower, the flux was lower than what it was initially without S(IV). As the S(IV) increased,

the chlorine flux increased until the gas film limit was reached. At the low inlet chlorine of 21 ppm, when the S(IV) concentration was 0.06 mM, the chlorine flux was the same as the flux in buffer alone. At lower concentrations, the flux is lower, and thus, the reaction seems to be inhibited by a little S(IV) but enhanced by greater amounts of S(IV).

Since Fogelman et al. (1989) have shown that HOCl reacts with sulfite, one possible mechanism for chlorine reaction with S(IV) is that the chlorine first hydrolyzes in water to form HOCl, and then the HOCl (not Cl₂ directly) reacts with S(IV). These overall reactions are shown below:



If this were the case, the rate of chlorine absorption in S(IV) would be equivalent to the rate of chlorine hydrolysis to form HOCl since chlorine hydrolysis is the rate limiting step. Then, the HOCl would react with S(IV). However, since the addition of S(IV) results in a greater chlorine removal rate than the chlorine hydrolysis rate, it must not depend on HOCl formation. Thus, chlorine itself reacts with S(IV) directly, and it is not necessary for HOCl to form before chlorine reaction with S(IV) occurs.

In the intermediate region of Figure 6.1, the flux is limited by S(IV) diffusion to the interface (depicted by flux increasing linearly with S(IV)) and/or kinetics (depicted by curvature). There is only a very small range (depicted by curvature) where the chlorine flux should be limited by the kinetics of the Cl₂/S(IV) reaction. Looking at the 265 ppm curve, the range of kinetics-limited data would be from 0.8 to 1.2 mM S(IV). For the 21 ppm inlet, the range is from 0.07 to 0.1 mM S(IV). Thus, it is hard to extract a precise rate constant from the data since most of the data falls in a region where the chlorine absorption is not limited by kinetics.

Even though it was difficult to obtain a precise value for the rate constant, an approximate value can be determined. Figures 6.2 to 6.4 illustrate with greater precision the extraction of a rate constant from the intermediate range of the data. The chlorine penetration ($Cl_{2,out}/Cl_{2,in}$) is shown as a function of the ratio of the dissolved S(IV) and the chlorine inlet partial pressure ($[S(IV)]_{bulk}/P_{Cl2,in}$). The model curves were calculated with various values of the rate constant. Figures 6.2 to 6.4 plot the same data (without separately labeling the points with oxygen) and use the same model (with different values for $k_{2,S(IV)}$) as in Figure 6.1.

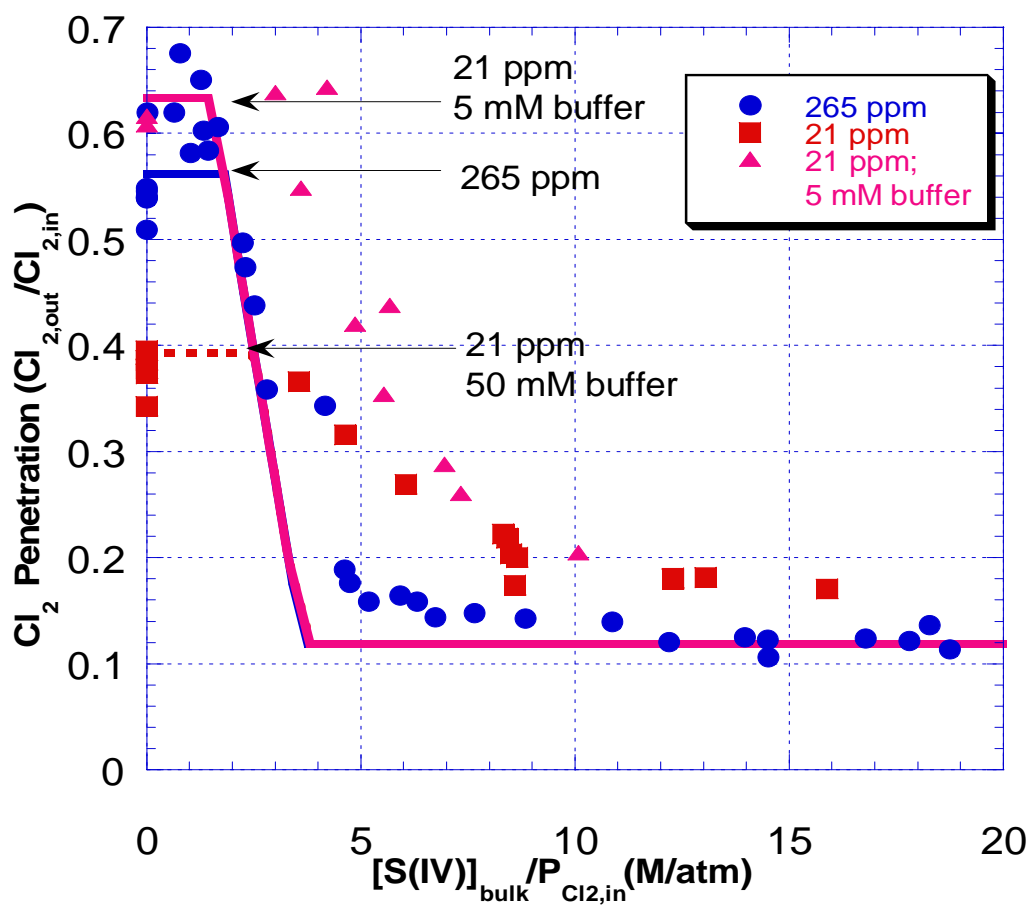


Figure 6.2. Chlorine penetration in buffered S(IV) in stirred cell, $k_{2,S(IV)} = 6$

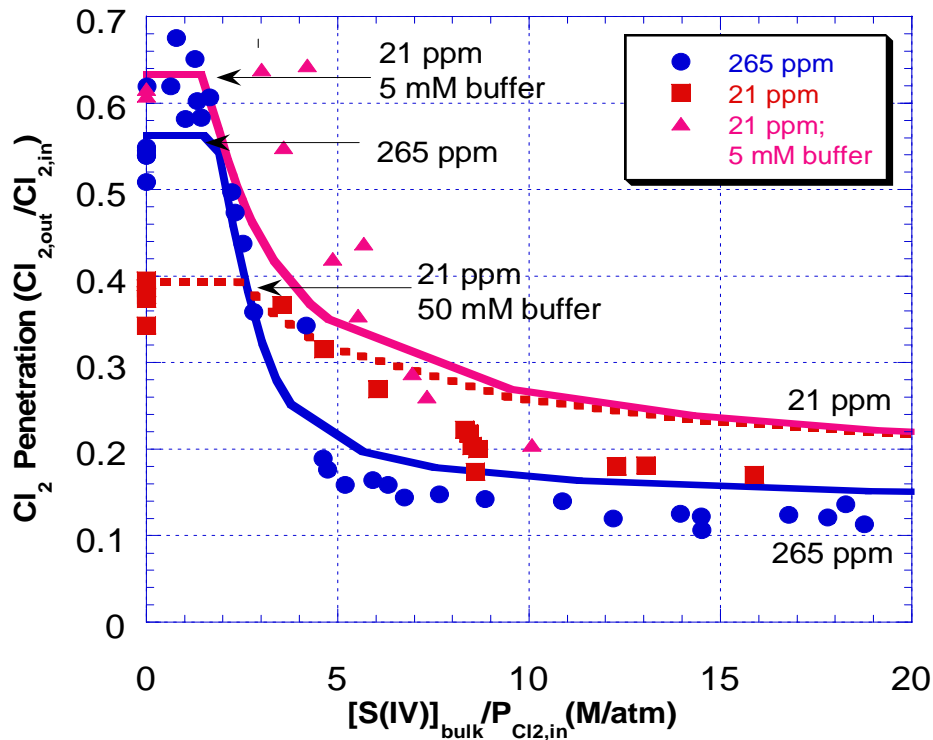


Figure 6.3. Chlorine penetration in buffered S(IV) in stirred cell reactor, $k_{2,S(IV)} = 2.5 \times 10^8$ L/mol-s

Figure 6.2 compares the measured values to those calculated with an infinite value for the rate constant for Cl_2 and S(IV). Since much of the data lie above the model curves, the chlorine penetration is significantly underpredicted with an infinite rate constant. This instantaneous reaction model predicts a greater rate of chlorine absorption than the experimental results.

The model curve in Figure 6.3 uses a lower rate constant of 2.5×10^8 L/mol-s. The penetration is overpredicted in most of the data, signifying greater chlorine removal than what is predicted from the model. Therefore, the actual rate constant must have a higher value than 2.5×10^8 L/mol-s.

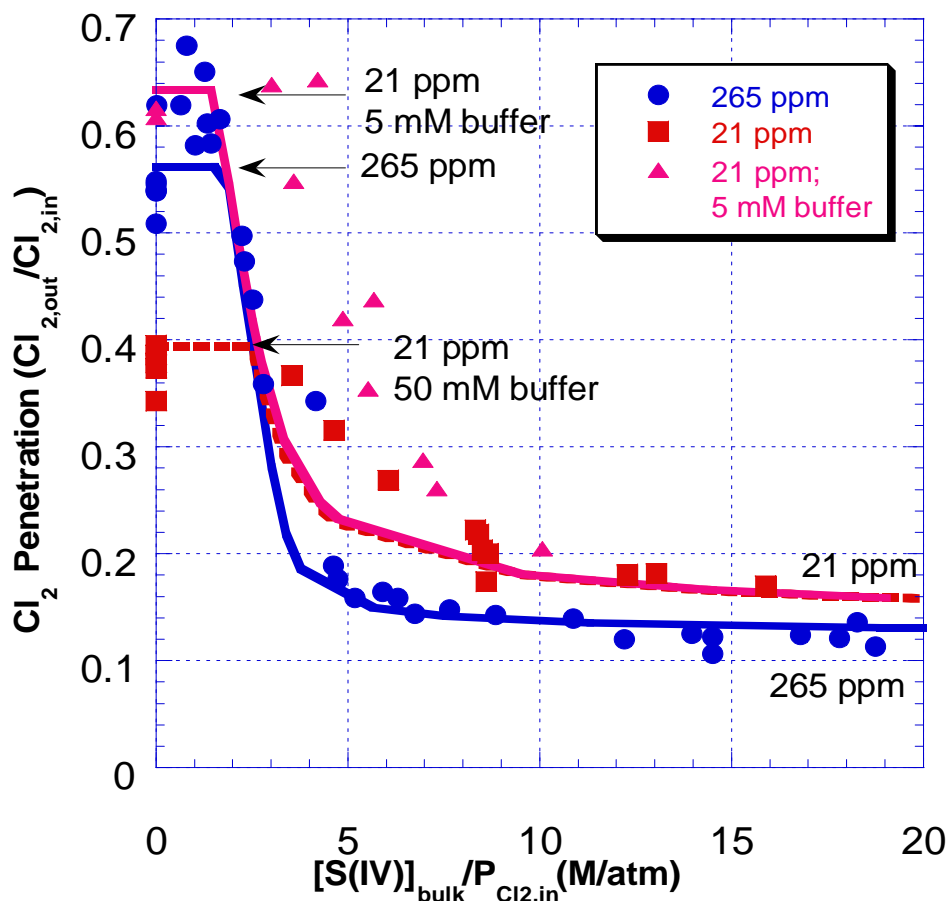


Figure 6.4. Chlorine penetration in buffered S(IV) in stirred cell reactor, $k_{2,S(IV)} = 2 \times 10^9 \text{ L/mol-s}$

Figure 6.4 depicts the calculated penetration with the best value of the rate constant, $2 \times 10^9 \text{ L/mol-s}$. However, at the lower inlet concentration of 21 ppm, the data do not fall on the model curve at S(IV) concentrations below 0.1 mM. These deviations result from the experimental uncertainty in the S(IV) concentration measurements at low S(IV). For example, if the iodometric analysis yielded an S(IV) concentration of 0.07 mM, the actual value could be 0.03 mM due to the analysis procedure not being as accurate at low S(IV) concentrations. Also, at the lower

concentrations, there could be less S(IV) at the interface than perceived due to oxidation by residual oxygen in the inlet gas. Up to 5 ppm oxygen may be present in the “pure” nitrogen.

The most probable value of the rate constant obtained from the stirred cell reactor data is 2×10^9 L/mol-s. In order to get a more precise rate constant, an apparatus with higher mass transfer coefficients is needed so that the absorption falls in a region controlled by reaction kinetics instead of being controlled by mass transfer.

6.2 CHLORINE ABSORPTION AS A FUNCTION OF AGITATION

In order to further investigate if it was possible to obtain a precise rate constant in the stirred cell reactor, experiments were conducted in which the mass transfer coefficients were varied by varying the agitation rates (n_g and n_L). For fast reactions controlled by kinetics, absorption should not be affected by changes in mass transfer coefficients. Therefore, if varying the agitation rates changes the flux of chlorine, kinetics cannot be extracted since mass transfer is being measured instead of kinetics.

6.2.1 *Experimental method*

Chlorine, entering at 21.2 ppm, was absorbed into 0 to 0.64 mM S(IV) at various agitation rates. The chlorine was analyzed using the IMS analyzer. The series of experiments began with chlorine absorption in 5 mM (5 mM succinic acid-5 mM NaOH) buffer. Then, S(IV) was injected, and agitation rates were varied. At the end of each series, a sample was withdrawn from the reactor for S(IV) analysis. As the S(IV) was depleted, more was injected, and the agitation rates were again varied. The S(IV) concentrations were not measured for each point.

6.2.2 Tabulated results

Table 6.4 tabulates the data in which the agitation rates were varied. Series A and B represent data obtained on two different days. Data were collected over the course of 5 to 6 hours each day, and the points are listed in chronological order. Also, for points in which n_L was changed (with other parameters constant), the change in flux with respect to n_L was tabulated between the two points by Equation 6-4.

$$\frac{d \ln N_{Cl_2}}{\ln n_L} = \frac{\ln \left(\frac{N_{Cl_2,1}}{N_{Cl_2,2}} \right)}{\ln \left(\frac{n_{L,1}}{n_{L,2}} \right)} \quad (6-4)$$

Table 6.4. Chlorine (21.2 ppm inlet) absorption in S(IV) solutions with 5 mM buffer at various agitation rates

	[S(IV)](mM)	n_g (rpm)	n_L (rpm)	$Cl_{2,out}$ (ppm)	N_{Cl_2} (kmol/m ² -s)	$d(\ln N_{Cl_2}/\ln n_L)$
A	0	720	780	16.8	4.43E-10	
A1	Inject S(IV)	720	780	4.69	1.67E-09	
A1		720	780	5.91	1.54E-09	0.600
A1		720	472	9.87	1.14E-09	
A1		720	472	10.5	1.08E-09	
A1		720	472	10.8	1.05E-09	0.504
A1		720	898	6.82	1.45E-09	0.078
A1		720	1029	6.67	1.47E-09	
A1		887	1036	7.16	1.42E-09	
A1		1007	1039	7.43	1.39E-09	
A1		1007	1039	7.74	1.36E-09	1.31
A1	0.11	752	757	12.3	8.97E-10	
A2	Inject S(IV)	752	757	5.30	1.60E-09	
A2		752	757	5.91	1.54E-09	0.131
A2		745	1053	5.23	1.61E-09	
A2		382	1063	6.06	1.53E-09	0.630
A2		382	330	13.9	7.30E-10	
A2		678	319	14.5	6.72E-10	
A2		926	319	14.8	6.44E-10	0.626
A2		926	695	10.8	1.05E-09	0.624

A2		926	1051	7.74	1.36E-09	1.17
A2		1051	757	12.0	9.25E-10	
A2	0.078	1051	757	13.1	8.17E-10	
B	0	730	708	14.8	6.44E-10	
B1	Inject S(IV)	730	708	7.10	1.42E-09	
B1		730	708	7.71	1.36E-09	
B1		1151	713	8.94	1.24E-09	
B1		344	713	9.86	1.14E-09	
B1		344	713	10.5	1.08E-09	0.903
B1		332	402	14.8	6.44E-10	
B1		332	402	15.1	6.16E-10	0.618
B1		330	1044	10.2	1.11E-09	
B1		330	1044	10.5	1.08E-09	
B1		974	1058	11.1	1.02E-09	
B1		974	1058	11.4	9.88E-10	1.23
B1	0.070	749	762	14.6	6.60E-10	0.314
B1		748	408	15.8	5.42E-10	0.236
B1		749	1057	14.4	6.78E-10	
B1		1140	1083	14.8	6.47E-10	0.598
B1		1153	722	16.1	5.08E-10	
B1		734	717	16.3	4.92E-10	
B2	0.028	734	717	16.6	4.61E-10	
B3	Inject S(IV)	734	717	4.35	1.70E-09	
B3		1054	715	4.10	1.72E-09	
B3		1054	715	4.38	1.70E-09	0.379
B3		1069	341	8.48	1.28E-09	
B3		478	336	9.24	1.20E-09	0.274
B3		467	990	5.14	1.62E-09	
B3		1103	1004	4.20	1.72E-09	
B3		720	1009	4.75	1.66E-09	0.304
B3	0.13	715	731	6.28	1.50E-09	
B4	Inject S(IV)	715	731	2.91	1.85E-09	0.014
B4		711	408	3.06	1.83E-09	
B4		369	403	4.10	1.72E-09	0.008
B4		366	938	3.98	1.74E-09	
B4		1100	946	2.42	1.89E-09	0.007
B4		1113	383	2.54	1.88E-09	0.005
B4		1117	713	2.48	1.89E-09	
B4	0.64	719	717	3.06	1.83E-09	

6.2.3 Discussion

To analyze the data, the variation of flux with n_L was investigated. From the first set of points in Table 6.4, when n_L was lowered from 780 rpm to 472 rpm, the flux changed by a factor of $n_L^{0.6}$. Based on the experiments to obtain the liquid film mass transfer coefficient of the reactor, k_{L,Cl_2}^o should be proportional to $n_L^{0.56}$. Since the flux depends on n_L , the rate of S(IV) diffusion to the interface (which is controlled by the liquid film mass transfer coefficient) is limiting the rate of chlorine absorption. For the points in Series A1, A2, and B1, the flux changes as n_L changes. For the points in Series B3, the overall dependence is less than the dependence in the above series, but there is still a dependence on n_L . For Series B4, the flux does not depend on the liquid agitation rate. Therefore, the flux is not being limited by S(IV) depletion at the interface.

Figure 6.5 was plotted to check if Series B4 was limited by the diffusion of chlorine to the interface, which is controlled by the gas film mass transfer coefficient, k_g . If the chlorine absorption were limited by k_g , the data in B4 would fall on a straight line corresponding to k_g .

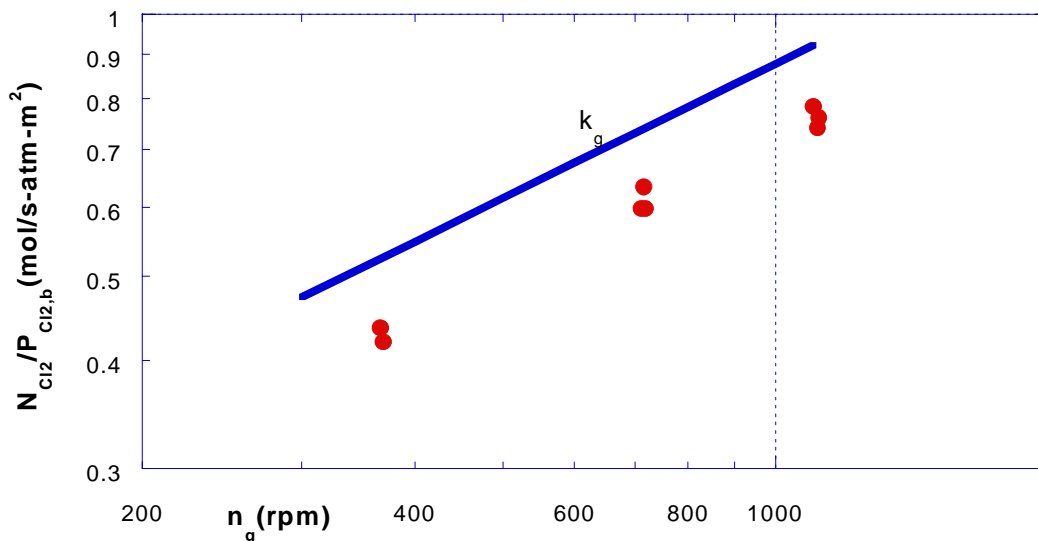


Figure 6.5. Data limited by k_g of stirred cell reactor

Figure 6.5 shows that the points in Series B4 are close to the k_g line. Since there is a dependence on n_g , kinetics cannot be extracted since these points are dependent on k_g .

Thus, the data show that the chlorine flux was never independent of the agitation rates. At S(IV) concentrations below 0.1 mM, the flux usually changed by a factor of $n_L^{0.6}$, which is consistent with the flux being limited by the rate of S(IV) diffusion to the gas/liquid interface. At 0.64 mM S(IV), the flux did not vary with n_L , but it varied as $n_g^{0.52}$, which is consistent with the flux being limited by gas film diffusion. At intermediate S(IV) concentrations, the overall dependence on n_g and n_L were less, but there still was a dependence. These data verified that the range of kinetics-limited data was very small, and it would be difficult to extract precise kinetics for the Cl_2 /S(IV) reaction using the existing stirred cell contactor.

6.3 EFFECT OF SUCCINATE BUFFER ON CHLORINE ABSORPTION AT PH 4.5

The enhancement of chlorine hydrolysis due to succinate buffer needed to be quantified. The reaction was assumed to be first order in both chlorine and succinate.

The data were modeled using mass transfer with chemical reaction theory. An equation similar to Equation 3-4 was used. However, the first two terms in the enhancement factor, Equation 3-3, were also included to account for the water reaction and the possibility of the reaction being slow. The rate constant was extracted using Equation 6-5.

$$N_{\text{Cl}_2} = k_{\text{L},\text{Cl}_2}^o \sqrt{1 + \frac{D_{\text{Cl}_2}}{k_{\text{L},\text{Cl}_2}^{o^2}} (k_{1,\text{H}_2\text{O}} + k_{2,\text{buf}} [\text{buffer}])} \frac{P_{\text{Cl}_{2,i}}}{H_{\text{Cl}_2}} \quad (6-5)$$

Even though Equation 6-5 was used, it should be noted that the data showed that the buffer enhancement was the dominant term in the enhancement factor. Therefore, Equation 6-5 would simplify to Equation 3-4, with [S(IV)] equal zero.

6.3.1 Experimental method

The absorption of chlorine into succinate buffer solutions was measured with no S(IV). The chlorine was analyzed using the IMS analyzer. The gas flow rate to the reactor was 1.15 L/min, and the chlorine inlet concentration was either 21 or 264 ppm. Throughout a single experimental series, the chlorine inlet concentration was kept constant. The experiment began with absorbing chlorine into distilled water (0 mM buffer). Then, succinate buffer was injected into the reactor solution. The cumulative succinate concentration (made from a stock solution of equimolar succinic acid and NaOH) ranged from 10 mM to 154 mM total succinate.

6.3.2 Tabulated results

Table 6.5 displays the data used in obtaining the rate of reaction with chlorine and succinate.

Table 6.5. Chlorine absorption with varying buffer concentration in pH 4.5 with 1.15 L/min gas at n_g/n_L of 700 rpm

Series	[buffer] (mM)	Cl _{2,in} (ppm)	Cl _{2,out} (ppm)	N _{Cl2} (kmol/m ² -s)
A	0	21.2	14.85	6.37E-10
	10.3	21.2	11.82	9.44E-10
	48	21.2	8.61	1.27E-09
	48	21.2	9.00	1.23E-09
	66	21.2	8.04	1.33E-09
	102	21.2	7.33	1.40E-09
	102	21.2	7.15	1.42E-09
	137	21.2	6.71	1.46E-09
	154	21.2	6.76	1.46E-09
B	0	263.9	225.0	3.77E-09
	10.3	263.9	187.4	7.41E-09
	48	263.9	148.6	1.12E-08
	66	263.9	143.0	1.17E-08
	102	263.9	132.0	1.28E-08
	102	263.9	136.4	1.24E-08
	137	263.9	129.2	1.31E-08
	154	263.9	126.7	1.33E-08
C	0	263.9	203.1	5.89E-09
	10.3	263.9	182.2	7.92E-09
	48	263.9	148.1	1.12E-08
	66	263.9	139.6	1.20E-08
	102	263.9	126.8	1.33E-08
	137	263.9	118.3	1.41E-08
	154	263.9	116.5	1.43E-08

6.3.3 Discussion

Figure 6.6 depicts the normalized flux (flux divided by the interfacial partial pressure of chlorine) as a function of the total succinate buffer concentration. These results show that the succinate buffer does enhance chlorine absorption. The extracted rate constants are depicted in Figure 6.6.

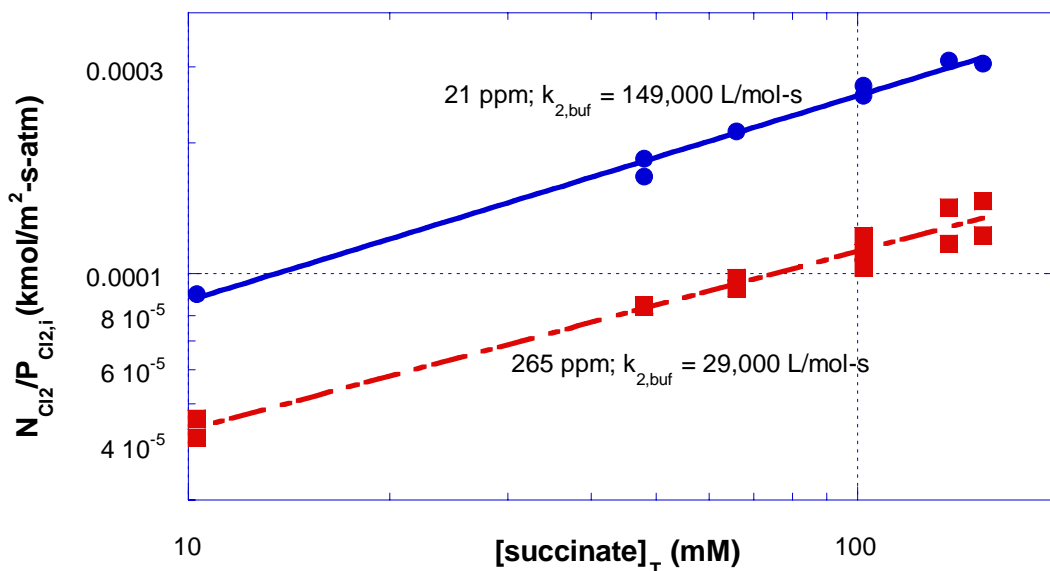


Figure 6.6. Obtaining kinetics for Cl₂ absorption in succinate buffer at pH 4.5

The rate constant, $k_{2,buf}$, was extracted from the data and found to have a slight dependence on the chlorine concentration. Therefore, the reaction may not be first order in chlorine. In order to verify the dependence on the chlorine concentration, experiments at an intermediate chlorine concentration should be done. However, since all that was needed was an empirical value to account for the enhancement, these results are good enough. At the chlorine inlet concentration of 265 ppm, the value for $k_{2,buf}$ used in the model was 3×10^4 L/mol-s; at inlet of 21 ppm, the value used for $k_{2,buf}$ was 1.5×10^5 L/mol-s.

Lifshitz and Perlmutter-Hayman (1962) only investigated the hydrolysis of Cl₂ in the presence of anions of weak monoprotic acids at low temperatures. Based on the data in this section, their correlation greatly underpredicts the rate constant for succinate, the anion of a diprotic acid, at ambient temperature. The regressed $k_{2,buf}$ at pH 5.7 is discussed in Section 7.2.3.1 and compared to the value obtained from this section at pH 4.5. A detailed comparison to the observations of Lifshitz and Perlmutter-Hayman is also discussed in Section 7.2.3.1.

6.4 S(IV) OXIDATION AT pH 4.5 BY CHLORINE AND OXYGEN

Chlorine and oxygen both oxidize S(IV) to sulfate, S(VI). Since oxygen is present in flue gas, it was added to the inlet gas. Since other oxidants, such as NO₂, are known to enhance oxygen absorption (Shen and Rochelle, 1998), experiments were conducted to see if chlorine enhanced oxygen absorption. These experiments established that Cl₂ is not a catalyst for the oxidation of S(IV) by oxygen.

6.4.1 Experimental method

The absorption of chlorine and oxygen into S(IV) was already discussed in Section 6.1. Most of these data were at high S(IV) concentrations since it is easier to observe S(IV) oxidation when the chlorine flux is constant due to complete gas film control. In addition, experiments were done in which only nitrogen and air (no chlorine) were absorbed into S(IV) solutions in the stirred cell reactor. The gas flow rate to the reactor was 1.15 L/min and consisted of either 14.5% or 20.5% oxygen. The oxygen concentration was varied by adjusting the flow of the pure nitrogen, which mixed with air before entering the reactor. Each series of experiments began with S(IV) injection into 50 mM buffer. Samples were periodically withdrawn to determine the S(IV) concentration as a function of time.

6.4.2 Tabulated results

The chlorine and oxygen absorption data discussed in this section have been tabulated in Table 6.1. The data for oxygen absorption in S(IV) is tabulated below in Table 6.6.

Table 6.6. S(IV) depletion resulting from oxygen absorption at pH 4.5 in 50 mM succinate buffer with 1.15 L/min gas and at n_g/n_L of 700 to 730 rpm

Series	$\Delta t(\text{min})$	$[\text{S(IV)}]_{\text{bulk}}(\text{mM})$	O ₂ (%)
A	0	6.06	14.5
	33	4.23	14.5
	37	4.07	14.5

	29	3.89	14.5
	57	3.86	14.5
	103	3.13	14.5
B	0	2.72	14.5
	53	2.36	14.5
C	0	4.88	20.5
	53	3.99	20.5
	42	3.64	20.5
	65	3.21	20.5
	60	2.66	20.5
	36	2.33	20.5
	37	2.18	20.5
	45	1.69	20.5
	57	1.27	20.5
	29	0.99	20.5

6.4.3 Discussion

Figures 6.7 and 6.8 show how the oxidation of S(IV) depends on oxygen and chlorine. The different symbols represent each series of experiments. The dashed lines represent experiments in which chlorine and oxygen are simultaneously absorbed. The values associated with each line represent the S(IV) oxidation rate for that series.

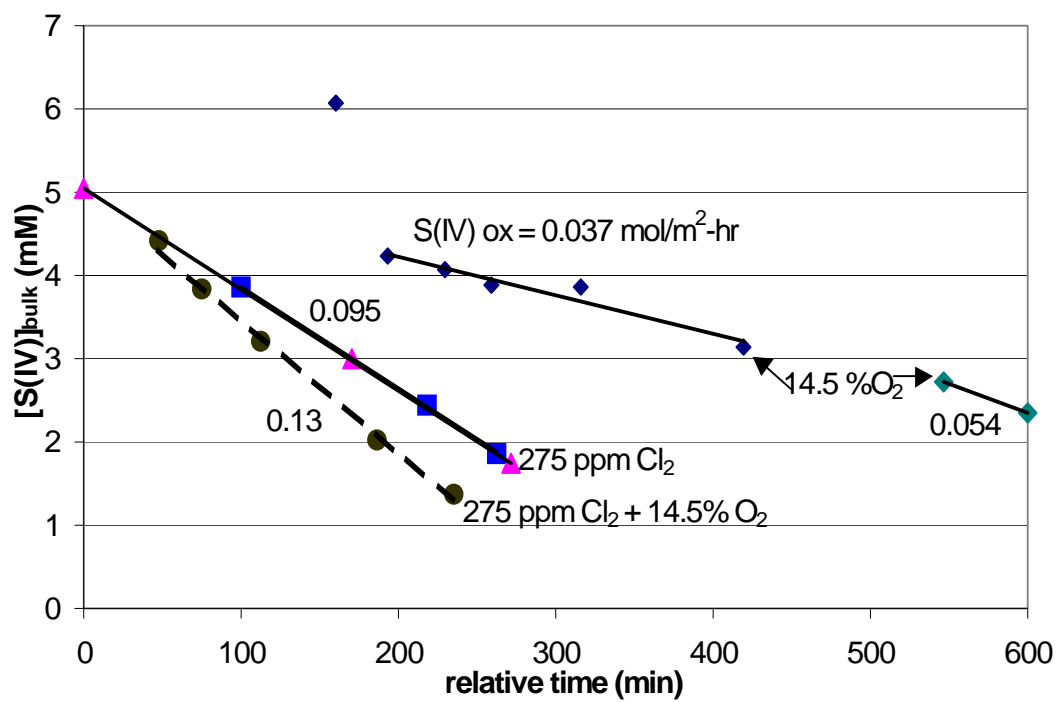


Figure 6.7. S(IV) oxidation by 275 ppm chlorine and 14.5% oxygen

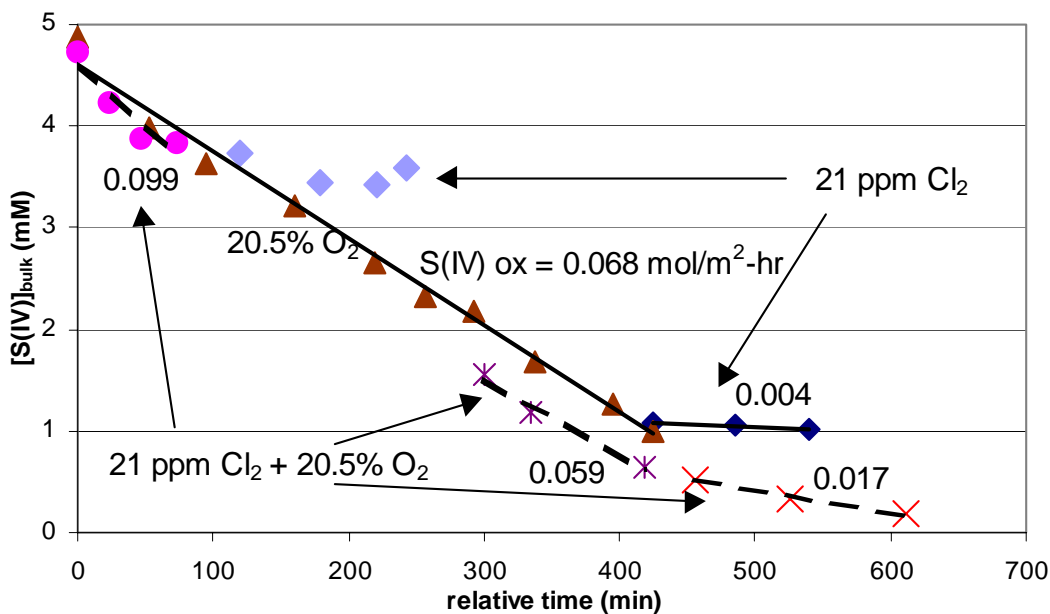


Figure 6.8. S(IV) oxidation by 21 ppm chlorine and 20.5% oxygen

Figure 6.7 shows that the effects of chlorine and oxygen on S(IV) oxidation may be additive when the inlet concentration is 275 ppm. For the points with no Cl₂, the first point at 6 mM was not used in the regression since the point seemed to deviate greatly from the rest. The expected oxidation rate of S(IV) resulting from the physical absorption of 14.5% O₂ was calculated to be 0.039 mol/m²-hr. This value agreed with the observed value of 0.037 mol/m²-hr. The observed S(IV) oxidation is calculated from the depletion rate of S(IV) observed over time.

When only chlorine is absorbed, the oxidation of S(IV) is 0.095 mol/m²-hr. There were two separate data series for these, and both data sets fell on the same line, resulting in the same S(IV) oxidation rate of 0.095 mol/m²-hr. The ratio of the rate of S(IV) oxidation to the rate of Cl₂ absorption was 1:1, confirming the 1:1 stoichiometry of the Cl₂/S(IV) reaction. When chlorine and oxygen are absorbed (corresponding to S(IV) oxidation rate of 0.13 mol/m²-hr), about three-fourths of the S(IV) oxidation is due to the reaction of chlorine with S(IV). In this case, the

chlorine does not seem to be catalyzing S(IV) oxidation since the S(IV) oxidation seems to be additive.

Figure 6.8 shows data in which the chlorine inlet concentration is significantly lower at 21 ppm. In this case, the oxidation of S(IV) due to reaction with chlorine alone is practically negligible. Physical absorption of 20.5% oxygen corresponds to S(IV) oxidation of $0.055 \text{ mol/m}^2\text{-hr}$. Thus, the oxidation rate of S(IV) without chlorine obtained experimentally is in the range of the calculated oxidation rate due to physical absorption of O_2 . At very low S(IV) concentrations ($< 0.5 \text{ mM}$), the S(IV) oxidation is much less ($0.017 \text{ mol/m}^2\text{-hr}$) than that expected from physical absorption of oxygen. This may occur because at these low concentrations, there is barely any S(IV) at the interface. When S(IV) is between 0.5 and 1.5 mM, it seems that the S(IV) oxidation is equivalent to that which would result from the physical absorption of oxygen. Thus, chlorine does not seem to enhance S(IV) oxidation in this case. At high S(IV) concentrations (around 4 mM), the slope of the line is steeper, and the S(IV) oxidation is much greater at $0.099 \text{ mol/m}^2\text{-hr}$. Chlorine may be catalyzing S(IV) oxidation, but it is hard to tell from looking at the figure. More data would need to be taken in this range.

6.5 ABSORPTION AT PH 4.5 USING ELECTROCHEMICAL CHLORINE ANALYZER

This section discusses some of the initial absorption experiments in which chlorine was absorbed into buffered S(IV) solutions. These data follow the same general trends as the data obtained using the IMS analyzer. The effect of chloride on the $\text{Cl}_2/\text{S(IV)}$ reaction rate is also discussed in this section.

The fraction gas film resistance is a parameter used in analyzing some of the data. The fraction gas film resistance is directly related to reaction kinetics:

$$\frac{K_{OG}}{k_g} = \frac{1}{1 + \frac{k_g H_{Cl_2}}{Ek_{L,Cl_2}^o}} = \text{fraction gas film resistance} \quad (6-6)$$

As the enhancement factor (E) increases, which corresponds to fast reaction rates, the total resistance to mass transfer ($1/K_{OG}$) becomes limited by gas film resistance ($1/k_g$). Under these conditions, the fraction gas film resistance (6-6) approaches unity and becomes independent of reaction kinetics. Thus, data which approach gas film resistance cannot be used for extracting kinetics. For these data, the gas film mass transfer coefficient (as opposed to kinetics) is being measured.

6.5.1 Experimental method

Chlorine absorption into S(IV) solutions in 50 mM buffer was measured using the electrochemical chlorine analyzer. The typical analyzer calibration is shown in Figure 4.2. In addition to S(IV) analysis, samples were withdrawn for chloride analysis (through ion chromatography). Chloride (as NaCl) was also added in some of the experiments. The chlorine inlet concentration was varied from 21 to 276 ppm. Throughout an experimental series, the chlorine inlet was kept constant, while the S(IV) concentration was varying.

6.5.2 Tabulated results

Table 6.7 tabulates the data discussed in this section. The chloride concentration for Series G is not noted since it was not measured. As usual, each series represents data obtained in a single day and are listed in chronological order.

Table 6.7. Chlorine absorption in S(IV) at pH 4.5, measured with electrochemical analyzer, in 50 mM succinate buffer with 1.2 L/min gas

Series	[S(IV)] _b (mM)	Cl _{2,in} (ppm)	Cl _{2,out} (ppm)	N _{Cl2} (kmol/m ² -s)	K _{OG} /k _g (%)	[Cl ⁻] (mM)	n _g (rpm)	n _L (rpm)
A	0	276	185	9.13E-09	8.2	0.36	619	645
	1.19	276	118	1.59E-08	22.5	0.5	619	645
	0.88	276	177	9.94E-09	9.4	0.76	619	645
	0.43	276	222	5.37E-09	4.0	1.1	619	645
	1.21	276	132	1.45E-08	18.3	1.65	619	645
	0.87	276	162	1.15E-08	11.8	6.56	619	645
	0.78	276	184	9.18E-09	8.2	19.7	632	649
B	0	276	174	1.02E-08	9.5	0.12	646	644
	1.45	276	70	2.06E-08	47.7	1.13	650	644
	0.95	276	141	1.35E-08	15.4	1.32	650	644
	0.84	129	43	8.86E-09	33.5	1.3	650	644
	0.62	129	50.4	8.07E-09	25.9	2.88	650	644
	0.58	276	181	9.55E-09	8.5	1.49	655	647
C	0	276	179	9.69E-09	8.3	0.17	710	691
	1.37	276	51.5	2.25E-08	37.0	0.86	710	683
	1.25	276	80.6	1.96E-08	29.5	1.61	710	683
	0.82	276	94.1	1.82E-08	53.7	1.9	710	683
	0.69	129	29.1	1.03E-08	8.8	2.31	719	683
D	1.16	21	2.9	1.85E-09	96.6	0.314	707	747
	1.14	21	2.9	1.85E-09	97.9	0.367	707	747
E	0.23	21	9.5	1.17E-09	18.5	0.176	728	717
	0.20	21	12.2	8.98E-10	11.0	0.356	728	717
	0.13	21	14.0	7.17E-10	7.7	0.27	728	717
F	0.20	21	9.9	1.13E-09	17.1	0.26	735	736
G	0.31	21	6.4	1.49E-09	35.8	n/a	701	732
	0.27	21	7.9	1.34E-09	26.1	n/a	701	732

6.5.3 Discussion

Figure 6.9 overlays the electrochemical data from Table 6.7 with the IMS data in Figure 6.1. The trends are similar, but the data from the electrochemical analyzer do not fit the model. The data obtained using the electrochemical analyzer are at a slightly lower k_L^0 value of 2.3×10^{-5} m/s, while the model curves were calculated

using the k_L^o value of 2.45×10^{-5} m/s (since this was the value for the data taken with the IMS analyzer). Even if the lower k_L^o value was used in the above model calculations, the electrochemical analyzer data would not fit the model. In order for the data to fit the model, the liquid film mass transfer coefficient used in the model would need to be approximately 1.23×10^{-5} m/s.

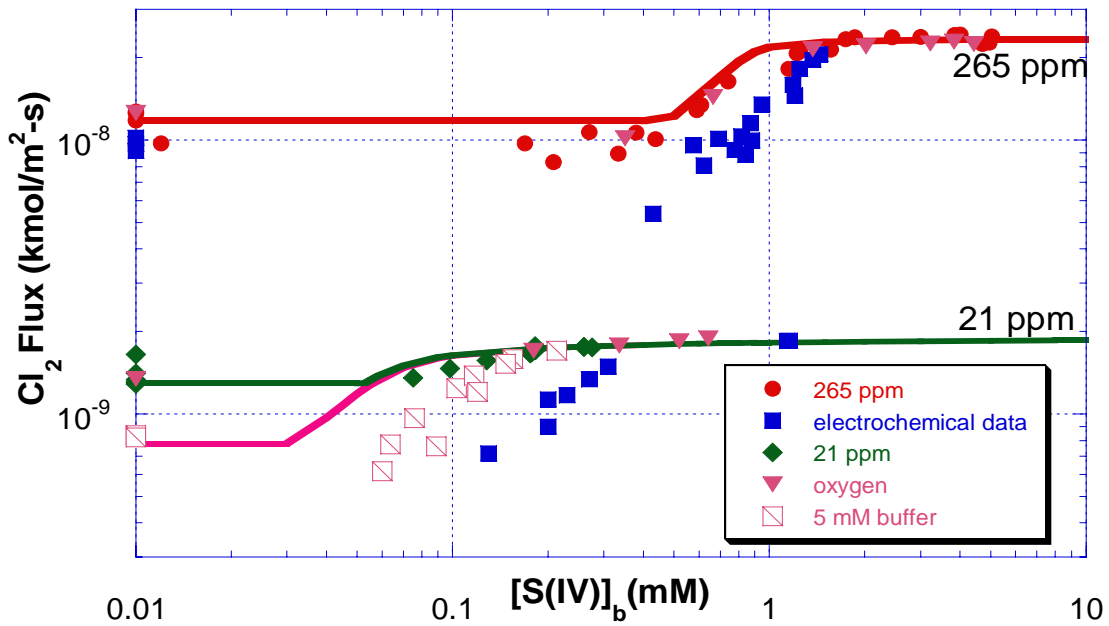


Figure 6.9. Electrochemical analyzer data overlaid onto IMS data

Figure 6.10 shows the electrochemical analyzer data in a separate figure to better see trends. As expected, the percent gas film resistance increases (signifying enhanced reaction) as S(IV) increases until 100% gas film control is reached. Figure 6.10 also shows that at the low chlorine concentration, the absorption is more likely to approach gas film control at lower S(IV) concentrations. This is expected since at lower chlorine concentrations, it takes less S(IV) to react completely with the chlorine. Figure 6.10 also shows that the point at 0.43 mM S(IV) seems to have a

lower reaction rate than the points with no S(IV). This is equivalent to the S(IV) inhibition seen with the IMS data.

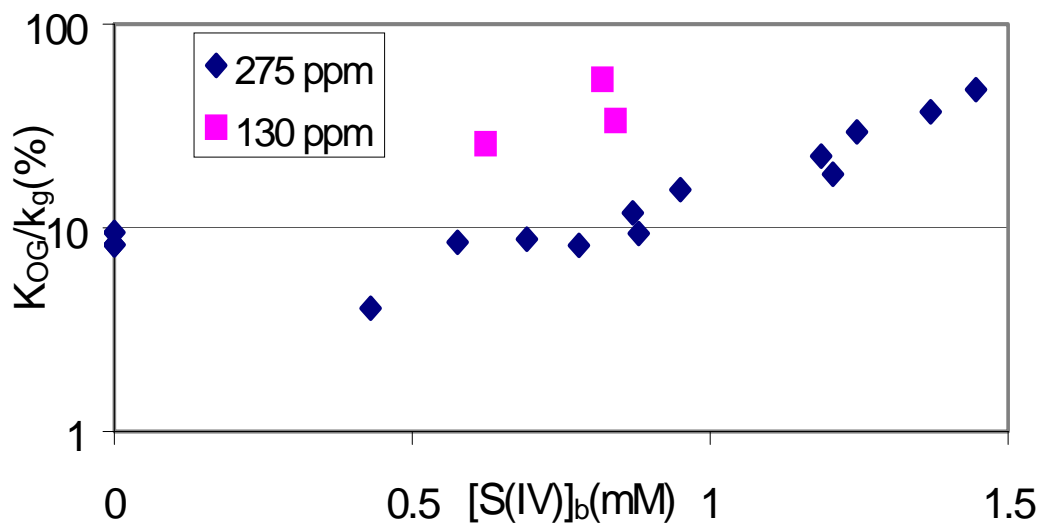


Figure 6.10. Chlorine absorption in 0 – 2 mM S(IV) in 50 mM buffer using electrochemical analyzer

6.5.3.1 Effect of chloride

Figure 6.11 shows that chloride (up to 20 mM) has no effect on the rate of chlorine absorption in S(IV). The two marked points have increased levels of chloride (stock solution of NaCl was added to reactor). The other points have chloride concentrations resulting from only chlorine absorbing to form chloride (no external addition of chloride). The chloride concentrations for these points range from 0.1 to 2 mM. The chloride does not seem to have any effect on the chlorine absorption since the two points with elevated chlorine seem to follow the trend of the other points. Thus, at chloride concentrations less than 0.02 M, there is no effect on the chlorine reaction with S(IV). This makes sense since chloride should not affect the Cl₂/S(IV)

reaction if the reaction is irreversible. Section 7.2.3.3 also shows that the $\text{Cl}_2/\text{S(IV)}$ reaction rate is not affected by greater chloride concentrations.

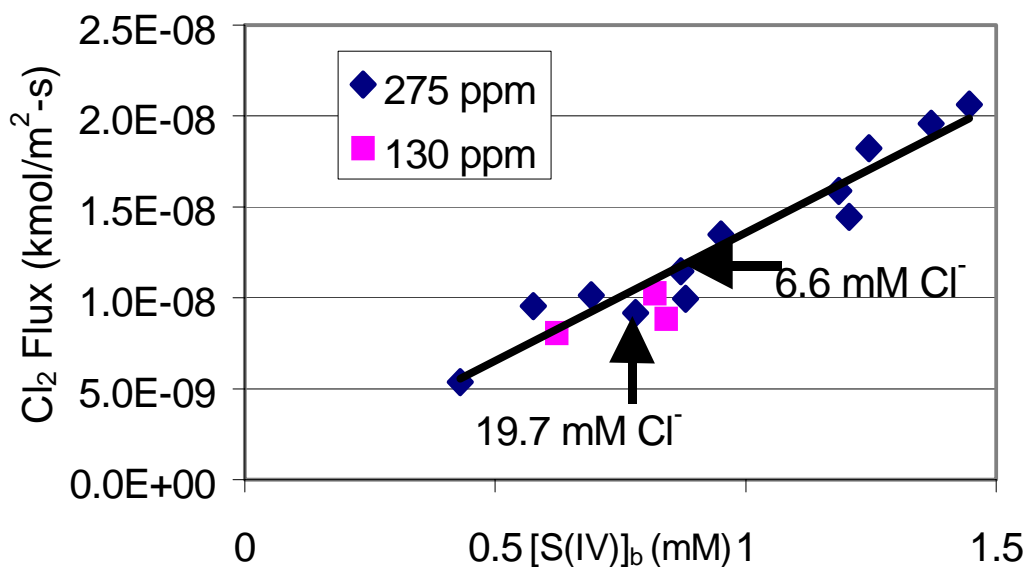


Figure 6.11. Effect of chloride on Cl_2 absorption in S(IV), obtained from data using electrochemical analyzer

6.6 ABSORPTION AT pH 6 TO 8.5 USING ELECTROCHEMICAL ANALYZER

This section discusses the first set of chlorine absorption experiments which were conducted. The solutions contained S(IV), but were not buffered. Due to the analytical imprecision for the early experiments (discussed in Chapter 4), the data can not be rigorously analyzed, but trends can be observed.

6.6.1 Experimental method

Chlorine absorption into S(IV) solutions was measured using the electrochemical analyzer. The chlorine inlet concentration was approximately 240 ppm. For solutions in which the pH was greater than 7, the S(IV) was obtained from a stock solution of sodium sulfite. For solutions in which the pH was between 6 and

7, a stock solution of equimolar sodium sulfite and sodium bisulfite (obtained from sodium meta-bisulfite) was used. A known quantity of S(IV) was taken from the stock solution and injected into the reactor.

6.6.2 Tabulated results

Table 6.8 tabulates the data discussed in this section.

Table 6.8. Chlorine absorption at pH 6 to 8.5 with 1.2 L/min gas, measured using electrochemical sensor analyzer

Series	pH	[S(IV)] _b (mM)	n _g (rpm)	n _L (rpm)	Cl _{2,in} (ppm)	Cl _{2,out} (ppm)	N _{Cl2} (kmol/m ² -s)
A	8	5.5	432	663	240	54	2.00E-08
	8.2	8.1	482	693	240	48	2.06E-08
	8.5	10	498	660	240	48	2.06E-08
	7.6	1.9	484	680	240	78	1.74E-08
B	water	0	533	609	245	204	4.38E-09
	6 - 7	2.51	533	609	245	76	1.81E-08
	6 - 7	2.48	533	609	245	60.8	1.98E-08

6.6.3 Discussion

These data show similar trends. The addition of S(IV) does enhance chlorine absorption. The data at S(IV) concentrations above 5 mM are completely gas film controlled, similar to that observed at pH 4.5. The data at lower S(IV) concentrations are very close to being gas film controlled. By comparing these data to those in the buffered solutions at pH 4.5, the higher pH seems to enhance absorption. At high pH, the Cl₂/OH rate would also be enhancing the absorption. However, because of the experimental uncertainties, it is not possible to obtain a reaction rate resulting from the high pH S(IV).

6.7 SUMMARY

The rate constant for the Cl₂/S(IV) reaction was too rapid to be precisely measured using the stirred cell reactor, due to mass transfer limitations. However, the most probable value for the rate constant was determined to be on the order of

magnitude of 2×10^9 L/mol-s. At low S(IV), the chlorine absorption was limited by the buffer-enhanced hydrolysis reaction. At moderate S(IV), it was limited by diffusion of S(IV) from the bulk solution to the interface. At high S(IV), the absorption was limited by diffusion of chlorine from the bulk gas to the interface.

The succinate buffer enhances chlorine absorption. However, lowering the succinate buffer concentration from 50 to 5 mM did not aid in extracting kinetics because there is not much of a range between the chlorine flux due to absorption in water and the maximum flux resulting from complete gas film control. Therefore, extracting kinetics for the S(IV) reaction will always be difficult in the existing stirred cell reactor apparatus. On one end, absorption is limited by the chlorine hydrolysis reaction, and on the other end, it is limited by gas film control in the stirred cell contactor.

Chloride does not affect chlorine absorption in S(IV) since the chlorine/S(IV) reaction is irreversible. Oxygen does not affect chlorine absorption in S(IV) either, nor does it seem to catalyze S(IV) depletion at the ranges investigated. When no oxygen is present, the rate of S(IV) oxidation equals the rate of chlorine absorption, confirming the 1:1 stoichiometry.

Chapter 7: Chlorine Absorption in Wetted Wall Column

This chapter presents the results of the chlorine absorption experiments conducted in the wetted wall column. The chlorine was analyzed using the IMS analyzer. The rate constant for the $\text{Cl}_2/\text{S(IV)}$ reaction was regressed at ambient temperature at an approximate pH of 4.7 and 5.7. The regression was done using a nonlinear parameter-estimation package called GREG (Generalized REGression package). The effect of 0.1 M sodium chloride was investigated. The enhancement of the succinate buffer at pH 5.7 was quantified.

7.1 CHLORINE ABSORPTION IN WETTED WALL COLUMN AT PH 4.7

The rate constant for the reaction of Cl_2 with S(IV) at pH 4.7 was regressed from the data discussed in this section. The model was calculated using Equations 3-8, 3-10, and 3-11.

7.1.1 *Experimental method*

The absorption of chlorine into buffered S(IV) solutions, with pH ranging from 4.5 to 4.7, was measured in the wetted wall column. The gas flow to the column was usually either 4.78 L/min or 9.52 L/min, and the liquid flow was 2.26 mL/s. The chlorine inlet concentration ranged from 21 to 46 ppm. Throughout each experimental series, the chlorine inlet was usually kept constant, while varying the S(IV) concentration. Each series started with chlorine absorption into 5 mM buffer (5mM succinic acid-5 mM NaOH). The 700 mL plexiglass reservoir was used for all the data, except those where the gas flow rate was 9.52 L/min. The 3.1 L reservoir was used for the final series discussed in this section, the series in which the gas flow to the column was 9.52 L/min.

7.1.2 Tabulated results

Table 7.1 tabulates the data discussed in this section. The outlet S(IV) divided by the chlorine inlet is also tabulated since the penetration was plotted against this normalized parameter.

Table 7.1. Chlorine absorption in S(IV) at pH 4.5 – 4.7 with 5 mM succinate buffer in wetted wall column

Series	G (L/min)	[S(IV)] _o (mM)	Cl _{2,in} (ppm)	Cl _{2,o} (ppm)	N _{Cl₂} (kmol/m ² s)	Cl _{2,o} /Cl _{2,in}	[S(IV)] _o /P _{Cl_{2,in}} (M/atm)
A	1.18	0	21.6	12.0	7.28E-10	0.556	0.0
B	1.18	0	21.8	13.5	6.30E-10	0.619	0.0
	1.18	0.5	21.8	3.70	1.37E-09	0.170	22.9
	1.18	0.5	21.8	3.45	1.39E-09	0.158	22.9
	4.78	0.5	23.5	7.74	4.84E-09	0.329	21.3
C	4.78	0	76	66	3.14E-09	0.866	0.0
D	4.78	0	23.5	19.9	1.11E-09	0.847	0.0
	4.78	0.074	23.5	12.2	3.47E-09	0.520	3.15
	4.78	0.074	23.5	13.6	3.04E-09	0.579	3.15
	4.78	0.258	23.5	9.35	4.35E-09	0.398	11.0
	4.78	0.144	23.5	9.60	4.27E-09	0.409	6.13
	4.78	0.144	23.5	10.1	4.11E-09	0.431	6.13
	4.78	0.34	23.5	8.24	4.69E-09	0.351	14.5
	4.78	0.34	23.5	8.31	4.67E-09	0.354	14.5
	4.78	0.16	23.5	9.60	4.27E-09	0.409	6.81
	4.78	0.525	23.5	7.28	4.98E-09	0.310	22.3
	4.78	0.45	23.5	7.26	4.99E-09	0.309	19.1
	4.78	1.7	23.5	6.77	5.14E-09	0.288	72.3
E	4.78	0	23.5	19.0	1.38E-09	0.809	0.0
	4.78	0.17	23.5	8.58	4.59E-09	0.365	7.23
	4.78	0.17	23.5	8.68	4.56E-09	0.369	7.23
	4.78	0.054	23.5	13.0	3.24E-09	0.551	2.30
	4.78	0.054	23.5	12.9	3.26E-09	0.549	2.30
	4.78	0.128	23.5	8.92	4.48E-09	0.380	5.45
	4.78	0.063	23.5	12.2	3.48E-09	0.519	2.68
	4.78	0.063	23.5	12.4	3.40E-09	0.529	2.68
	4.78	0.063	23.5	11.9	3.55E-09	0.508	2.68
F	9.52	0	45.5	41.7	2.31E-09	0.917	0.0

	9.52	0.169	45.5	25.9	1.20E-08	0.568	3.71
	9.52	0.126	45.5	31.9	8.34E-09	0.701	2.77
	9.52	0.111	45.5	35.2	6.33E-09	0.773	2.44
	9.52	0.164	45.5	29.1	1.00E-08	0.640	3.60
	9.52	0.139	45.5	32.3	8.06E-09	0.711	3.05
	9.52	0.227	45.5	26.5	1.16E-08	0.583	4.99
	9.52	0.172	45.5	30.2	9.34E-09	0.665	3.78
	9.52	0.298	45.5	22.9	1.38E-08	0.503	6.55
	9.52	0.389	45.5	21.8	1.45E-08	0.479	8.55
	9.52	0.313	45.5	24.8	1.27E-08	0.545	6.88
	9.52	0.61	45.5	20.1	1.56E-08	0.442	13.4
	9.52	0.507	45.5	20.7	1.52E-08	0.456	11.1
	9.52	0.292	45.5	23.7	1.34E-08	0.521	6.42

7.1.3 Discussion

Figure 7.1 compares the stirred cell model predictions (as shown in Figure 6.1) to the wetted wall column prediction, using a value of 2×10^9 L/mol-s for the $\text{Cl}_2/\text{S(IV)}$ rate constant. The wetted wall column model shows that the range between the buffer-enhanced chlorine hydrolysis rate and gas film control is greater than it was in the stirred cell reactor. The curvature is also broader, which signifies a region where the absorption is limited by kinetics.

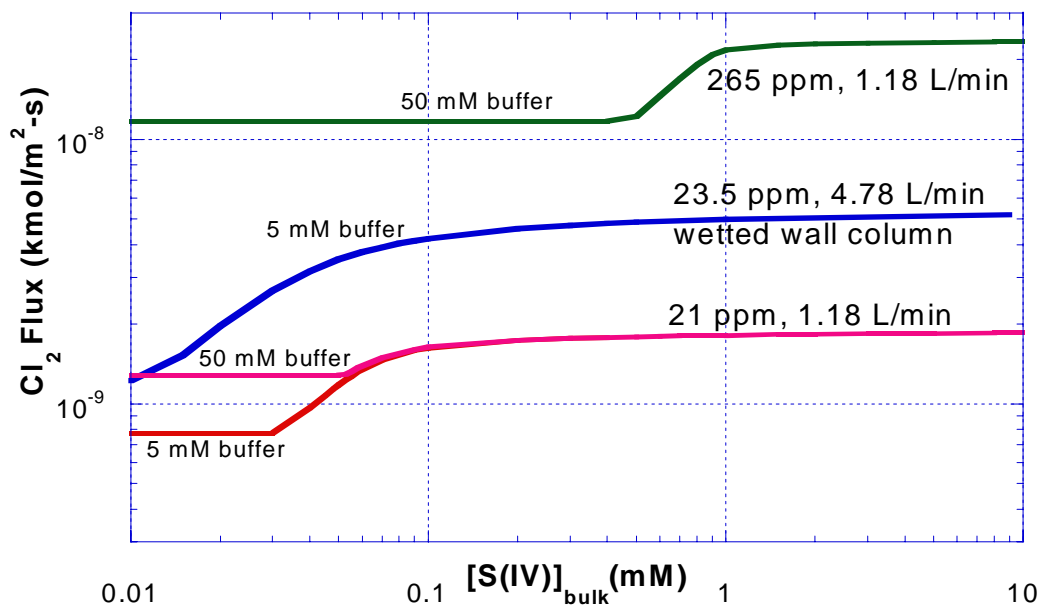


Figure 7.1. Comparison of predicted fluxes in wetted wall column to that in stirred cell at pH 4.7 using $k_{2,S(IV)} = 2 \times 10^9$ L/mol-s

7.1.3.1 Regressed rate constant

Figure 7.2 depicts the chlorine penetration at two different flow rates and chlorine inlet concentrations. The curves were calculated using Equations 3-8, 3-10, and 3-11. The value used for $k_{2,buf}$ was 1.5×10^5 L/mol-s, which is the same value used for the stirred cell reactor experiments (in which the inlet chlorine was under 50 ppm). The mass transfer coefficients used in the model were representative of the data. The $k_{L,S(IV)}^0$ was 8.53×10^{-5} m/s. At the gas flow of 4.78 L/min, the k_g used in the model was 0.4 mol/s-atm-m². At the gas flow of 9.52 L/min, the k_g used was 0.7 mol/s-atm-m². A rate constant with a 95% confidence interval of $(1.0 \pm 0.2) \times 10^9$ L/mol-s was regressed from the data and used to calculate the model curves depicted in Figure 7.2.

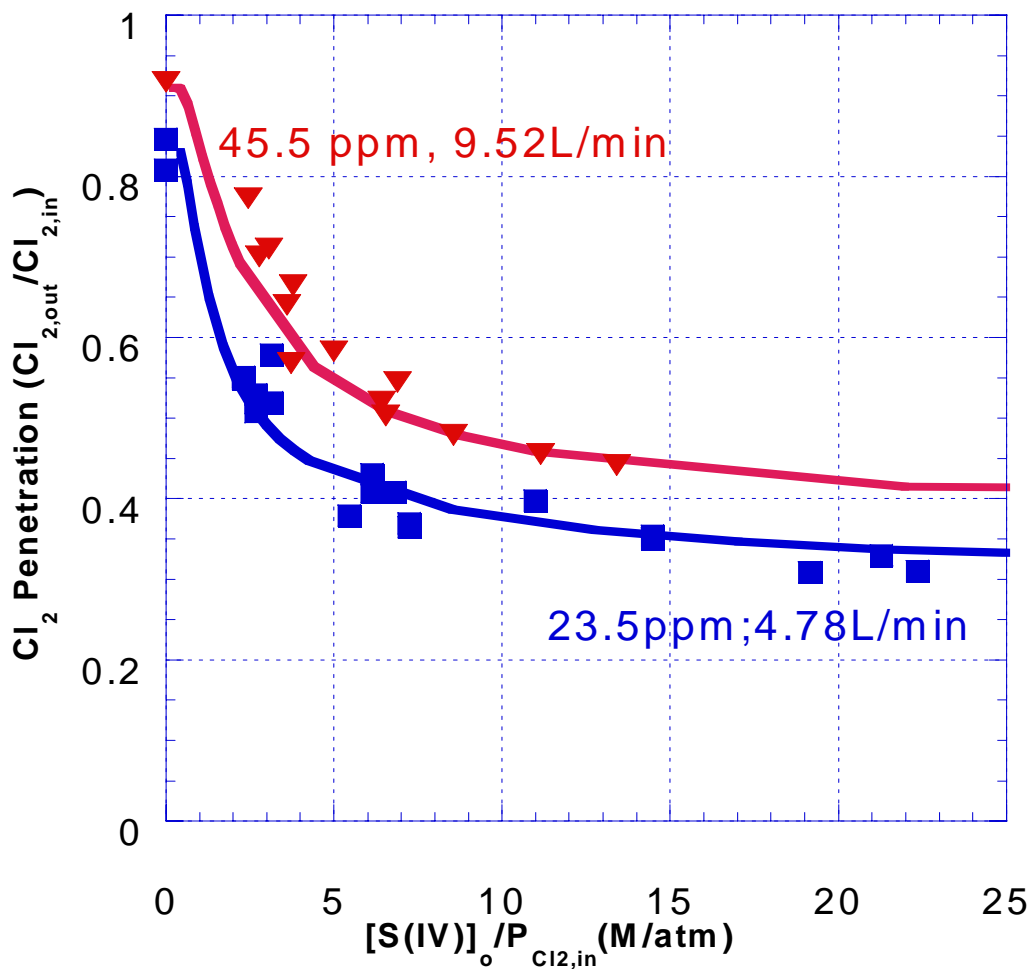


Figure 7.2. Chlorine penetration in buffered S(IV), $k_{2,S(IV)} = 1.0 \times 10^9$ L/mol-s, in wetted wall column at pH 4.7

This rate constant fits the data very well and is also the same order of magnitude predicted from the stirred cell data. Figure 7.2 also depicts the same general trends as the stirred cell data. At high S(IV), the chlorine penetration flattens since the limit of gas film resistance is approached. Figure 7.3 plots the stirred cell data using the new $k_{2,S(IV)}$ of 1.0×10^9 L/mol-s and confirms that this rate constant fits the stirred cell reactor data also.

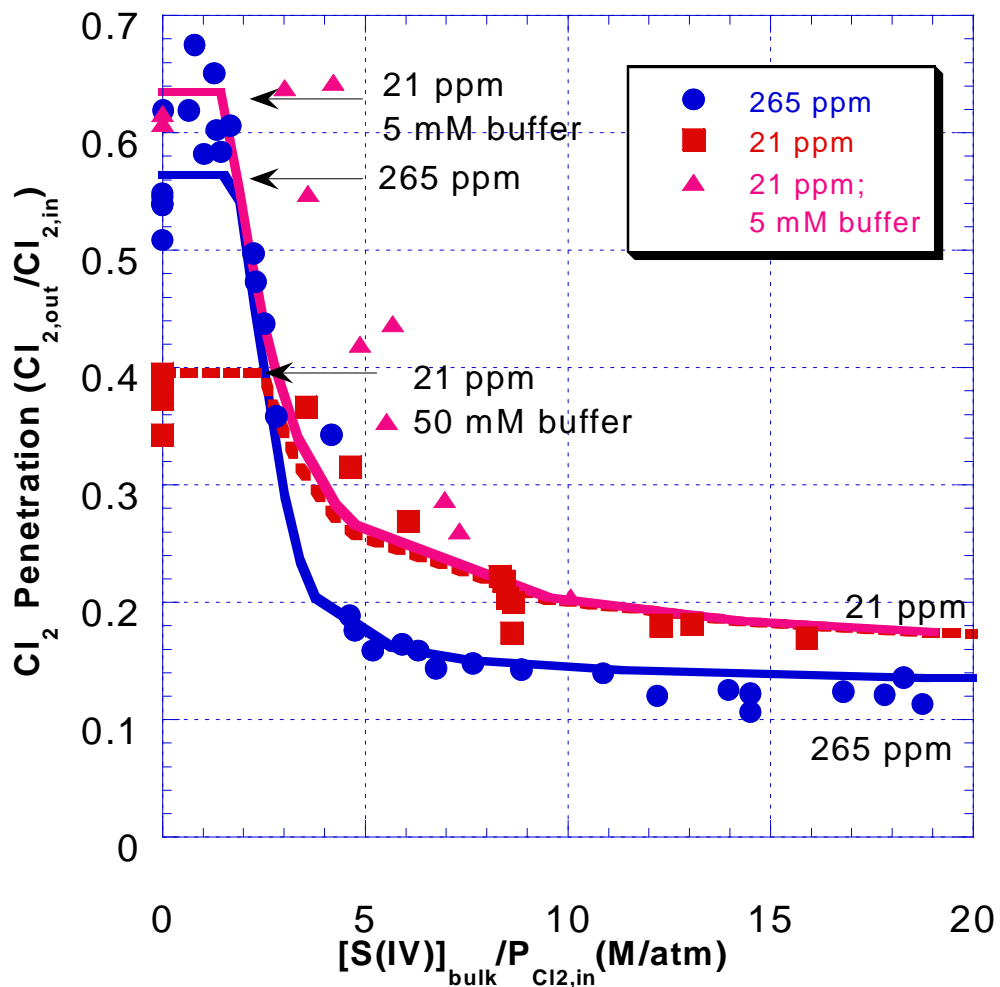


Figure 7.3. Chlorine penetration in buffered S(IV) in stirred cell reactor, $k_{2,S(IV)} = 1.0 \times 10^9 \text{ L/mol-s}$

7.1.3.2 Section profiles

As mentioned before, the model was integrated to obtain the bulk concentrations at each point in the column. The S(IV) concentrations in Figure 7.2 are represented as the outlet concentration (normalized by the chlorine inlet) because the liquid was sampled at the outlet. The S(IV) concentration exiting the column is slightly less than that entering the column (due to reaction with Cl_2). The chlorine

concentration also changes throughout the column. At a given $[S(IV)]_o$, the absorption in the column may go through all three regimes: limited by gas film diffusion, limited by reaction kinetics, and limited by S(IV) diffusion.

Tables 7.2 to 7.4 tabulate section profiles calculated using the model. The model divides the column into 36-3 cm² sections. Section 0 represents the bottom section, and Section 105 represents the top section. The inlet concentration for the three profiles was 23.5 ppm. Other than the S(IV) concentration, the other variables remain constant for the profile calculations. The tabulated fraction gas film resistance (K_{OG}/k_g) is the ratio of the flux for the section to the flux that would result from complete gas film control (Equation 3-12). The last row tabulates the overall flux and penetration; the experimental values were compared to these values to regress the rate constant.

Table 7.2 shows the profile at an outlet S(IV) concentration of 0.01 mM. At this low S(IV) concentration, there is essentially no S(IV) at the interface. The rate of absorption is dominated by the rate of the buffer-enhanced chlorine hydrolysis.

Table 7.2. Chlorine section profile at 23.5 ppm and 0.01 mM S(IV)

Section	$P_{Cl_2,b}$ (atm)	$[S(IV)]_b$ (mM)	$[S(IV)]_i$ (mM)	N_{Cl_2} (kmol/m ² -s)	$Cl_{2,out}/Cl_{2,in}$	K_{OG}/k_g (%)
0	2.350E-05	0.01	0	1.28E-09	0.995	13.6
3	2.338E-05	0.01	0	1.27E-09	0.995	13.6
6	2.327E-05	0.01	0	1.27E-09	0.995	13.6
9	2.315E-05	0.011	0	1.26E-09	0.995	13.6
12	2.304E-05	0.011	0	1.26E-09	0.995	13.6
15	2.293E-05	0.011	0	1.25E-09	0.995	13.6
18	2.281E-05	0.011	0	1.24E-09	0.995	13.6
21	2.270E-05	0.011	0	1.24E-09	0.995	13.6
24	2.259E-05	0.011	0	1.23E-09	0.995	13.6
27	2.248E-05	0.012	0	1.23E-09	0.995	13.6
30	2.237E-05	0.012	0	1.22E-09	0.995	13.6
33	2.226E-05	0.012	0	1.21E-09	0.995	13.6
36	2.215E-05	0.012	0	1.21E-09	0.995	13.6
39	2.204E-05	0.012	0	1.20E-09	0.995	13.6

42	2.193E-05	0.012	0	1.20E-09	0.995	13.6
45	2.182E-05	0.012	0	1.19E-09	0.995	13.6
48	2.172E-05	0.013	0	1.18E-09	0.995	13.6
51	2.161E-05	0.013	0	1.18E-09	0.995	13.6
54	2.150E-05	0.013	0	1.17E-09	0.995	13.6
57	2.140E-05	0.013	0	1.17E-09	0.995	13.6
60	2.129E-05	0.013	0	1.16E-09	0.995	13.6
63	2.119E-05	0.013	0	1.15E-09	0.995	13.6
66	2.108E-05	0.014	0	1.16E-09	0.995	13.7
69	2.098E-05	0.014	0	1.17E-09	0.995	13.9
72	2.087E-05	0.014	0	1.18E-09	0.995	14.1
75	2.076E-05	0.014	0	1.19E-09	0.995	14.3
78	2.066E-05	0.014	0.0001	1.20E-09	0.995	14.6
81	2.055E-05	0.014	0.0001	1.22E-09	0.995	14.8
84	2.044E-05	0.014	0.0001	1.23E-09	0.995	15
87	2.033E-05	0.015	0.0001	1.24E-09	0.994	15.3
90	2.022E-05	0.015	0.0001	1.25E-09	0.994	15.5
93	2.010E-05	0.015	0.0002	1.27E-09	0.994	15.7
96	1.999E-05	0.015	0.0002	1.28E-09	0.994	16
99	1.987E-05	0.015	0.0002	1.29E-09	0.994	16.2
102	1.976E-05	0.016	0.0002	1.30E-09	0.994	16.5
105	1.964E-05	0.016	0.0002	1.32E-09	0.994	16.8
Overall				1.22E-09	0.831	

Table 7.3 tabulates the section profile for an outlet S(IV) of 0.06 mM. Under these conditions, the absorption is limited by kinetics. As the gas flows through the column, the chlorine decreases, while the S(IV) at the interface increases. Therefore, the fraction gas film resistance increases. At this S(IV) concentration, the reaction is not yet gas film controlled. Also, there is S(IV) at the interface; therefore, the absorption is not limited by S(IV) diffusion to the interface.

Table 7.3. Chlorine section profile at 23.5 ppm and 0.06 mM S(IV)

Section	$P_{Cl_2,b}$ (atm)	$[S(IV)]_b$ (mM)	$[S(IV)]_i$ (mM)	N_{Cl_2} (kmol/m ² -s)	$Cl_{2,out}/Cl_{2,in}$	K_{OG}/k_g (%)
0	2.350E-05	0.06	0.01	4.26E-09	0.984	45.4
3	2.311E-05	0.061	0.011	4.26E-09	0.983	46.1
6	2.273E-05	0.061	0.011	4.25E-09	0.983	46.8

9	2.235E-05	0.062	0.012	4.24E-09	0.983	47.5
12	2.196E-05	0.062	0.013	4.23E-09	0.983	48.2
15	2.158E-05	0.063	0.013	4.22E-09	0.982	48.9
18	2.120E-05	0.063	0.014	4.20E-09	0.982	49.5
21	2.082E-05	0.064	0.015	4.18E-09	0.982	50.2
24	2.044E-05	0.064	0.016	4.16E-09	0.982	50.8
27	2.007E-05	0.065	0.017	4.13E-09	0.981	51.5
30	1.969E-05	0.066	0.017	4.11E-09	0.981	52.1
33	1.932E-05	0.066	0.018	4.08E-09	0.981	52.7
36	1.895E-05	0.067	0.019	4.04E-09	0.981	53.3
39	1.859E-05	0.067	0.02	4.01E-09	0.981	53.9
42	1.822E-05	0.068	0.021	3.97E-09	0.98	54.5
45	1.787E-05	0.068	0.022	3.93E-09	0.98	55
48	1.751E-05	0.069	0.023	3.89E-09	0.98	55.6
51	1.716E-05	0.069	0.024	3.85E-09	0.98	56.1
54	1.681E-05	0.07	0.025	3.81E-09	0.98	56.6
57	1.647E-05	0.07	0.026	3.76E-09	0.979	57.1
60	1.613E-05	0.071	0.027	3.71E-09	0.979	57.5
63	1.579E-05	0.071	0.028	3.66E-09	0.979	58
66	1.546E-05	0.072	0.029	3.61E-09	0.979	58.4
69	1.513E-05	0.072	0.031	3.56E-09	0.979	58.9
72	1.481E-05	0.073	0.032	3.51E-09	0.979	59.3
75	1.449E-05	0.073	0.033	3.46E-09	0.978	59.7
78	1.418E-05	0.074	0.034	3.41E-09	0.978	60.1
81	1.387E-05	0.074	0.035	3.35E-09	0.978	60.4
84	1.357E-05	0.075	0.036	3.30E-09	0.978	60.8
87	1.327E-05	0.075	0.037	3.25E-09	0.978	61.1
90	1.298E-05	0.075	0.038	3.19E-09	0.978	61.5
93	1.269E-05	0.076	0.039	3.14E-09	0.978	61.8
96	1.241E-05	0.076	0.04	3.08E-09	0.978	62.1
99	1.213E-05	0.077	0.041	3.03E-09	0.977	62.4
102	1.186E-05	0.077	0.042	2.97E-09	0.977	62.7
105	1.159E-05	0.077	0.043	2.92E-09	0.977	63
Overall				3.74E-09	0.482	

Table 7.4 depicts the profile at 1 mM S(IV). Under these conditions, the absorption is almost completely gas film controlled throughout the column. There is

a lot of S(IV) at the interface, but there is essentially no chlorine since it reacts with the S(IV) as soon as it diffuses to the interface.

Table 7.4. Chlorine profile at 23.5 ppm and 1 mM S(IV)

Section	$P_{Cl_2,b}$ (atm)	$[S(IV)]_b$ (mM)	$[S(IV)]_i$ (mM)	N_{Cl_2} (kmol/m ² -s)	$Cl_{2,out}/Cl_{2,in}$	K_{OG}/k_g (%)
0	2.350E-05	1	0.902	8.32E-09	0.968	88.6
3	2.275E-05	1.00	0.907	8.06E-09	0.968	88.6
6	2.202E-05	1.00	0.911	7.80E-09	0.968	88.6
9	2.131E-05	1.00	0.915	7.56E-09	0.968	88.6
12	2.063E-05	1.00	0.919	7.32E-09	0.968	88.6
15	1.997E-05	1.01	0.922	7.08E-09	0.968	88.7
18	1.933E-05	1.01	0.926	6.86E-09	0.968	88.7
21	1.871E-05	1.01	0.929	6.64E-09	0.968	88.7
24	1.811E-05	1.01	0.933	6.43E-09	0.968	88.7
27	1.753E-05	1.01	0.936	6.22E-09	0.968	88.7
30	1.697E-05	1.01	0.939	6.02E-09	0.968	88.8
33	1.642E-05	1.01	0.942	5.83E-09	0.968	88.8
36	1.590E-05	1.01	0.945	5.65E-09	0.968	88.8
39	1.539E-05	1.01	0.948	5.47E-09	0.968	88.8
42	1.489E-05	1.01	0.951	5.29E-09	0.968	88.8
45	1.441E-05	1.01	0.953	5.12E-09	0.968	88.8
48	1.395E-05	1.01	0.956	4.96E-09	0.968	88.8
51	1.350E-05	1.02	0.958	4.80E-09	0.968	88.9
54	1.307E-05	1.02	0.961	4.65E-09	0.968	88.9
57	1.265E-05	1.02	0.963	4.50E-09	0.968	88.9
60	1.224E-05	1.02	0.966	4.35E-09	0.968	88.9
63	1.185E-05	1.02	0.968	4.21E-09	0.968	88.9
66	1.147E-05	1.02	0.970	4.08E-09	0.968	88.9
69	1.110E-05	1.02	0.972	3.95E-09	0.968	88.9
72	1.074E-05	1.02	0.974	3.82E-09	0.968	88.9
75	1.040E-05	1.02	0.976	3.70E-09	0.968	88.9
78	1.006E-05	1.02	0.978	3.58E-09	0.968	89
81	9.739E-06	1.02	0.980	3.47E-09	0.968	89
84	9.426E-06	1.02	0.981	3.36E-09	0.968	89
87	9.123E-06	1.02	0.983	3.25E-09	0.968	89
90	8.829E-06	1.02	0.985	3.14E-09	0.968	89
93	8.545E-06	1.02	0.986	3.04E-09	0.968	89
96	8.270E-06	1.02	0.988	2.95E-09	0.968	89
99	8.004E-06	1.02	0.989	2.85E-09	0.968	89

102	7.747E-06	1.02	0.991	2.76E-09	0.968	89
105	7.497E-06	1.02	0.992	2.67E-09	0.968	89
Overall				4.993E-09	0.309	

7.1.3.3 Model sensitivity

In order to ensure that the regressed rate constant was not sensitive to errors in the mass transfer characteristics, the sensitivity of the model was examined. These analyses were done using an inlet concentration of 23.5 ppm, with a gas flow of 4.78 L/min to the column. Since the mass transfer properties were not expected to vary more than 10% of the values calculated in Chapter 5, the model sensitivity was studied by varying each of the parameters by $\pm 10\%$ and seeing the resulting effect on the predicted penetration, as depicted in Figures 7.4 through 7.6. The solid line in each figure represents the base case. The values for the parameters for the base case are listed in Table 7.5. The dashed lines in the figures represent the predicted penetration obtained by varying a parameter by 10%.

Table 7.5. Parameters used for base case model sensitivity analyses at pH 4.7

Parameter	Value
G (L/min)	4.78
[succinate buffer] (mM)	5
$k_{2,buf}$ (L/mol-s)	1.5×10^5
$k_{2,S(IV)}$ (L/mol-s)	2×10^9
$P_{Cl_2,in}$ (atm)	2.35×10^{-5}
k_g (mol/s-atm-m ²)	0.4
$k_{L,S(IV)}^0$ (m/s)	8.53×10^{-5}
Area (cm ²)	108

Figure 7.4 depicts the result in varying the k_g by 10%. The k_g was varied to 0.36 and 0.44 mol/s-atm-m². The variation in k_g mainly affects the data at high S(IV); this is the region in which the absorption becomes gas film controlled.

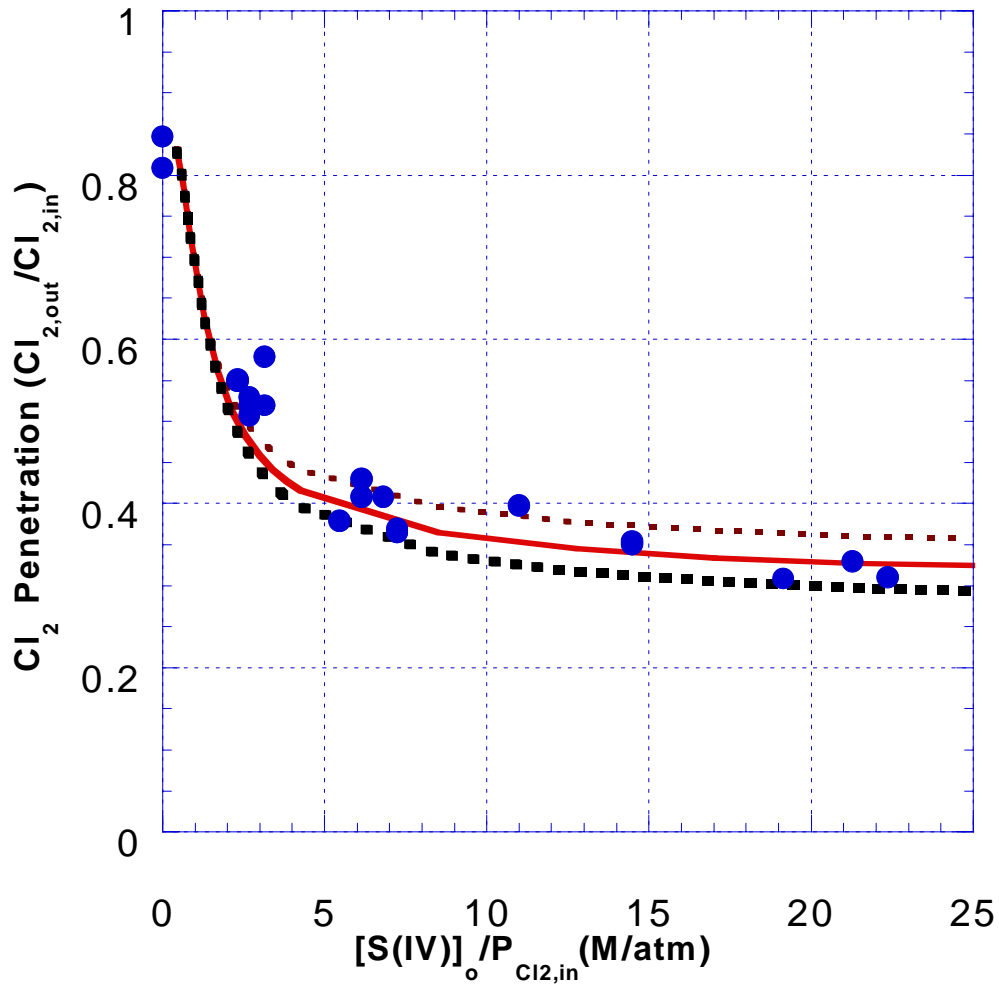


Figure 7.4 Effect of varying k_g on predicted chlorine penetration

Figure 7.5 shows how varying $k_{L,S(IV)}^o$ affects the predicted penetration. The $k_{L,S(IV)}^o$ is varied from 7.58×10^{-5} to 9.48×10^{-5} m/s. The value of $k_{L,S(IV)}^o$ has a negligible effect. The biggest impact is in the region of very low S(IV), where the absorption is limited by S(IV) diffusion. However, when plotting penetration, the

impact is negligible. Since the reaction is a fast reaction, it makes sense that the absorption should not be very sensitive to the $k_{L,S(IV)}^0$ value.

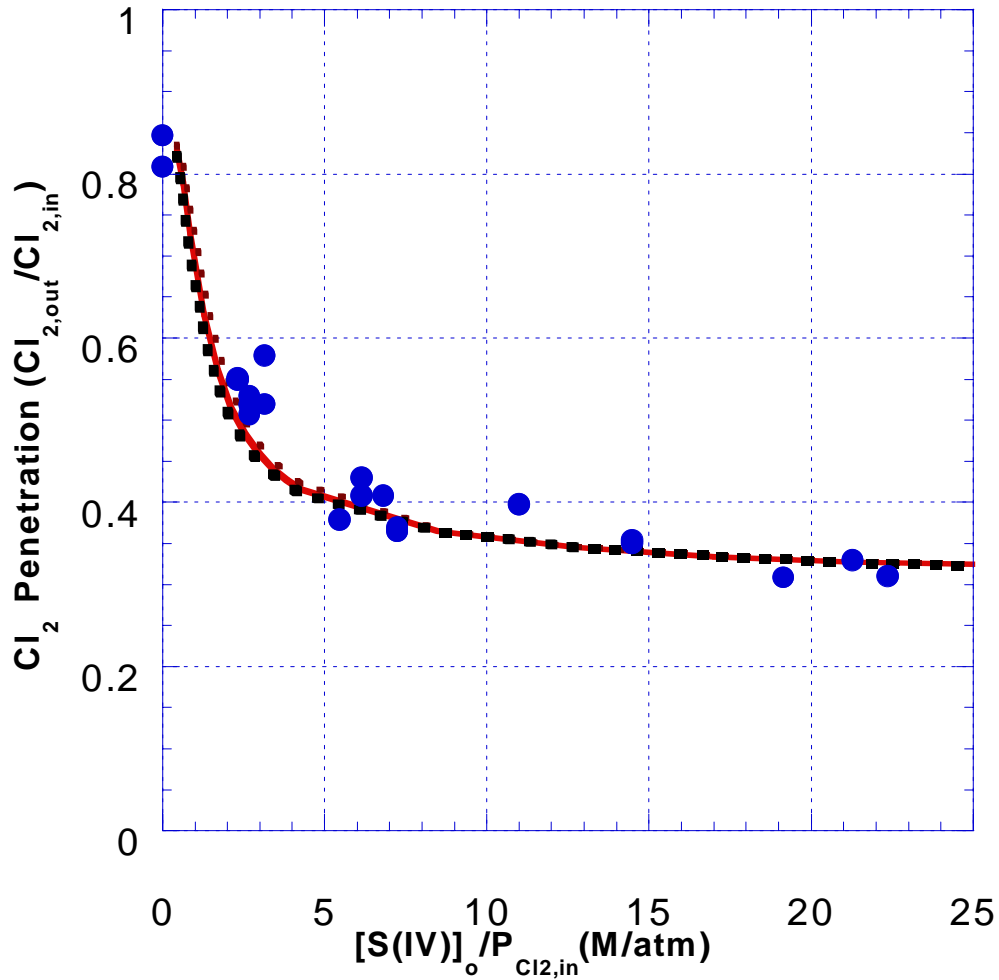


Figure 7.5 Effect of varying $k_{L,S(IV)}^0$ on predicted chlorine penetration

Figure 7.6 shows the affect of varying the area from 99 to 117 cm². For these calculations, the model still divides the column into 3-cm² sections. For the lower area, the model divides the column into 33 sections. For the higher area, there are 39 sections. Just as with k_g , the area does have a slight effect on the predicted penetration.

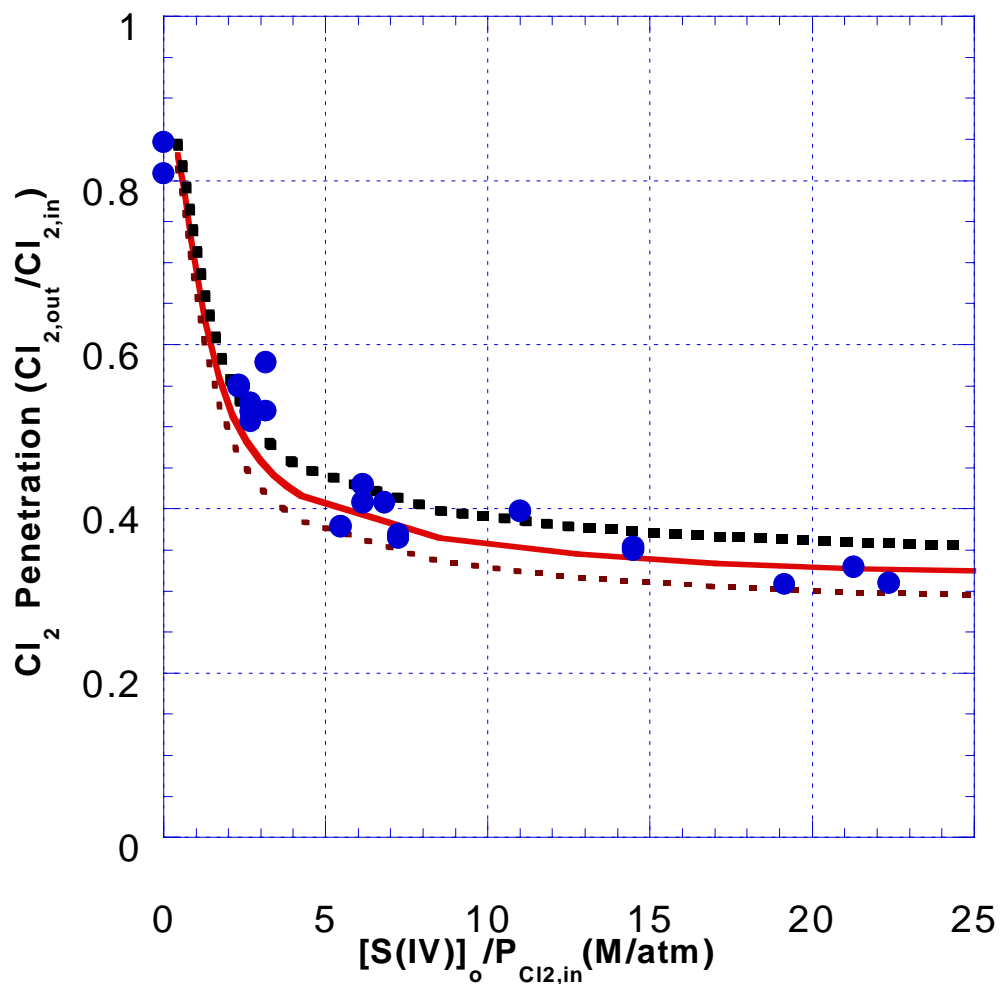


Figure 7.6. Effect of varying area on chlorine penetration

Sensitivity analyses to the rate constants were also done. The $k_{2,S(IV)}$ was regressed using a higher $k_{2,buf}$ of 3.5×10^5 L/mol-s. Increasing the buffer rate had no effect on the regressed constant for the rate $Cl_2/S(IV)$ reaction. Also, varying the $k_{2,S(IV)}$ had no impact on regressing $k_{2,buf}$. The original $k_{2,buf}$ of 1.5×10^5 L/mol-s fit the absorption in buffer data better than the higher value of 3.5×10^5 L/mol-s, but the S(IV) data were unaffected.

Figure 7.7 shows the effect on the penetration when the $k_{2,S(IV)}$ is varied by an order of magnitude.

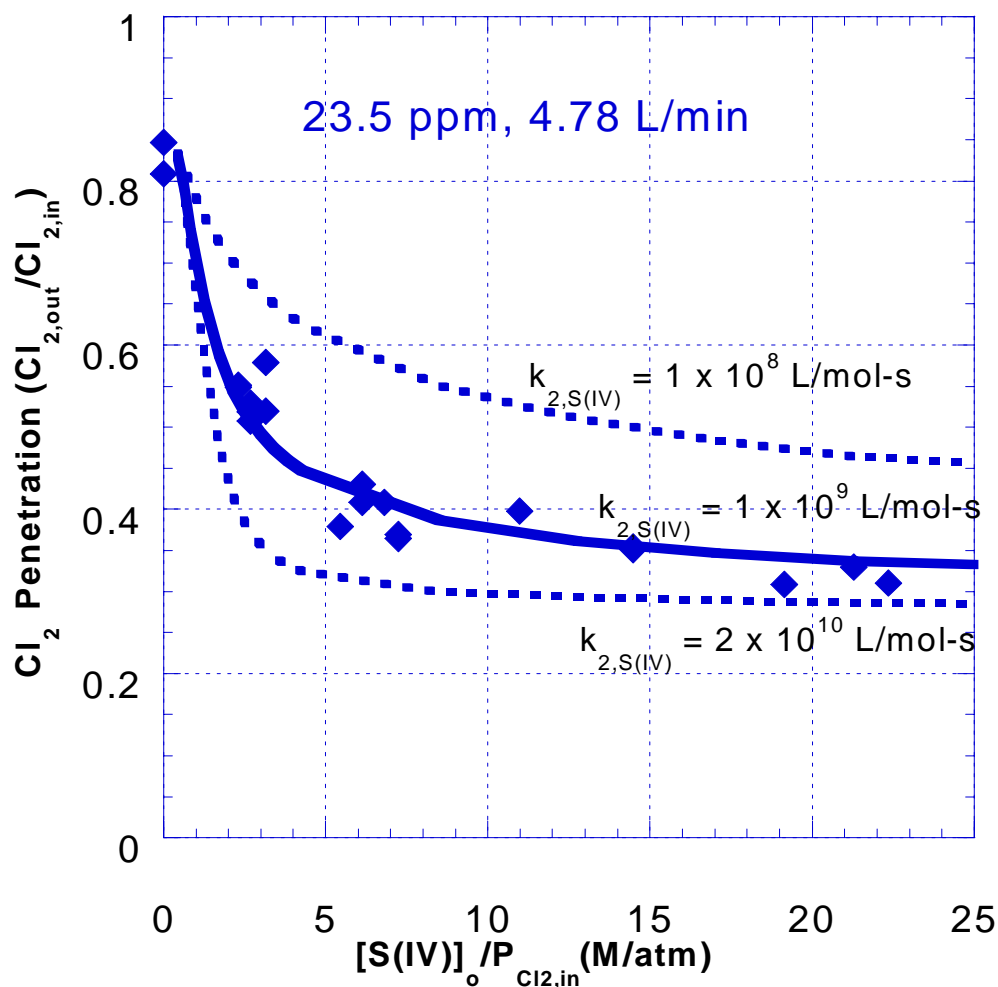


Figure 7.7 Effect of varying $k_{2,S(IV)}$ on chlorine penetration

These analyses show that the model was primarily sensitive to the $Cl_2/S(IV)$ reaction rate. Thus, the wetted wall column resulted in the extraction of a more precise rate constant, with a value of $(1.0 \pm 0.2) \times 10^9$ L/mol-s, than the stirred cell reactor.

7.2 CHLORINE ABSORPTION IN WETTED WALL COLUMN AT pH 5.7

The rate constant for the reaction of Cl_2 with S(IV) at pH 5.7 was regressed from the data discussed in this section. The data were collected from the simultaneous absorption of Hg and Cl_2 . Since the flux of Hg is three orders of magnitude less than the Cl_2 flux, the chlorine absorption was not affected by the presence of mercury. The mercury absorption data will be discussed in Chapter 8. The same model, as in the last section, was used to regress the Cl_2 /S(IV) rate constant.

7.2.1 *Experimental method*

The absorption of mercury and chlorine into buffered S(IV) solutions was measured at pH 5.7. An experiment was also done in buffered S(IV) solution containing 0.1 M NaCl. The 3.1 L plexiglass reservoir was used for all the experiments discussed in this section. The gas flow to the column was 4.78 L/min, and the liquid flow was 2.26 mL/s. The chlorine inlet concentration was varied from 6 to 40 ppm. In previous experiments, the chlorine concentration was kept constant while the S(IV) concentration was varied. However, a different procedure was used here. The experiment started with absorption in buffer, while varying the chlorine inlet. Then, S(IV) was added, and the chlorine inlet was again varied. The Cl_2 inlet was varied at several S(IV) concentrations. The S(IV) was periodically sampled, but (unlike previous data) it was not measured at each of the data points shown in Table 7.6.

To buffer at pH 5.7, the equimolar succinic acid/NaOH buffer could not be used. Instead, a ratio of 1:1.8 of succinic acid: NaOH was used. The buffer concentration for all the experiments at pH 5.7 was 2.78 mM succinic acid-5 mM NaOH. The enhancement of this buffer on chlorine absorption was quantified and is discussed in Section 7.2.3.1.

7.2.2 Tabulated results

Table 7.6 tabulates the chlorine absorption data at pH 5.7. The data in Series B contain 0.1 M NaCl, in addition to the buffered S(IV).

Table 7.6. Chlorine absorption in buffered S(IV) at pH 5.65 – 5.75

Series	G (L/min)	[S(IV)] ₀ (mM)	Cl _{2,in} (ppm)	Cl _{2,o} (ppm)	N _{Cl₂} (kmol/m ² s)	Cl _{2,o} /Cl _{2,in}	[S(IV)] ₀ /P _{Cl_{2,in}} (M/atm)
A	4.78	0	6.3	4.41	5.80E-10	0.701	0.0
	4.78	0	12	8.29	1.14E-09	0.691	0.0
	4.78	0	22.4	15.69	2.06E-09	0.701	0.0
	4.78	0	17	11.99	1.54E-09	0.706	0.0
	4.78	0.176	17	6.04	3.37E-09	0.356	10.4
	4.78	0.176	12	4.41	2.33E-09	0.368	14.7
	4.78	0.176	22.4	8.63	4.23E-09	0.385	7.9
	4.78	0.102	39.4	20.56	5.79E-09	0.522	2.6
	4.78	0.102	31.3	14.99	5.01E-09	0.479	3.3
	4.78	0.102	22.4	10.0	3.81E-09	0.447	4.6
	4.78	0.102	12	5.16	2.10E-09	0.430	8.5
	4.78	0.175	12	4.16	2.41E-09	0.346	14.6
	4.78	0.175	22.4	7.83	4.48E-09	0.349	7.8
	4.78	0.175	22.4	7.91	4.45E-09	0.353	7.8
	4.78	0.175	39.4	17.79	6.64E-09	0.451	4.4
	4.78	0.342	39.4	13.26	8.03E-09	0.337	8.7
	4.78	0.342	22.4	6.85	4.78E-09	0.306	15.3
	4.78	0.342	12	3.84	2.51E-09	0.320	28.5
	4.78	0.618	12	3.66	2.56E-09	0.305	51.5
	4.78	0.618	22.4	6.33	4.94E-09	0.283	27.6
	4.78	0.618	39.4	12.25	8.34E-09	0.311	15.7
	4.78	0.618	31.3	9.33	6.75E-09	0.298	19.7
	4.78	0.618	17	4.93	3.71E-09	0.290	36.4
B	4.78	0.213	22.4	7.19	4.68E-09	0.321	9.5

7.2.3 Discussion

The experimental values were compared to the predicted values to regress the Cl₂/S(IV) rate constant. Table 7.7 tabulates the parameters used in the model.

Table 7.7. Parameters used in model for pH 5.7 chlorine absorption

Parameter	Value
G (L/min)	4.78
k_g (mol/s-atm-m ²)	0.4
$k_{L,S(IV)}^o$ (m/s)	8.53×10^{-5}
Area (cm ²)	108

7.2.3.1 Regressed $k_{2,buf}$ at pH 5.7

Before the $Cl_2/S(IV)$ rate constant can be regressed, the buffer enhancement at pH 5.7 must be quantified. The value for $k_{2,buf}$ was regressed from the first four data points in Table 7.6 (data in which no S(IV) is present). The buffer reaction rate was written in terms of the anion equivalents, $[A^-]$. The reaction rate was expressed as:

$$\text{rate} = k_{2,buf}[Cl_2][A^-] \quad (7-1)$$

Another way to express the rate is in terms of the total succinate concentration as shown in Equation 7-2.

$$\text{rate} = k_{2,buf}[Cl_2][\text{succinate}]_T \quad (7-2)$$

At pH 4.5, both rate expressions would yield the same rate constant since the concentrations are equal (resulting from equimolar succinic acid/NaOH). In the pH 4.5 data, the buffer was essentially the mono-succinate ion since the pK_{a1} is 4.21 (Lide, 2000). Since succinic acid is a diprotic acid with a pK_{a2} of 5.64 (Lide, 2000), at pH 5.7, di-succinate is primarily present. Since the succinic acid: NaOH ratio used here was 1:1.8, the concentration of total succinate is 2.78 mM, while the concentration of equivalent anions is 5 mM. The buffer reaction rate was regressed using the formulation in Equation 7-1.

The regressed $k_{2,buf}$ value used to obtain the $Cl_2/S(IV)$ reaction rate at pH 5.7 was $(8.5 \pm 0.5) \times 10^5$ L/mol-s. This rate is higher than the rate for enhancement in pH

4.5 buffer, which was discussed in Section 6.3. This observation agrees with that of Lifshitz and Perlmutter-Hayman (1962), who correlated the rate constant (k_A) with the K_a values for various weak acid systems at 9.5°C.

$$k_A = 1.6 (K_a)^{-0.54} \quad (7-3)$$

The rate constant increases with decreasing K_a (increasing pK_a). The pK_{a2} for succinic acid (dissociation of mono-succinate ion to di-succinate ion) is greater than the pK_{a1} (dissociation of succinic acid to mono-succinate ion); thus, the rate constant is higher at pH 5.7 than at pH 4.7. In order to do a quantitative comparison of the results of this work to that of Lifshitz and Perlmutter-Hayman, the correlation must be at the same temperature as the data. The K_a values used by Lifshitz and Perlmutter-Hayman (1962) at 9.5°C are very similar to the values at 25°C (Lide, 2000) as shown in Table 7.8.

Table 7.8 Comparison of K_a values at 9.5°C and 25°C

Acid	pK_a at 9.5°C	pK_a at 25°C
acetic	4.759	4.756
chloroacetic	2.81	2.87
formic	3.72	3.75

Table 7.8 shows that the K_a is not very sensitive to temperature. However, depending on the activation energy, rate constants may be very sensitive to temperature. Therefore, instead of comparing the absolute rate constants obtained from this work directly to Equation 7-3, the dependence on K_a was compared. The correlation that best fit the $k_{2,buf}$ regressed in this work is shown by Equation 7-4.

$$k_A = 770 (K_a)^{-0.54} \quad (7-4)$$

This correlation has the same dependence on K_a as the correlation obtained by Lifshitz and Perlmutter-Hayman (1962). Table 7.9 compares the observed values to those predicted by Equation 7-4.

Table 7.9 Correlation for $k_{2,buf}$ as a function K_a at ambient temperature

pH	pK _a	Observed $k_{2,buf}$ (L/mol-s)	Predicted $k_{2,buf}$ (L/mol-s)
4.5-4.7	4.21	1.5×10^5	1.45×10^5
5.7	5.64	8.5×10^5	8.55×10^5

As previously mentioned in Section 7.1.3.3, the regression of the $Cl_2/S(IV)$ rate constant is not sensitive to the $k_{2,buf}$ value. This was confirmed at pH 5.7. The $Cl_2/S(IV)$ rate constant was also regressed with a lower value of 3.5×10^5 L/mol-s. Lowering the buffer rate had no effect on the regressed value for $k_{2,S(IV)}$.

7.2.3.2 Regressed $k_{2,S(IV)}$ at pH 5.7

All of the data in Series A of Table 7.6 were used to regress the $Cl_2/S(IV)$ rate constant. However, Figures 7.8 and 7.9 only show the data and model predictions at the three inlet concentrations of 12, 22.4, and 39.4 ppm. These are the concentrations which have the most data points and in which the variation of S(IV) was the greatest. The model curves were calculated using the regressed $k_{2,S(IV)}$ of $(1.4 \pm 0.5) \times 10^9$ L/mol-s and $k_{2,buf}$ of $(8.5 \pm 0.5) \times 10^5$ L/mol-s.

Figure 7.8 shows how the predicted flux compares with the observed flux. Since the buffer enhancement is greater at pH 5.7, the range of flux is much narrower than it was with the pH 4.7 data (as shown in Figure 7.1).

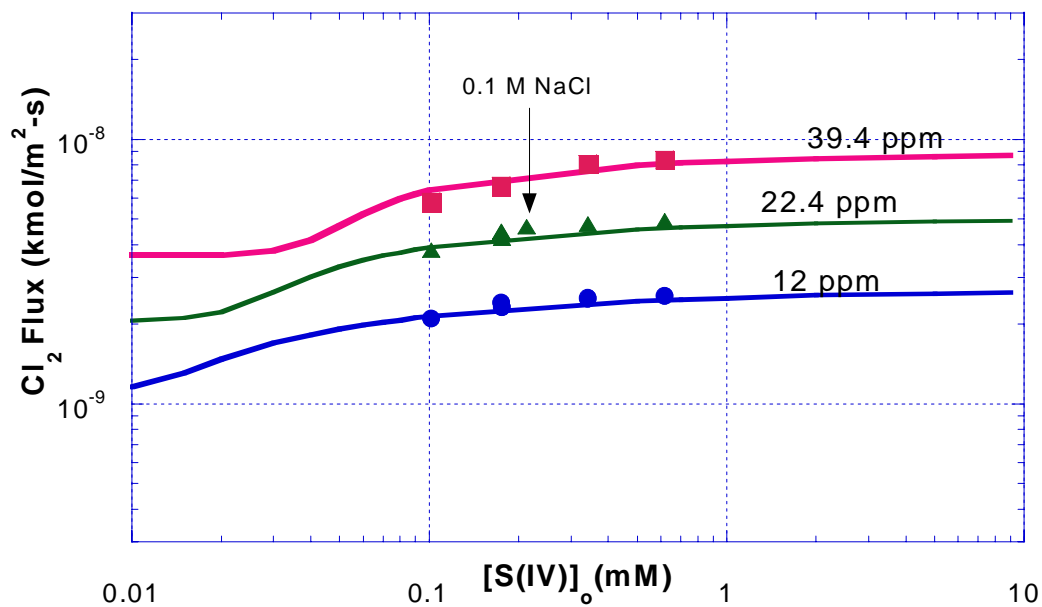


Figure 7.8. Chlorine absorption in buffered S(IV) at pH 5.7, $k_{2,S(IV)} = 1.4 \times 10^9$ L/mol-s

Figure 7.9 compares the observed penetration to the predicted penetration.

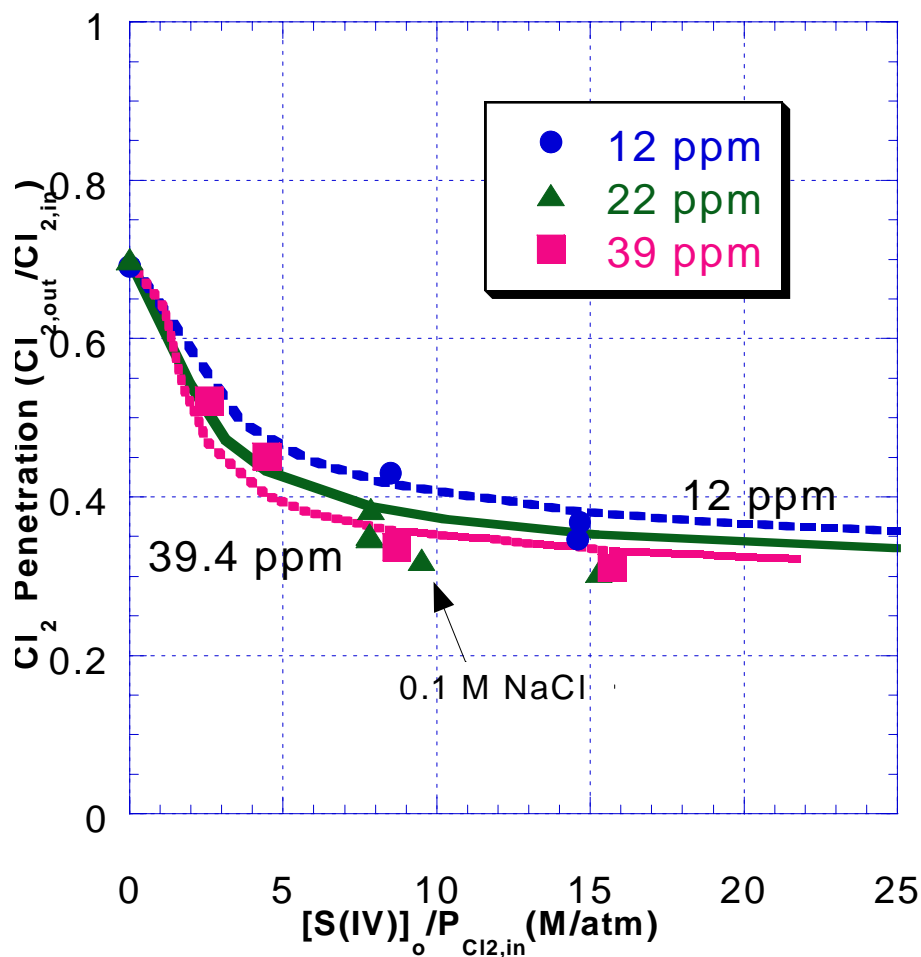


Figure 7.9 Chlorine penetration in buffered S(IV) at pH 5.7, $k_{2,S(IV)} = 1.4 \times 10^9$ L/mol-s

The $\text{Cl}_2/\text{S(IV)}$ rate constant at pH 5.7 is slightly greater than the value at pH 4.7. However, the uncertainty is greater also. The lack of precision at pH 5.7 probably results from the difference in procedure and the narrower range in observable flux/penetration.

7.2.3.3 Effect of 0.1 M NaCl

The data point in 0.1 M sodium chloride is plotted in Figure 7.8 and 7.9. The chloride did not have a statistically significant effect on the $\text{Cl}_2/\text{S(IV)}$ reaction rate. This observation was also seen in Section 6.5.3.1. Since the $\text{Cl}_2/\text{S(IV)}$ reaction is irreversible, the addition of chloride should not affect the absorption rate, unless the solution is at a very high ionic strength where activity coefficient corrections may become significant.

7.3 COMPARISON OF S(IV) REACTION RATES WITH $\text{Cl}_2/\text{HOCl}/\text{OCl}^-$

Fogelman et al. (1989) quantified the reaction rates of S(IV) with hypochlorous acid (HOCl) and hypochlorite (OCl^-). The reaction rate decreased with pH, as the HOCl was converted to OCl^- . Table 7.10 tabulates the rate constants for the reaction of S(IV) with Cl_2 (obtained from this work), HOCl, and OCl^- . All reaction rates were first order in S(IV) and first order in the chlorine species.

Table 7.10. Reaction rates of S(IV) with chlorine species at 25°C

Chlorine species	Rate constant for reaction with S(IV) (L/mol-s)
Cl_2	1.1×10^9
HOCl	7.6×10^8
OCl^-	2.3×10^4

At high pH, OCl^- is the dominant species. As the pH is decreased, HOCl becomes the dominant species, and the reaction rate with S(IV) is four orders of magnitude faster (Fogelman et al., 1989). As the pH is decreased further, chlorine is the dominant species, resulting in an even faster reaction rate with S(IV).

7.4 SUMMARY

Chlorine absorption in the wetted wall column resulted in the regression of a more precise rate constant, compared to the stirred cell reactor. The basic trends in the data were the same as that observed in the data from the stirred cell reactor.

However, the range of kinetics-limited absorption was greater using the wetted wall column. At pH 4.7 and 5.7, the $\text{Cl}_2/\text{S(IV)}$ rate constant with a 95 % confidence interval was $(1.0 \pm 0.2) \times 10^9 \text{ L/mol-s}$ and $(1.4 \pm 0.5) \times 10^9 \text{ L/mol-s}$, respectively. Since the rate constants were very similar, an average value of $(1.1 \pm 0.3) \times 10^9 \text{ L/mol-s}$ can be reported for the $\text{Cl}_2/\text{S(IV)}$ reaction rate. The reaction rate of S(IV) with Cl_2 is greater than that with HOCl and OCl^- . The addition of 0.1 M sodium chloride did not affect this reaction rate. The greater uncertainty at pH 5.7 resulted from the increased scatter in the data due to the imprecision in the experimental procedure (varying Cl_2 and S(IV) without measuring S(IV) at each point).

Section profiles can be calculated to observe how concentrations change throughout the column. As the gas goes through the column, Cl_2 concentration decreases as it is absorbed. As the liquid flows through the column, the S(IV) concentration also decreases as it is depleted through reaction with Cl_2 . The Cl_2 concentration is the least at the top of the column, while the S(IV) concentration is the greatest. Therefore, at the top of the column, the absorption is closer to gas film control than at the bottom. The model uses the concentrations in each section to calculate the overall chlorine flux and penetration. These predicted values are compared with the experimental values in order to regress the $\text{Cl}_2/\text{S(IV)}$ rate constant.

Sensitivity analyses showed that the model is very sensitive to the $\text{Cl}_2/\text{S(IV)}$ rate constant. The buffer rate constant does not affect the regression of the $\text{Cl}_2/\text{S(IV)}$ rate constant. The effect of varying $k_{\text{L,S(IV)}}^0$ is negligible, but there is a slight effect of varying k_{g} and area.

The buffer enhancement was quantified at pH 5.7. The rate constant was regressed with a 95 % confidence interval, $(8.5 \pm 0.5) \times 10^5 \text{ L/mol-s}$. A more precise value is not needed since $k_{2,\text{buf}}$ does not affect the regression of $k_{2,\text{S(IV)}}$. At pH 5.7, the buffer is primarily the di-succinate ion. Since the $\text{pK}_{\text{a}2}$ is higher than the $\text{pK}_{\text{a}1}$ of succinic acid, the rate constant is greater than that at pH 4.5.

Chapter 8: Simultaneous Absorption of Mercury and Chlorine

This chapter presents the results of the simultaneous absorption of mercury and chlorine into buffered S(IV) experiments conducted in the wetted wall column. The rate constant for the Hg/Cl₂ reaction was regressed (using the same Generalized Regression package) at ambient temperature at an approximate pH of 4.7 and 5.7. The effect of adding mercuric chloride (HgCl₂) to the solution was observed. Also, the effects of adding sodium hypochlorite and sodium chloride to the solution were studied. The rates were compared to the results from previous researchers (Zhao, 1997; Nene and Rane, 1981), and mechanisms are proposed to elucidate the chemistry occurring. The implications of these results on mercury removal in a typical limestone slurry scrubber are also discussed in this chapter.

8.1 ABSORPTION OF MERCURY AND CHLORINE INTO S(IV) AT PH 4.7

The rate constant for the reaction of Hg and Cl₂ at pH 4.7 was regressed from the data in this section.

8.1.1 *Experimental method*

The absorption of Hg and Cl₂ into buffered S(IV) solutions, with pH ranging from 4.7 to 4.8, was measured in the wetted wall column. The gas flow to the column was 4.78 L/min, and the liquid flow was 2.26 mL/s. The chlorine was analyzed using the IMS analyzer, and the Hg was analyzed using the CVAA analyzer. The 3.1 L plexiglass reservoir was used for all the data. The Hg inlet concentration was approximately 46 ppb, while the chlorine inlet ranged from 6 to 40 ppm. The experiment started with absorption into 5 mM buffer (5 mM succinic acid-5 mM NaOH), while varying the chlorine inlet. Then, S(IV) was injected into the buffer,

and the chlorine inlet was varied again. The chlorine inlet was varied at several S(IV) concentrations, ranging from 0 to 1 mM. This procedure is analogous to that described in Section 7.2.1.

8.1.2 Tabulated results

Table 8.1 tabulates the data discussed in this section. The data are at pH 4.7 to 4.75. However, the data at high S(IV) (greater than 0.8 mM) are at pH 4.8 to 4.85. The Hg inlet concentration is 46 ppb. During all of these experiments, the chlorine mass flow controller drifted during the experiment, causing greater Cl₂ flow towards the end of each data series. Even though the chlorine flow controller did occasionally drift, the data in this section is the only data set in which the drift occurred during an experiment. Also, some of the data in Series C do not report the outlet chlorine concentration because the concentration was above the range of the analyzer.

Table 8.1. Mercury and chlorine absorption in buffered S(IV) at pH 4.7

Series	[S(IV)] _o (mM)	Hg _o (ppb)	Hg _o /Hg _{in}	N _{Hg} (kmol/m ² s)	Cl _{2,in} (ppm)	Cl _{2,o} (ppm)	N _{Cl2} (kmol/m ² s)	Cl _{2,o} /Cl _{2,in}
A	0	46	1	0	0	0	0	n/a
	1	46	1	0	0	0	0	n/a
B	0	24.8	0.54	6.51E-12	22.4	16.5	1.81E-09	0.737
	0	26.7	0.58	5.95E-12	17.1	12.8	1.34E-09	0.746
	0	28.5	0.62	5.39E-12	12	8.92	9.46E-10	0.743
	0.044	34.2	0.74	3.63E-12	12	5.93	1.87E-09	0.494
	0.044	34.4	0.75	3.56E-12	12	6.29	1.75E-09	0.524
	0.044	31.4	0.68	4.47E-12	17.1	10.3	2.08E-09	0.604
	0.033	24.8	0.54	6.51E-12	29.4	21.5	2.42E-09	0.732
	0.033	26.2	0.57	6.09E-12	22.4	15.8	2.03E-09	0.705
	0.033	25.5	0.55	6.30E-12	22.4	16.6	1.77E-09	0.743
	0.044	27.8	0.60	5.60E-12	22.4	12.2	3.15E-09	0.542
	0.044	32.8	0.71	4.05E-12	12	5.48	2.00E-09	0.457
	0.044	31.7	0.69	4.40E-12	17.1	8.77	2.56E-09	0.513
	0.044	24.8	0.54	6.51E-12	29.4	18.9	3.22E-09	0.644
C	0	32.9	0.72	4.03E-12	6.3	5.06	3.82E-10	0.803
	0	28.9	0.63	5.27E-12	17.1	13.1	1.23E-09	0.766
	0	25.2	0.55	6.41E-12	22.4	17.5	1.51E-09	0.781

	0	23.0	0.50	7.06E-12	31.3	n/a	n/a	n/a
	0	20.9	0.45	7.71E-12	39.4	n/a	n/a	n/a
	0	20.6	0.45	7.81E-12	39.4	n/a	n/a	n/a
	0	27.0	0.59	5.85E-12	12	10.04	6.04E-10	0.836
	0.23	32.9	0.72	4.03E-12	13.3	4.30	2.76E-09	0.324
	0.23	38.1	0.83	2.43E-12	7.6	2.59	1.54E-09	0.341
	0.23	30.1	0.66	4.87E-12	40.9	14.47	8.12E-09	0.354
	0.23	33.9	0.74	3.73E-12	23.2	7.91	4.70E-09	0.341
	0.23	33.7	0.73	3.77E-12	23.2	8.17	4.62E-09	0.352
	0.23	35.1	0.76	3.34E-12	18	6.17	3.64E-09	0.343
	0.86	35.1	0.76	3.34E-12	18	4.90	4.03E-09	0.272
	0.86	38.6	0.84	2.26E-12	7.6	2.28	1.63E-09	0.300
	0.86	37.9	0.82	2.49E-12	7.6	2.28	1.63E-09	0.300
	0.86	36.2	0.79	3.02E-12	13.3	3.73	2.94E-09	0.281
	0.86	31.8	0.69	4.35E-12	40.9	10.66	9.30E-09	0.261
	0.86	32.6	0.71	4.12E-12	33	8.40	7.56E-09	0.255
	0.86	32.6	0.71	4.12E-12	33	8.45	7.54E-09	0.256
	0.86	35.0	0.76	3.37E-12	23.2	6.35	5.18E-09	0.274
	0.86	33.3	0.72	3.90E-12	23.2	6.38	5.17E-09	0.275

8.1.3 Discussion

Series A in Table 8.1 shows that the buffered S(IV) solution does not absorb any Hg. Experiments showed that Hg did not absorb into distilled water, 5 mM buffer, or S(IV) unless chlorine was also present in the column. Thus, there is no direct reaction of Hg with S(IV). The addition of S(IV) results in a decrease in chlorine, which causes an increase in the mercury penetration.

8.1.3.1 Regressing $k_{2,Hg}$ at pH 4.7

The Hg/Cl₂ rate constant was regressed from all the data in Series B and C. Table 8.2 tabulates the parameters used in the model.

Table 8.2. Parameters used to regress Hg/Cl₂ reaction rate at pH 4.7

Parameter	Value
G (L/min)	4.78
[succinate buffer] (mM)	5
$k_{2,buf}$ (L/mol-s)	1.5×10^5
$k_{2,S(IV)}$ (L/mol-s)	1.0×10^9
$P_{Hg,in}$ (atm)	4.6×10^{-8}
k_{g,Cl_2} (mol/s-atm-m ²)	0.4
$k_{g,Hg}$ (mol/s-atm-m ²)	0.4
k_{L,Cl_2}^o (m/s)	9.0×10^{-5}
$k_{L,S(IV)}^o$ (m/s)	8.53×10^{-5}
Area (cm ²)	108

The regressed $k_{2,Hg}$ with a 95 % confidence interval was $(6.2 \pm 0.8) \times 10^9$ L/mol-s, which is much lower than what Zhao (1997) predicted from absorbing Hg into NaOCl/NaCl solutions at high pH. The differences will be discussed in Section 8.4.

Figure 8.1 shows the model calculations using this rate constant. For this calculation, the S(IV) concentration was varied from 0 to 9 mM, and the Cl₂ inlet was varied from 6 to 80 ppm. Figure 8.2 shows the data, along with the appropriate model curves. The data at 0.044 mM and 0.033 mM S(IV) are not shown since these S(IV) concentrations are not significant, but these data were used in the regression of the rate constant.

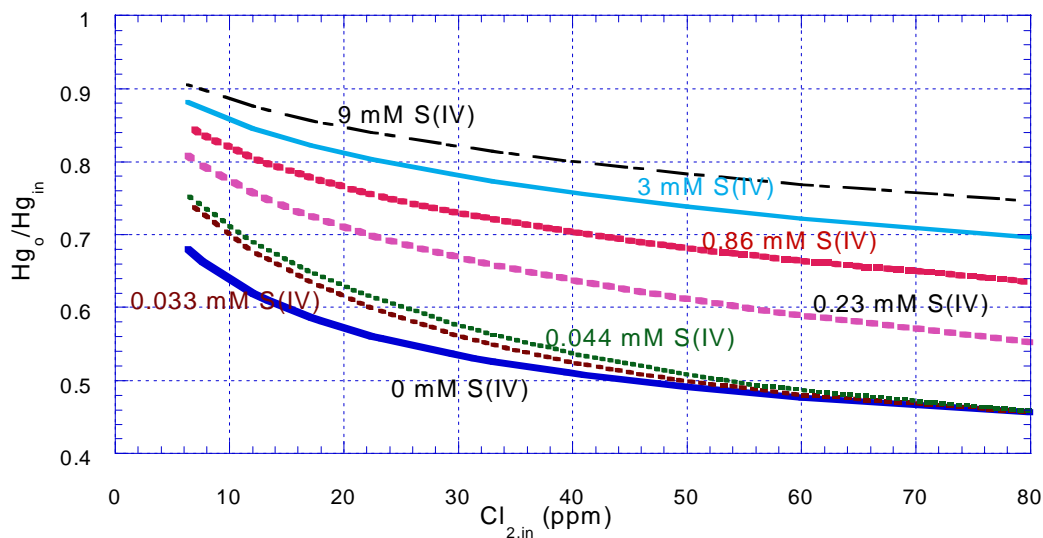


Figure 8.1. Predicted Hg penetration at various Cl_2 and S(IV) at pH 4.7 to 4.8

Figure 8.1 shows that as the chlorine inlet increases, the Hg penetration decreases since more chlorine is available to react with the Hg. Even at 80 ppm chlorine, the Hg penetration is still slightly decreasing. The penetration will decrease until complete gas film control is reached. Figure 8.1 shows that as the S(IV) concentration increases, the Hg penetration decreases since there is less Cl_2 at the interface to react with the Hg. As S(IV) is increased, the Cl_2 concentration does not change significantly since the chlorine absorption becomes gas film controlled, resulting in the Hg penetration curves becoming closer together at high S(IV).

Figure 8.2 shows that there is some scatter in the data, which probably results from the imprecision in the measured concentrations. As noted before, the Hg analyzer drifts, and the chlorine flow controller drifted during these experiments. Therefore, calibration needed to be checked frequently.

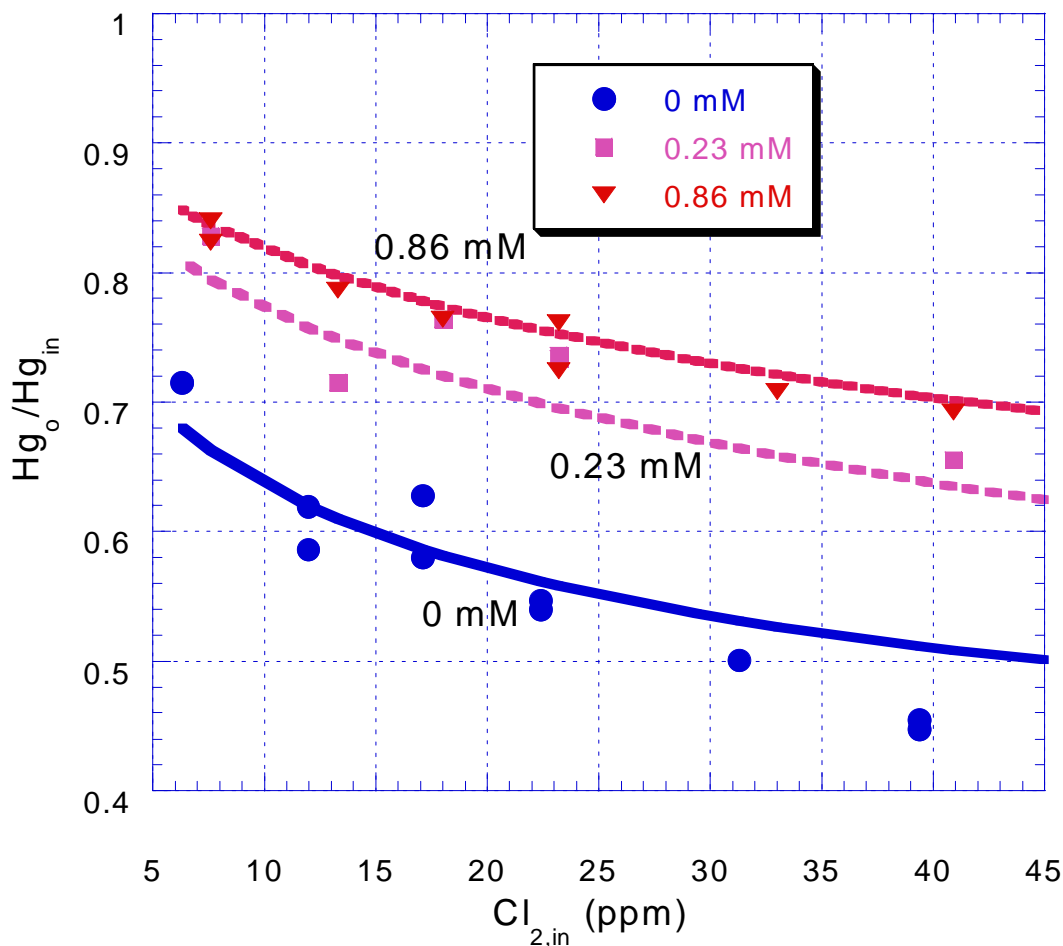


Figure 8.2 Mercury penetration in S(IV) at pH 4.7, $k_{2,Hg} = 6.2 \times 10^9$ L/mol-s

Before the Hg/Cl_2 rate constant was regressed, the new chlorine absorption data from this section were used to confirm the regressed $Cl_2/S(IV)$ rate constant of 1.0×10^9 L/mol-s. The same $k_{2,S(IV)}$ was regressed from the data in this section, confirming the value regressed in Section 7.1. However, there was more scatter present than in the data discussed in Section 7.1.3.1. This scatter is probably due to the different procedures used. In Section 7.1, the S(IV) concentration was varied and analyzed at several points at the same chlorine inlet. In these experiments, the S(IV)

concentration was not measured at each point. The chlorine inlet was varied, assuming the S(IV) concentration was constant (which is reasonable since the time scale between samples was small enough that significant S(IV) depletion would not occur).

8.1.3.2 Section profiles

As in the Cl₂/S(IV) model, the Hg/Cl₂/S(IV) model is also integrated to obtain the bulk concentrations at each point in the column. Using the conditions at the bottom of the column (inlet Hg and Cl₂ and outlet S(IV) concentrations), the model calculates the overall penetration and flux. The parameters in Table 8.2, along with the regressed k_{2,Hg}, were used to calculate the section profiles shown below in Tables 8.3 to 8.6. The profiles show the different “extremes” that occur.

Table 8.3 shows the profile at an outlet S(IV) concentration of 0.01 mM and a chlorine inlet of 7.6 ppm. Since there is very little S(IV), most of the chlorine is available to react with Hg.

Table 8.3. Mercury section profile at 7.6 ppm Cl₂ and 0.01 mM S(IV)

Section	P _{Hg,b} (atm)	[S(IV)] _b (mM)	P _{Cl₂,b} (atm)	[Cl ₂] _b (mM)	[Cl ₂] _i (mM)	[S(IV)] _i (mM)	N _{Hg} (kmol/m ² -s)	Hg _{out} /Hg _{in}
0	4.60E-08	0.01	7.60E-06	4.55E-04	3.51E-04	0.0019	5.73E-12	0.99
3	4.55E-08	0.01	7.54E-06	4.51E-04	3.47E-04	0.002	5.64E-12	0.99
6	4.50E-08	0.01	7.48E-06	4.48E-04	3.43E-04	0.002	5.55E-12	0.99
9	4.45E-08	0.01	7.41E-06	4.44E-04	3.39E-04	0.0021	5.47E-12	0.99
12	4.40E-08	0.01	7.35E-06	4.40E-04	3.35E-04	0.0022	5.39E-12	0.99
15	4.35E-08	0.01	7.29E-06	4.36E-04	3.32E-04	0.0023	5.31E-12	0.99
18	4.30E-08	0.011	7.22E-06	4.32E-04	3.28E-04	0.0023	5.23E-12	0.99
21	4.25E-08	0.011	7.16E-06	4.29E-04	3.24E-04	0.0024	5.15E-12	0.99
24	4.21E-08	0.011	7.10E-06	4.25E-04	3.20E-04	0.0025	5.07E-12	0.99
27	4.16E-08	0.011	7.03E-06	4.21E-04	3.16E-04	0.0026	4.99E-12	0.99
30	4.12E-08	0.011	6.97E-06	4.17E-04	3.12E-04	0.0027	4.92E-12	0.99
33	4.07E-08	0.011	6.91E-06	4.13E-04	3.08E-04	0.0028	4.84E-12	0.99
36	4.03E-08	0.011	6.84E-06	4.10E-04	3.04E-04	0.0029	4.77E-12	0.99
39	3.99E-08	0.011	6.78E-06	4.06E-04	3.01E-04	0.003	4.70E-12	0.99
42	3.94E-08	0.011	6.71E-06	4.02E-04	2.97E-04	0.0031	4.63E-12	0.99

45	3.90E-08	0.011	6.65E-06	3.98E-04	2.93E-04	0.0031	4.56E-12	0.99
48	3.86E-08	0.011	6.59E-06	3.94E-04	2.89E-04	0.0032	4.49E-12	0.99
51	3.82E-08	0.012	6.52E-06	3.91E-04	2.85E-04	0.0033	4.42E-12	0.99
54	3.78E-08	0.012	6.46E-06	3.87E-04	2.82E-04	0.0034	4.35E-12	0.99
57	3.74E-08	0.012	6.40E-06	3.83E-04	2.78E-04	0.0035	4.29E-12	0.99
60	3.70E-08	0.012	6.33E-06	3.79E-04	2.74E-04	0.0037	4.22E-12	0.99
63	3.66E-08	0.012	6.27E-06	3.75E-04	2.71E-04	0.0038	4.16E-12	0.99
66	3.63E-08	0.012	6.21E-06	3.72E-04	2.67E-04	0.0039	4.10E-12	0.99
69	3.59E-08	0.012	6.14E-06	3.68E-04	2.64E-04	0.004	4.04E-12	0.99
72	3.55E-08	0.012	6.08E-06	3.64E-04	2.60E-04	0.0041	3.98E-12	0.99
75	3.52E-08	0.012	6.02E-06	3.60E-04	2.57E-04	0.0042	3.92E-12	0.99
78	3.48E-08	0.012	5.96E-06	3.57E-04	2.53E-04	0.0043	3.86E-12	0.99
81	3.45E-08	0.013	5.89E-06	3.53E-04	2.50E-04	0.0044	3.80E-12	0.99
84	3.41E-08	0.013	5.83E-06	3.49E-04	2.46E-04	0.0045	3.74E-12	0.99
87	3.38E-08	0.013	5.77E-06	3.45E-04	2.43E-04	0.0046	3.69E-12	0.99
90	3.34E-08	0.013	5.71E-06	3.42E-04	2.39E-04	0.0048	3.63E-12	0.99
93	3.31E-08	0.013	5.64E-06	3.38E-04	2.36E-04	0.0049	3.58E-12	0.99
96	3.28E-08	0.013	5.58E-06	3.34E-04	2.33E-04	0.005	3.53E-12	0.99
99	3.25E-08	0.013	5.52E-06	3.31E-04	2.29E-04	0.0051	3.47E-12	0.99
102	3.22E-08	0.013	5.46E-06	3.27E-04	2.26E-04	0.0052	3.42E-12	0.99
105	3.19E-08	0.013	5.40E-06	3.23E-04	2.23E-04	0.0054	3.37E-12	0.99
Overall							4.44E-12	0.69

Table 8.4 shows the profile at an outlet S(IV) concentration of 9 mM and a chlorine inlet of 7.6 ppm. Since the chlorine absorption is gas film controlled throughout the column, there is not much chlorine at the interface to react with the Hg. Thus, the Hg penetration is greater in Table 8.4 than in Table 8.3.

Table 8.4. Mercury section profile at 7.6 ppm Cl₂ and 9 mM S(IV)

Section	P _{Hg,b} (atm)	[S(IV)] _b (mM)	P _{Cl₂,b} (atm)	[Cl ₂] _b (mM)	[Cl ₂] _i (mM)	[S(IV)] _i (mM)	N _{Hg} (kmol/m ² -s)	Hg _{out} /Hg _{in}
0	4.60E-08	9	7.60E-06	4.55E-04	2.49E-05	8.97	1.98E-12	0.996
3	4.58E-08	9	7.34E-06	4.40E-04	2.41E-05	8.97	1.94E-12	0.996
6	4.57E-08	9.00	7.09E-06	4.25E-04	2.33E-05	8.97	1.90E-12	0.996
9	4.55E-08	9.00	6.85E-06	4.10E-04	2.25E-05	8.97	1.87E-12	0.996
12	4.53E-08	9.00	6.61E-06	3.96E-04	2.17E-05	8.97	1.83E-12	0.996
15	4.51E-08	9.00	6.39E-06	3.82E-04	2.10E-05	8.97	1.79E-12	0.996
18	4.50E-08	9.00	6.17E-06	3.69E-04	2.02E-05	8.97	1.76E-12	0.996

21	4.48E-08	9.00	5.96E-06	3.57E-04	1.95E-05	8.98	1.73E-12	0.997
24	4.47E-08	9.00	5.76E-06	3.45E-04	1.89E-05	8.98	1.69E-12	0.997
27	4.45E-08	9.00	5.56E-06	3.33E-04	1.82E-05	8.98	1.66E-12	0.997
30	4.44E-08	9.00	5.37E-06	3.21E-04	1.76E-05	8.98	1.63E-12	0.997
33	4.42E-08	9.00	5.19E-06	3.10E-04	1.70E-05	8.98	1.60E-12	0.997
36	4.41E-08	9.00	5.01E-06	3.00E-04	1.64E-05	8.98	1.57E-12	0.997
39	4.39E-08	9.00	4.84E-06	2.90E-04	1.59E-05	8.98	1.54E-12	0.997
42	4.38E-08	9.00	4.67E-06	2.80E-04	1.53E-05	8.98	1.51E-12	0.997
45	4.37E-08	9.01	4.51E-06	2.70E-04	1.48E-05	8.98	1.48E-12	0.997
48	4.35E-08	9.01	4.36E-06	2.61E-04	1.43E-05	8.99	1.45E-12	0.997
51	4.34E-08	9.01	4.21E-06	2.52E-04	1.38E-05	8.99	1.43E-12	0.997
54	4.33E-08	9.01	4.07E-06	2.43E-04	1.33E-05	8.99	1.40E-12	0.997
57	4.31E-08	9.01	3.93E-06	2.35E-04	1.29E-05	8.99	1.37E-12	0.997
60	4.30E-08	9.01	3.79E-06	2.27E-04	1.24E-05	8.99	1.35E-12	0.997
63	4.29E-08	9.01	3.66E-06	2.19E-04	1.20E-05	8.99	1.32E-12	0.997
66	4.28E-08	9.01	3.54E-06	2.12E-04	1.16E-05	8.99	1.30E-12	0.997
69	4.27E-08	9.01	3.42E-06	2.05E-04	1.12E-05	8.99	1.27E-12	0.997
72	4.25E-08	9.01	3.30E-06	1.98E-04	1.08E-05	8.99	1.25E-12	0.997
75	4.24E-08	9.01	3.19E-06	1.91E-04	1.04E-05	8.99	1.23E-12	0.997
78	4.23E-08	9.01	3.08E-06	1.84E-04	1.01E-05	8.99	1.20E-12	0.997
81	4.22E-08	9.01	2.97E-06	1.78E-04	9.74E-06	8.99	1.18E-12	0.997
84	4.21E-08	9.01	2.87E-06	1.72E-04	9.41E-06	8.99	1.16E-12	0.998
87	4.20E-08	9.01	2.77E-06	1.66E-04	9.09E-06	8.99	1.14E-12	0.998
90	4.19E-08	9.01	2.68E-06	1.60E-04	8.78E-06	9.00	1.12E-12	0.998
93	4.18E-08	9.01	2.59E-06	1.55E-04	8.48E-06	9.00	1.10E-12	0.998
96	4.17E-08	9.01	2.50E-06	1.50E-04	8.19E-06	9.00	1.08E-12	0.998
99	4.16E-08	9.01	2.41E-06	1.44E-04	7.9E-06	9.00	1.06E-12	0.998
102	4.15E-08	9.01	2.33E-06	1.40E-04	7.64E-06	9.00	1.04E-12	0.998
105	4.14E-08	9.01	2.25E-06	1.35E-04	7.37E-06	9.00	1.02E-12	0.998
Overall							1.44E-12	0.90

Table 8.5 shows the profile at an outlet S(IV) concentration of 0.01 mM and a chlorine inlet of 22.4 ppm. Since there is very little S(IV), most of the chlorine is available to react with Hg. Also, since the chlorine inlet is greater than that in Table 8.3, the Hg penetration is lower.

Table 8.5. Mercury section profile at 22.4 ppm Cl₂ and 0.01 mM S(IV)

Section	P _{Hg,b} (atm)	[S(IV)] _b (mM)	P _{Cl₂,b} (atm)	[Cl ₂] _b (mM)	[Cl ₂] _i (mM)	[S(IV)] _i (mM)	N _{Hg} (kmol/m ² -s)	Hg _{out} /Hg _{in}
0	4.60E-08	0.01	2.24E-05	1.34E-03	1.16E-03	0	8.29E-12	0.98
3	4.53E-08	0.01	2.23E-05	1.33E-03	1.15E-03	0	8.15E-12	0.98
6	4.45E-08	0.01	2.22E-05	1.33E-03	1.15E-03	0	8.00E-12	0.98
9	4.38E-08	0.01	2.21E-05	1.32E-03	1.14E-03	0	7.86E-12	0.98
12	4.31E-08	0.011	2.20E-05	1.32E-03	1.14E-03	0	7.72E-12	0.98
15	4.24E-08	0.011	2.19E-05	1.31E-03	1.13E-03	0	7.59E-12	0.98
18	4.17E-08	0.011	2.18E-05	1.30E-03	1.12E-03	0	7.46E-12	0.98
21	4.10E-08	0.011	2.16E-05	1.30E-03	1.12E-03	0	7.33E-12	0.98
24	4.04E-08	0.011	2.15E-05	1.29E-03	1.11E-03	0	7.20E-12	0.98
27	3.97E-08	0.011	2.14E-05	1.28E-03	1.11E-03	0	7.07E-12	0.98
30	3.91E-08	0.012	2.13E-05	1.28E-03	1.10E-03	0	6.95E-12	0.98
33	3.84E-08	0.012	2.12E-05	1.27E-03	1.10E-03	0	6.83E-12	0.98
36	3.78E-08	0.012	2.11E-05	1.26E-03	1.09E-03	0	6.71E-12	0.98
39	3.72E-08	0.012	2.10E-05	1.26E-03	1.09E-03	0	6.59E-12	0.98
42	3.66E-08	0.012	2.09E-05	1.25E-03	1.08E-03	0	6.48E-12	0.98
45	3.60E-08	0.012	2.08E-05	1.25E-03	1.08E-03	0	6.37E-12	0.98
48	3.55E-08	0.012	2.07E-05	1.24E-03	1.07E-03	0	6.25E-12	0.98
51	3.49E-08	0.013	2.06E-05	1.23E-03	1.07E-03	0	6.15E-12	0.98
54	3.43E-08	0.013	2.05E-05	1.23E-03	1.06E-03	0	6.04E-12	0.98
57	3.38E-08	0.013	2.04E-05	1.22E-03	1.05E-03	0	5.94E-12	0.98
60	3.33E-08	0.013	2.03E-05	1.22E-03	1.05E-03	0	5.83E-12	0.98
63	3.27E-08	0.013	2.02E-05	1.21E-03	1.04E-03	0	5.73E-12	0.98
66	3.22E-08	0.013	2.01E-05	1.20E-03	1.03E-03	0.0001	5.63E-12	0.98
69	3.17E-08	0.014	2.00E-05	1.20E-03	1.03E-03	0.0001	5.52E-12	0.98
72	3.12E-08	0.014	1.99E-05	1.19E-03	1.02E-03	0.0001	5.43E-12	0.98
75	3.07E-08	0.014	1.98E-05	1.18E-03	1.01E-03	0.0002	5.33E-12	0.98
78	3.02E-08	0.014	1.97E-05	1.18E-03	1.00E-03	0.0002	5.23E-12	0.98
81	2.98E-08	0.014	1.96E-05	1.17E-03	9.94E-04	0.0002	5.14E-12	0.98
84	2.93E-08	0.014	1.95E-05	1.17E-03	9.86E-04	0.0003	5.05E-12	0.98
87	2.88E-08	0.014	1.94E-05	1.16E-03	9.78E-04	0.0003	4.96E-12	0.98
90	2.84E-08	0.015	1.92E-05	1.15E-03	9.69E-04	0.0003	4.87E-12	0.99
93	2.80E-08	0.015	1.91E-05	1.15E-03	9.61E-04	0.0004	4.78E-12	0.99
96	2.75E-08	0.015	1.90E-05	1.14E-03	9.53E-04	0.0004	4.70E-12	0.99
99	2.71E-08	0.015	1.89E-05	1.13E-03	9.45E-04	0.0004	4.61E-12	0.99
102	2.67E-08	0.015	1.88E-05	1.13E-03	9.36E-04	0.0005	4.53E-12	0.99
105	2.63E-08	0.015	1.87E-05	1.12E-03	9.28E-04	0.0005	4.45E-12	0.99
Overall							6.19E-12	0.56

Table 8.6 shows the profile at an outlet S(IV) concentration of 9 mM and a chlorine inlet of 22.4 ppm. Since the chlorine absorption is gas film controlled throughout the column, there is not much chlorine at the interface to react with the Hg. Thus, the Hg penetration is greater in Table 8.6 than in Table 8.5. Since the chlorine inlet is higher, the penetration is less than it is in Table 8.4. The absorption depicted by Tables 8.4 and 8.6 is gas film controlled for both cases. However, since the inlet chlorine is higher here, there is slightly more Cl₂ at the interface, resulting in the decrease in Hg penetration in Table 8.6.

Table 8.6. Mercury section profile at 22.4 ppm Cl₂ and 9 mM S(IV)

Section	P _{Hg,b} (atm)	[S(IV)] _b (mM)	P _{Cl₂,b} (atm)	[Cl ₂] _b (mM)	[Cl ₂] _i (mM)	[S(IV)] _i (mM)	N _{Hg} (kmol/m ² -s)	Hg _{out} /Hg _{in}
0	4.60E-08	9	2.24E-05	1.34E-03	7.38E-05	8.90	3.16E-12	0.994
3	4.57E-08	9.00	2.16E-05	1.30E-03	7.12E-05	8.91	3.09E-12	0.994
6	4.54E-08	9.00	2.09E-05	1.25E-03	6.88E-05	8.91	3.03E-12	0.994
9	4.52E-08	9.00	2.02E-05	1.21E-03	6.64E-05	8.91	2.97E-12	0.994
12	4.49E-08	9.00	1.95E-05	1.17E-03	6.41E-05	8.92	2.91E-12	0.994
15	4.46E-08	9.01	1.88E-05	1.13E-03	6.19E-05	8.92	2.85E-12	0.994
18	4.44E-08	9.01	1.82E-05	1.09E-03	5.98E-05	8.93	2.79E-12	0.994
21	4.41E-08	9.01	1.76E-05	1.05E-03	5.77E-05	8.93	2.73E-12	0.994
24	4.39E-08	9.01	1.70E-05	1.02E-03	5.58E-05	8.93	2.68E-12	0.994
27	4.36E-08	9.01	1.64E-05	9.81E-04	5.38E-05	8.94	2.62E-12	0.995
30	4.34E-08	9.01	1.58E-05	9.47E-04	5.20E-05	8.94	2.57E-12	0.995
33	4.32E-08	9.01	1.53E-05	9.15E-04	5.02E-05	8.94	2.52E-12	0.995
36	4.29E-08	9.01	1.48E-05	8.84E-04	4.85E-05	8.95	2.47E-12	0.995
39	4.27E-08	9.01	1.43E-05	8.54E-04	4.68E-05	8.95	2.42E-12	0.995
42	4.25E-08	9.01	1.38E-05	8.24E-04	4.52E-05	8.95	2.37E-12	0.995
45	4.23E-08	9.01	1.33E-05	7.96E-04	4.37E-05	8.95	2.32E-12	0.995
48	4.21E-08	9.01	1.28E-05	7.69E-04	4.22E-05	8.96	2.28E-12	0.995
51	4.19E-08	9.02	1.24E-05	7.43E-04	4.07E-05	8.96	2.23E-12	0.995
54	4.17E-08	9.02	1.20E-05	7.17E-04	3.93E-05	8.96	2.19E-12	0.995
57	4.15E-08	9.02	1.16E-05	6.93E-04	3.80E-05	8.96	2.15E-12	0.995
60	4.13E-08	9.02	1.12E-05	6.69E-04	3.67E-05	8.97	2.10E-12	0.995
63	4.11E-08	9.02	1.08E-05	6.46E-04	3.54E-05	8.97	2.06E-12	0.995
66	4.09E-08	9.02	1.04E-05	6.24E-04	3.42E-05	8.97	2.02E-12	0.996

69	4.07E-08	9.02	1.01E-05	6.03E-04	3.30E-05	8.97	1.98E-12	0.996
72	4.05E-08	9.02	9.73E-06	5.82E-04	3.19E-05	8.98	1.94E-12	0.996
75	4.04E-08	9.02	9.39E-06	5.62E-04	3.08E-05	8.98	1.91E-12	0.996
78	4.02E-08	9.02	9.07E-06	5.43E-04	2.98E-05	8.98	1.87E-12	0.996
81	4.00E-08	9.02	8.76E-06	5.25E-04	2.87E-05	8.98	1.83E-12	0.996
84	3.99E-08	9.02	8.46E-06	5.07E-04	2.77E-05	8.98	1.80E-12	0.996
87	3.97E-08	9.02	8.17E-06	4.89E-04	2.68E-05	8.98	1.76E-12	0.996
90	3.95E-08	9.02	7.89E-06	4.73E-04	2.59E-05	8.99	1.73E-12	0.996
93	3.94E-08	9.02	7.62E-06	4.57E-04	2.50E-05	8.99	1.69E-12	0.996
96	3.92E-08	9.02	7.36E-06	4.41E-04	2.41E-05	8.99	1.66E-12	0.996
99	3.91E-08	9.02	7.11E-06	4.26E-04	2.33E-05	8.99	1.63E-12	0.996
102	3.89E-08	9.02	6.87E-06	4.11E-04	2.25E-05	8.99	1.60E-12	0.996
105	3.88E-08	9.02	6.63E-06	3.97E-04	2.17E-05	8.99	1.57E-12	0.996
Overall							2.26E-12	0.84

Figures 8.3 and 8.4 illustrate the section profiles tabulated in Tables 8.5 and 8.6, respectively.

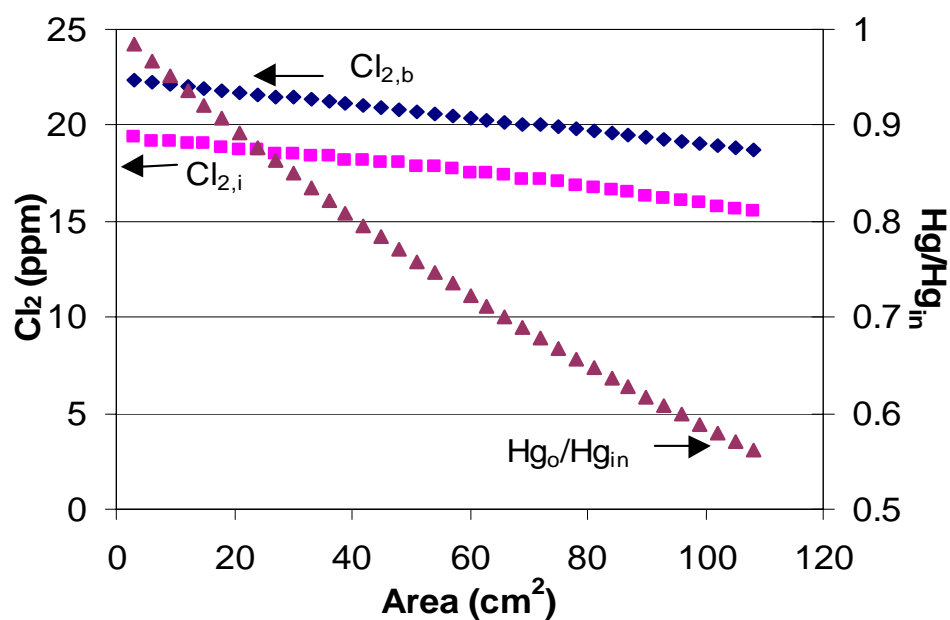


Figure 8.3. Concentration profile at 22.4 ppm Cl_2 and 0.01 mM S(IV)

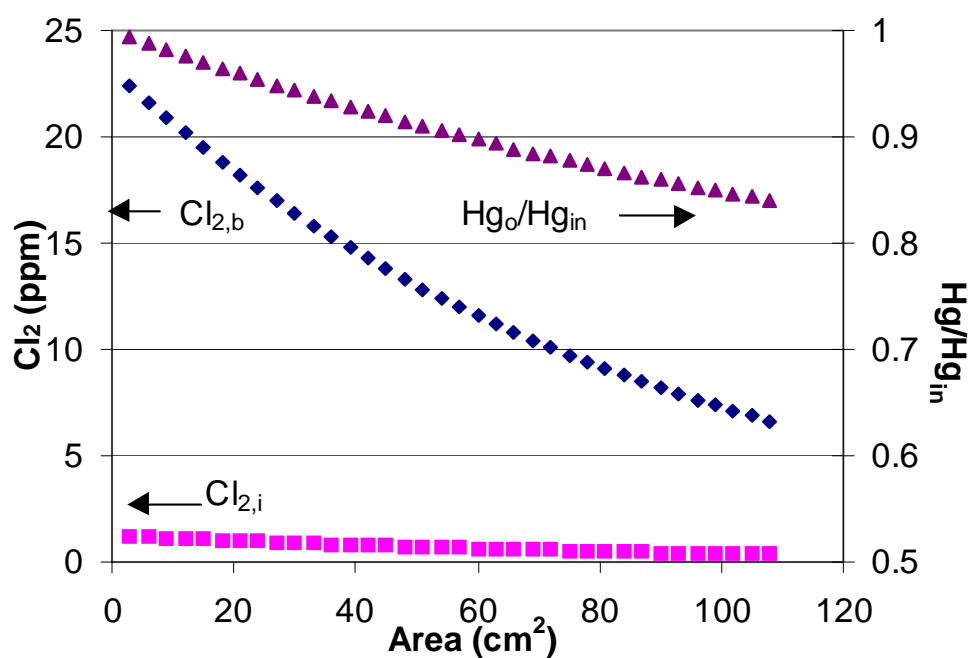


Figure 8.4. Concentration profile at 22.4 ppm Cl_2 and 9 mM S(IV)

Due to the greater S(IV) concentration, the chlorine concentration profile in Figure 8.4 decreases rapidly, and there is not much chlorine available at the interface to react with Hg. Therefore, the Hg penetration curve is less steep in Figure 8.4 than in Figure 8.3. Since the S(IV) concentration in Figure 8.3 is low, the chlorine at the interface is very close to the chlorine in the bulk. Since there is more chlorine available to react with Hg, the Hg penetration curve in Figure 8.3 is much steeper than that in Figure 8.4.

8.2 ABSORPTION OF MERCURY AND CHLORINE INTO S(IV) AT pH 5.7

The rate constant for the reaction of Hg and Cl₂ at pH 5.7 was regressed from the data in this section.

8.2.1 Experimental method

The experimental methods are essentially the same as that detailed in Section 8.1.1. However, to buffer at pH 5.7, the ratio of succinic acid: NaOH was 1:1.8 instead of the equimolar composition used to buffer at pH 4.5 to 4.7. The solution buffer composition for the experiments discussed in this section was 2.78 mM succinic acid-5 mM NaOH.

8.2.2 Tabulated results

Table 8.7 tabulates the data used to regress the Hg/Cl₂ rate constant. The pH ranges from 5.65 to 5.75. The Hg inlet concentration is 46 ppb. The chlorine mass flow controller did not drift during these experiments. Some of the data do not report the chlorine outlet because the concentration was over the range of the analyzer. The chlorine data shown below have been detailed in Table 7.6.

Table 8.7 Mercury and chlorine absorption in buffered S(IV) at pH 5.65 to 5.75

[S(IV)] _o (mM)	Hg _o (ppb)	Hg _o /Hg _{in}	N _{Hg} (kmol/m ² s)	Cl _{2,in} (ppm)	Cl _{2,o} (ppm)	N _{Cl2} (kmol/m ² s)	Cl _{2,o} /Cl _{2,in}
0	36.4	0.79	2.94E-12	6.3	4.41	5.80E-10	0.701
0	29.8	0.65	4.98E-12	12	8.29	1.14E-09	0.691

0	26.3	0.57	6.04E-12	22.4	15.7	2.06E-09	0.701
0	23.1	0.50	7.05E-12	39.4	n/a	n/a	n/a
0	28.8	0.63	5.28E-12	17	12.0	1.54E-09	0.706
0.176	33.1	0.72	3.95E-12	17	6.04	3.37E-09	0.356
0.176	34.4	0.75	3.58E-12	12	4.41	2.33E-09	0.368
0.176	32.5	0.71	4.14E-12	22.4	8.63	4.23E-09	0.385
0.176	29.2	0.63	5.17E-12	39.4	20.0	5.95E-09	0.509
0.102	28.6	0.62	5.35E-12	39.4	20.6	5.79E-09	0.522
0.102	30.5	0.66	4.77E-12	31.3	15.0	5.01E-09	0.479
0.102	31.1	0.68	4.59E-12	22.4	10.0	3.81E-09	0.447
0.102	35.4	0.77	3.26E-12	12	5.16	2.10E-09	0.430
0.175	31.6	0.69	4.43E-12	22.4	7.83	4.48E-09	0.349
0.175	31.7	0.69	4.40E-12	22.4	7.91	4.45E-09	0.353
0.175	29.2	0.63	5.17E-12	39.4	17.8	6.64E-09	0.451
0.342	31.7	0.69	4.40E-12	39.4	13.3	8.03E-09	0.337
0.342	34.4	0.75	3.57E-12	22.4	6.85	4.78E-09	0.306
0.342	36.7	0.80	2.85E-12	12	3.84	2.51E-09	0.320
0.618	33.7	0.73	3.78E-12	22.4	6.33	4.94E-09	0.283
0.618	31.0	0.67	4.62E-12	39.4	12.25	8.34E-09	0.311
0.618	32.1	0.70	4.28E-12	31.3	9.33	6.75E-09	0.298
0.618	35.4	0.77	3.26E-12	17	4.93	3.71E-09	0.290

8.2.3 Discussion

The experimental values were compared to the predicted values to obtain the Hg/Cl₂ rate constant. Table 8.8 tabulates the parameters used in the model, including the rate constant obtained from all the data in Table 8.7.

Table 8.8 Parameters used to model Hg and Cl₂ absorption at pH 5.7

Parameter	Value
G (L/min)	4.78
P _{Hg,in} (atm)	4.6 x 10 ⁻⁸
k _{g,Cl2} (mol/s-atm-m ²)	0.4
k _{g,Hg} (mol/s-atm-m ²)	0.4
k ^o _{L,Cl2} (m/s)	9.0 x 10 ⁻⁵

$k_{L,S(IV)}^o$ (m/s)	8.53×10^{-5}
Area (cm ²)	108
$k_{2,buf}$ (L/mol-s)	8.5×10^5
$k_{2,S(IV)}$ (L/mol-s)	1.4×10^9
$k_{2,Hg}$ (L/mol-s)	6.0×10^9

8.2.3.1 Regressed $k_{2,Hg}$ at pH 5.7

The regressed $k_{2,Hg}$ with a 95 % confidence interval was $(6.0 \pm 0.7) \times 10^9$ L/mol-s. This value is within the same range as the rate at pH 4.7. Figure 8.5 shows the data and the model curves at the four S(IV) concentrations of 0, 0.1, 0.175, 0.34, and 0.62 mM.

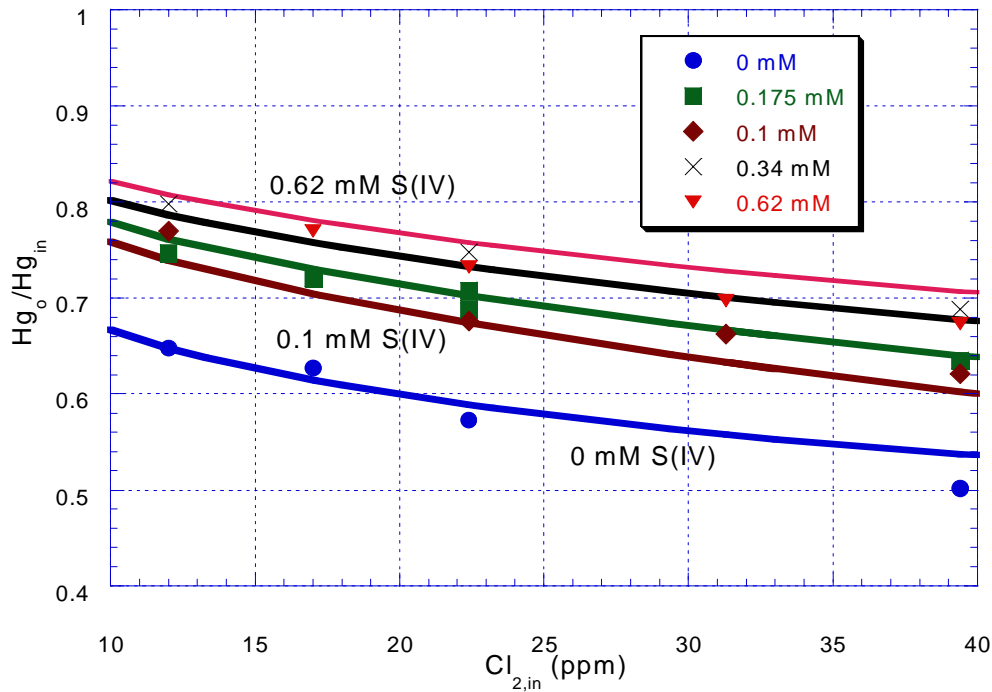


Figure 8.5. Mercury penetration in S(IV) at pH 5.7, $k_{2,Hg} = 6.0 \times 10^9$ L/mol-s

The data seem to have less scatter than the data in Figure 8.2. The better fit may result from the chlorine flow controller not drifting and more frequent sampling of S(IV). The same trends, as discussed in Section 8.1.3.1, are seen here. At 0.34 mM S(IV), the chlorine absorption is mostly gas film controlled. Therefore, the values at 0.62 mM are very close to those at 0.34 mM.

8.2.3.2 Model sensitivity

The sensitivity of the model was investigated by varying selected parameters ($k_{g,Hg}$, $k_{2,Hg}$, $k_{2,S(IV)}$) and observing the resulting effect on the predicted mercury penetration as depicted in Figures 8.6, 8.7, and 8.8. The solid line each figure represents the base case, which is calculated using the values in Table 8.8. The dashed lines in each figure represent the predicted penetration obtaining by changing the value of the selected parameter, while keeping the other values constant. Since

the same results were obtained for all the S(IV) curves, only the data and models at 0 mM and 0.175 mM S(IV) are shown.

Figure 8.6 shows the effect of varying $k_{g,Hg}$. The $k_{g,Hg}$ was decreased to 0.36 (10 % decrease) and 0.30 (25 % decrease) mol/s-atm-m². Lowering the value by 10% barely increases the Hg penetration. The most significant effect is at higher chlorine concentrations and when the $k_{g,Hg}$ is reduced by 25 % (top dashed curve), as the Hg absorption approaches gas film control

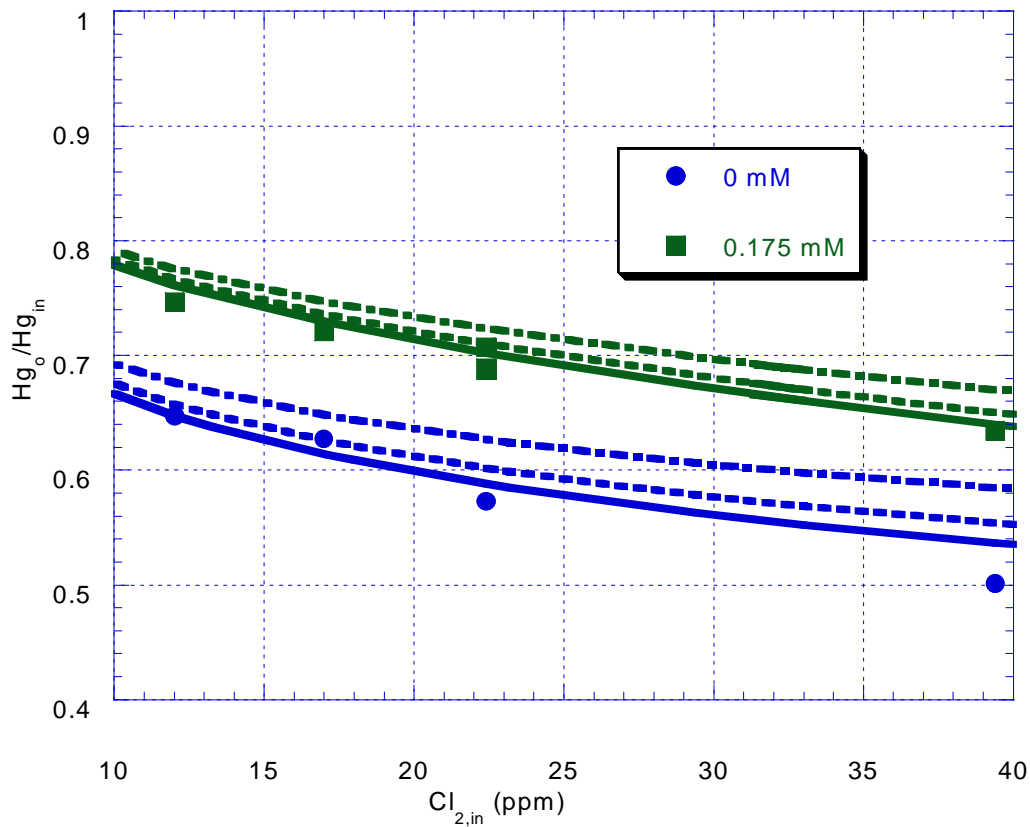


Figure 8.6. Effect of varying $k_{g,Hg}$ on predicted Hg penetration

Figure 8.7 shows the effect of varying $k_{2,Hg}$. The $k_{2,Hg}$ was increased to 9×10^9 L/mol-s. It was also decreased to 1×10^9 and 5×10^9 L/mol-s; in addition to a lower $k_{2,Hg}$, these two curves also had a lower $k_{g,Hg}$ of 0.36 mol/s-atm-m². As shown

by Figure 8.7, the most dramatic effect occurred when the was $k_{2,\text{Hg}}$ lowered to $1 \times 10^9 \text{ L/mol-s}$ (at $k_{g,\text{Hg}}$ of $0.36 \text{ mol/s-atm-m}^2$).

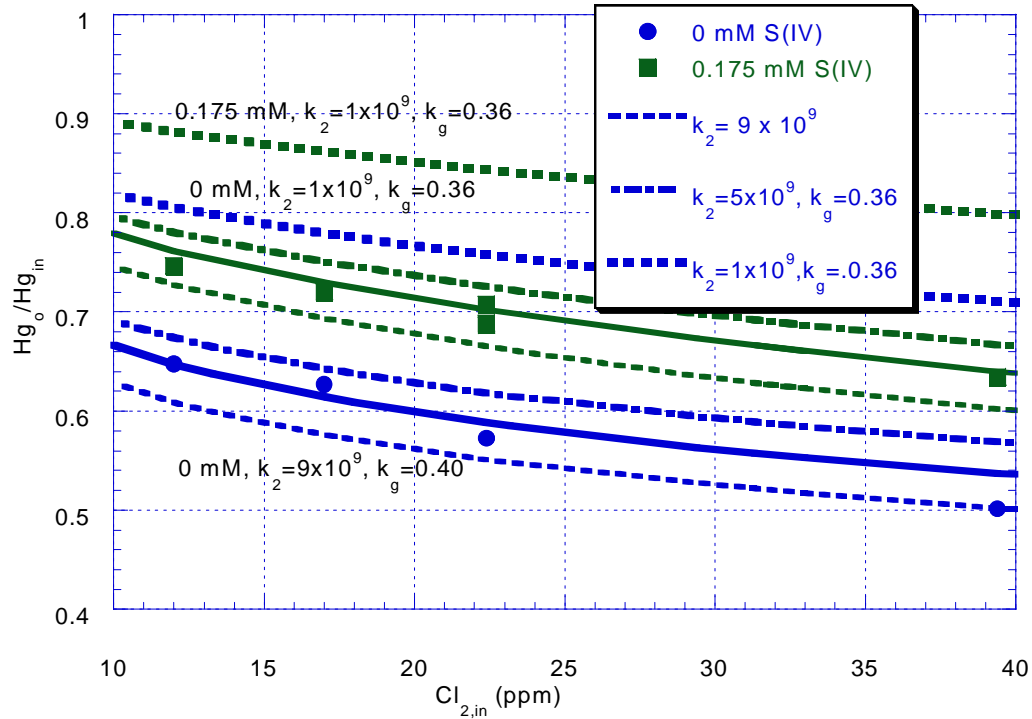


Figure 8.7. Effect of varying $k_{2,\text{Hg}}$ on predicted Hg penetration

Figure 8.8 depicts the effect of varying of lowering $k_{2,\text{S(IV)}}$ from 1.4×10^9 to $9.0 \times 10^8 \text{ L/mol-s}$. Varying the $\text{Cl}_2/\text{S(IV)}$ rate constant has no effect on the rate of mercury absorption (with chlorine) into buffer; the dashed line is exactly the same as the solid line at 0 mM S(IV).

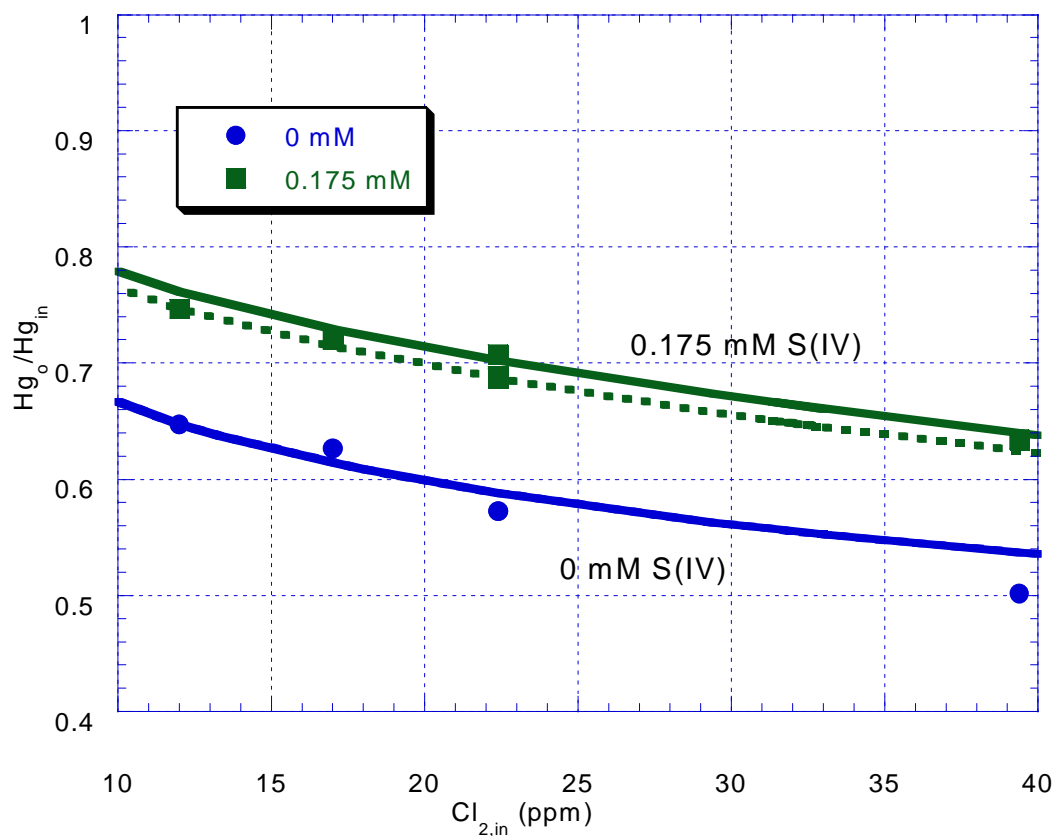


Figure 8.8. Effect of varying $k_{2,\text{S(IV)}}$ on predicted Hg penetration

In addition, the effect of varying $k_{2,\text{S(IV)}}$ was studied by regressing $k_{2,\text{Hg}}$ with a lower $k_{2,\text{S(IV)}}$. When the $k_{2,\text{S(IV)}}$ was lowered from 1.4×10^9 to 1.0×10^9 L/mol-s, the regressed $k_{2,\text{Hg}}$ was $(5.4 \pm 0.6) \times 10^9$ L/mol-s. This value is slightly lower, but still in the same range as the original $k_{2,\text{Hg}}$ of 6.0×10^9 L/mol-s.

Even though the uncertainty in the Hg/ Cl_2 rate constant is greater than the uncertainty in the $\text{Cl}_2/\text{S(IV)}$ rate constant, the model is still primarily sensitive to $k_{2,\text{Hg}}$. Furthermore, the rate is in the range of other rates of reaction for Hg with other aqueous oxidants, which range from 10^6 to 10^9 L/mol-s (Lin and Pehkonen, 1999).

Thus, the value for the regressed $k_{2,\text{Hg}}$ seems reasonable. A detailed analysis of this value and the possible chemistry is discussed in Section 8.4.

8.3 EFFECT OF MERCURIC CHLORIDE AT PH 5.7

The effect of adding Hg(II) to the solution was studied at ambient temperature at pH 5.7. Zhao (1997) observed that Hg(II) catalyzed the absorption of elemental Hg in certain aqueous oxidants, such as various acids, hydrogen peroxide and potassium dichromate. Typical concentrations of Hg(II) added ranged from 10^{-6} to 10^{-3} M. The presence of divalent Hg caused the Hg to absorb much faster than if only the oxidant was present (Zhao, 1997; Zhao and Rochelle, 1998). Zhao also observed that Hg(II) enhanced Hg absorption in water (with no oxidant present). However, the addition of HgCl_2 did not affect Hg absorption in sodium hypochlorite/chloride solutions (Zhao, 1997).

In the absorption experiments previously discussed in this chapter, the typical accumulation of Hg(II) in the bulk solution is approximately 10^{-7} M. Therefore, HgCl_2 was added to see if Hg(II) affects the absorption of elemental Hg.

8.3.1 Experimental method

The methods are similar to that discussed in Section 8.2.1. However, there was no S(IV) in the solution. The experiments started with only Hg (no Cl_2) contacting the buffer solution (2.78 mM succinic acid-5 mM NaOH). The measured pH varied from 5.64 to 5.66. Mercuric chloride was periodically injected into the buffer. Then, the flow of Cl_2 through the column was started. The chlorine inlet was varied (from 12 to 22 ppm), as HgCl_2 was periodically added. After the Cl_2 flow was stopped, Hg absorption into the buffered HgCl_2 solution was still measured, as more HgCl_2 was added. The added Hg(II) throughout the entire experiment ranged from 2.5×10^{-6} to 4×10^{-5} M. The Hg inlet was 46 ppb.

8.3.2 Tabulated results

Table 8.8 tabulates the data. For the first five data points, there was no chlorine going through the column. For these data, as HgCl_2 was added, the mercury concentration would initially decrease and remained stable for approximately one minute. Then, the Hg concentration would continually increase, even after 10 to 20 minutes. For points 3 through 5, the initial Hg concentration (immediately after HgCl_2 addition) and the last Hg concentration (immediately before the next HgCl_2 injection) are reported in Table 8.8. For point 2, only the last concentration is reported. All HgCl_2 concentrations are cumulative. Points 12 and 13 represent data at the end of the experiment, when the chlorine was no longer going through the column.

Table 8.8 Absorption of Hg and Cl_2 in buffered HgCl_2 at pH 5.64 to 5.66

Point	$[\text{HgCl}_2]$ (M)	Hg_o (ppb)	$\text{Hg}_o/\text{Hg}_{in}$	N_{Hg} ($\text{kmol}/\text{m}^2\text{s}$)	$\text{Cl}_{2,in}$ (ppm)	$\text{Cl}_{2,o}$ (ppm)	N_{Cl_2} ($\text{kmol}/\text{m}^2\text{s}$)	$\text{Cl}_{2,o}/\text{Cl}_{2,in}$
1	0	46	1	0	0	0	0	n/a
2	2.56E-06	54.2	n/a	n/a	0	0	0	n/a
3	5.12E-06	52.9, 55.4	n/a	n/a	0	0	0	n/a
4	9.00E-06	53.5, 57.9	n/a	n/a	0	0	0	n/a
5	1.68E-05	56.6, 60.0	n/a	n/a	0	0	0	n/a
6	1.68E-05	25.3	0.55	6.35E-12	22.4	16.36	1.86E-09	0.730
7	1.68E-05	27.0	0.59	5.83E-12	17.0	12.27	1.45E-09	0.722
8	1.68E-05	28.4	0.62	5.40E-12	12.0	8.80	9.85E-10	0.733
9	2.40E-05	27.5	0.60	5.69E-12	12.0	8.87	9.61E-10	0.739
10	2.40E-05	24.5	0.53	6.61E-12	22.4	16.39	1.85E-09	0.732
11	3.21E-05	22.6	0.49	7.18E-12	22.4	16.46	1.82E-09	0.735
12	3.21E-05	35.5	0.77	3.21E-12	0	0	0	n/a
13	3.98E-05	34.1	0.74	3.66E-12	0	0	0	n/a

8.3.3 Discussion

For the first five data points, no oxidants are present in solution. The first point confirms that succinate buffer does not enhance Hg absorption. When only Hg

contacts the buffer with no HgCl_2 , the Hg exiting the column is the same as that entering. Points 2 through 5 show that the injection of HgCl_2 initially decreases the Hg concentration, but then the added Hg(II) is reduced and stripped from the solution. Therefore, the exiting Hg concentration increases continuously, as the added Hg(II) is reduced to elemental Hg and desorbed. The initial decrease results since immediately after injection, the added HgCl_2 exists as Hg(II) and has not yet been reduced. However, since no oxidants are present, the solution may have a strong reducing potential. For example, succinate buffer contains iron impurities; thus, in a reducing environment, Fe(II) may be present. Since Hg(II) can easily be reduced to elemental Hg by reducing agents, such as sulfite (Munthe et al., 1991), it is reasonable to assume that the reductants in the solution are reducing the added Hg(II) to elemental Hg.

As soon as the Cl_2 flow is started, the oxidizing environment enhances Hg absorption. Even after the Cl_2 flow through the column is stopped, the Hg(II) still oxidizes the Hg and enhances the Hg absorption. The solution now has a strong oxidizing potential. Therefore, any impurities such as iron are now present in their oxidized states.

Figure 8.9 shows the Hg absorption in buffer data and predicted penetration from Figure 8.5. Figure 8.9 also shows the observed penetration when HgCl_2 is present (Points 6 through 11 from Table 8.8).

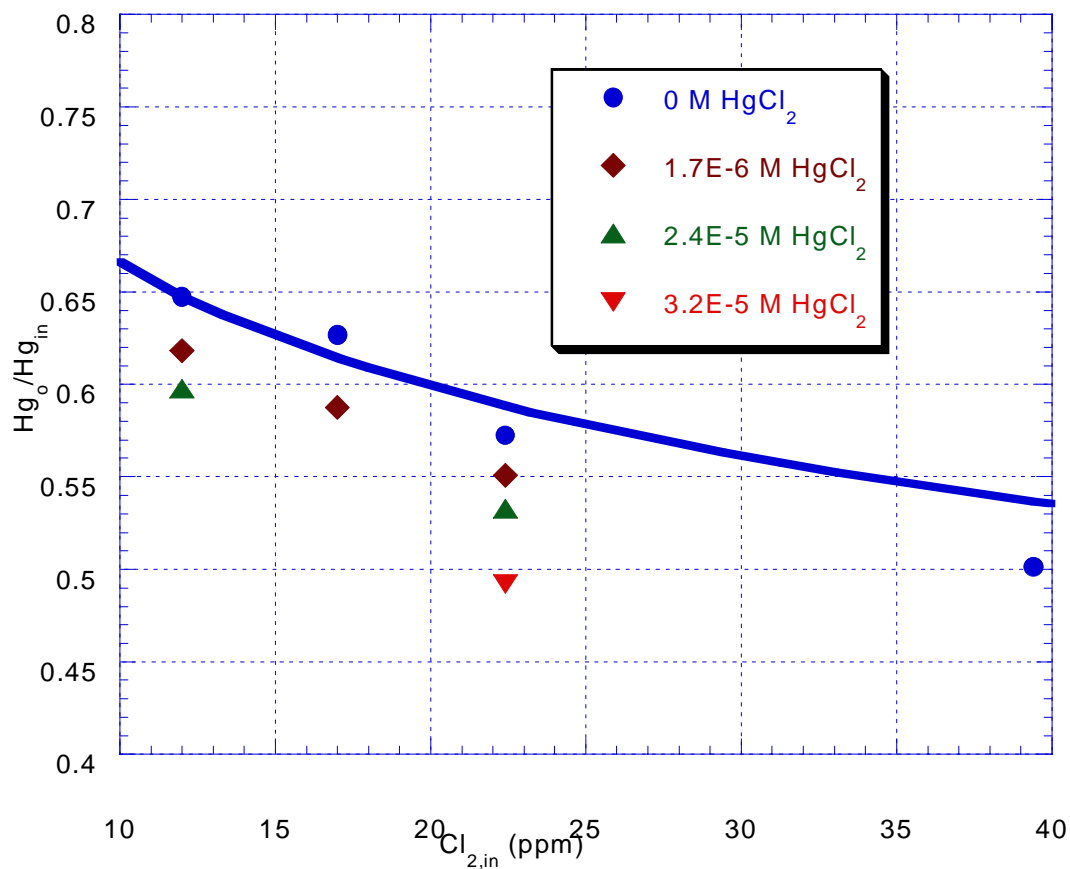


Figure 8.9. Hg penetration in buffered $HgCl_2$ at pH 5.65

The $HgCl_2$ does seem to slightly enhance the Hg absorption. Since the enhancement is so small, it is not possible to regress a precise rate from the data. However, a quantitative analysis can still be done. The observed enhancement may result from the two reactions ($Hg/Hg(II)$ and Hg/Cl_2) occurring in parallel. Therefore, a term accounting for the $Hg/Hg(II)$ reaction must be added to Equation 3-14, as shown in Equation 8-1.

$$N_{Hg} = \frac{P_{Hg_i}}{H_{Hg}} \sqrt{D_{Hg} (k_{2,Hg} [Cl_2]_i + k_{2,Hg(II)} [Hg(II)]_i)} \quad (8-1)$$

This expression must be integrated throughout the column, similar to Equation 3-16 with the Hg(II) term added. The corresponding rate expression for the Hg/Hg(II) reaction is:

$$\text{reaction rate} = k_{2,\text{Hg(II)}}[\text{Hg}][\text{Hg(II)}] \quad (8-2)$$

The $[\text{Hg(II)}]_i$ can be calculated from Equation 8-3.

$$[\text{Hg(II)}]_i = [\text{Hg(II)}]_{\text{injected}} + [\text{Hg(II)}]_{\text{absorbed}} - \frac{N_{\text{Hg}}}{k_{L,\text{Hg(II)}}^o} \quad (8-3)$$

The last two terms are negligible compared to the injected Hg(II). Therefore, only the concentration of the Hg(II) injected was supplied to the model.

Zhao (1997) obtained $k_{2,\text{Hg(II)}}$ in the presence of various oxidants. The average $k_{2,\text{Hg(II)}}$ was 9×10^6 L/mol-s, with the highest value at 2×10^8 L/mol-s (Zhao, 1997; Zhao and Rochelle, 1998). Table 8.9 compares the observed Hg flux and penetration (Points 6 through 9 from Table 8.8) to the predicted flux and penetration using different values for $k_{2,\text{Hg(II)}}$.

Table 8.9 Predicted and observed Hg absorption in HgCl₂ with Cl₂ present

Observed		$k_{2,\text{Hg(II)}} = 9 \times 10^6$ L/mol-s		$k_{2,\text{Hg(II)}} = 1 \times 10^8$ L/mol-s	
N_{Hg} (kmol/m ² -s)	Hg _o /Hg _{in}	N_{Hg} (kmol/m ² -s)	Hg _o /Hg _{in}	N_{Hg} (kmol/m ² -s)	Hg _o /Hg _{in}
6.35E-12	0.55	5.86E-12	0.59	6.20E-12	0.56
5.83E-12	0.59	5.50E-12	0.61	5.95E-12	0.58
5.40E-12	0.62	5.06E-12	0.64	5.65E-12	0.60
5.69E-12	0.60	5.09E-12	0.64	5.85E-12	0.59
6.61E-12	0.53	5.88E-12	0.58	6.34E-12	0.55
7.18E-12	0.49	5.89E-12	0.58	6.47E-12	0.54

A value of 1×10^8 L/mol-s seems to best fit the Hg/Cl₂/HgCl₂ data. For points 12 and 13, there is no chlorine present. A value for $k_{2,\text{Hg(II)}}$ can also be obtained from these data by setting the Cl₂ concentration equal to zero in Equation 8-1. Table 8.10 compares the observed Hg flux to the predicted flux using different values of $k_{2,\text{Hg(II)}}$.

Table 8.10 Predicted and observed Hg flux in HgCl₂ without Cl₂

Observed	$k_{2,\text{Hg(II)}} = 2.4 \times 10^7 \text{ L/mol-s}$	$k_{2,\text{Hg(II)}} = 1 \times 10^8 \text{ L/mol-s}$
$N_{\text{Hg}}(\text{kmol/m}^2\text{-s})$	$N_{\text{Hg}}(\text{kmol/m}^2\text{-s})$	$N_{\text{Hg}}(\text{kmol/m}^2\text{-s})$
3.21E-12	3.39E-12	5.66E-12
3.66E-12	3.68E-12	6.00E-12

Table 8.10 shows that a $k_{2,\text{Hg(II)}}$ of $2.4 \times 10^7 \text{ L/mol-s}$ best fits the data when no Cl₂ is present (Points 12 and 13 in Table 8.8). A $k_{2,\text{Hg(II)}}$ of $1 \times 10^8 \text{ L/mol-s}$ over-predicts the flux for these points. Since a single value of $k_{2,\text{Hg(II)}}$ does not fit both data sets (with and without Cl₂), the reactions probably do not occur as independent parallel reactions. Since $k_{2,\text{Hg(II)}}$ is higher when Cl₂ is present, it is probable that Hg(II) catalyzes Hg absorption with Cl₂.

8.4 EFFECT OF SODIUM HYPOCHLORITE AND CHLORIDE

As mentioned earlier in this chapter, the reaction rate between Hg and Cl₂ obtained is much lower than the reaction rate Zhao (1997) obtained from measuring Hg absorption in sodium hypochlorite/chloride solutions at high pH. Both rate constants were correlated using the same rate expression (Equation 3-15), but the value obtained by Zhao is several orders of magnitude higher. The differences result from the different chemistry occurring. In this section, sodium hypochlorite and sodium chloride were added to the solution in order to simulate the conditions Zhao used and obtain a better understanding of the chemistry.

8.4.1 Theory

Since the solution contains NaOCl/NaCl, the free chlorine in solution must be calculated from the equilibrium relationships shown in Equations 2-1 and 2-2. Since ionic strength may have a considerable impact, the activities of the aqueous components were used instead of concentrations. Low pH and high chloride concentration increases the activity of chlorine in solution.

Iodometric titration results in the determination of the total concentration of all chlorine species, resulting in Equation 8-4.

$$[\text{Total NaOCl}] = [\text{Cl}_2] + [\text{HOCl}] + [\text{OCl}^-] \quad (8-4)$$

The activity of HOCl can be written in terms of the activity of chlorine through Equation 2-2, and the activity of hypochlorite can also be written in terms of the activity of chlorine using both equilibrium relationships. The values for K_1 and K_2 were given in Section 2.3.1.

$$a_{\text{HOCl}} = \gamma_{\text{HOCl}}[\text{HOCl}] = \frac{a_{\text{Cl}_2} K_2}{a_{\text{Cl}^-} a_{\text{H}^+}} \quad (8-5)$$

$$a_{\text{OCl}^-} = \gamma_{\text{OCl}^-}[\text{OCl}^-] = \frac{a_{\text{Cl}_2} K_1 K_2}{a_{\text{Cl}^-} a_{\text{H}^+}^2} \quad (8-6)$$

Substituting into Equation 8-4 and solving for chlorine activity yields:

$$a_{\text{Cl}_2} = \frac{[\text{Total NaOCl}]}{\frac{1}{\gamma_{\text{Cl}_2}} + \frac{K_2}{\gamma_{\text{HOCl}} a_{\text{Cl}^-} a_{\text{H}^+}} + \frac{K_1 K_2}{\gamma_{\text{OCl}^-} a_{\text{Cl}^-} a_{\text{H}^+}^2}} \quad (8-7)$$

The activity coefficients for Cl_2 and HOCl are assumed to be 1. The activity coefficients for chloride and hypochlorite are assumed to be equal to that of sodium chloride (Zhao, 1997). The γ_{NaCl} at 0.1 M NaCl and 25°C is 0.779 (Zhao, 1997; Robinson and Harned, 1941; Lobo and Quaresma, 1989). Thus, Equation 8-7 can be simplified to Equation 8-8.

$$a_{\text{Cl}_2} = \frac{[\text{Total NaOCl}]}{1 + \frac{K_2}{\gamma_{\text{NaCl}} [\text{Cl}^-] a_{\text{H}^+}} + \frac{K_1 K_2}{\gamma_{\text{NaCl}}^2 [\text{Cl}^-] a_{\text{H}^+}^2}} \quad (8-8)$$

For these experiments, the chlorine at the interface depends on the liquid chlorine activity calculated from Equation 8-8, in addition to that resulting from

chlorine absorption from the gas (Equation 3-1). If the chlorine in the bulk liquid is not negligible, it must be included in Equation 3-4 as shown below in Equation 8-9.

$$N_{Cl_2} = \frac{P_{Cl_2,i} - P_{Cl_2,b}^*}{H_{Cl_2}} \sqrt{D_{Cl_2} (k_{2,S(IV)} [S(IV)]_i + k_{2,buf} [buffer]_i)} \quad (8-9)$$

If the chlorine at the interface only depends on Equation 8-8 because there is no chlorine in the gas, Equation 3-16 simplifies to Equation 8-10. Equations 8-8 and 8-10 are identical to the expressions Zhao (1997) used to correlate her data.

$$N_{Hg} = \frac{1}{H_{Hg}} \left(P_{Hg,b} - \frac{N_{Hg}}{k_{g,Hg}} \right) \sqrt{D_{Hg} k_{2,Hg} a_{Cl_2,i}} \quad (8-10)$$

8.4.2 *Experimental method*

The absorption of mercury and chlorine into buffered sodium hypochlorite/sodium chloride solutions at pH 5.76 was measured in the wetted wall column. The methods are similar to that discussed in Section 8.2.1. The gas flow to the column was 4.78 L/min, and the liquid flow was 2.26 mL/s. The 3.1 L plexiglass reservoir was used for all the data. The experiment started with the absorption of Hg and Cl₂ into solution containing 0.1 M sodium chloride (NaCl) and 2.78 mM succinic acid-5 mM NaOH buffer, with no S(IV) present. The Hg inlet concentration was 46 ppb, while the chlorine inlet was varied from 6 to 22 ppm. Sodium hypochlorite (NaOCl) was periodically injected into the solution, and the chlorine inlet was varied. Afterwards, the chlorine flow through the column was stopped, while the absorption of Hg was still measured, and additional NaOCl was added.

The added NaOCl ranged from 3.6 x 10⁻⁶ to 3.6 x 10⁻⁵ M. The NaOCl was added by injecting a known quantity of sodium hypochlorite solution (Fisher Scientific, Purified Grade, 4 to 6 wt %). The exact NaOCl concentration was obtained through iodometric titration (Zhao, 1997; Lagowski, 1995; Kolthoff and Belcher,

1957). This procedure is detailed in Appendix G. At pH 5.76 and 0.1 M NaCl, most of the NaOCl is present as HOCl.

S(IV) was added towards the end of the experiment. Then, the chlorine flow was again started through the column. The absorption of Hg and Cl₂ into buffered S(IV) at 0.1 M NaCl was measured.

8.4.3 Tabulated results

Table 8.11 tabulates the data in which absorption into NaOCl was measured, and Table 8.12 tabulates the data in which absorption into S(IV) was measured. All of the data are at pH 5.76 in 0.1 M NaCl. All sodium hypochlorite concentrations are cumulative, based on the amount injected into solution. For Points 13 through 16, the chlorine bypassed the column.

Table 8.11 Absorption of Hg and Cl₂ in NaOCl/0.1 M NaCl at pH 5.76

Point	[NaOCl] _T (M)	Hg _o (ppb)	Hg _o /Hg _{in}	N _{Hg} (kmol/m ² s)	Cl _{2,in} (ppm)	Cl _{2,o} (ppm)	N _{Cl2} (kmol/m ² s)	Cl _{2,o} /Cl _{2,in}
1	0	26.7	0.58	5.93E-12	6.3	5.11	3.65E-10	0.812
2	0	24.3	0.53	6.67E-12	12	10.07	5.95E-10	0.839
3	0	22.0	0.48	7.36E-12	17	14.11	8.88E-10	0.830
4	0	21.1	0.46	7.65E-12	22.4	18.54	1.18E-09	0.828
5	3.58E-06	21.0	0.46	7.70E-12	22.4	17.90	1.38E-09	0.799
6	3.58E-06	21.5	0.47	7.52E-12	22.4	17.95	1.37E-09	0.801
7	8.96E-06	20.8	0.45	7.75E-12	22.4	17.30	1.57E-09	0.772
8	8.96E-06	21.2	0.46	7.62E-12	22.4	17.27	1.58E-09	0.771
9	8.96E-06	26.5	0.58	6.00E-12	6.3	5.40	2.77E-10	0.857
10	8.96E-06	23.3	0.51	6.98E-12	12	9.96	6.26E-10	0.830
11	1.43E-05	23.6	0.51	6.88E-12	12	10.01	6.11E-10	0.834
12	1.43E-05	21.5	0.47	7.54E-12	22.4	18.03	1.34E-09	0.805
13	1.43E-05	36.3	0.79	2.97E-12	0	0	0	n/a
14	3.05E-05	35.6	0.77	3.21E-12	0	0	0	n/a
15	3.58E-05	35.5	0.77	3.23E-12	0	0	0	n/a

Table 8.12 Absorption of Hg and Cl₂ in S(IV)/0.1 M NaCl at pH 5.76

Point	[S(IV)] _o (mM)	Hg _o (ppb)	Hg _o /Hg _{in}	N _{Hg} (kmol/m ² s)	Cl _{2,in} (ppm)	Cl _{2,o} (ppm)	N _{Cl2} (kmol/m ² s)	Cl _{2,o} /Cl _{2,in}
16	0.213	44	0.96	6.1E-13	0	0	0	n/a
17	0.213	31.3	0.68	4.51E-12	22.4	7.19	4.68E-09	0.32

8.4.4 Discussion

This section first details the experimental observations and trends, followed by a discussion of the possible chemistry and conclusions that can be drawn by comparing this work to previous work with Hg absorption in chlorine-containing (NaOCl/NaCl) solutions.

8.4.4.1 Overview of data

The chlorine absorption data in Table 8.11 show that the chlorine hydrolysis is slightly suppressed by the addition of 0.1 M NaCl. When there is no chloride added to solution, the chlorine penetration in buffer is 0.7 (as shown in Table 8.7); however, with 0.1 M chloride, the penetration is 0.8. When no chloride is added to the solution (as in the data in Table 8.7), the chloride accumulating in solution from chlorine absorption is at most 10⁻⁴ M, which is negligible compared to 0.1 M. Point 17 in Table 8.12, which has already been discussed in Section 7.2.3.3, shows that chloride has no effect on the chlorine/S(IV) reaction rate.

The Hg absorption data in Table 8.11 show that the addition of 0.1 M NaCl greatly enhances the rate of Hg absorption. Figure 8.10 plots this data (Points 1 through 12 from Table 8.11), along with the observed and predicted Hg penetration in buffer (with no added NaOCl or NaCl) from Figure 8.5.

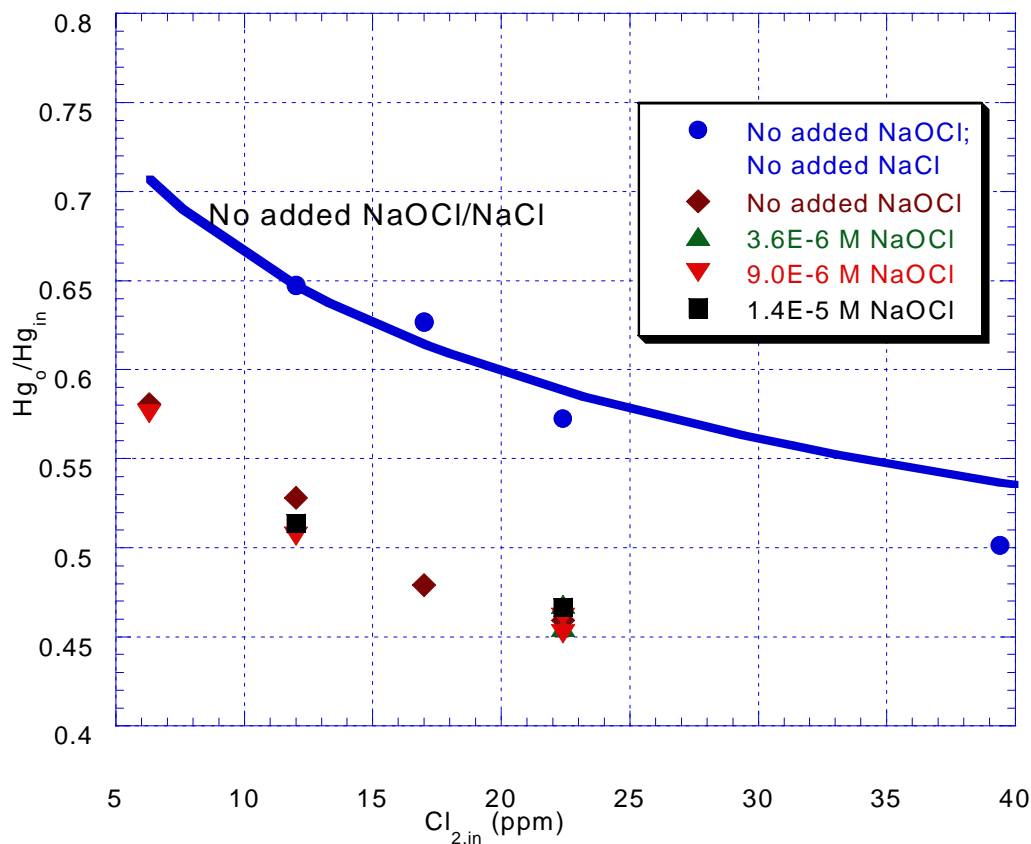


Figure 8.10. Mercury penetration in buffered NaOCl/0.1 M NaCl at pH 5.76

Figure 8.10 shows that the additional NaOCl did not enhance Hg absorption. The decrease in Hg penetration is due to the presence of 0.1 M NaCl. The NaOCl added exists as HOCl in solution. Even when no NaOCl was added, there was still HOCl present, resulting from chlorine hydrolysis.

Points 13 to 15 from Table 8.11 show that the NaOCl/NaCl enhances Hg absorption, even without the presence of chlorine in the gas. These data are similar to that collected by Zhao (1997) and were analyzed similarly.

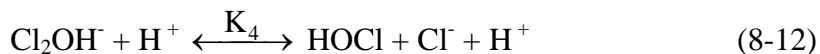
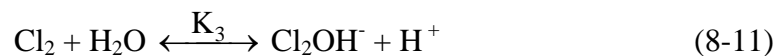
Point 16 from Table 8.12 was measured after S(IV) was added to the solution. Since S(IV) reacts with HOCl, the Hg absorption decreases as the HOCl is depleted. The chlorine flow was started through the column after S(IV) was added, as shown in

Point 17. Since the Hg flux and penetration at this point are similar to that of the points with no chloride present (Table 8.7), chloride does not affect the rate of absorption of Hg when S(IV) is present. Therefore, the addition of chloride only affects the rate of Hg and Cl₂ absorption when no S(IV) is present.

8.4.4.2 Analysis of results obtained by previous researchers

In order to understand the chemistry of the Hg/Cl₂ system, the raw data obtained by Zhao (1997) and Nene and Rane (1981) were re-analyzed, along with the data obtained from this work. Even though Zhao developed a single correlation to represent data at any pH, [Cl⁻], and [NaOCl]_T, the data used to obtain this correlation were primarily at pH 9 to 11, where hypochlorite (OCl⁻) is the dominant species in solution. Therefore, it may not be possible to directly extrapolate this correlation to predict Hg absorption in acidic pH ranges (where HOCl is the dominant species). Furthermore, the $k_{2,Hg}$ of 1.7×10^{15} L/mol-s Zhao obtained is higher than the diffusion-limited reaction rate, which signifies that the reaction cannot proceed according to the mechanism Zhao proposed. Therefore, Cl₂ was not the active species reacting with Hg in Zhao's experiments. Reaction rates in solution cannot be faster than the diffusion-limited rate of 10^{10} (for molecules) to 10^{11} (for ions) L/mol-s (Connors, 1990).

Zhao (1997) observed that the Hg absorption depended on chloride and pH, in addition to HOCl/OCl⁻. It is probable that Zhao observed the reaction of Hg with a chlorine intermediate, which is in equilibrium with HOCl, Cl⁻, and OCl⁻ (similar to Cl₂) instead of observing the direct reaction between Hg and Cl₂. A possible species is Cl₂OH⁻, which is a proposed intermediate in the chlorine hydrolysis reaction (Eigen and Kustin, 1962).



The rate-determining step is the reaction in Equation 8-11. Furthermore, at high pH, the relative stability of Cl_2OH^- with respect to Cl_2 and OH^- is quite large (Eigen and Kustin, 1962).



At 20°C, the forward rate constant for Equation 8-13 is 10^{10} L/mol-s, and the equilibrium constant, K_5 , is 10^5 L/mol (Eigen and Kustin, 1962).

The data obtained by Nene and Rane (1981) were also carefully analyzed. Using their raw data, the activity of chlorine was calculated by Equation 8-8. The data were all at 30°C and at either pH 9 or 11. There were some data at pH 2, but these data seemed to be gas film controlled (even though the authors did not state this); the gas film mass transfer coefficient was obtained from the pH 2 data, and used in Equation 8-10 to calculate a $k_{2,\text{Hg}}$. The highest $[\text{Cl}^-]$ used in their work was 4.4 M. For the experiments with low chloride (10^{-3} M), the $k_{2,\text{Hg}}$ ranged from 10^{14} to 10^{16} L/mol-s, which is above the diffusion-limited rate and in a similar range as the rate obtained by Zhao (1997). Therefore, a similar mechanism may exist as that observed in Zhao's high pH data.

For the experiments with 4.4 M chloride, the calculated $k_{2,\text{Hg}}$ ranged from 10^{11} to 10^{12} L/mol-s, which is still above the diffusion-limited rate. At this high chloride concentration, there may be other interactions that need to be accounted for, such as the formation of the trichloride ion, Cl_3^- (Zimmerman and Strong, 1957; Sherrill and Izard, 1931; Halford, 1940).

The data of Nene and Rane (1981) and Zhao (1997) show that Hg reacts in solutions containing species resulting from chlorine hydrolysis and that Hg absorption is enhanced by chloride. However, it is incorrect to propose that the elementary reaction mechanism consists of Hg reacting with Cl_2 directly.

8.4.4.3 Analysis of this work in the context of previous work

The chlorine at the interface resulting from chlorine absorption into buffer ranges from 10^{-6} M (with 22 ppm inlet Cl_2) to 10^{-7} M (with 7 ppm inlet). The concentration of chlorine at the interface is detailed in the section profiles in Tables 8.3 and 8.5 and were calculated using the integrated model discussed in Chapter 3. The Cl_2 concentration at the interface in Zhao's experiments (calculated from Equation 8-8) ranged from 10^{-15} to 10^{-11} M. Zhao observed significant Hg absorption in this range, with gas film control observed with an a_{Cl_2} of only 10^{-11} M. Thus, if the kinetics were the same as that observed by Zhao, the absorption would have been gas film controlled since the $[\text{Cl}_2]_i$ resulting from absorption was much higher than 10^{-11} M. Since the Hg absorption in this work was not gas film controlled, either the reaction mechanism is different from that observed in the experiments conducted by Zhao (1997) or the reaction is slower at lower pH.

The $k_{2,\text{Hg}}$ obtained from this work is lower than the diffusion-limit, but it is very close to this upper limit. It is probable that the reaction between elemental Hg and Cl_2 is the elementary reaction step, which determines the reaction rate. In the Hg absorption experiments in NaOCl/NaCl at high pH, an intermediate was likely involved in the rate-determining step. However, in this work, it is probable that Hg is reacting directly with Cl_2 . The same value for $k_{2,\text{Hg}}$ was regressed for absorption into buffer (with no chloride present) and into S(IV) , signifying the same mechanism for both systems.

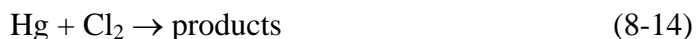
Figure 8.10 showed that the addition of NaCl significantly enhanced Hg absorption when no S(IV) is present. Zhao (1997) postulated that increased chloride enhanced Hg absorption due to increased Cl_2 formation, but this work shows that hypothesis is not valid. The addition of 0.1 M NaCl results in a chlorine activity of 10^{-9} M, which is negligible compared to the chlorine concentration at the interface. Therefore, increasing the chloride concentration did not increase the chlorine

concentration at the interface; the increased Hg absorption cannot be explained by the direct reaction of Hg and Cl₂ since the reaction rate increased without an increase in the Cl₂ at the interface.

Thus, in the presence of 0.1 M NaCl and with no S(IV), the dominant reaction pathway is not the direct reaction of Hg and Cl₂ since the reaction rate depends on the concentration of chloride. The increased chloride may be reacting with the HOCl present (from Cl₂ hydrolysis and/or NaOCl injection) to form an intermediate, which enhances Hg absorption. The addition of 0.1 M NaCl increases the a_{Cl₂} from 10⁻¹² M to 10⁻⁹ M. Therefore, if the reaction rate depends on the formation of an intermediate (whose concentration depends on the concentrations of HOCl and Cl⁻), the concentration of the intermediate will be a few orders of magnitude higher in the presence of 0.1 M NaCl.

8.4.4.4 Parallel reactions

The Hg/Cl₂ reaction likely occurs by two parallel reaction pathways, as shown by Equations 8-14 and 8-15.



Another possibility is that the increased Cl⁻ results in the formation of the trichloride ion (Cl₃⁻). The equilibrium constant for this reaction is 0.18 L/mol at 25°C (Zimmerman and Strong, 1956). The Cl₃⁻ may have a faster reaction rate with Hg, enhancing its absorption. However, at the conditions of this work, it is unlikely that enough trichloride could form to result in the significant enhancement observed at 0.1 M NaCl.

Thus, the parallel reactions listed in Equations 8-14 and 8-15 seem to be the most probable reaction pathway. Increasing the chloride concentration increases the concentration of the Cl₂ intermediate, which is in equilibrium with HOCl and Cl⁻.

The presence of the intermediate increases the Hg reaction rate, beyond what it would be with just Cl_2 . The NaOCl addition did not have an effect on the reaction rate since the increase was not as substantial. Point 17 in Table 8.12 showed that in the presence of S(IV), the chloride does not affect the reaction rate. When S(IV) is present, no HOCl will be present. Therefore, the intermediate will not be present either; so, the reaction rate will not be affected by the addition of chloride and will occur by Equation 8-14.

The rate expression accounting for both mechanisms can be written as the sum of the two parallel reaction rates. The reaction pathway in Equation 8-14 can be represented by the $k_{2,\text{Hg}}$ obtained in this work. The pathway with the intermediate can be represented with the rate constant obtained by Zhao (1997). Even though the rate expression obtained by Zhao does not represent the elementary reaction mechanism, the expression may be adapted to correlate the data.

The rate expression by Zhao must be written in terms of HOCl instead of chlorine, and the volatility of HOCl must be accounted for. At pH 4 to 7, HOCl is the predominant chlorine species in solution, and the desorption of HOCl may be significant (Lahiri et al., 1983; Blatchley and Johnson, 1991; Holzwarth et al., 1984). Therefore, the concentration of HOCl at the interface will be significantly lower than the bulk value and must be accounted for in the rate expression. This would result in the concentration of the intermediate (reacting with Hg) to be less at the interface. If the HOCl volatility was not accounted for, the rate expression would be the same as what Zhao used and would over-predict the data by several orders of magnitude.

The HOCl at the interface can be obtained by setting the rate of desorption equal to the rate of diffusion in the liquid plus the rate of HOCl formation through chlorine absorption. The depletion of HOCl to form dichlorine monoxide (Cl_2O) is not accounted for because the formation rate of Cl_2O should not be significant at the

low HOCl concentrations discussed in this work (Lahiri et al., 1982; Renard and Bolker, 1976; Soper, 1924; Secoy and Cady, 1941).

$$k_g (H_{\text{HOCl}}[\text{HOCl}]_i - 0) = k_L([\text{NaOCl}]_{\text{T,b}} - [\text{NaOCl}]_{\text{T,i}}) + N_{\text{Cl}_2} \quad (8-16)$$

By writing the concentration of total chlorine species in terms of HOCl and solving for HOCl at the interface, Equation 8-17 is obtained.

$$[\text{HOCl}]_i = \frac{k_L[\text{NaOCl}]_{\text{T}} + N_{\text{Cl}_2}}{k_g H_{\text{HOCl}} + k_L \left(\frac{K_1}{a_{\text{H}^+} \gamma_{\text{NaCl}}} + 1 \right)} \quad (8-17)$$

The Henry's law constant for HOCl was taken to be 46 atm-L/mol at 30°C (Renard and Bolker, 1976). The rate expression and corresponding flux expression representing the parallel reaction rates are shown below in Equations 8-18 and 8-19.

$$\text{rate} = [\text{Hg}]_i \left(k_{2,\text{Hg}} [\text{Cl}_2]_i + \frac{k_{2,\text{Zhao}}}{K_2} \gamma_{\text{NaCl}} [\text{Cl}^-] [\text{H}^+] [\text{HOCl}]_i \right) \quad (8-18)$$

$$N_{\text{Hg}} = \frac{P_{\text{Hg}_i}}{H_{\text{Hg}}} \sqrt{D_{\text{Hg}} \left(k_{2,\text{Hg}} [\text{Cl}_2]_i + \frac{k_{2,\text{Zhao}}}{K_2} \gamma_{\text{NaCl}} [\text{Cl}^-] [\text{H}^+] [\text{HOCl}]_i \right)} \quad (8-19)$$

Equation 8-19 was used to analyze the data in this work and the data by Zhao (1997) to see if the developed model could accurately predict Hg absorption throughout the pH range of 5 to 11. Table 8.13 tabulates selected data from Zhao. Even though Zhao was not able to correlate the data at low pH, the data were reported in her dissertation (Zhao, 1997). Using Zhao's original model (Equation 8-10), the data at low pH were over-predicted by several orders of magnitude. The Hg inlet concentration was 98 ppb (Zhao, 1997). Two of the data points contained HgCl_2 ; therefore, the rate expression for Hg(II) was added to Equation 8-19 in order to calculate the predicted flux for these two points. Table 8.14 tabulates the data in

Table 8.11 and shows how the predicted flux from Equation 8-19 compares with the observed flux.

Table 8.13 Mercury absorption in NaOCl/NaCl at pH 5 to 11, $Hg_{in} = 98$ ppb (Zhao, 1997)

$P_{Hg,i}$ (atm)	Observed N_{Hg} ($kmol/m^2 \cdot s$)	$[NaOCl]_T$ (M)	γ_{NaCl}	pH	$[Cl^-]$ (M)	$[HOCl]_i$ (M)	Predicted N_{Hg} ($kmol/m^2 \cdot s$)	Predicted $N_{Hg}/$ Observed N_{Hg}
8.80E-08	1.02E-12	3.71E-02	0.8	11.12	3.71E-02	6.67E-06	8.67E-13	0.85
8.20E-08	1.42E-12	3.71E-02	0.8	10.9	3.71E-02	1.03E-05	1.29E-12	0.91
7.60E-08	1.84E-12	3.71E-02	0.8	10.77	3.71E-02	1.31E-05	1.57E-12	0.85
8.10E-08	1.51E-12	3.63E-03	0.92	9.86	3.63E-03	4.24E-06	9.11E-13	0.60
5.00E-08	3.64E-12	8.53E-06	0.97	5.8	8.53E-06	1.38E-08	1.34E-11*	3.69
2.60E-08	5.32E-12	8.52E-06	0.97	4.89	8.52E-06	1.38E-08	1.03E-11*	1.95
2.60E-08	5.33E-12	3.90E-05	0.657	8.97	1	5.89E-08	1.35E-12	0.25
7.70E-08	1.76E-12	8.80E-03	0.657	11.1	1	1.38E-06	1.66E-12	0.95
4.70E-08	3.86E-12	1.70E-03	0.657	10.18	1	1.30E-06	2.84E-12	0.74
4.60E-08	3.90E-12	2.70E-06	0.657	5.08	1	4.36E-09	5.71E-11	14.6
3.80E-08	4.50E-12	4.10E-06	0.657	5.15	1	6.62E-09	5.36E-11	11.9
9.60E-08	4.70E-13	9.00E-07	0.779	6.31	0.1	1.45E-09	5.75E-12	12.2
8.80E-08	1.00E-12	3.40E-06	0.779	6.42	0.1	5.49E-09	9.02E-12	9.02
9.70E-08	3.40E-13	2.10E-06	0.779	6.67	0.1	3.39E-09	5.86E-12	17.2
9.50E-08	5.10E-13	4.10E-06	0.779	6.74	0.1	6.61E-09	7.40E-12	14.5

* Points with $Hg(II)$, $k_{2,Hg(II)}$ (2.4×10^7 L/mol-s) term added to rate expression

Table 8.14 Mercury flux predictions in 0.1 M NaCl at pH 5.76

Point	$P_{Hg,i}$ (atm)	Observed N_{Hg} ($kmol/m^2 \cdot s$)	$[NaOCl]_T$ (M)	γ_{NaCl}	$[HOCl]_i$ (M)	Predicted N_{Hg} ($kmol/m^2 \cdot s$)	Predicted $N_{Hg}/$ Observed N_{Hg}
1	2.07E-08	5.93E-12	0	0.779	1.97E-08	9.40E-12	1.59
2	1.73E-08	6.67E-12	0	0.779	3.22E-08	1.02E-11	1.53
3	1.42E-08	7.36E-12	0	0.779	4.80E-08	1.01E-11	1.37
4	1.28E-08	7.65E-12	0	0.779	6.41E-08	1.06E-11	1.39
5	1.26E-08	7.70E-12	3.58E-06	0.779	9.23E-08	1.21E-11	1.58
6	1.34E-08	7.52E-12	3.58E-06	0.779	9.14E-08	1.29E-11	1.72
7	1.24E-08	7.75E-12	8.96E-06	0.779	1.28E-07	1.38E-11	1.78
8	1.30E-08	7.62E-12	8.96E-06	0.779	1.29E-07	1.45E-11	1.90
9	2.03E-08	6.00E-12	8.96E-06	0.779	5.86E-08	1.50E-11	2.50
10	1.59E-08	6.98E-12	8.96E-06	0.779	7.75E-08	1.37E-11	1.97
11	1.64E-08	6.88E-12	1.43E-05	0.779	1.03E-07	1.61E-11	2.34
12	1.33E-08	7.54E-12	1.43E-05	0.779	1.42E-07	1.56E-11	2.06
13	3.35E-08	2.97E-12	1.43E-05	0.779	6.96E-08	2.62E-11	8.80

14	3.25E-08	3.21E-12	3.05E-05	0.779	1.48E-07	3.71E-11	11.6
15	3.24E-08	3.23E-12	3.58E-05	0.779	1.74E-07	4.01E-11	12.4

Figure 8.11 depicts the data in Tables 8.13 and 8.14, showing how the observed flux compares with that predicted using Equation 8-19. The triangles (including the inverted triangles) represent the data from this work (Table 8.14); the inverted triangles represent points in which no chlorine was in the gas (Points 13 through 15 from Table 8.14). The rest of the points represent data from Zhao (1997), as listed in Table 8.13.

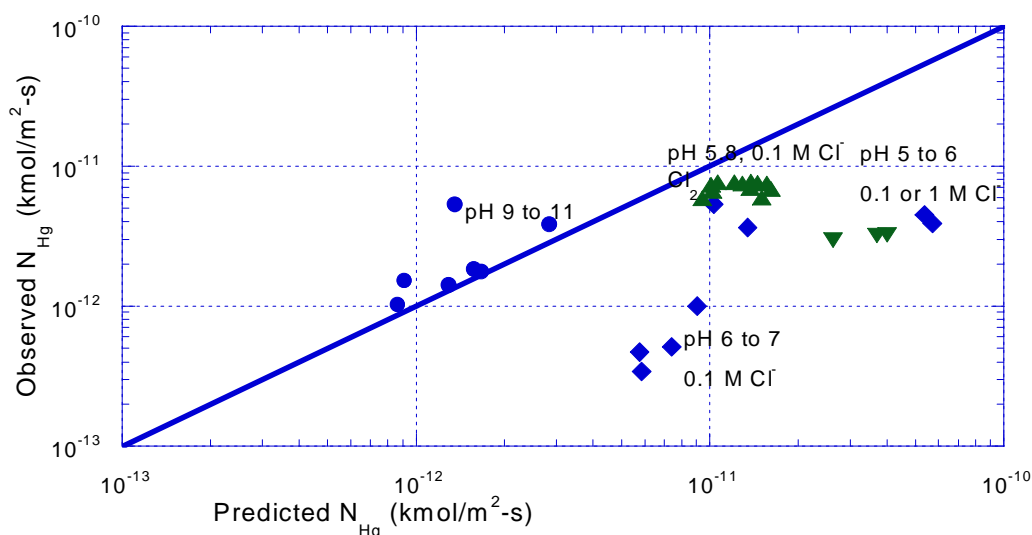


Figure 8.11. Using parallel reaction model to correlate data with NaOCl/NaCl

The developed model predicts the pH 9 to 11 data from Zhao (1997) very well. At high pH, OCl^- is the dominant species; therefore, the correction for HOCl volatility is not significant. Since the model utilized the rate constant obtained by Zhao at high pH, the model was expected to fit the high pH data. The model predicts the rest of the data (pH 5 to 7) within a factor of 10. Even though this model is not very accurate, it predicts the absorption much better than the original model Zhao developed. Her model could only predict the absorption rate of Hg into NaOCl/NaCl

at high pH; it greatly over-predicted the absorption at lower pH. By accounting for HOCl volatility, this model predicts the lower pH data within one order of magnitude.

The pH 5 to 7 data would be predicted accurately if the rate constant were lowered by a factor of 100. Therefore, if the formation of the intermediate were slower at low pH, it would explain why the low pH data do not fit using the same rate constant that fits the high pH data. At pH 5 to 7, HOCl is the dominant species. More HOCl may be disappearing from the interface due to a mechanism not accounted for in the model, resulting in the model over-predicting the flux by a factor of 10. The parallel reaction model developed in this work attempts to connect the Hg absorption with Cl_2 to absorption in HOCl/OCl⁻. However, further research is required to understand the chemistry and develop a more accurate model that accounts for all the reactions.

8.5 IMPLICATIONS ON MERCURY REMOVAL IN A TYPICAL LIMESTONE SLURRY SCRUBBER

A model was developed to predict mercury removal through injection of Cl_2 in a limestone slurry scrubber. The expected mercury removal was calculated using the regressed rate constants obtained from this work and typical mass transfer characteristics for a scrubber. The mercury removal model must be supplied with a given chlorine inlet and a constant S(IV) concentration. The model accounts for the two simultaneous reactions occurring at the gas/liquid interface: the depletion of chlorine through reaction with S(IV) ($k_{2,\text{S(IV)}}$) and the reaction of elemental mercury with chlorine ($k_{2,\text{Hg}}$). The calculations were done at 25°C using the parameters listed in Table 8.15.

Table 8.15. Parameters used to predict mercury removal in a scrubber at 25°C

Properties	Value
$k_{2,S(IV)}$ (L/mol-s)	1×10^9
$k_{2,Hg}$ (L/mol-s)	6×10^9
k_g (kmol/s-atm-m ²)	0.001
D_{Cl_2} (m ² /s)	1.48×10^{-9}
D_{Hg} (m ² /s)	1.19×10^{-9}
H_{Hg} (atm-m ³ /kmol)	8.91
H_{Cl_2} (atm-m ³ /kmol)	16.7

Since the concentrations change through the scrubber, the model integrates the Hg and Cl₂ concentrations. However, to simplify the calculations, the S(IV) was assumed to be constant throughout the spray scrubber. The chlorine at the interface must be calculated in order to predict Hg absorption. The bulk chlorine in the scrubber depends on the number of gas phase mass transfer units (N_g), which is defined as $k_g A/G$. The total number of gas phase mass transfer units in a typical scrubber is 6.9; this value assumes the absorption is gas film controlled. By expressing the rate of chlorine absorption in terms of the overall gas phase mass transfer coefficient (K_{OG}) and N_g , the bulk chlorine can be calculated from Equation 8-20.

$$P_{Cl_2,b} = P_{Cl_2,in} \exp\left(-\frac{K_{OG}}{k_g} N_g\right) \quad (8-20)$$

The fraction gas film resistance (K_{OG}/k_g) was calculated by substituting the enhancement factor into Equation 6-6, as shown in Equation 8-21.

$$\frac{K_{OG}}{k_g} = \frac{1}{1 + \frac{k_g H_{Cl_2}}{\sqrt{D_{Cl_2} k_{2,S(IV)} [S(IV)]}}} \quad (8-21)$$

The chlorine flux calculated from Equation 3-1 must equal the flux from Equation 3-4, thus allowing the chlorine concentration at the interface to be determined when the S(IV) concentration is provided. The succinate buffer term in Equation 3-4 was neglected. The chlorine at the interface was calculated from Equation 8-22.

$$[Cl_2]_i = \frac{k_g P_{Cl_2, in} \exp\left(-\frac{K_{OG}}{k_g} N_g\right)}{k_g H_{Cl_2} + \sqrt{D_{Cl_2} k_{2, S(IV)} [S(IV)]}} \quad (8-22)$$

To predict mercury absorption, the enhancement of mercury removal due to reaction with chlorine was calculated:

$$E_{Hg} k_{L, Hg}^o = \sqrt{D_{Hg} k_{2, Hg} [Cl_2]_i} \quad (8-23)$$

The rate at which mercury is absorbed is the product of the driving force (mole fraction of Hg in gas, y_{Hg}) and the overall gas phase mass transfer coefficient (K_{OG}) given in Equation 8-24.

$$K_{OG} = \frac{k_g}{1 + \frac{k_g H_{Hg}}{E_{Hg} k_{L, Hg}^o}} \quad (8-24)$$

Thus, the rate of mercury absorption in a scrubber is given by Equation 8-25:

$$-G dy_{Hg} = y_{Hg} \frac{k_g}{1 + \frac{k_g H_{Hg}}{\sqrt{D_{Hg} k_{2, Hg} [Cl_2]_i}}} dA \quad (8-25)$$

Substituting N_g for $k_g A/G$ and integrating:

$$\int_{y_{\text{Hg},\text{in}}}^{y_{\text{Hg}}} \frac{dy_{\text{Hg}}}{y_{\text{Hg}}} = - \int_0^{6.9} \frac{1}{1 + \frac{k_g H_{\text{Hg}}}{\sqrt{D_{\text{Hg}} k_{2,\text{Hg}} [\text{Cl}_2]_i}}} dN_g \quad (8-26)$$

Equation 8-26 was used to quantify mercury removal. The Cl_2 exiting the scrubber and the Hg penetration were calculated at various Cl_2 inlet and S(IV) concentrations, as shown in Table 8.16.

Table 8.16. Predicted Hg penetration in a scrubber with Cl_2 injection at inlet

[S(IV)] (mM)	$\text{Cl}_{2,\text{in}}$ (ppm)	$\text{Cl}_{2,\text{out}}$ (ppm)	$\text{Hg}_o/\text{Hg}_{\text{in}}$
0.001	10	6.3	0.32
0.001	25	15.6	0.19
0.001	50	31.3	0.12
0.001	500	313	0.02
0.01	50	13.7	0.18
1.0	10	0.08	0.74
1.0	50	0.41	0.53
1.0	500	4.1	0.20
1.0	2000	16.3	0.08
10.0	50	0.12	0.70

At a given S(IV), mercury removal increases (penetration decreases) as the chlorine injected increases; however, the Cl_2 exiting the scrubber also increases. Mercury removal decreases as S(IV) increases due to greater depletion of chlorine at the interface. Less chlorine is needed to achieve the same Hg removal when there is less S(IV). However, when there is less S(IV), the chlorine exiting the scrubber is greater. To obtain 80% Hg removal, only 25 ppm Cl_2 is needed at 0.001 mM S(IV), while 500 ppm Cl_2 is required at 1 mM S(IV). However, the chlorine emissions are less using 500 ppm Cl_2 because the S(IV) concentration is greater. Thus, the process feasibility will depend on the S(IV) concentration of the scrubber, the desired Hg removal, and the amount of Cl_2 which can be tolerated.

In addition to studying the effect of Cl_2 injection at the inlet, Cl_2 injection near the top of the scrubber was also studied. Since less S(IV) is present near the top of the scrubber, more chlorine would remain at the interface. Thus, less chlorine would be required to enhance Hg absorption. The model was the same as for Cl_2 injection at the inlet, except the value for N_g was lowered to 2.3. Table 8.17 displays the predicted performance of Hg removal at low S(IV) with Cl_2 injection near the top of the scrubber.

Table 8.17. Predicted Hg penetration in a scrubber with Cl_2 injection near top

[S(IV)] (mM)	$\text{Cl}_{2,\text{in}}$ (ppm)	$\text{Cl}_{2,\text{out}}$ (ppm)	$\text{Hg}_o/\text{Hg}_{\text{in}}$
0.001	10	8.6	0.67
0.001	25	21.4	0.56
0.001	50	42.8	0.47
0.001	500	428	0.25

Since the S(IV) concentration is low, most of the Cl_2 exits the scrubber. Therefore, if Cl_2 were injected near the top of the scrubber, the Cl_2 would need to be scrubbed with sodium hydroxide before being released to the atmosphere.

8.5.1 Other factors affecting Hg removal in a limestone slurry scrubber

The developed model does not account for all the variables which may impact the process feasibility in a limestone slurry scrubber. As mentioned before, the model assumes that the S(IV) concentration throughout the scrubber is constant. Even though the S(IV) concentration is probably not constant, assuming an average value should not have a significant effect on the model predictions.

Limestone slurry typically contains Fe^{+2} and Mn^{+2} . Gilliland et al. (1958) have shown that Fe^{+2} reacts with Cl_2 at low pH, but the reaction rate is negligible compared to the reaction rate of Cl_2 with S(IV). Ulrich et al. (1986) have shown that transition metal cations, including Fe^{+2} and Mn^{+2} , catalyze S(IV) oxidation through the formation of free radicals. Even though Section 6.4 showed that Cl_2 alone does

not catalyze S(IV) oxidation, it is possible that in the presence of $\text{Fe}^{+2}/\text{Mn}^{+2}$, the S(IV) oxidation may be enhanced. The enhanced oxidation of S(IV) would result in more available Cl_2 at the interface, resulting in greater Hg absorption. However, the Cl_2 exiting the scrubber would also be greater. Munthe and McElroy (1992) have shown that Fe^{+2} can enhance Hg absorption in the presence of H_2O_2 through the formation of free radicals.

Limestone slurry scrubbers usually operate at 55°C . At this temperature, the diffusivities and Henry's law constants would be slightly higher. Depending on the activation energy, the rate constants would also be higher. Therefore, at the higher temperature, there would be less chlorine at the interface due to the higher reaction rate of chlorine with S(IV). However, since the reaction rate of mercury and chlorine also increases with temperature, the overall effect may be similar to that calculated in this section, using the values at 25°C .

The presence of NO in the gas was not accounted for in the model. Since the reaction rate of Cl_2 with NO is slow at 55°C , this reaction will have a negligible effect on the Cl_2 and NO concentrations in the flue gas (Chen and Rochelle, 2000; Ashmore and Chanmugam, 1953; Ashmore and Spencer, 1959; Clark et al., 1966).

Even though there are parameters which the developed model did not include, the same tradeoffs will always be present. If there is low $\text{SO}_2/\text{S(IV)}$, less Cl_2 will be required to remove the Hg. However, more chlorine would exit the scrubber. If there is high $\text{SO}_2/\text{S(IV)}$, good chlorine removal will occur, but more would need to be injected in order to achieve good Hg removal. Therefore, the process feasibility depends on what concentrations of Hg and Cl_2 can be tolerated.

8.6 SUMMARY

The simultaneous absorption of Hg and Cl_2 into buffered S(IV) solutions was measured in the wetted wall column at ambient temperature at pH 4.7 and 5.7.

Mercury does not absorb (at either pH) into distilled water, buffer, or S(IV) unless an oxidant (Cl_2 , Hg(II) , NaOCl) is present. As the Cl_2 inlet concentration increases, the Hg penetration decreases until the gas film control limit is reached. As S(IV) increases, the Cl_2 decreases and eventually becomes gas film controlled; therefore, at high S(IV), less Hg is absorbed since barely any Cl_2 exists at the interface to enhance Hg absorption. The regressed values for $k_{2,\text{Hg}}$ at pH 4.7 and 5.7 were $(6.2 \pm 0.8) \times 10^9$ and $(6.0 \pm 0.7) \times 10^9$ L/mol-s, respectively. Since the values at both pH are essentially the same, an average value of $(6.1 \pm 0.8) \times 10^9$ L/mol-s can be reported as the Hg/ Cl_2 rate constant. Sensitivity analyses showed that the model is very sensitive to the $k_{2,\text{Hg}}$.

The absorption of Hg and Cl_2 into buffered HgCl_2 solutions was also studied in the wetted wall column at pH 5.7. In a reducing solution, the added HgCl_2 was reduced to elemental Hg and desorbed. In an oxidizing environment, the Hg(II) enhanced the absorption of elemental Hg. The reaction rate in the presence of Hg(II) and Cl_2 was slightly higher than the sum of the individual reaction rates. Therefore, in the presence of Cl_2 , the HgCl_2 seems to be slightly catalyzing the absorption of Hg.

Absorption experiments were also performed in 0.1 M NaCl at pH 5.76, with the addition of either NaOCl (which is present as HOCl) or S(IV). The addition of 0.1 M NaCl greatly enhanced Hg absorption in buffer with Cl_2 present, while the addition of 10^{-6} to 10^{-5} M NaOCl had no effect on the Hg absorption. The NaOCl/NaCl did enhance Hg absorption when no Cl_2 was present. The addition of 0.1 M NaCl had no effect on the absorption of Hg with Cl_2 in S(IV). The addition of S(IV) depletes the HOCl in the solution.

The Hg/ Cl_2 reaction can be modeled as two parallel reactions: the direct reaction of Hg with Cl_2 and reaction of Hg with a Cl_2 -intermediate. In the Hg/ Cl_2 /S(IV) system, the Hg reacts directly with Cl_2 . The addition of S(IV) results in decreased Hg absorption because of the lower chlorine concentration at the gas/liquid

interface. When no S(IV) is present, other Cl_2 oxidants may be present in solution. A Cl_2 -intermediate, which is in equilibrium with HOCl and Cl^- , may enhance Hg absorption. Therefore, at high concentrations of this intermediate species (such as that obtained in 0.1 M NaCl), the reaction rate with Hg is much higher than what it is for the direct reaction between Hg and Cl_2 .

To model the Hg reaction with the intermediate, the expression by Zhao (1997) was rewritten in terms of HOCl, and the volatility of HOCl was accounted for. The parallel reaction model attempts to connect this work (mainly Hg/ Cl_2 and some Hg/ Cl_2 /NaOCl/NaCl) to that of Zhao (Hg/NaOCl/NaCl). The model predicted the Hg/ Cl_2 data very well and the data from Zhao (1997) within a factor of ten. This model prediction was much more accurate than that of the model Zhao (1997) developed.

Using the rate constants obtained in this work, it is possible to predict the removal of Hg in a typical limestone slurry scrubber by Cl_2 injection. Less chlorine is needed to achieve the same Hg removal when less S(IV) is present. However, the Cl_2 exiting the scrubber is greater when there is less S(IV). Thus, the process feasibility will depend on the SO_2 /S(IV) concentration of the scrubber, the desired Hg removal, and the amount of Cl_2 which can be tolerated.

Chapter 9: Conclusions and Recommendations

This work studied the chemical reaction kinetics for the aqueous $\text{Hg}/\text{Cl}_2/\text{S(IV)}$ system. Absorption was measured in either a stirred cell reactor or a wetted wall column. The wetted wall column was designed to have a higher liquid film mass transfer coefficient (necessary to obtain kinetics for fast reactions) than the stirred cell reactor and to minimize surface and bulk gas reactions. The absorption was modeled using the theory of mass transfer with chemical reaction.

9.1 CONCLUSIONS

9.1.1 *Chlorine absorption in succinate buffer/S(IV)*

The addition of S(IV) significantly enhances Cl_2 absorption. The rate constant was too rapid to be precisely measured in the stirred cell reactor, due to mass transfer limitations. The absorption always varied with the mass transfer coefficients in the stirred cell reactor. Using the wetted wall column, the rate constant was determined to be $(1.1 \pm 0.3) \times 10^9 \text{ L/mol-s}$. The S(IV) reacts with chlorine directly, not through the formation of HOCl. The reaction rate of S(IV) with Cl_2 is greater than that with HOCl and OCl^- . The $\text{Cl}_2/\text{S(IV)}$ reaction is very rapid, requiring only 0.2 mM S(IV) to become gas film controlled with 20 ppm Cl_2 . The amount of S(IV) required to reach gas film control depends on the chlorine concentration. When the partial pressure of the inlet chlorine (in atm) is 10 times less than the S(IV) concentration (in mol/L), the absorption becomes gas film controlled.

At low S(IV) concentrations, chlorine absorption was limited by the buffer-enhanced hydrolysis reaction. The enhancement by the succinate buffer was

quantified. The di-succinate results in greater enhancement of Cl_2 absorption than the mono-succinate anion. This enhancement was correlated as a function of pK_a .

The addition of up to 0.1 M sodium chloride did not affect the rate of Cl_2 absorption in S(IV) since this is an irreversible reaction, but it did slightly suppress the reversible chlorine hydrolysis reaction when no S(IV) was present.

Oxygen did not affect the rate of chlorine absorption in S(IV) or catalyze S(IV) oxidation at the conditions investigated. With no oxygen present, the rate of S(IV) oxidation was equal to the rate of chlorine absorption, confirming the reaction stoichiometry of 1 mole Cl_2 per 1 mole S(IV).

9.1.2 Simultaneous absorption of mercury and chlorine

Mercury does not absorb into distilled water, buffer, or S(IV) unless an oxidant is present. The aqueous reaction of Hg and Cl_2 is very rapid, only slightly below the diffusion-limited reaction rate. The rate constant was determined to be $(6.1 \pm 0.8) \times 10^9 \text{ L/mol}\cdot\text{s}$. As the Cl_2 concentration increases, the Hg absorption increases until the gas film control limit is reached. The addition of S(IV) decreases the chlorine at the interface, thus decreasing the rate of Hg absorption.

The addition of 0.1 M sodium chloride greatly enhanced the rate of absorption of Hg with Cl_2 in buffer with no S(IV) present, but had no effect when S(IV) was present. In the Hg/ Cl_2 /S(IV) system, the Hg reacts directly with Cl_2 . When no S(IV) is present, HOCl from chlorine hydrolysis is present in solution. An intermediate species, which is in equilibrium with HOCl and Cl^- , may form and enhance Hg absorption. Therefore, at high concentrations of this intermediate (such as that obtained with 0.1 M NaCl), the reaction rate with Hg is much faster than what it is for the direct reaction between Hg and Cl_2 .

The Hg/ Cl_2 reaction was modeled as two parallel reactions: the direct reaction of Hg with Cl_2 and reaction of Hg with a Cl_2 -intermediate. The rate expression used

by Zhao (1997) was modified to represent the reaction of Hg with the intermediate. The developed model predicted the data from Zhao (1997) and from this work in NaOCl/NaCl within a factor of ten. This model prediction was much more accurate than that of the model Zhao (1997) developed. This model can predict the rate of absorption of Hg in Cl₂-containing solutions from pH 5 to 11.

The effect of adding HgCl₂ to the solution was also studied. If the solution had a reducing potential, the added HgCl₂ was reduced to elemental Hg and desorbed. In an oxidizing environment, Hg(II) enhanced Hg absorption. Furthermore, in the presence of Cl₂, the Hg(II) seemed to slightly catalyze the absorption of elemental Hg.

9.1.3 Predicting Hg removal in a limestone slurry scrubber

The developed model shows that to obtain 80% Hg removal, only 25 ppm Cl₂ is needed at 0.001 mM S(IV), while 500 ppm Cl₂ is required at 1 mM S(IV). However, the chlorine emissions are less using 500 ppm Cl₂ because the S(IV) reacts with the Cl₂. Thus, the feasibility of introducing Cl₂ to remove Hg depends on the SO₂/S(IV) concentration of the scrubber, the desired Hg removal, and the amount of Cl₂ which can be tolerated.

9.2 RECOMMENDATIONS

9.2.1 Understanding Hg/Cl₂ reaction pathway

Further study is needed to develop a model which accurately predicts Hg absorption with Cl₂ in the presence of NaOCl/NaCl. A model that contains all the chemistry and is valid for all pH ranges and concentrations is needed. The structure of the intermediate and the formation rate at different pH may be important. The dependence of the reaction rate on pH, [Cl⁻], and [HOCl] need to be verified. Mercury/chlorine absorption experiments should be conducted with increased concentrations of NaOCl/Cl⁻ so that the activity of chlorine in the liquid is similar to

that at the gas/liquid interface. This increased a_{Cl_2} should be obtained in various ways in order to see if each method yields the same enhancement on Hg absorption. The a_{Cl_2} can be increased by increasing the chloride concentration, at a small HOCl concentration, until the desired value for a_{Cl_2} is reached. The a_{Cl_2} can also be increased by only increasing the HOCl concentration at a small NaCl concentration. If both of these results yield the same enhancement, then the Hg absorption is probably being enhanced by the formation of an intermediate which is in equilibrium with HOCl and Cl^- . If the enhancement is lower (at the same a_{Cl_2}) when the NaOCl is added than it was with NaCl addition, then the enhancement probably results from the formation of an intermediate which only depends on the chloride concentration (such as Cl_3^-).

Other parameters to vary include buffer concentration and pH. Increasing the buffer concentration would increase the chlorine hydrolysis rate. Therefore, more HOCl and Cl^- would be present. Lowering pH would result in an increase in the activity of chlorine in the liquid.

9.2.2 Experimental conditions to simulate limestone slurry scrubber

To simulate experimental conditions in a typical scrubber, reaction kinetics should be determined at 55°C. The effects of adding NO_x and SO_2 to the gas should be studied. Absorption should be studied in the pH range of 2.5 to 6.

Furthermore, experiments should be done with Fe^{+2} and Mn^{+2} since these transition metal cations are present in limestone slurry scrubbers and may affect chlorine absorption in S(IV). Also, the effects of Ca^{+2} and Mg^{+2} on Hg/Cl_2 absorption should be studied.

9.2.3 Improved Hg analytical capabilities

Purchasing a new Hg analyzer, which has less drift and a longer cell path length, would be very beneficial. It would allow measurement at much lower Hg

concentrations. It would also aid in shortening the experimental time and increasing productivity.

Appendix A: Gas film mass transfer coefficient for stirred cell

The gas film mass transfer coefficient for the stirred cell reactor was obtained by absorbing chlorine into 0.28 M NaOH. At a constant gas flow rate, the gas phase agitation was varied in order to obtain a correlation for k_g . Data were taken using both chlorine analyzers. Table A-1 tabulates the data obtained using the IMS analyzer. These data were used to obtain the correlation that was used for all the data obtained using the IMS analyzer. Table A-2 tabulates the data obtained using the electrochemical analyzer. These data were used to obtain the correlation that was used for the data obtained using electrochemical analyzer.

Table A-1. Gas film mass transfer coefficient (k_g) for stirred cell reactor, obtained using IMS analyzer

n_g (rpm)	$Cl_{2,in}$ (ppm)	$Cl_{2,out}$ (ppm)	N_{Cl_2} (kmol/m ² -s)	k_g (mol/s-atm-m ²)
750	21.2	2.47	1.89E-09	0.765
623	21.2	2.69	1.87E-09	0.694
500	21.2	3.00	1.84E-09	0.613
762	21.2	2.50	1.89E-09	0.755

Table A-2. Gas film mass transfer coefficient (k_g) for stirred cell reactor, obtained using electrochemical analyzer

n_g (rpm)	$Cl_{2,in}$ (ppm)	$Cl_{2,out}$ (ppm)	N_{Cl_2} (kmol/m ² -s)	k_g (mol/s-atm-m ²)
629	195	26.2	1.69E-08	0.65
474	195	30.6	1.65E-08	0.54
352	195	34.5	1.61E-08	0.47
707	195	24.9	1.71E-08	0.69
484	195	31.6	1.64E-08	0.52
710	195	25.3	1.70E-08	0.67
710	149	19.7	1.31E-08	0.66
710	93	12.8	8.25E-09	0.65
490	93	16.5	7.87E-09	0.48

362	93	18.2	7.69E-09	0.42
711	93	12.6	8.27E-09	0.65
616	197	27.8	1.70E-08	0.61
519	197	31.7	1.66E-08	0.52
412	197	36.7	1.61E-08	0.44
330	197	41.3	1.56E-08	0.38
597	197	30.9	1.67E-08	0.54
342	197	39.8	1.58E-08	0.40
720	197	26.6	1.71E-08	0.64
428	197	36.1	1.61E-08	0.45
288	197	41.9	1.56E-08	0.37
704	197	27.0	1.71E-08	0.63

Figure A-1 depicts the data and correlations for obtaining k_g , and Table A-3 lists the correlation parameters. The k_g correlations were compared with other correlations developed by previous researchers who used a similar apparatus. Zhao, who used the exact same apparatus, developed a k_g correlation for mercury by absorbing mercury into aqueous permanganate. Her correlation was: $k_g(\text{mol/s-atm-m}^2) = 0.0344(n_g)^{0.38}$ (Zhao and Rochelle, 1996). Dutchuk, who used a similar apparatus (but not identical), developed a k_g correlation for sulfur dioxide by absorbing SO_2 into sodium hydroxide. His correlation was: $k_g(\text{mol/s-atm-m}^2) = 0.0552(n_g)^{0.385}$ (Dutchuk, 1999). Figure A-1 and Table A-3 display all the correlations.

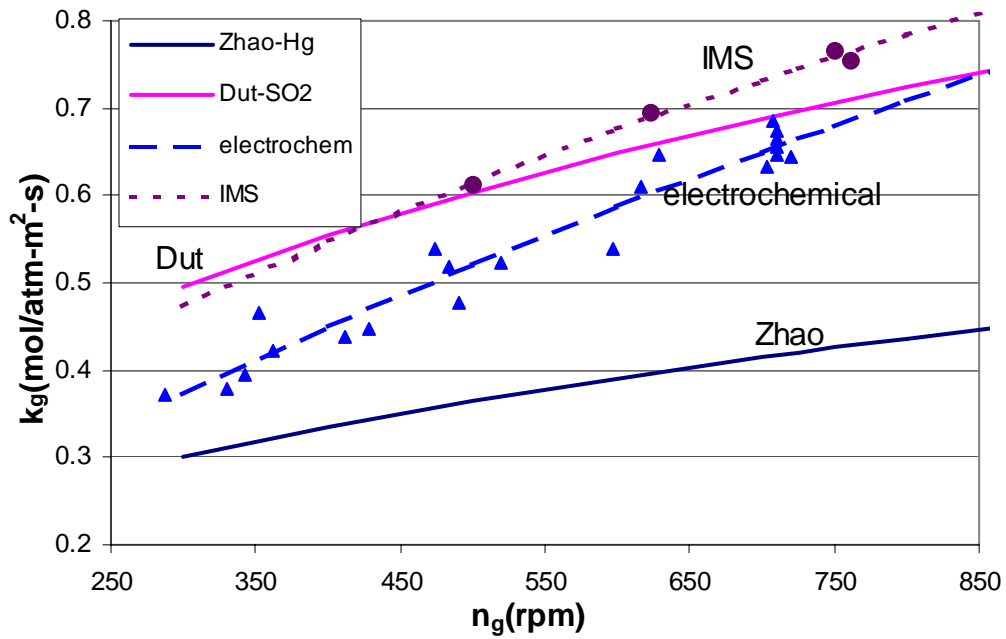


Figure A-1. Data and correlations for gas film mass transfer coefficient

Table A-3. Parameters for gas film mass transfer correlations

Series	$k_g = a n_g^b$	
	a	b
IMS	0.0252	0.5142
electrochem	0.0089	0.655
Zhao-Hg	0.0344	0.38
Dutchuk-SO ₂	0.0552	0.385

Appendix B: Liquid film mass transfer coefficient for stirred cell

As mentioned in Section 5.2, the physical liquid film mass transfer coefficient can be determined from Cl_2 desorption from HOCl in 0.1 M HCl . From a plot of $\ln P_{\text{Cl}_2, \text{out}}$ vs time, the liquid film mass transfer coefficient can be extracted from the slope. Table B-1 tabulates the raw data at different liquid agitation speeds. All the data were taken with the IMS analyzer.

Table B-1. Data used to determine $k_{\text{L}, \text{Cl}_2}^0$ correlations for stirred cell reactor

$n_L(\text{rpm})$	$t(\text{min})$	$\text{Cl}_{2, \text{out}}(\text{ppm})$	$\ln P_{\text{Cl}_2}(\text{atm})$
729	0	284	-8.17
	6	264	-8.24
	12	248	-8.30
	18	232	-8.37
	20.6	222	-8.41
	24	213	-8.46
	30	203	-8.50
	36	186	-8.59
	42	168	-8.69
	48	158	-8.76
	54	148	-8.82
	60	135	-8.91
	64.8	129	-8.96
	75	112	-9.10
305	0	56.7	-9.78
	6	53.8	-9.83
	12	51.2	-9.88
	18	50.2	-9.90
	25.1	47.3	-9.96
504	0	65.4	-9.63
	6	61.9	-9.69
	12	58.6	-9.74
	14.2	57.0	-9.77
	18	56.3	-9.78

	24	52.1	-9.86
734	0	66.4	-9.62
	4.2	63.5	-9.66
	12	57.0	-9.77
	18	53.4	-9.84
	24	50.5	-9.89
	32.4	45.7	-9.99
699	0	289	-8.15
	6	275	-8.20
	9.6	264	-8.24
	12	257	-8.27
	18	238	-8.34
	24	218	-8.43
	30	203	-8.50
	36	186	-8.59
	42	171	-8.67
	48	156	-8.76
228	0	62.3	-9.68
	6	58.7	-9.74
	12	58.0	-9.75
	18	54.8	-9.81
	24	54.1	-9.82
	27.6	51.5	-9.87
600	0	104.0	-9.17
	3.6	98.4	-9.23
	7.2	95.8	-9.25
	9.6	91.9	-9.29
	15.6	88.7	-9.33
	21.6	84.1	-9.38
	25.2	78.6	-9.45
306	0	45.0	-10.01
	6	43.4	-10.05
	12	40.4	-10.12
	18	39.1	-10.15
	24	36.5	-10.22
514	0	54.4	-9.82
	2.4	52.8	-9.85
	8.4	49.5	-9.91
	14.4	47.3	-9.96
	20.4	44.3	-10.02
	26.4	41.1	-10.10
718	0	52.5	-9.86

	2.4	50.5	-9.89
	8.4	46.6	-9.97
	14.4	43.4	-10.05
	20.4	39.8	-10.13
	26.4	37.5	-10.19

For each n_L , a plot of $\ln P_{Cl_2}$ against time was generated, and the liquid film mass transfer coefficient was determined from the slope of the line. Figures B-1 through B-10 depict the best-fit lines used to obtain the k_L . Table B-2 lists the k_{L,Cl_2}^o values obtained from the slopes of these lines.

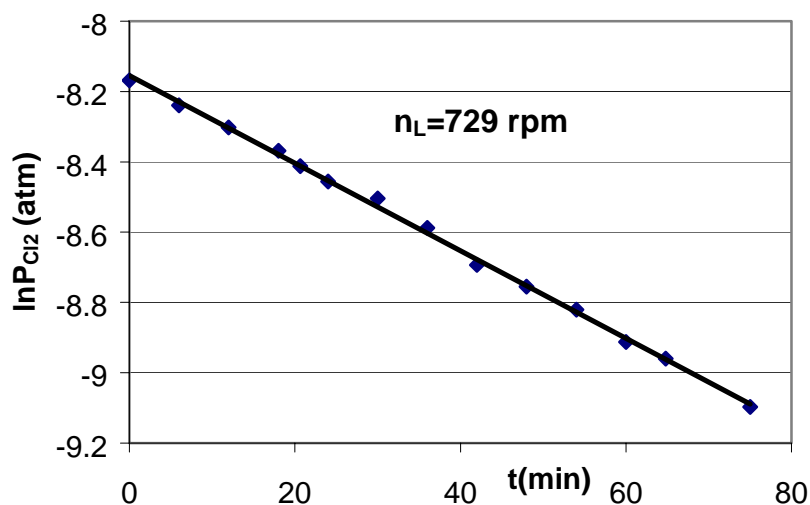


Figure B-1. Extracting k_{L,Cl_2}^o at 729 rpm

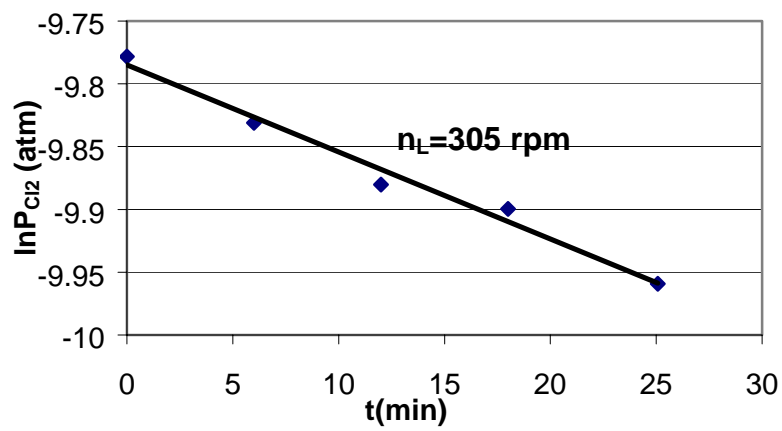


Figure B-2. Extracting k_{L,Cl_2}^0 at 305 rpm

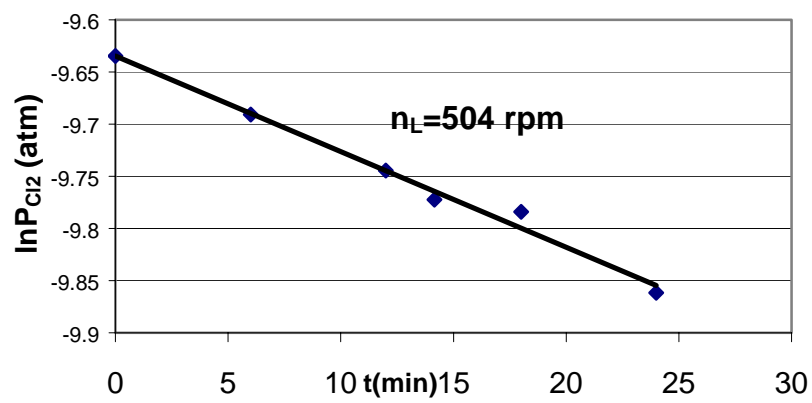


Figure B-3. Extracting k_{L,Cl_2}^0 at 504 rpm

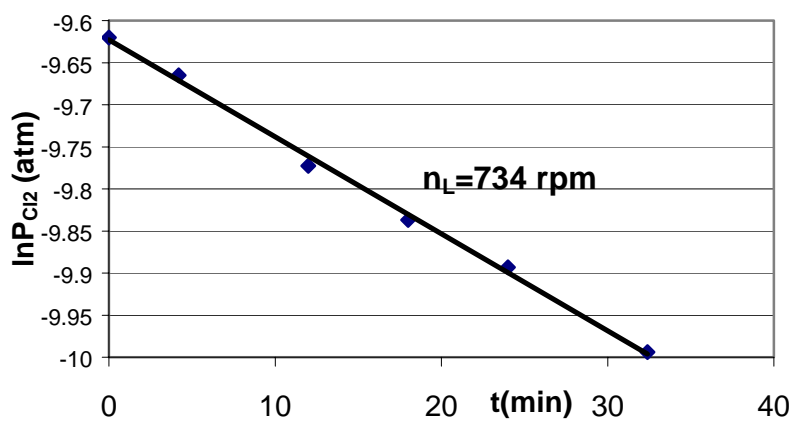


Figure B-4. Extracting k_{L,Cl_2}^0 at 734 rpm

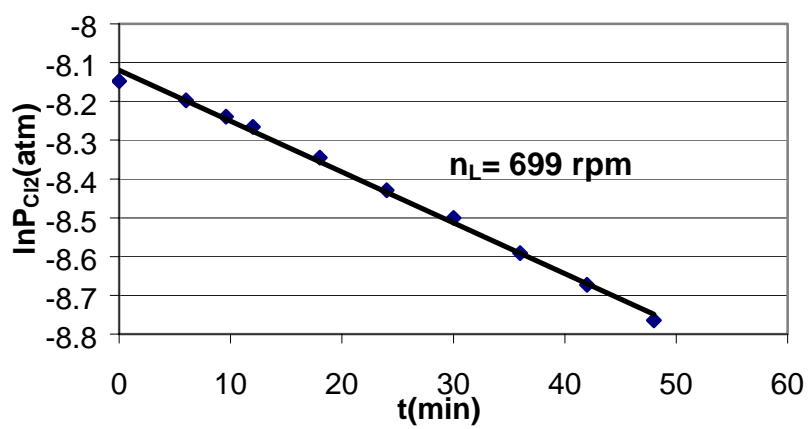


Figure B-5. Extracting k_{L,Cl_2}^0 at 699 rpm

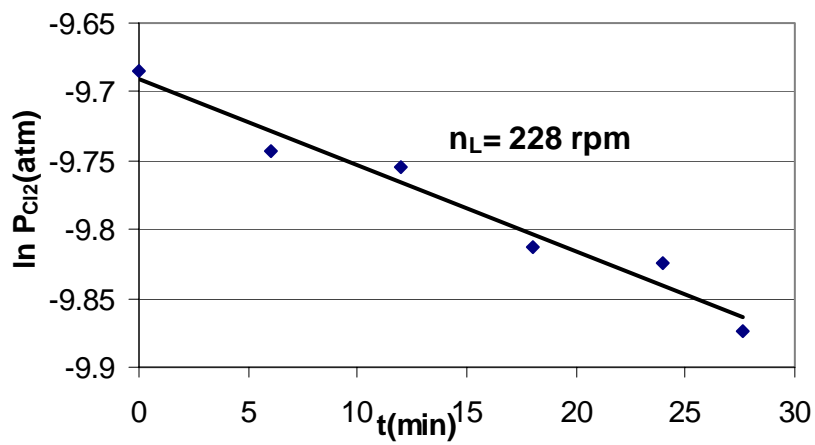


Figure B-6. Extracting k_{L,Cl_2}^0 at 228 rpm

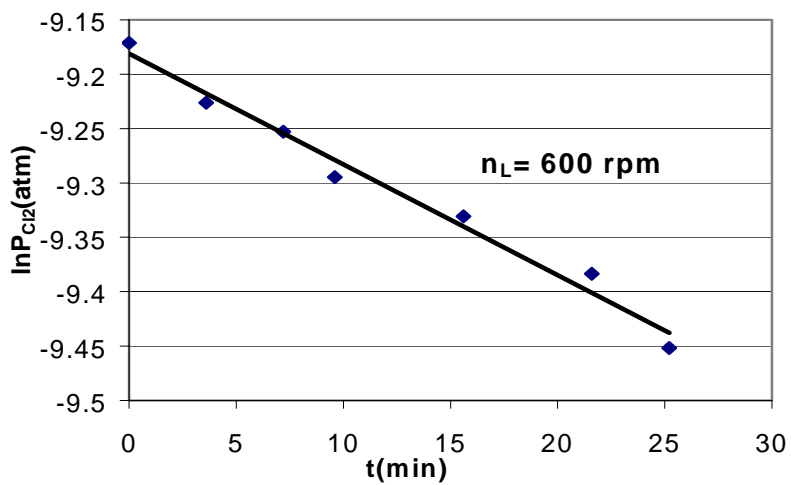


Figure B-7. Extracting k_{L,Cl_2}^0 at 600 rpm

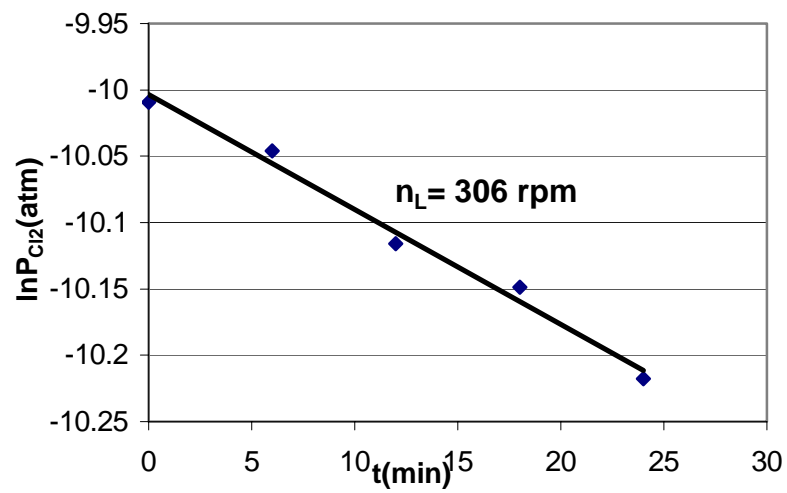


Figure B-8. Extracting k_{L,Cl_2}^0 at 306 rpm

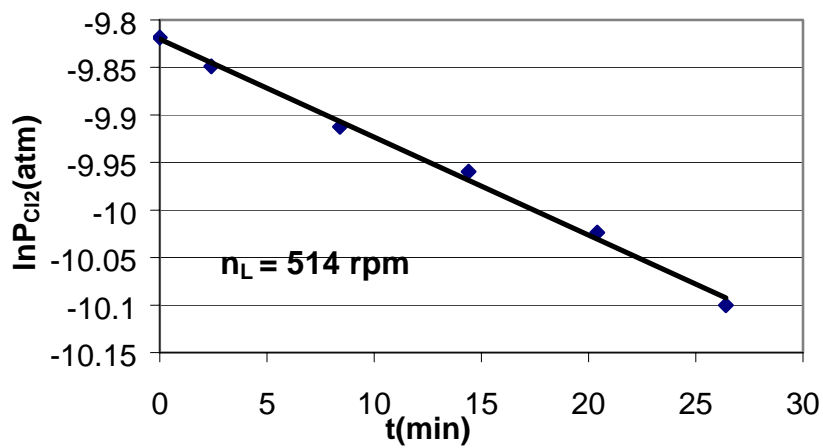


Figure B-9. Extracting k_{L,Cl_2}^0 at 514 rpm

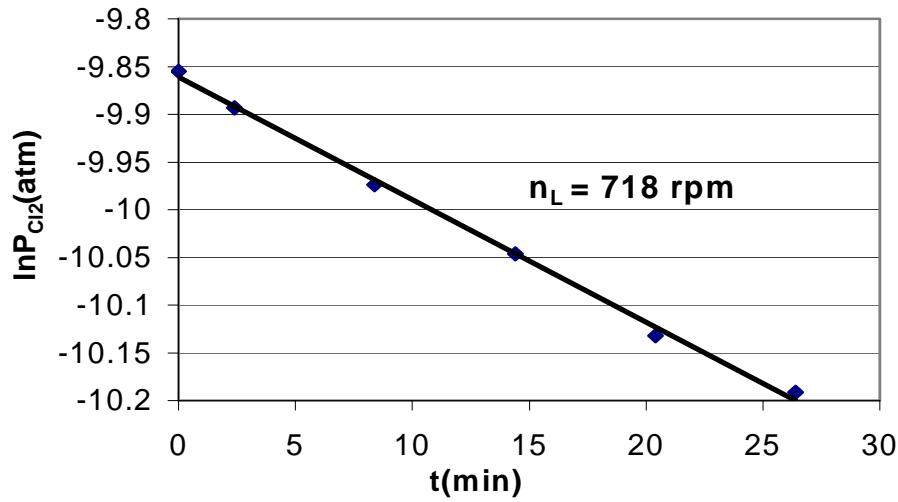


Figure B-10. Extracting k_{L,Cl_2}^0 at 718 rpm

Table B-2. Liquid film mass transfer coefficient for stirred cell reactor

n_L (rpm)	k_{L,Cl_2}^0 (m/s)
729	2.73E-05
305	1.51E-05
504	2.01E-05
734	2.51E-05
699	2.86E-05
228	1.37E-05
600	2.23E-05
306	1.90E-05
514	2.25E-05
718	2.80E-05

Figure B-11 shows the data and correlations for the liquid film mass transfer coefficient. The k_{L,Cl_2}^0 correlation was compared with Zhao's correlation. Zhao performed mercury desorption experiments in the stirred cell contactor and found the correlation for mercury to be $k_{L,Hg}^0$ (m/s) = $2.42 \times 10^{-7} (n_L)^{0.73}$ (Zhao, 1997). The

correlation for mercury was converted to a correlation for chlorine by correcting for diffusivities:

$$k_{L,Cl_2}^o = k_{L,Hg}^o \sqrt{\frac{D_{Cl_2}}{D_{Hg}}} \quad (B-1)$$

Applying this correction resulted in: $k_{L,Cl_2}^o \text{ (m/s)} = 2.7 \times 10^{-7} (n_L)^{0.73}$. Figure B-11 shows how the correlation from this work compares with Zhao's corrected correlation. The solid line represents Zhao's correlation.

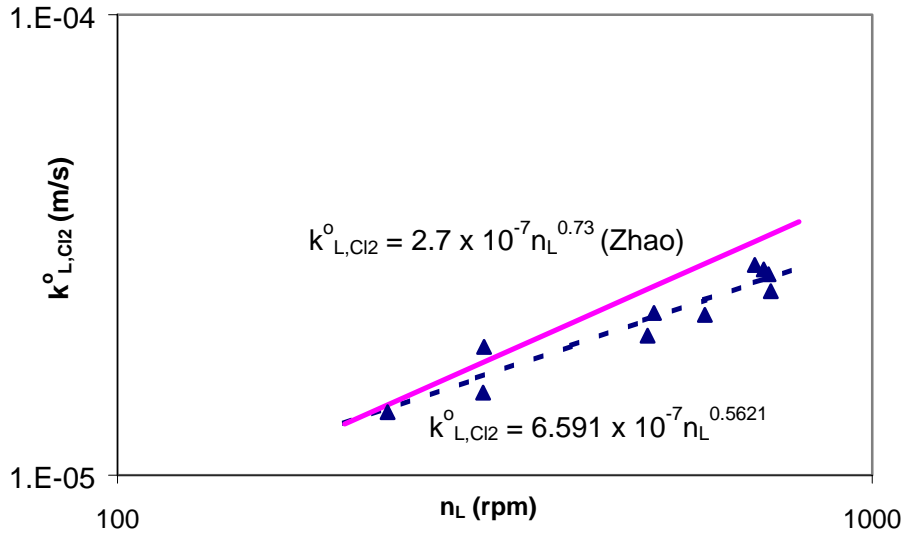


Figure B-11. Data and correlations for physical liquid film mass transfer coefficient for stirred cell reactor

In order to calculate the S(IV) at the interface, the liquid film transfer coefficient for S(IV) was needed. Thus, the above correlation, $k_{L,Cl_2}^o \text{ (m/s)} = 6.591 \times 10^{-7} (n_L)^{0.56}$, was corrected for S(IV) by correcting for the diffusivities, which resulted in $k_{L,S(IV)}^o \text{ (m/s)} = 6.248 \times 10^{-7} (n_L)^{0.56}$.

Appendix C: Chloride analysis through ion chromatography

Chloride concentrations were determined using ion chromatography (IC). A Dionex (Model 2000i/SP) analyzer equipped with a Hewlett-Packard 3390A reporting integrator was used. The guard column was Dionex Model AG4A, and the separator column was Dionex Model AS4A. The eluant was an aqueous solution containing 1.7 mM NaHCO_3 and 1.8 mM Na_2CO_3 . The regenerant solution was 25 mM H_2SO_4 .

A standard solution of NaCl was made. The concentration of this standard was similar to the concentrations of the samples. At the beginning of each experimental series, the standard solution was injected (using 3 mL samples) into the IC. Duplicate analyses were done on all samples injected into the IC. A step-by-step procedure for sample analysis is provided below.

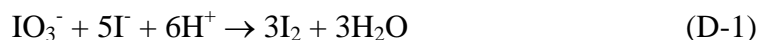
1. Using a clean syringe, withdraw a 3 mL sample from the stirred cell reactor.
2. Inject the sample into a 100 mL volumetric flask partially filled with distilled water. The flask should be weighed before and after sample addition to accurately determine the quantity of reactor sample.
3. Dilute with distilled water to get 100 mL of solution in the flask.
4. Using a magnetic stirrer, stir the solution in the volumetric flask.
5. Using a clean syringe, withdraw 3 mL of solution from the volumetric flask and inject into IC. Do duplicate analyses.
6. From IC output, calculate peak height and use calibration to determine chloride concentration.

Appendix D: S(IV) analysis through iodometric titration

Iodometric titration was used to determine the S(IV) concentration (Kolthoff and Belcher, 1957). A starch indicator solution is required in this procedure. Details on how to make a 2% starch solution, preserved with salicylic acid, are provided below.

1. Weigh 1 g of soluble starch (Fisher Scientific) into a beaker containing 50 mL distilled water.
2. Stir, while heating, until starch is completely dissolved.
3. Add 0.25 g salicylic acid. Continue to heat and stir until completely dissolved.
4. Let solution cool to room temperature and transfer to a dropper-bottle. Solution must be at room temperature before being used in titrations.

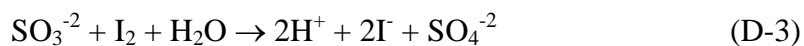
Standard solutions of iodine (I_2) and sodium thiosulfate are also required. The thiosulfate can be standardized against a standard potassium iodate (KIO_3) solution in the presence of excess potassium iodide and H_2SO_4 as shown in Equation D-1. It should be noted that 1 N KIO_3 is the same as 1/6 M KIO_3 , and 1 N I_2 is equal to 0.5 M I_2 .



The iodine solution can be standardized against the thiosulfate solution.



S(IV) reacts directly with I_2 to form iodide and sulfate as shown in Equation D-3. However, iodine cannot be used to directly titrate the S(IV) sample since S(IV) rapidly oxidizes to sulfate. Therefore, the S(IV) sample should be injected into excess iodine to avoid air oxidation to sulfate. The iodine should then be back-titrated with thiosulfate.



The above titrations should not be performed in basic solutions, or in solutions that are very acidic. Either extreme causes disproportionation and side reactions. Titrations in this work were performed in pH 4 to 6. This analysis procedure was verified with known S(IV) standards. Depending on the expected S(IV) concentration, either 0.003 N or 0.01 N standard solutions were used. Detailed procedure is provided below for sample analysis.

1. Pipet 3mL of standard iodine solution into an Erlenmeyer flask, and stopper the flask. This flask should be weighed now and again after adding S(IV) sample to accurately determine quantity of reactor fluid sampled.
2. Using a clean syringe, withdraw sample from the stirred cell reactor.
3. Immediately inject the sample into the flask containing 3mL I_2 . Ensure the syringe needle is completely immersed in the iodine solution to prevent air oxidation of S(IV) during sampling. Stopper the flask after sample addition and weigh.
4. While stirring the solution in the flask with a magnetic stirring bar, titrate the iodine solution using sodium thiosulfate.
5. When the yellow color of the iodine starts to fade (as the iodine is converted to iodide), add a couple drops of starch indicator to enhance the detection of the endpoint. (Do NOT add the starch to the iodine solution before this point.) The endpoint is reached when the blue solution turns clear. Record the volume of thiosulfate used.

Appendix E: Calculation of $D_{\text{Cl}_2\text{-N}_2}$ using Chapman-Enskog theory

Chapman and Enskog related the properties of low density gases to the forces acting between the molecules and developed, with Hirschfelder et al. (1954), the following equation to predict the diffusivity (D_{AB}) for nonpolar gas pairs (Hines and Maddox, 1995).

$$D_{AB} = \frac{1.858 \times 10^{-27} T^{3/2}}{P \sigma_{AB}^2 \Omega_D} \sqrt{\frac{1}{M_A} + \frac{1}{M_B}} \quad (\text{E-1})$$

In order to obtain the value of Ω_D , which is the collision integral based on the Lennard-Jones potential, the energy parameter (ε/k) is required. Also, the value for the collision diameter (σ_{AB}) is required for Equation E-1. These parameters are tabulated for various molecules (Hines and Maddox, 1985). The collision diameter is the arithmetic mean of the collision diameters for the 2 molecules, while the energy parameter is the geometric mean of the 2 values. The collision diameters for Cl_2 and N_2 are 4.217×10^{-10} and 3.798×10^{-10} m, respectively, resulting in an average σ_{AB} of 4.0075×10^{-10} m. The energy parameters for Cl_2 and N_2 are 316.0 and 71.4 K, resulting in a geometric average of 150.2. At 298 K, the value for kT/ε is 1.984, resulting in a Ω_D of 1.075. Using Equation E-1, the diffusion coefficient for Cl_2 through N_2 at 298 K and 1 atm was $1.23 \times 10^{-5} \text{ m}^2/\text{s}$.

The diffusion coefficient for Hg through N_2 can be similarly calculated. The collision diameter for Hg is 2.969×10^{-10} m and the energy parameter is 750. Using Equation E-1, the diffusion coefficient for Hg through N_2 at 298 K and 1 atm was $1.32 \times 10^{-5} \text{ m}^2/\text{s}$.

Appendix F: Liquid film mass transfer coefficient for wetted wall

This appendix details the data used to obtain the physical liquid film mass transfer coefficient for chlorine (k_{L,Cl_2}^0) in the wetted wall column. Table F-1 tabulates the raw data at a liquid flow rate of 2.26 mL/s. Table F-2 tabulates the data at a liquid rate of 2.96 mL/s.

Table F-1. Data used to determine k_{L,Cl_2}^0 at 2.26 mL/s

t(s)	Cl _{2,out} (ppm)	lnP _{Cl₂} (atm)
0	39.4	-10.14
36	35.7	-10.24
108	32.8	-10.33
180	30.1	-10.41
252	27.5	-10.50
324	24.9	-10.60
396	22.5	-10.70
468	20.5	-10.80
0	47.6	-9.95
72	44.3	-10.03
144	40.9	-10.10
216	36.8	-10.21
288	33.4	-10.31
360	30.5	-10.40
432	28.0	-10.48
504	24.9	-10.60
0	80.5	-9.43
72	72.4	-9.53
144	66.1	-9.62
216	59.8	-9.73
288	53.4	-9.84
360	48.7	-9.93
432	43.8	-10.04
504	39.7	-10.13

576	35.6	-10.24
648	31.9	-10.35
720	28.8	-10.46
792	26.1	-10.55
864	23.6	-10.65
936	21.6	-10.74
1008	19.2	-10.86
0	79.5	-9.44
36	75.1	-9.50
72	71.5	-9.55
108	68.8	-9.58
144	66.1	-9.62
180	63.4	-9.67
216	59.9	-9.72
252	56.6	-9.78
324	51.5	-9.87
396	46.3	-9.98
468	41.7	-10.09
576	35.8	-10.24
648	32.0	-10.35
756	27.7	-10.49
828	25.2	-10.59
936	21.6	-10.74
0	39.6	-10.14
72	38.5	-10.17
144	37.2	-10.20
216	35.2	-10.25
324	32.0	-10.35
396	29.6	-10.43
504	25.8	-10.57
612	22.3	-10.71
684	20.2	-10.81
792	17.2	-10.97
864	15.6	-11.07
1044	12.0	-11.33
1116	11.1	-11.41
0	39.9	-10.13
36	34.9	-10.26
72	33.6	-10.30
108	32.2	-10.34

144	31.1	-10.38
180	29.6	-10.43
216	28.3	-10.47
252	27.0	-10.52
288	25.7	-10.57
0	12.8	-11.26
72	12.0	-11.33
108	11.5	-11.38
180	10.4	-11.47
252	9.40	-11.58
324	8.55	-11.67
360	8.11	-11.72
432	7.41	-11.81
540	6.51	-11.94
612	5.92	-12.04
720	5.22	-12.16
792	4.86	-12.23
900	4.27	-12.36

Table F-2. Data used to determine k_{L,Cl_2}^0 at 2.96 mL/s

t(s)	Cl _{2,out} (ppm)	lnP _{Cl2} (atm)
0	78.7	-9.45
36	74.2	-9.51
72	69.7	-9.57
108	65.4	-9.64
144	62.3	-9.68
180	58.4	-9.75
216	55.7	-9.80
252	52.6	-9.85
288	49.8	-9.91
324	46.7	-9.97
396	41.8	-10.08
468	37.1	-10.20
540	32.8	-10.33
612	29.1	-10.44
684	26.1	-10.55
756	23.4	-10.66
828	20.8	-10.78

936	18.2	-10.91
-----	------	--------

For each data set, a plot of $\ln P_{\text{Cl}_2}$ against time was generated, and the liquid film mass transfer coefficient was determined from the slope of the line. Since all the data generate similar figures, only two of the plots are shown below. Figure F-1 plots the first data set from Table F-1, and Figure F-2 plots the data set from Table F-2. Table 5.2 lists the $k_{\text{L,Cl}_2}^0$ values obtained from the slopes of the best-fit lines for all the data sets listed in Tables F-1 and F-2.

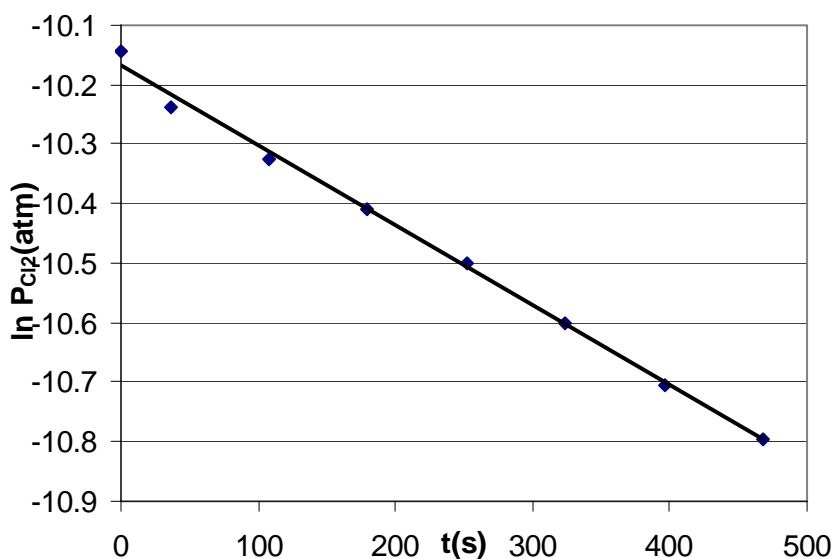


Figure F-1. Extracting $k_{\text{L,Cl}_2}^0$ at 2.26 mL/s for wetted wall column

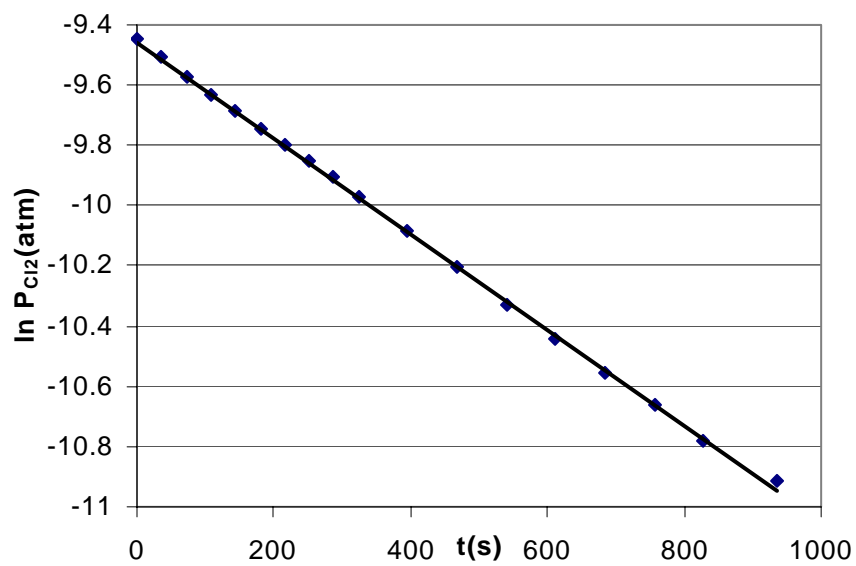
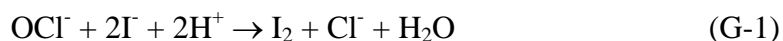


Figure F-2. Extracting k_{L,Cl_2}^0 at 2.96 mL/s for wetted wall column

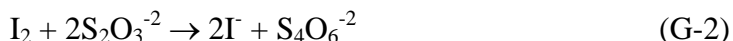
Appendix G: NaOCl Analysis through Iodometric Titration

Iodometric titration was used to determine the NaOCl concentration of the stock solution (Zhao, 1997; Lagowski, 1995; Kolthoff and Belcher, 1957). Starch indicator and standard thiosulfate solution are required in this procedure. Details on these solutions are provided in Appendix D.

Hypochlorite reacts with excess iodide in acid to form iodine.



The iodine produced must then be titrated with thiosulfate solution.



Detailed procedure for NaOCl analysis is provided below.

1. Add 1 g of solid KI and 5 mL of 0.5 M H_2SO_4 to 100 mL Erlenmeyer flask.
2. Weigh the above flask with solution.
3. Add approximately 1 mL of NaOCl from the stock solution to the previously weighed Erlenmeyer flask. The solution will turn yellow-orange instantaneously (resulting from I_2 formation)
4. Weigh the flask again to determine the amount of sample added.
5. Immediately titrate the above solution with standard sodium thiosulfate. When the yellow color of the I_2 starts to fade, add a couple drops of starch to enhance the detection of the endpoint.
6. Repeat steps 1 through 6 several times.

The NaOCl concentration can now be calculated using Equation G-3. For this calculation, the density of the NaOCl solution needs to be determined. In this work, the density was determined to be 1.08 g/mL.

$$[\text{NaOCl}] = \frac{V_{\text{thiosulfate}} [\text{thiosulfate}]}{2V_{\text{sample}}} \quad (\text{G-3})$$

Bibliography

- Adam, L.C., I. Fabian, K. Suzuki, and G. Gordon, "Hypochlorous Acid Decomposition in the pH 5-8 Region," *Inorg. Chem.*, 31(17), 3534-3541 (1992).
- Afonso, R.F. and C.L. Senior, "Assessment of Mercury Removal by Existing Air Pollution Control Devices in Full Scale Power Plants," proceedings of Mega Symposium, presented at the US EPA-DOE-EPRI Combined Power Plant Air Pollutant Control Symposium, Chicago, IL, August 20-23, 2001.
- Aieta, E.M., "The Kinetics of Chlorine Dioxide Generation for Water Treatment," Ph.D. Dissertation, Stanford University, February 1984.
- Aieta, E.M. and P.V. Roberts, "Application of Mass-Transfer Theory to the Kinetics of a Fast Gas-Liquid Reaction: Chlorine Hydrolysis," *Environ. Sci. Technol.*, 20(1), 44-49 (1986a).
- Aieta, E.M. and P.V. Roberts, "Kinetics of the Reaction Between Molecular Chlorine and Chlorite in Aqueous Solution," *Environ. Sci. Technol.*, 20(1), 50-55 (1986b).
- Ashmore, P.G. and J. Chanmugam, "Reactions in the System Hydrogen, Chlorine, Nitric Oxide, and Nitrosyl Chloride," *Trans. Faraday Soc.*, 49, 270 (1953).
- Ashmore, P.G. and M.S. Spencer, "Concurrent Molecular and Chlorine Atom Mechanisms in the Reversible Dissociation of Nitrosyl Chloride," *Trans. Faraday Soc.*, 55, 1868 (1959).
- Ashour, S.S., E.B. Rinker, and O.C. Sandall, "Absorption of Chlorine into Aqueous Bicarbonate Solutions and into Aqueous Hydroxide Solutions," *AIChE J.*, 42(3), 671-682 (1996).
- Askew, W. C. and S. J. Morisani, "Determining Chlorine Concentrations in Air and Water Samples for Scrubbing Studies Using Ion Chromatography," *J. Chromatogr. Sci.*, 27, 42-46 (1989).
- Astarita, G., D.W. Savage, and A. Bisio, *Gas Treating with Chemical Solvents*, Wiley-Interscience Publication (1983).
- Atkins, P.W., *Physical Chemistry*, 4th ed., W.H. Freeman and Company, New York (1990).

- Ayres, G.H., *Quantitative Chemical Analysis*, 2nd ed., Harper and Row, New York, NY (1968).
- Bacon, T., J. Taylor and K. Webber, "Chlorine and Hydrogen Chloride Monitoring Utilizing Ion Mobility Spectroscopy (IMS)," *ISA Tech/Expo Technol. Update*, 2(6), 141-145 (1998).
- Bird, R.B. and W.E. Stewart, and E.N. Lightfoot, *Transport Phenomena*, John Wiley and Sons, Inc., New York, NY (1960).
- Bishnoi, S., "Carbon Dioxide Absorption and Solution Equilibrium in Piperazine Activated Methyldiethanolamine," Ph.D. Dissertation, The University of Texas at Austin, December 2000.
- Blatchley III, E.R. and R.W. Johnson, "Hypohalous Acid and Haloamine Flashoff in Industrial Evaporative Cooling Systems," *CTI Journal*, 12(1), 19 (1991).
- Blauwhoff, P.M.M. and W.P.M. Van Swaaij, "Simultaneous Mass Transfer of H₂S and CO₂ with Complex Chemical Reactions in an Aqueous Di-isopropanolamine Solution," *Chem. Eng. Process*, 19, 67 - 83 (1985).
- Blythe, G.M. and C.F. Richardson, "Catalytic Oxidation of Mercury in Flue Gas for Enhanced Removal In Wet FGD Systems," proceedings of Mega Symposium, presented at the US EPA-DOE-EPRI Combined Power Plant Air Pollutant Control Symposium, Chicago, IL, August 20-23, 2001.
- Brian, P.L.T., J.E. Vivian, and C. Piazza, "The Effect of Temperature on the Rate of Absorption of Chlorine into Water," *Chem. Eng. Sci.*, 21, 551-558 (1966).
- Brogren, C. and Karlsson, H.T. "Modeling the Absorption of SO₂ in a Spray Scrubber Using the Penetration Theory," *Chem. Eng. Sci.*, 52(18), 3085-3099 (1997).
- Burke, M., J. Tenney, B. Indu, M.F. Hoq, S. Carr, and W.R. Ernst, "Kinetics of Hydrogen Peroxide-Chlorate Reaction in the Formation of Chlorine Dioxide," *Ind. Eng. Chem. Res.*, 32(7), 1449-1456 (1993).
- Carson, W.N., Jr., "Automatic Titrator Using Electrolytically Generated Titrants," *Anal. Chem.*, 25(2), 226-230 (1953).
- Castner, T.G. and Känzig, W., "The Electronic Structure of V-Centers," *J. Phys. Chem. Solids*, 3, 178-195 (1957).
- Chang, C.S., "Mass Transfer with Equilibrium Chemical Reaction, Sulfur Dioxide Absorption in Aqueous Solutions," Ph.D. Dissertation, The University of Texas at Austin, December 1979.

- Chang, C.S. and G.T. Rochelle, "SO₂ Absorption into NaOH and Na₂SO₃ Aqueous Solutions," *Ind. Eng. Chem. Fundam.*, 24, 7-11 (1985).
- Chen, E. and G.T. Rochelle, "Mercury Removal from Stack Gas by Aqueous Scrubbing with Injection of Chlorine Oxidants," from the Annual Report to the Gulf Coast Hazardous Substance Research Center (GCHSRC) 098UTA0724, August 2000.
- Chu, P., G. Behrens, and D. Laudal, "Estimating Total and Speciated Mercury Emissions from U.S. Coal-Fired Power Plants," proceedings of Mega Symposium, presented at the US EPA-DOE-EPRI Combined Power Plant Air Pollutant Control Symposium, Chicago, IL, August 20-23, 2001.
- Clark, T.C., M.A.A. Clyne, and D.H. Stedman, "Mechanism of Formation of Triatomic Combination Reactions," *Trans. Faraday Soc.*, 62, 3354 (1966).
- Clever, H.L., S.A. Johnson, and M.E. Derrick, "The Solubility of Mercury and Some Sparingly Soluble Mercury Salts in Water and Aqueous Electrolyte Solutions," *J. Phys. Chem. Ref. Data*, 14(3), 631 (1985).
- Connick, R.E. and Y. Chia, "The Hydrolysis and Its Variation with Temperature," *J. Am. Chem. Soc.*, 81, 1280-1284 (1959).
- Connors, K.A., *Chemical Kinetics: The Study of Reaction Rates in Solutions*, VCH Publishers, Inc., New York, NY (1990).
- Coulson, D.M. and L.A. Cavanagh, "Automatic Chloride Analyzer," *Anal. Chem.*, 32(10), 1245-1247 (1960).
- Critchfield, J.E., "CO₂ Absorption/Desorption in Methyldiethanolamine Solutions Promoted with Monoethanolamine and Diethanolamine: Mass Transfer and Reaction Kinetics," Ph.D. Dissertation, The University of Texas at Austin, 1988.
- Danckwerts, P.V., *Gas-Liquid Reactions*, McGraw-Hill Book Co., New York, NY (1970).
- Davies, R., B. Kipling, and A.G. Sykes, "Mechanistic Studies of One- and Two-Equivalent Oxidations of the Mercury(I) Dimer," *J. Am. Chem. Soc.*, 95(22), 7250-7256 (1973).
- Dutchuk, M.J., "Nitrogen Dioxide Absorption in Aqueous Dithionite," M.S. Thesis, The University of Texas at Austin, May 1999.
- Edwards, J.R., R.K. Sricastava, C.W. Lee, J.D. Kilgore, and S.B. Ghorishi, "A Computational and Experimental Study of Mercury Speciation as Facilitated by the Deacon Process," proceedings of Mega Symposium, presented at the

- US EPA-DOE-EPRI Combined Power Plant Air Pollutant Control Symposium, Chicago, IL, August 20-23, 2001.
- Eigen, M. and K. Kustin, "The Kinetics of Halogen Hydrolysis," *J. Am. Chem. Soc.*, 84, 1355-1361 (1962).
- EPA, *Acid Rain Program: Overview*. Available from <http://www.epa.gov/airmarkets/arp/overview.html> (2001).
- EPA, *Mercury*. Available from <http://www.epa.gov/mercury/information.html> (2000).
- Fabian, I. and G. Gordon, "Complex Formation Reactions of the Chlorite Ion," *Inorg. Chem.*, 30(19), 3785-3787 (1991).
- Fabian, I. and G. Gordon, "Iron(III)-Catalyzed Decomposition of the Chlorite Ion: An Inorganic Application of the Quenched Stopped-Flow Method," *Inorg. Chem.*, 31(11), 2144-2150 (1992).
- Fickert, S., F. Helleis, J.W. Adams, G.K. Moortgat, and J.N. Crowley, "Reactive Uptake of ClNO₂ on Aqueous Bromide Solution," *J. Phys. Chem. A*, 102, 10689-10696 (1998).
- Finlayson, A.C., "The pH Range of the Mohr Titration for Chloride Ion Can Be Usefully Extended to 4-10.5," *J. Chem. Educ.*, 69(7), 559 (1992).
- Fogelman, K.D., D.M. Walker, and D.W. Margerum, "Non-Metal Redox Kinetics: Hypochlorite and Hypochlorous Acid Reactions With Sulfite," *Inorg. Chem.*, 28, 986-993 (1989).
- Franson, M.H., *Standard Methods for the Examination of Water and Wastewater 19th ed.*, American Public Health Association, American Water Works Association, Water Pollution Control Federation, Washington, D.C. (1995).
- Gilliland, E.R., R.F. Baddour, and P.L.T. Brian, "Gas Absorption Accompanied by a Liquid-Phase Chemical Reaction," *AIChE J.*, 4(2), 223-230 (1958).
- Gilliland, E.R. and T.K. Sherwood, "Diffusion of Vapors into Air Streams," *Ind. Eng. Chem.*, 26(5), 516-523, (1934).
- Gordon, G. and F. Emmenegger, "Complex Ion Formation between ClO₂ and ClO₂^{-*}," *Inorg. Nucl. Chem. Letters*, 2(12), 395-398 (1966).
- Gordon, G. and S. Tachiyashiki, "Kinetics and Mechanism of Formation of Chlorate Ion from the Hypochlorous Acid/Chlorite Ion Reaction at pH 6-10," *Environ. Sci. Technol.*, 25(3), 468-474 (1991).

- Gordon, G., B. Sloodmaekers, S. Tachiyashiki, and D.W. Wood, III, "Minimizing Chlorite Ion and Chlorate Ion in Water Treated with Chlorine Dioxide," *American Water Works Association Journal*, 82, 160-165 (1990).
- Greenewalt, C.H., "Absorption of Water Vapor by Sulfuric Acid Solutions," *Ind. Eng. Chem.*, 18(22), 1291-1295 (1926).
- Gutmann, V., *Main Group Elements—Group VI-VII*, Inorganic Chemistry v. 5, University Park Press, London (1972).
- Halford, R.S., "A Lower Limit for the Velocities of Formation of the Tri-Halide Ions in Aqueous Solution," *J. Am. Chem. Soc.*, 62, 3233-3236 (1940).
- Hall, B., "An Experimental Study of Mercury Reactions in Combustion Flue Gases," Ph.D. Dissertation, Goteborgs Universitet (Sweden), 1992.
- Hall, B., P. Schager, and O. Lindqvist, "Chemical Reactions of Mercury in Combustion Flue Gases," *Water, Air, Soil Pollut.*, 56, 3-14 (1991).
- Halperin, J. and H. Taube, "The Transfer of Oxygen Atoms in Oxidation-Reduction Reactions. III. The Reaction of Halogens with Sulfite in Aqueous Solution," *J. Am. Chem. Soc.*, 74, 375-380 (1952).
- Harris, D.C., *Quantitative Chemical Analysis*, 2nd ed., W.H. Freeman., New York, NY (1987).
- Hikita, H., S. Asai, Y. Himukashi, and T. Takatsuka, "Absorption of Chlorine into Aqueous Sodium Hydroxide Solutions," *Chem. Eng. J.*, 5, 77-84 (1973).
- Hines, A.L. and R.N. Maddox, *Mass Transfer: Fundamentals and Applications*, Prentice-Hall: Englewood Cliffs, NJ (1985).
- Hirschfelder, J.O., C.F. Curtiss, and R.B. Bird, *Molecular Theory of Gases and Liquids*, Wiley, New York, NY (1954).
- Hobler, T., *Mass Transfer and Absorbers*, Pergamon Press, Oxford, London, New York (1966).
- Holzwarth, G., R.G. Balmer, and L. Soni, "The Fate of Chlorine and Chloramines in Cooling Towers: Henry's Law Constants for Flashoff," *Water Res.*, 18(11), 1421-1427 (1984).
- Hong, C.C., F. Lenzi, and W.H. Rapson, "The Kinetics and Mechanism of the Chloride-Chlorate Reaction," *Can. J. Chem. Eng. J. Chem. Eng.*, 45, 349-355 (1967).
- Huheey, J.E., *Inorganic Chemistry: Principles of Structure and Reactivity*, 3rd ed., Harper and Row, New York (1983).

- Indu, B., W.R. Ernst, and M.F. Hoq, "Influence of Mercuric Nitrate on Species and Reactions Related to Chlorine Dioxide Formation," *Ind. Eng. Chem. Res.*, 36, 11-16 (1997).
- Iverfeldt, A. and O. Lindqvist, "Atmospheric Oxidation of Elemental Mercury by Ozone in the Aqueous Phase," *Atmos. Environ.*, 20(8), 1567-1573 (1986).
- Jensen, J.S. and G. R. Helz, "Rates of Reduction of N-Chlorinated Peptides by Sulfite: Relevance to Incomplete Dechlorination of Wastewaters," *Environ. Sci. Technol.*, 32, 516-522 (1998).
- Kaczur, J.J., "Oxidation Chemistry of Chloric Acid in NO_x/SO_x and Air Toxic Metal Removal from Gas Streams," *Environ. Prog.*, 15(4), 245-254 (1996).
- Keating, M.H., K.R. Mahaffey, R. Schoeny, G.E. Rice, and O.R. Bullock, *Mercury Study Report to Congress*, Office of Air Quality Planning and Standards, EPA/452/R-97-003 (NTIS PB124738), U.S. Environmental Protection Agency, Research Triangle Park, NC, December 1997.
- Kieffer, R. and G. Gordon, "Disproportionation of Chlorous Acid. I. Stoichiometry," *Inorg. Chem.*, 7(2), 235-239 (1968).
- Kieffer, R. and G. Gordon, "Disproportionation of Chlorous Acid. II. Kinetics," *Inorg. Chem.*, 7(2), 239-244 (1968).
- Kiil, S., "Experimental and Theoretical Investigations of Wet Flue Gas Desulphurisation," Ph.D. Thesis, Technical University of Denmark, 1998.
- Kolthoff, I.M. and R. Belcher, *Volumetric Analysis, Volume III*, 199-374, Interscience Publishers, Inc., New York, NY (1957).
- Kolthoff, I.M., E.J. Meehan and S. Bruckenstein, *Quantitative Chemical Analysis 4th ed.*, Macmillan., New York, NY (1969).
- Kolthoff, I.M. and V.A. Stenger, *Volumetric Analysis, Volume II*, 2nd ed. Interscience Publishers, Inc., New York, NY (1947).
- Lagowski, "Bleach Analysis by Redox Titration," *Experiences in Chemistry*, 124-126, McGraw-Hill, Inc. (1995).
- Lahiri, R.N., G.D. Yadav, and M.M. Sharma, "Absorption of Chlorine in Aqueous Solutions of Sodium Hydroxide," *Chem. Eng. Sci.*, 38(7), 1119-1133 (1983).
- Li, M-H. and M-D Lai, "Solubility and Diffusivity of N₂O and CO₂ in (Monoethanolamine + N-Methyldiethanolamine + Water) and in (Monoethanolamine 2-Amino-2-methyl-1-propanol + Water)," *J. Chem. Eng. Data*, 40(2), 486-492 (1995).

- Lide, D.R. (ed.), *CRC Handbook of Chemistry and Physics*, 81st ed., CRC Press, Inc., New York and Washington DC (2000).
- Lifshitz, A. and B. Perlmutter-Hayman, "The Kinetics of the Hydrolysis of Chlorine. I. Reinvestigation of the Hydrolysis in Pure Water," *J. Phys. Chem.*, 64, 1663-1665 (1960).
- Lifshitz, A. and B. Perlmutter-Hayman, "The Kinetics of the Hydrolysis of Chlorine. II. The Hydrolysis in the Presence of Acetate," *J. Phys. Chem.*, 65, 753-758 (1961).
- Lifshitz, A. and B. Perlmutter-Hayman, "The Kinetics of the Hydrolysis of Chlorine. III. The Reaction in the Presence of Various Bases, and a Discussion of the Mechanism," *J. Phys. Chem.*, 66, 701-705 (1962).
- Lin, C-J. and S.O. Pehkonen, "Aqueous Phase Reactions of Mercury with Free Radicals and Chlorine: Implications for Atmospheric Mercury Chemistry," *Chemosphere*, 38(6), 1253-1263 (1999).
- Lin, C-J. and S.O. Pehkonen, "Two-Phase Model of Mercury Chemistry in the Atmosphere," *Atmos. Environ.*, 32(14/15), 2543-2558 (1998).
- Lindqvist, O., "Transformation and Deposition Processes," *Water, Air, and Soil Pollution*, 55, 49-63 (1991).
- Lingane, J.J., "Automatic Coulometric Titration with Electrolytically Generated Silver: Determination of Chloride, Bromide, and Iodide Ions," *Anal. Chem.*, 26(4), 622-626 (1954).
- Lisensky, G. and K. Reynolds, "Chloride in Natural Waters: An Environmental Application of a Potentiometric Titration," *J. Chem. Edu.*, 68(4), 334-335 (1991).
- Lister, M.W. and P. Rosenblum, "Rates of Reaction of Hypochlorite Ions with Sulphite and Iodide Ions," *Can. J. Chem.*, 41, 3013-3020 (1963).
- Livengood, C.D. and M.H. Mendelsohn, "Improved Mercury Control in Wet Scrubbing through Modified Speciation," presented at the EPRI-DOE-EPA Combined Utility Air Pollutant Control Symposium, Washington, D.C., August 25-29, 1997.
- Lobo, V.M.M. and J.L. Quaresma, *Handbook of Electrolyte Solutions*, Elsevier Science Publishing Company, Inc., New York (1989).
- Medhekar, A.K., M. Rokni, D.W. Trainor, and J.H. Jacob, "Surface Catalyzed Reaction of $\text{Hg} + \text{Cl}_2$," *Chemical Physics Letters*, 65(3), 600-604 (1979).

- Melton, C.E., G.A. Ropp and P.S. Rudolph, "Mass Spectrometric Observation of Triatomic Ions in Chlorine and Bromine Gases," *J. Chem. Phys.*, 29, 968-969 (1958).
- Menke, R. and G. Wallis, "Detection of Mercury in Air in the Presence of Chlorine and Water Vapor," *Am. Ind. Hyg. Assoc. J.*, 41, 120-124 (1980).
- Milobowski, M.G., G.T. Amrhein, G.A. Kudlac, and D.M. Yurchison, "Wet FGD Enhanced Mercury Control for Coal-Fired Utility Boilers," proceedings of Mega Symposium, presented at the US EPA-DOE-EPRI Combined Power Plant Air Pollutant Control Symposium, Chicago, IL, August 20-23, 2001.
- Morris, J.C., "The Acid Ionization Constant of HOCl from 5 to 35°C," *J. Phys. Chem.*, 70, 3798-3805 (1966).
- Mullaly, J.M. and H. Jacques, "The Diffusion of Mercury and of Iodine Vapor Through Nitrogen," *Philos. Mag.*, 48(288), 1105-1022 (1924).
- Munthe, J., "The Aqueous Oxidation of Elemental Mercury by Ozone," *Atmos. Environ.*, 26A(8), 1461-1468 (1992).
- Munthe, J. and W.J. McElroy, "Some Aqueous Reactions of Potential Importance in the Atmospheric Chemistry of Mercury," *Atmos. Environ.*, 26A(4), 553-557 (1992).
- Munthe, J., F. Xiao and O. Lindqvist, "The Aqueous Reduction of Divalent Mercury by Sulfite," *Water, Air, Soil Pollut.*, 56, 621-630 (1991).
- Nagy, G., K. Tóth and E. Pungor, "Novel Programmed Coulometric Titration Technique: Chloride Determination in Streaming Solutions," *Anal. Chem.*, 47(8), 1460-1462 (1975).
- Nakayama, K., "An Accurate Measurement of the Mercury Vapor Drag Effect in the Pressure Region of Transition Flow," *Japanese Journal of Applied Physics*, 7(9), 1114 (1968).
- Nene, S. and V.C. Rane, "Kinetics of the Absorption of Mercury," *Indian J. Technol.*, 19(1), 20-25 (1981).
- Niksa, S. and J.J. Helble, "Interpreting Laboratory Test Data on Homogeneous Mercury Oxidation in Coal-Derived Exhausts," proceedings of Mega Symposium, presented at the US EPA-DOE-EPRI Combined Power Plant Air Pollutant Control Symposium, Chicago, IL, August 20-23, 2001.
- Noblett, J.G., Jr., F.B. Meserole, D.M. Seeger, and D.R. Owens, "Control of Air Toxics from Coal-Fired Power Plants Using FGD Technology," presented at the 1993 SO₂ Control Symposium, August 24-27, Boston, MA (1993).

- Oskarsson, K., A. Berglund, R. Deling, U. Snellman, O. Stenback, and J.J. Fritz, *A Planner's Guide for selecting Clean-Coal Technologies for Power Plants*. World Bank Technical Paper 387, The World Bank: Washington, DC (1997).
- Pacheco, M., "Mass Transfer, Kinetics and Rate-Based Modeling of Reactive Absorption," Ph.D. Dissertation, The University of Texas at Austin, May 1998.
- Peintler, G., I. Nagypal, and I.R. Epstein, "Kinetics and Mechanism of the Reaction between Chlorite Ion and Hypochlorous Acid," *J Phys. Chem.*, 94(7), 2954-2958 (1990).
- Pigford, R.L. "Counter-Diffusion in a Wetted Wall Column," Ph.D. Dissertation, The University of Illinois/Urbana, 1941.
- Pinsent, B.R.W., L. Pearson, and F.J.W. Roughton, "The Kinetics of Combination of Carbon Dioxide with Hydroxide Ions," *Trans. Faraday Soc.*, 52, 1512-1520 (1956)
- Pohorecki, R. and W. Moniuk, "Kinetics of Reaction between Carbon Dioxide and Hydroxyl Ions in Aqueous Electrolyte Solutions," *Chem. Eng. Sci.*, 43(7), 1677-1684 (1988).
- Prokopov, T.S., "Potentiometric Titration of Halides in Their Mixtures," *Anal. Chem.*, 42(9), 1096-1098 (1970).
- Renard, J.J. and H.I. Bolker, "The Chemistry of Chlorine Monoxide (Dichlorine Monoxide)," *Chem. Rev.*, 76(4), 487-508 (1976).
- Richardson, C., T. Machalek, S. Miller, C. Dene, and R. Chang, "Effect of NO_x Control Processes on Mercury Speciation in Utility Flue Gas," proceedings of Mega Symposium, presented at the US EPA-DOE-EPRI Combined Power Plant Air Pollutant Control Symposium, Chicago, IL, August 20-23, 2001.
- Robertson, A.J.B. and P. Williams, "The Formation of Negative Ions by Field Ionization," *Proc. Chem. Soc.*, 286-287 (1964)
- Robinson, R.A. and H.S. Harned, "Some Aspects of the Thermodynamics of Strong Electrolytes from Electromotive Force and Vapor Pressure Measurements," *Chem. Rev.*, 28, 419 (1941).
- Rodríguez, S.J., T-G. Lee, E. Hendrick, and P. Biswas, "Iodine Room Temperature Sorbents for Mercury Capture in Combustion Exhausts," proceedings of Mega Symposium, presented at the US EPA-DOE-EPRI Combined Power Plant Air Pollutant Control Symposium, Chicago, IL, August 20-23, 2001.

- Ropp, G.A., C.J. Danby, and D.A. Dominey, "Studies Involving Isotopically Labeled Formic Acid and Its Derivatives. II. Relation of the Absolute Reaction Rates to the Magnitudes of the Isotope Effects in the Oxidation of Formic-C¹³ Acid by Halogen Atoms," *J. Am. Chem. Soc.*, 79, 4944-4948 (1957).
- Rostam-Abadi, M., S. Chen, A.A. Lizzio, H-C. Hsi, C.M.B. Lehmann, M.J. Rood, R. Chang, C. Richardson, T. Machalek, and M. Richardson, "Development of Low-Cost Sorbents for Mercury Removal from Utility Flue Gas," proceedings of Mega Symposium, presented at the US EPA-DOE-EPRI Combined Power Plant Air Pollutant Control Symposium, Chicago, IL, August 20-23, 2001.
- Schroeder, W.H., G. Yarwood, and H. Niki, "Transformation Processes Involving Mercury Species in the Atmosphere -- Results from a Literature Survey," *Water, Air, Soil Pollut.*, 56, 653-666 (1991).
- Scott, W.W., *Standard Methods of Chemical Analysis 5th ed.*, D. Van Nostrand Company, Inc (1939).
- Secoy, C.H. and G.H. Cady, "The Effect of Temperature and Pressure on the Solubility of Chlorine Monoxide in Water," *J. Am. Chem. Soc.*, 63, 2504 (1941).
- Seigneur, C., E. Constantinou, and J. Wrobel, "A Chemical Kinetic Mechanism for Atmospheric Inorganic Mercury," *Environ. Sci. Technol.*, 28(9), 1589-1597 (1994).
- Serjeant, E.P., *Potentiometry and Potentiometric Titrations*, Wiley-Interscience Publication (1984).
- Shaffer, P.A., Jr., A. Briglio, Jr., and J.A. Brockman, Jr., "Instrument for Automatic Continuous Titration," *Anal. Chem.*, 20(11), 1008-1014 (1948).
- Shen, C.H., "Nitrogen Dioxide Absorption in Aqueous Sodium Sulfite," Ph.D. Dissertation, The University of Texas at Austin, May 1997.
- Shen, C.H. and G.T. Rochelle, "Nitrogen Dioxide Absorption and Sulfite Oxidation in Aqueous Sulfite," *Environ. Sci. Technol.*, 32(13), 1994-2003 (1998).
- Sherrill, M.S. and E.F. Izard, "The Solubility of Chlorine in Aqueous Solutions of Chlorides and the Free Energy of Trichloride Ion," *J. Am. Chem. Soc.*, 53, 1667-1674 (1931).
- Singer, C.F., B. Ghorishi, and C. Sedman, "Lime Based Multi-Pollutant Sorbents," proceedings of Mega Symposium, presented at the US EPA-DOE-EPRI Combined Power Plant Air Pollutant Control Symposium, Chicago, IL, August 20-23, 2001.

- Sitaraman, R., S.H. Ibrahim, and N.R. Kuloor, "A Generalized Equation for Diffusion in Liquids," *J. Chem. Eng. Data*, 8(2), 198 (1963).
- Sjostrom, S., T. Ebner, T. Ley, R. Slye, C. Richardson, T. Machalek, M. Richardson, R. Chang, and F. Meserole, "Assessing Sorbents for Mercury Control in Coal-Combustion Flue Gas," proceedings of Mega Symposium, presented at the US EPA-DOE-EPRI Combined Power Plant Air Pollutant Control Symposium, Chicago, IL, August 20-23, 2001.
- Skare, I. and R. Johansson, "Reactions Between Mercury Vapor and Chlorine Gas at Occupational Exposure Levels," *Chemosphere*, 24(11), 1633-1644 (1992).
- Skipnik, V.A., L.F. Fedorovskaya, L.I. Kravetskii, and I.M. Umanskaya, "Mechanism and Kinetics of Mercury Oxidation by Chlorine-Containing Solutions," translated from *Zhurnal Prikladnoi Khimii*, 52(6), 1233-1237 (1979).
- Soper, F.G., "The Ionisation Constant of Hypochlorous Acid," *J. Chem. Soc.*, 125, 2227 (1924).
- Spalding, C.W., "Reaction Kinetics in the Absorption of Chlorine into Aqueous Media," *AIChE J.*, 8(5), 685 (1962).
- Spier, J.L., "The Determination of the Coefficient of Diffusion of Mercury Vapor and Cadmium Vapor in Nitrogen," *Physica*, 7(5), 381-384 (1940).
- Stock, J.T., *Amperometric Titrations*, Interscience Publishers, New York, NY (1965).
- Stoddart, E.M., "The Kinetics of the Reaction between Chlorine and Nitric Oxide," *J. Chem. Soc.*, 388-393 (1944).
- Suzuki, K. and G. Gordon, "Stoichiometry and Kinetics of the Reaction between Chlorine Dioxide and Sulfur(IV) in Basic Solutions," *Inorg. Chem.*, 17(11), 3115-3118 (1978).
- Sznopce, J.L. and T.G. Goonan., *The Materials Flow of Mercury in the Economies of the United States and the World*, U.S. Geological Survey Circular 1197. Available from <http://geology.cr.usgs.gov/pub/circulars/c1197> (2000).
- Tang, T. and G. Gordon, "Stoichiometry of the Reaction Between Chlorite Ion and Hypochlorous Acid at pH 5," *Environ. Sci. Technol.*, 18(3), 212-216 (1984).
- Ulrich, R.K., G.T. Rochelle, and R.E. Prada, "Enhanced Oxygen Absorption into Bisulphite Solutions Containing Transition Metal Ion Catalysts," *Chem. Eng. Sci.*, 41(8), 2183-2191 (1986).

- Utter, R.G., J.B. Burkholder, C.J. Howard, and A.R. Ravishankara, "Measurement of the Mass Accommodation Coefficient of Ozone on Aqueous Surfaces," *J. Phys. Chem.*, 96, 4973-4979 (1992).
- Vivian, J.E. and D.W. Peaceman, "Liquid-Side Resistance in Gas Absorption," *AIChE J.*, 2(4), 437-443 (1965).
- Wang, T.X. and D.W. Margerum, "Kinetics of Reversible Chlorine Hydrolysis: Temperature Dependence and General-Acid/Base-Assisted Mechanisms," *Inorg. Chem.*, 33, 1050-1055 (1994).
- Weilert, C.V. and D.W. Randall, "Analysis of ICR Data for Mercury Removal from Wet and Dry FGD," proceedings of Mega Symposium, presented at the US EPA-DOE-EPRI Combined Power Plant Air Pollutant Control Symposium, Chicago, IL, August 20-23, 2001.
- West, H.L. and G.K. Rollefson, "The Photochemical Reaction of Chlorine with Formic Acid," *J. Am. Chem. Soc.*, 58, 2140-2144 (1936).
- White, G., *The Handbook of Chlorination*, New York: Van Nostrand Reinhold Co (1986).
- Yarwood, G. and H. Niki, "A Critical Review of Available Information on Transformation Pathways for Mercury Species in the Atmospheric Environment," report prepared for Atmospheric Environment Service, Environment Canada, Downsview, Ontario, Canada (1990).
- Yih, S.M. and K.P. Shen, "Kinetics on Carbon Dioxide Reaction with Sterically Hindered 2-Amino-2 methyl-1-propanol Aqueous Solutions," *Ind. Eng. Chem. Res.*, 27(12), 2237-2247 (1988).
- Yiin, B.S., D.W. Margerum, "Kinetics of Hydrolysis of the Chlorosulfate Ion," *Inorg. Chem.*, 27, 1670-1672 (1988).
- Zetemeisl, M.J. and D.F. Laurence, "Trace Chloride Determination by Rate Controlled Coulometric Titration," *Anal. Chem.*, 49 (11), 1557-1562 (1977).
- Zimmerman, G. and F.C. Strong, "Equilibria and Spectra of Aqueous Chlorine Solutions," *J. Am. Chem. Soc.*, 79, 2063-2066 (1957).
- Zhao, L.L., "Mercury Absorption in Aqueous Solutions," Ph.D. Dissertation, The University of Texas at Austin, May 1997.
- Zhao, L.L. and G.T. Rochelle, "Mercury Absorption in Aqueous Hypochlorite," *Chem. Eng Sci.*, 54, 655-662 (1999).

Zhao, L.L. and G.T. Rochelle, "Mercury Absorption in Aqueous Oxidants Catalyzed by Mercury (II)," *Ind. Eng. Chem. Res.*, 37, 380-387 (1998).

Zhao, L.L. and G.T. Rochelle, "Mercury Absorption in Aqueous Permanganate," *AIChE J.*, 42 (1996).

Vita

Sharmistha Roy was born in Boston, Massachusetts, on January 18, 1976, the daughter of Baidya and Bharati Roy. After graduating from Lakeside High School in 1993, she entered Georgia Institute of Technology in Atlanta, GA. During the summers of 1995 and 1996, she interned at Dow Chemical Company. In 1997, she received the Bachelor of Science with Highest Honor in Chemical Engineering. That summer, she interned at Exxon Production Research Company in Houston, TX. In the fall of 1997, she entered the graduate school of Chemical Engineering at The University of Texas at Austin. Full time employment has been accepted with ExxonMobil Chemical Company.

Permanent Address: 710 Whittington's Ridge
Evans, GA 30809

This dissertation was typed by the author.